



ulm university universität
uulm

Design of Polymer Nanoarchitectures by DNA Origami Technology

Dissertation zur Erlangung des Doktorgrades Dr. rer. nat. am Fachbereich Chemie der
Fakultät für Naturwissenschaften der Universität Ulm

vorgelegt von

Yu Tokura

aus Japan

2018

Dissertation der Universität Ulm:

Amtierender Dekan: Prof. Dr. Peter Dürre

1. Gutachter: Prof. Dr. Tanja Weil

2. Gutachter: Prof. Dr. Mika Lindén

3. Gutachter: Prof. Dr. habil. Hans Börner

Tag der Promotion: 31 Jan 2018

Universität Ulm, Fakultät für Naturwissenschaften, 2018

Abstract

This dissertation explores a novel concept and new methodologies for the fabrication of precision (bio)synthetic polymer architectures in nanoscale resolution by merging DNA nanotechnology and polymer chemistry. Polymeric materials are versatile and play important roles in modern nanotechnologies including nano-optics / electronics, nanofluidics, nanosensors, nanomedicine, and so on. To further develop these applications in the future, the rational design of polymeric materials with a high structural precision in the low nanoscale dimensions is highly attractive. I have particularly focused on DNA nanotechnology, more precisely, represented as “DNA origami”, and utilized this technique as a template for synthesizing novel polymeric nanostructures. The high programmability of DNA origami was employed for the first time to design and create a suitable chemical reactor to control polymerization reactions in nanoscale environments with great structural precision.

The integration of controlled radical polymerization (CRP) and DNA origami was established for the first time, which could create desired polymer nanopatterned surfaces in a controlled fashion. Through these investigations, unique features were found such as altered surface properties of DNA origami by grown polymers that inspired the next step. Further developments were achieved by making use of an established in-situ polymerization system for creating defined DNA / polymer hybrid nanomaterials. The step-wise design to convert the common two-dimensional rectangular DNA origami to a three-dimensional tube-shape structure with an outer polymer coating could potentially protect DNA origami from external stimuli (in particularly, against nuclease digestion), which is one of the current issues limiting various applications of DNA origami-based materials / systems. Additionally, the remaining interior space of the tube was available for further reactive environment, which was demonstrated by incorporation of multiple DNA-based enzyme moieties.

In addition, polydopamine, a bio-inspired polymer whose polymerization is more challenging to control, was also successfully fabricated in a defined manner on DNA origami for the first time. Properly designing the catalytic domain on DNA origami could allow us to fabricate various shapes and sizes of polydopamine nanoarchitectures in high precision. The adhesive property of polydopamine was successfully expressed on DNA origami to dynamically control its conformation as a supramolecular glue. On the other hand, the rigidly crosslinked polymer structure of polydopamine allowed us to rapidly liberate the grown polydopamine with programmed geometry from DNA origami template by a facile acid treatment.

To summarize, the integration of polymer chemistry and DNA nanotechnology was studied in the thesis, which emerged as a unique and promising approach to fabricate

various polymeric nanoarchitectures in a defined manner. Versatility and uniqueness of the reported methods could cause a stir in the design concepts of polymeric nanomaterials and pave the way for the further development of nanotechnology in future.

Table of Contents

1. Introduction	5
1-1. Nanotechnology	5
1-2. Design and synthesis of precision polymers	6
1-3. Defined polymer assembly	7
1-4. Fabrication of micro/nano patterned polymer brush surfaces	10
1-5. The characterization of polymer brushes	12
1-6. Use of biomacromolecule as template for directing polymerization reactions or biomolecule-templated polymer synthesis	14
1-7. Bio/polymer hybrid	17
1-8. The programmability of DNA	18
1-9. DNA synthesis	19
1-10. Programming DNA assembly	22
1-11. Incorporation of functionalities into DNA origami	25
1-12. The modification of staple DNA strand	28
1-13. DNA origami as template for assembling nanomaterials	29
1-14. DNA origami-templated synthesis of nanomaterials	31
1-15. The stability of DNA origami	35
1-16. DNA origami and polymer synthesis	37
2. Motivation	38
3. Investigated systems	40
[3-1] Fabrication of defined nanopatterned polymers by surface-initiated atom transfer radical polymerization on DNA origami	40
[3-2] Step-wise design of precision polymer tube by DNA origami templated synthesis	44
[3-3] DNAzyme-assisted fabrication of polydopamine nanostructure on DNA origami template	48
[3-4] Systematic study on intercellular supramolecular assembly of oligothiophene analogues	52
4. Conclusion and Outlook	54
5. References	57
6. Publications	70
[6-1] Bottom-Up Fabrication of Nanopatterned Polymers on DNA Origami by In Situ Atom-Transfer Radical Polymerization	70
[6-2] Polymer tube nanoreactors by DNA-origami templated synthesis	91
[6-3] Fabrication of defined polydopamine nanostructures by DNA origami-templated polymerization	119

[6-4] Directing intracellular supramolecular assembly with N-heteroaromatic quaterthiophene analogues	143
7. Curriculum vitae	175
8. List of publications	176
9. List of conferences	177
10. Abbreviations	178
11. List of figures	180
12. Declaration of Originality in academic work	181
13. Acknowledgement	182

1. Introduction

The scientific results included in this thesis originated from an inspiration from both polymer chemistry and DNA nanotechnology to create unique DNA-polymer hybrid architectures of greatest structural precision. First, an excursion into polymer nanotechnology will be discussed, focusing on the design and synthesis of single precision polymers, their assembled states, characterization methods also emphasizing their advances in the last decades and currently faced problems and demands. The second part of the introduction will emphasize the unique opportunities of DNA nanotechnology, which is a key technique for structuring with greatest precision. Here, the structure of DNA and its functions, design principles of DNA nanotechnology with its applications in the nanotechnology fields are discussed in detail. Not all of the writing might be directly found within the work conducted in the thesis, however the author believes that the future developments of the project can potentially reach to integrate with and contribute to broad subjects in the nanotechnology field, therefore several promising techniques, applications and directions are also described herein.

1-1. Nanotechnology

The intensive advances of the various nanotechnology fields in the past decades has enlightened new visions and future possibilities of science and technology. Nanotechnology is the discipline for manipulating materials of nanometer (10^{-9} m = 1 nm) sizes, which basically is the world of atoms, molecules, and their assembled states. Due to the wide range of materials nanotechnology benefits, the applications of nanotechnology can cover a wide variety of science and technology fields involving information technology (IT), life science, energy science, and so on. Among nanomaterials, polymers or polymeric nanomaterials are not the exception. Recent advances in polymer chemistry have made synthetic polymers no longer just simple plastics but a man-made soft matter that can be tuned and functionalized to give desired properties. Manipulation of polymer nanotechnology can start from the design and the synthesis of single polymers to control the size, polydispersity, and compositions, which decide both the functionality of polymers and the final architecture (nanoparticle, micelle, fiber, and micro/nanofilm) by self-assembly or self-folding. Each step will be comprehensively described in the following sections.

1-2. Design and synthesis of precision polymers

In the past decades, new design and synthesis strategies have emerged to create synthetic polymers with controlled shapes, sizes, and functionalities. Especially, the controlled radical polymerization (atom transfer radical polymerization (ATRP) first reported in 1995^{1,2} and reversible addition-fragmentation chain transfer (RAFT) polymerization first reported in 1998³) have developed rapidly since they were found to be versatile methods to achieve polymers with different sections (di / tri block copolymer) with very low polydispersity. This is feasible because there are only initiation and propagation reactions present while transfer or stop reactions in the polymerization are minimized (Figure 1). Therefore, the size of the resulting polymers (molecular weight) mainly depends on the ratio between monomers and initiators. In addition, the initiator also provides the terminating group of the growing polymers, so additional functional groups can be easily introduced. It should also be noted that ATRP and RAFT are quite robust in the presence of a wide variety of functional groups and tolerate various solvents to tailor the desired properties. The versatility of these methods are crucial since the final architecture of the polymers is a result of their self-folding, self-assembly, and self-organization features, which are influenced by their length, solvophobicity, charge, hydrogen bonding capability, and bulkiness of synthesized polymers.

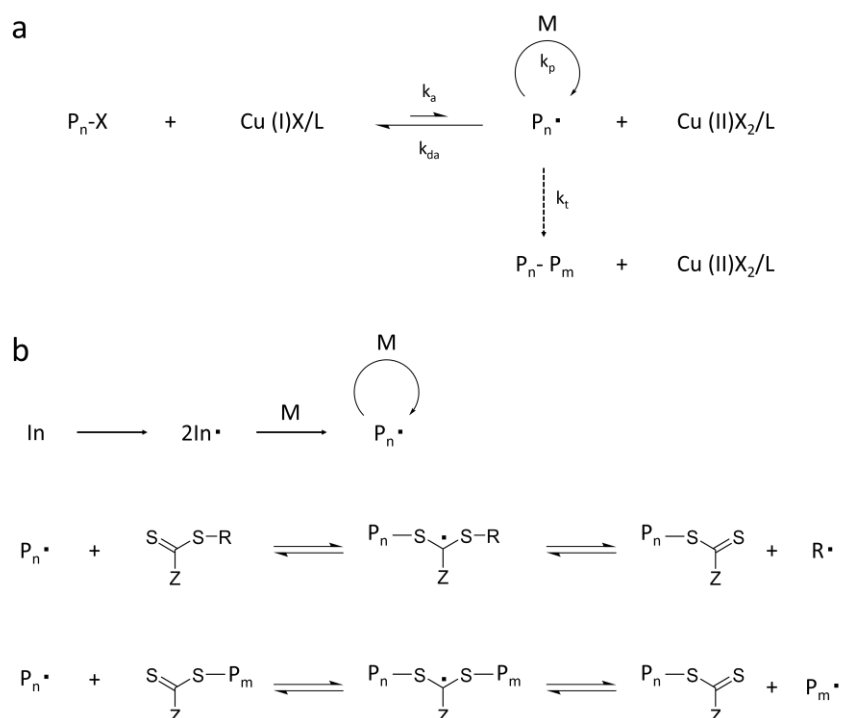


Figure 1. The basic scheme of ATRP. Alkyl halide (R-X) serve as the initiator. In typical cases, a transition metal complex is employed as the catalyst. The initiator or the dormant species is activated by the catalyst to generate radicals. Simultaneously, the catalyst is

oxidized while capturing the halide. Since the equilibrium is predominantly shifted to the dormant species, it assures very low radical concentrations, resulting in the same probability of the polymers to propagate with monomers. (RAFT: Z and R group must be chosen according to the monomer and the temperature.)

1-3. Defined polymer assembly

Recent advances in controlling precision polymer synthesis has provided new avenues for achieving single polymer chains with well-defined lengths and compositions to control their self-assembly and organized states of multiple polymers in the micro/nanoscale. It has been demonstrated that amphiphilic AB-block copolymers could form nanostructures such as spherical/wormlike micelles and vesicles (polymersome) (Figure 2a)^{4,5}. These polymer self-assemblies have been investigated as drug carriers, as artificial cell systems, and so on. In addition, it has been demonstrated that the geometry and the sizes of these nano-objects have a considerable influence on their optical⁶, electronic⁷ and biomedical functions^{8,9}. These studies clearly indicated that the precise control of polymeric nanostructures is a key-factor to conceive advanced polymeric nanomaterials. To design such nanostructured polymer assemblies, the bottom-up approach based on the design of monomers, the block length/ratio, and the geometry of the block polymers would essentially allow atomic control over the structure and high production yields. D. J. Pochan and co-workers have demonstrated a multi geometry polymer assembly in a systematic fashion by blending the designed block copolymers¹⁰. Further rational guidelines for the self-assembly of linear ABC triblock terpolymers into a variety of polymeric nanostructures with different hydrophilic or hydrophobic patches were reported by Axel H.E. Müller and co-workers (Figure 2b)¹¹. In their work, each block length of polystyrene-block-polybutadiene-block-poly(tert-butyl methacrylate) (PS-PB-PT) was fine-tuned, from which the geometry and the microphase separation could be predicated.

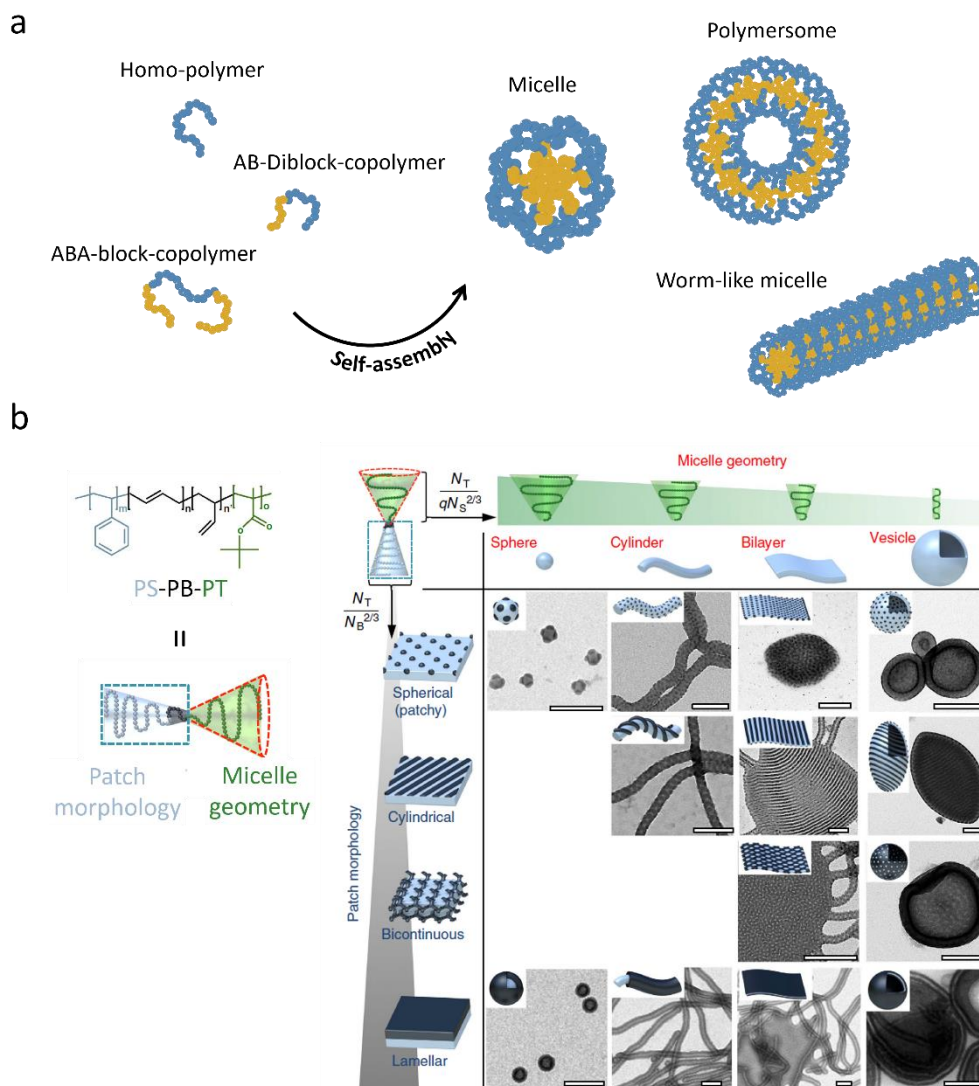


Figure 2. Design of polymer assembly. (a) General scheme of polymer self-assembly into micro/nanostructured architectures. (b) Rational design of ABC triblock terpolymer with controlled geometry and patch morphology. (b) was adapted with permission from “Lobling, T. I. et al. Rational design of ABC triblock terpolymer solution nanostructures with controlled patch morphology. Nat. Commun. 7, doi:Artn 12097 10.1038/Ncomms12097 (2016).” Copyright (2016) Nature Publishing Group and Creative Commons Attribution 4.0 International License (<http://creativecommons.org/licenses/by/4.0/>).

Polymer brushes – ensembles of densely packed polymer chains tethered on various surfaces - are another class of polymeric micro/nano architecture (Figure 3)¹²⁻¹⁴. Depending on the density and size of surface-anchored polymer chains, polymer brushes can adopt various conformations such as so-called “mushroom”, “pancake”, and “brush” architectures. Due to the fact that various chemical and physical properties of synthetic polymers can be incorporated onto the surface of interest, polymer brush formation has

been investigated as versatile method for surface functionalization and tailoring the surface morphology. Additionally, more sophisticated systems such as block copolymer brushes and mixed polymer brushes with different chemical components or stimuli/environment responsiveness can impart smart functionalities on to the surface, like switchable wetting behaviors^{15,16}.

In general, there are two major strategies for the design and the construction of polymer brushes; namely the “grafting to” and “grafting from”¹² strategies. In the former approach, end-functionalized polymers prepared by “in-solution-based synthesis” are directly transferred to the surface by reacting with the respective functional groups on the surface. Although the chemical/physical information of the grafted polymers can be analyzed before grafting, the steric hindrance of polymers with large molecular weights or bulky building blocks can make it difficult to graft these polymers in high densities. On the other hand, in the “grafting from” approach, polymers are grown directly from the initiator moieties immobilized on the surface (in other words, surface-initiated polymerization).

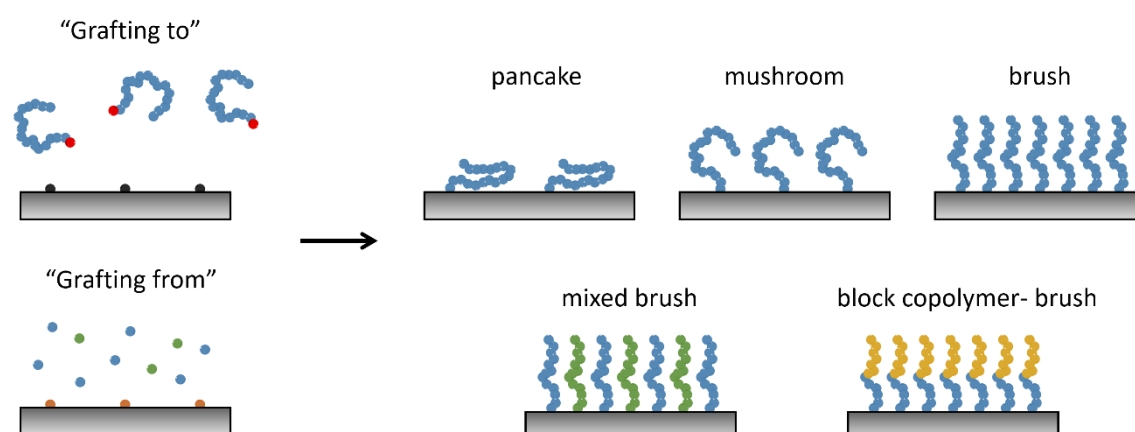


Figure 3. General scheme of polymer brush fabrication. Polymer brush surfaces can be prepared by either the “grafting to” method (direct immobilization of end-functional polymers to the corresponding functional groups on the surface) or the “grafting from” method (surface-initiated polymerization from the initiator-immobilized surface). The tethered polymer surface can show different morphologies (pancake, mushroom, and brush) relying on the density and the length of grown polymers. Step-wise growth of polymers or a combination of different polymerization reactions allows fabrication of more complicated architectures such as mixed polymer brush surfaces and block copolymer-brush surfaces.

A number of surface initiated controlled radical polymerizations such as

surface-initiated atom transfer radical polymerization (SI-ATRP), surface-initiated reversible-addition fragmentation chain transfer (SI-RAFT) polymerization, and surface-initiated nitroxide-mediated polymerization (SI-NMP) represent very versatile methods due to their unique advantages such as compatibility to a wide variety of monomers and solvents¹⁷. Particularly among all the CRP methods, SI-ATRP has been most extensively investigated due to the easy anchoring of the alkyl bromide initiator molecules, tenability, versatility, and robust chemistry. During the development of SI-ATRP, there are several key findings. First, to achieve a controlled polymerization from the initiator immobilized on the surface, the addition of free initiator as sacrificial initiators was sometimes necessary to maintain the adequate initiator and deactivating Cu^{2+} concentrations¹⁸. Secondly, the concentration of the metal catalyst could be reduced to a few ppm at the same time retaining the tolerance toward oxygen or other radical traps by using reducing agents such as ascorbic acid. This ATRP variant is denoted especially as activators (re)generated by electron transfer ATRP (A(R)GET ATRP). These improvements could solve mainly the concerns of the presence of residual amounts of metal catalysts in the grown polymers that may cause unwanted toxicities in (bio)medical application. Last but not least, the development of ATRP chemistry has broadened its versatility by proposing a variety of photo-induced ATRP (photoATRP), and so on.

1-4. Fabrication of micro/nano patterned polymer brush surfaces

The patterning of polymer brushes with micro/nanoscale spatial resolution is not only of fundamental interest to study, for instance, swelling and friction properties, but also for practical applications from micro/nano electronics to bionanotechnology fields^{19,20}. For example, micropatterned thermoresponsive polymer brush surface prepared by a combination of RAFT and photolithography exhibits tunable and spatial bioadhesion properties that are especially applicable for the orientation and alignment of fibroblast cells which can be cleaved off as a “cell sheet” just by lowering the temperature under the lower critical solution temperature²¹. G. P. López and co-workers have reported a dual-nanopatterned polymer brush/bioactive molecules surface to demonstrate the controlled attachment, killing and release of bacteria (Figure 4a)²².

Preparation of micro- or nanopatterned polymer brushes with desired spatial resolutions, polymer lengths, and chemical compositions, using the combination of surface-initiated polymerization and a variety of lithographical techniques has been shown as a promising strategy (Figure 4b). Basically, the patterning strategy can be categorized to two areas; “top-down” approach and “bottom-up” approach. In the top-down approach, electron beam lithography can be used to directly pattern polymer

brushes in a single step from non-patterned polymer brush surface²³. Although the spatial resolution can be down to about 10 nm, there are several limitations including high instrumental costs, long operation time, and low production yield. Alternatively, in the “bottom-up” approach, the initiator moieties are immobilized/self-assembled onto the surface of the interest by using the proper chemistry (alkyl thiol/gold surface, silane/oxide surface) and pre-patterning by lithographical techniques, followed by the surface-initiated polymerization. Depending on the area size and the material of the surface used, different lithographical techniques such as micro-contact printing, photo lithography, electron beam lithography, scanning probe lithography, nanoimprint lithography, and so on can be options.

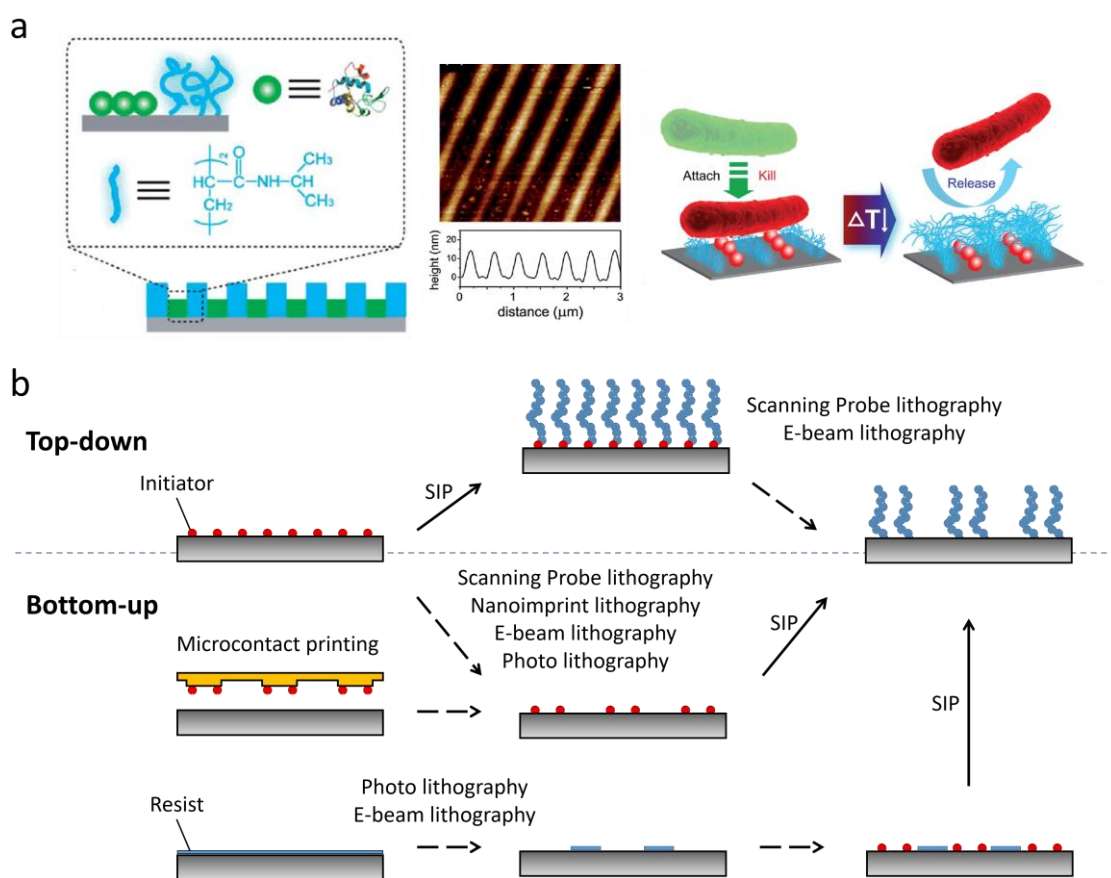


Figure 4. Fabrication of a micro/nano patterned polymer brush surface. (a) Schematic depiction of nanopatterned thermoresponsive poly(N-isopropylacrylamide) (PNIPAAm) / Lysozyme surface (AFM image in the middle). After attaching bacteria with the collapsed dehydrated PNIPAAm chains at 37 degree, lysozyme proteins kill the bacteria, followed by the release of killed bacteria by hydrated PNIPAAm chains at 25 degree. (b) The overview of various approaches for preparing micro/nano patterned polymer brushes. SIP: surface-initiated polymerization. (a) was adapted with permission from “Yu, Q. et al.

Nanopatterned Smart Polymer Surfaces for Controlled Attachment, Killing, and Release of Bacteria. ACS Appl. Mater. Interfaces 5, 9295-9304, doi:10.1021/am4022279 (2013).” Copyright (2017) American Chemical Society.

1-5. The characterization of polymer brushes

In general, the characterization methods for polymer brushes can be classified into two categories, investigating chemical properties (molecular weight, chemical compositions, and dispersity) and physical properties (thickness, grafting density). Although the conventional, well-established analytical techniques for characterizing polymers created in solution are also useful to obtain the information of polymers on the surface especially for those prepared by the grafting-to methods, there are some challenges for characterizing polymers on surface in general. For example, in the bottom-up approach, molecular weights of grown polymers are often determined by GPC analysis of polymers grown in solution from free or sacrificial initiators during surface initiated polymerization. Although there is an assumption and experimental proof that molecular weights of free polymers have a relatively good agreement with that of polymers on surface, this is not always the case. To precisely determine the molecular weight information, the cleavage of the polymers from the surface followed by GPC analysis is required.

Here, some of the most common and useful characterization techniques that are also employed in the thesis are introduced.

AFM / AFM-IR: AFM has been a powerful characterization tool for acquiring information on the topology, thickness, roughness of the polymer surface. Although other microscopy techniques like SEM and TEM are also essential tools for imaging the polymer surface, AFM can provide specially the mechanical properties of the surface such as elasticity, deformation and adhesion in nanometer spatial resolution. The basic AFM setup is shown in Figure 5. The tip attached on the cantilever moves across the sample surface for imaging. The forces between the tip and the surface are measured as the deflection of the cantilever that information was reflected to the change of the laser reflection by the photo detector. There are currently several modes for imaging such as contact, noncontact, and tapping. Tapping mode eliminates the major drawbacks of contact mode (sample destruction) and noncontact mode (low resolution in lateral and z-axis). Nowadays, tapping mode is the most frequently used mode in measurement in air and in solution. In this mode, the cantilever oscillates up and down at its resonance frequency. When the oscillating cantilever gets close to the surface, the interactions between the tip and the sample (Van der Waals force, dipole-dipole interaction, electrostatic interaction and so on)

cause a change of the oscillation amplitude. This amplitude change is used as the parameter and a feedback loop adjusts the height of the cantilever to maintain the oscillation amplitude. For obtaining mechanical information of the surface, the force measurement is used. In the measurement, the cantilever moves towards the sample surface, contacts the sample, then the tip experiences a force due to the deflection of the cantilever. By recording the force versus distance of the cantilever from the sample surface, a force curve is obtained, from which the information on the mechanical properties of the sample such as elastic modulus, adhesion, deformation, and dissipation can be determined.

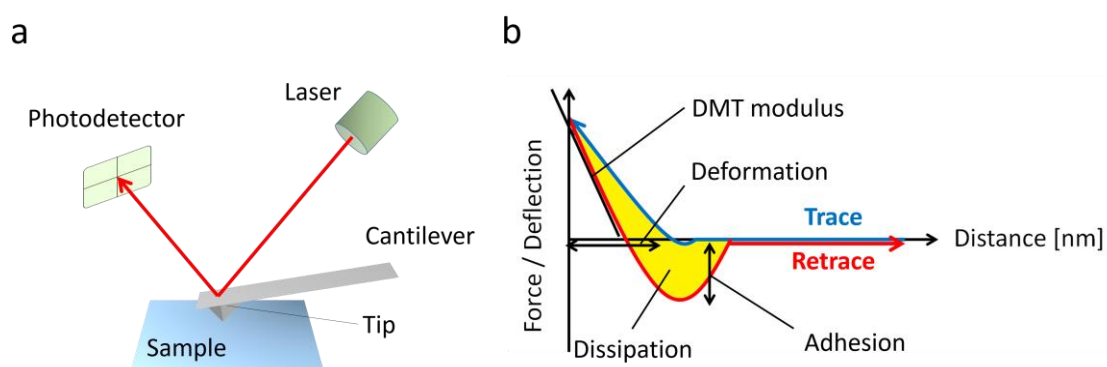


Figure 5. General AFM scheme. (a) General setup of AFM instrument. (b) Force curve.

Recent developments of AFM technology have proposed combinations of the AFM instrument with confocal laser microscopy, photo conductivity, and especially, infrared spectroscopy (AFM-IR)^{24,25}. AFM-IR provides a nanoscale infrared spectrum to map the different chemical components on the surface. Wavelengths in which the sample absorbs the light of corresponding wavelength will cause greater heating and thus the rapid expansions. This causes the modulation of the oscillating cantilever at the characteristic resonant frequencies of the cantilever. The induced resonance amplitude in the cantilever is proportional to the absorption of the IR illumination in the sample. Although early AFM-IR instruments had a limited spatial resolution down to micrometer scale due to the thermal diffusion, significant improvement was achieved by using pulsed infrared laser sources to reduce consequently the thermal diffusion²⁶, achieving the spatial resolutions down to around 20 - 30 nm²⁷. Chemical compositional mapping is usually conducted by imaging the sample with a single wavelength corresponding to a specific molecular resonance and can be made at different absorption bands to reveal the distribution of different chemical species. The IR band range of AFM-IR is typically mid-IR, between 1000 cm⁻¹ to 3600 cm⁻¹ covering the polymer backbone conformation region. Applications of AFM-IR spans from characterizing blended polymer films²⁸, nanofabricated polymer

patterns²⁹ to elucidating the nanostructure of polymer networks³⁰, and also other nanotechnology fields.

Time-of-Flight Secondary Ion Mass Spectrometry (ToF-SIMS): Nowadays, ToF-SIMS has become one of the most important tools to analyze polymeric materials in solids owing to the high surface sensitivity, molecular specificity, and sub-micrometer imaging resolution^{31,32}. ToF-SIMS can be used to acquire the chemical information of the polymer nanostructures on surfaces. During a ToF-SIMS measurement, the sample surface is bombarded with primary ions, which dislodge chemical species on the uppermost surface as the secondary ions (Figure 6). Usually, the irradiation dose of ions is very low ($<10^{13}$ ions per cm^2) so that the same surface spot is not bombarded again and the information obtained should reflect the surface of nanometer depth. The generated secondary ions are accelerated in the flight path towards the mass detector measuring time of flight. The secondary ions are usually series of multiple monomer units (oligomers) or characteristic fragmentation ions that provides the “fingerprint” spectrum to determine the chemical structure of polymers.

Recent developments in ToF-SIMS has enlarged its usage to determine the end-functional group distribution of polymer semi-crystalline surface³³, the morphology of polymer blends³⁴, 3D mapping of multilayer polymer films³⁵ and so on.

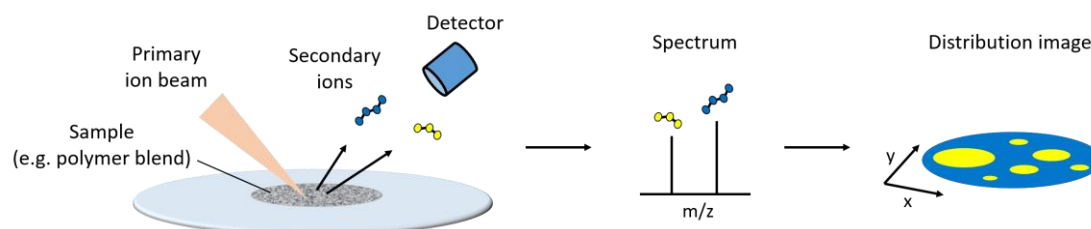


Figure 6. General schematic depiction of ToF-SIMS.

1-6. Use of biomacromolecule as template for directing polymerization reactions or biomolecule-templated polymer synthesis

Peptides, proteins, and DNA are biopolymers that evolved over billions of years. They have a sequence precision, wide variety of monomers (amino acids and nucleotides), intermolecular interactions for self-folding into unique 3D structures for performing biochemical reactions, and intramolecular interactions to self-assemble into nano/meso architectures with high order. The structural and functional perfection of bio-macromolecules and their assembled states like peptide fibers and virus capsid

proteins, cage proteins provide unique interior cavities or amino acid-patterned surfaces with nanoscale precision. For this reason, biomacromolecules have been exploited as promising nano-sized templates or nanoreactors to realize novel chemical reactions³⁶, to build inorganic nanomaterials (particles³⁷, wires³⁸) and also to synthesize new polymeric materials³⁹. These reactions in confined nanoscale environments have shown the allowance for enhanced reaction kinetics, decreasing side reactions, and shape / size control. Encapsulation of metal catalysts inside ferritin has offered a bionanoreactor that could successfully polymerize phenyl acetylene with a narrower polydispersity compared to the same reaction conducted without the ferritin (Figure 7a)⁴⁰. Bruns and co-workers covalently bound the metal catalyst for ATRP to the cavity surface of chaperonins to polymerize NIPAM and oligo(ethylene glycol)ethyl ether acrylate (OEGA)⁴¹. Both products after the reaction showed lower molecular weights and a narrower molecular weight distribution than the products synthesized in bulk solution

As shown above, protein assemblies offer a unique confined space, on the other hand, DNA templates have been used to program the sequence information of polymers. Sequence-defined polymer synthesis represents a challenge in polymer chemistry. Inspired by DNA transcription and replication systems in nature, DNA templates have been investigated as promising scaffolds for controlling the sequence of the polymers (Figure 7b)⁴². Strand-displacement systems⁴³ and the DNA machinery⁴⁴ have been employed to synthesize oligomers and peptides with desired sequences in a stepwise manner. Although these methods had the limitation that only relatively small polymers or oligomers could be synthesized in low yields, the major advance was achieved by Liu's group (Figure 7c). They mimicked the ribosomal translation system by designing macrocyclic monomer units composed of a polymer block and peptide nucleic acid (PNA) connected with cleavable linker, emulating transfer- ribonucleic acid (tRNA). PNA is an artificial derivative of DNA or RNA and has N-(2-aminoethyl)-glycine units linked by peptide bonding as backbone⁴⁵. Due to the lack of electrostatic repulsion between backbones, PNA can show a stronger binding affinity to its complementary sequence compared to DNA and RNA. The specific alignment of each monomer unit composed of PNA adapter with 5 nucleobases onto the DNA template and conjugation by oxime formation, hydrazone formation, and copper(I)-catalyzed azide alkyne cycloaddition (CuAAC) click chemistry gave the sequence-defined polymers that could be cleaved from the DNA template. This method allowed usage of peptides as building block to synthesize sequence-defined biopolymers with a molecular weight of about 26 kDa (90 amino acids) with high efficiency (~70 %)⁴⁶ based on the precise self-assembling features of DNA.

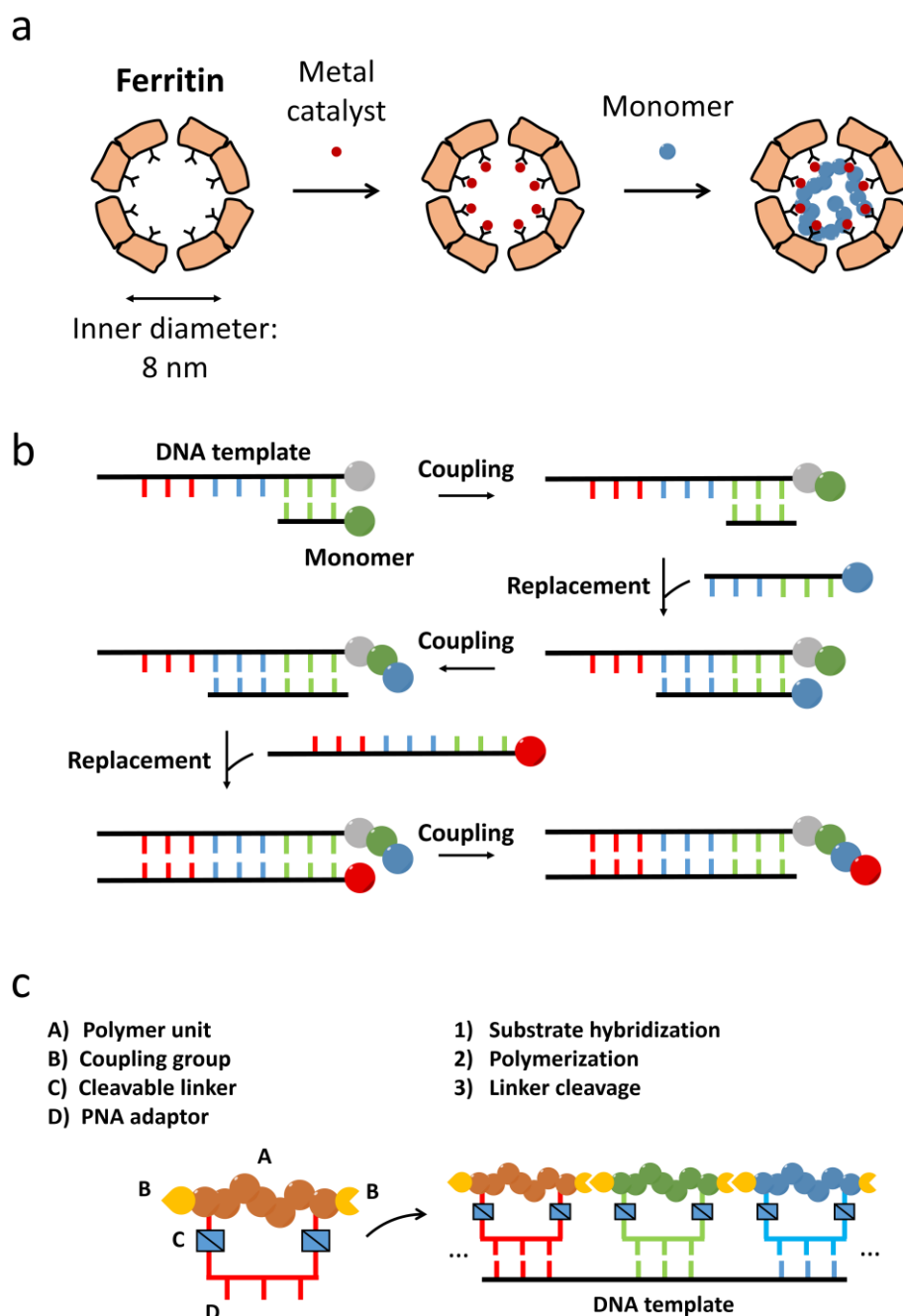


Figure 7. Biomacromolecular templated polymer synthesis. (a) The scheme of protein cage-templated polymer synthesis. The interior cavity of ferritin was modified with metal catalysts followed by supplying the monomer and the polymerization⁴⁰. (b) DNA templated sequence-controlled polymer synthesis by strand-displacement method⁴³. The ds DNA was used to bring the monomer and the last group of the growing polymer in close proximity. Repetitive coupling and replacement of the hybridized DNA strand with the longer complementary DNA strand produce the sequence defined polymer. (c) DNA templated sequence-controlled polymer synthesis by using macrocyclic monomer unit⁴⁶. The aligned substrate on DNA template allows the one-pot synthesis of sequence-defined polymer that can be cleaved from the template afterwards.

1-7. Bio/polymer hybrid

In addition to using biomacromolecules as templates to synthesize polymers as described in the last paragraph, merging the functionalities and properties of polymers with biomacromolecules would be interesting to create advanced bio/polymer hybrid nanomaterials⁴⁷. PEGylation of protein has been known to reduce the immunogenicity of proteins and increases their circulation time⁴⁸. PEGylated DNA has been found to show solubility in organic solvent while preserving its 3D structure⁴⁹. Polymers loaded or synthesized within protein cages offer the possibility of increasing the loading density of cargos such as drug molecules, nucleic acids, and agents for magnetic resonance imaging contrast, and increased stabilities against mechanical stress⁵⁰. In addition, block polymers composed of hydrophobic synthetic polymer units and hydrophilic biopolymer moieties have been demonstrated to form unique micelle or other self-assembled structures. Stimuli responsive polymers could introduce new functionalities to biomacromolecules⁵¹.

For designing and creating polymer biohybrid nanomaterials, several approaches have been exploited. "Grafting to" is a facile synthesis method that allows introduction of fully characterized synthesized polymers to biomacromolecules. The main limitations of the "grafting to" approaches are 1) the purification of the polymer biohybrids from unreacted polymers or biopolymers can be laborious, and 2) the conjugation of the polymers with high molecular weight may result in low loading yield due to the steric repulsion. To address these issues, the "grafting from" approach has been studied intensively³⁹. Again, controlled radical polymerization (ATRP, RAFT) is preferably suited due to its compatibility to aqueous solvent and very small amounts (ppm) of catalyst is necessary or even without transition metals (Metal-free ATRP^{52,53}). The attachment of initiator molecules could be conducted by using the reactive amino acid residues (thiol, amine, carboxylic acid) on the surface of macromolecules. The site directed mutation of amino acids made it possible to precisely tune the position and the number of the initiator molecules on the surface of biomacromolecules.

Compared to the protein assemblies that mostly offer symmetric structures and defined dimensions, which makes the modulation of shape (asymmetric structures) or the size of cavities quite challenging and laborious, the development of DNA nanotechnology has made it possible to design 2D/3D nanostructures with high programmability of size, shape and functionalities from which arises the possibility of using DNA as a template not only for synthesizing single precision polymers but polymer nanoarchitectures with a high order of control.

1-8. The programmability of DNA

In nature, DNA is carried by all known living organisms and many viruses as a carrier of genetic information to sustain their life through the processes of cell replication and protein syntheses. This essential role of DNA is attributed to its high programmability, in other words, high specific recognition ability and diversity (uniqueness). As shown in Figure 8, the 3D structure of DNA is a right-handed double helix composed of an anti-parallel pair of single-stranded DNA (ssDNA) strands which are complementary with each other⁵⁴. The ssDNA is a biopolymer consisting of repeating units of its monomers, called nucleotides. Nucleotides are composed of deoxyribose, phosphate groups, and one of four different bases; adenine (A), cytosine (C), guanine (G), and thymine (T). Each nucleotide is connected by a phosphodiester linkage between the 3' hydroxyl group of one deoxyribose unit and the 5' hydroxyl group of a neighboring deoxyribose, which gives a ssDNA strand the directionality which is typically presented from 5' to 3'. In the double helical structure of DNA, each base is specifically paired with just one type of base out of four; A-T and C-G (Watson-Crick base pair), via hydrogen bonding. There are two hydrogen bonding between A and T, and three between C-G which give stronger interactions. DNA double helix is also stabilized by π - π stacking of the aromatic bases. Totally, the highly specific base pairing and hybridization to double helical structure allow DNA strands to be unique with programmable features.

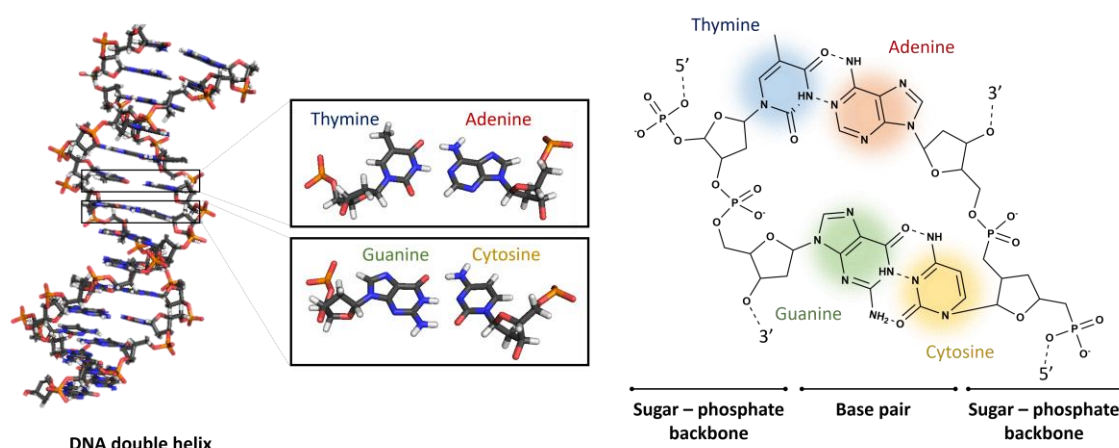


Figure 8. 3D Structure of dsDNA. Double helical structure and base pairings are shown on left. On the right, the molecular structure of each base pairing is drawn with sugar-phosphate backbones. dsDNA images were created from PDB: 2M2C⁵⁵ by PyMOL (The PyMOL Molecular Graphics System, Version 2.0 Schrödinger, LLC).

1-9. DNA synthesis

Recent developments in the chemical synthesis of DNA has turned DNA from an expensive and laborious compound to a designable material with desired sequence and functionality. Nowadays, the most common setup for DNA synthesis is implemented with nucleotide loaded solid-supports by coupling desired phosphoramidites with protected bases one by one in an automated instrument (Figure 9). The chemical DNA synthesis goes from 3' to 5' which is different from enzymatic DNA synthesis done in nature (5' to 3'). The following paragraph introduced the general steps conducted in one cycle of chain elongation of DNA.

The 3' nucleotide of the desired DNA strand is immobilized on a solid-support, usually controlled pore glass (CPG). The 5' of the immobilized nucleotide and phosphoramidites are protected by 4,4'-dimethoxytrityl (DMT) group which is labile to acid. The first step is to remove the DMT group by acid solution, usually trichloroacetic acid (TCA). The cleaved DMT cation is orange colored which is monitored by a UV-Vis detector to evaluate the yield of this step (and later the yield of phosphoramidite coupling). The second step is to couple deprotected 5' hydroxyl group of the nucleotide with the next phosphoramidite activated by acidic azole catalyst like 1H-tetrazole and 5-ethylthio-1H-tetrazole. It should be noted that to ensure the high yield of coupling (otherwise, 90 % yield of each coupling can result in only total yield of 12 % after 20 couplings), usually 1.5-20-fold excess of phosphoramidite is used for the coupling. The third step is capping, which is to treat the remaining unreacted 5' hydroxyl group with a mixture of acetic anhydride and 1-methylimidazole so that it won't react again during the next coupling cycle which will result in a shorter DNA sequences than designed. The last step is the oxidation of the phosphite triester linkage with iodine to a phosphate triester. These four steps fulfill one cycle to introduce new nucleotide onto the 5' of existing DNA sequence on a solid-support.

After DNA synthesis, the synthesized DNA sequences are eluted from the solid-support by ammonium hydroxide solution treatment which also cleaves the protecting group on the bases. By leaving the DMT group on the last introduced phosphoramidite (5' of DNA sequence), the DMT-bearing correct DNA sequence (product) can be separated from other DMT-missing shorter DNA sequences (byproduct) by reverse phase high performance liquid chromatography (RP-HPLC), followed by manual detritylation with acetic acid treatment.

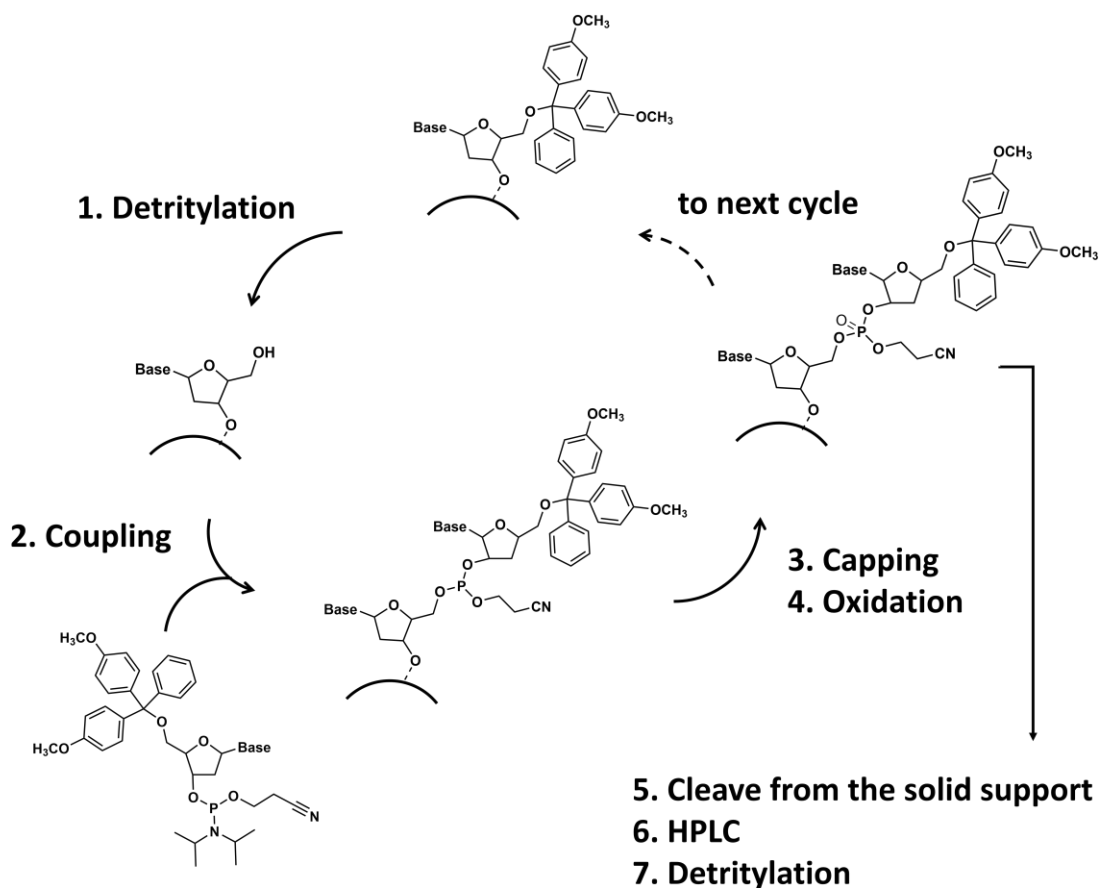


Figure 9. The general scheme on one cycle of DNA synthesis.

It should be noted that automated DNA synthesis still has a drawback that only relatively short DNA sequences, i. e. until around 50 nucleotides can be synthesized due to increasing steric hindrance and less than 100 % coupling yield. On the other hand, it allows employment of not only phosphoramidites with normal bases (A, C, G, and T) but also non-nucleoside monomers to prepare tailor-made DNA sequences with desired functionalities at desired positions. Phosphoramidites modified with functional groups (amine, thiol, alkyne, azide, and so on) or fluorescent molecules are able to be incorporated into the DNA sequences by automated DNA synthesis (Figure 10a). Obtained DNA with functional groups are able to be post-modified with the corresponding molecules (amine / N-hydroxysuccinimide (NHS) ester, thiol / maleimide, alkyne / azide, azide / dibenzocyclooctyl and so on) to incorporate further functionalities (Figure 10b).

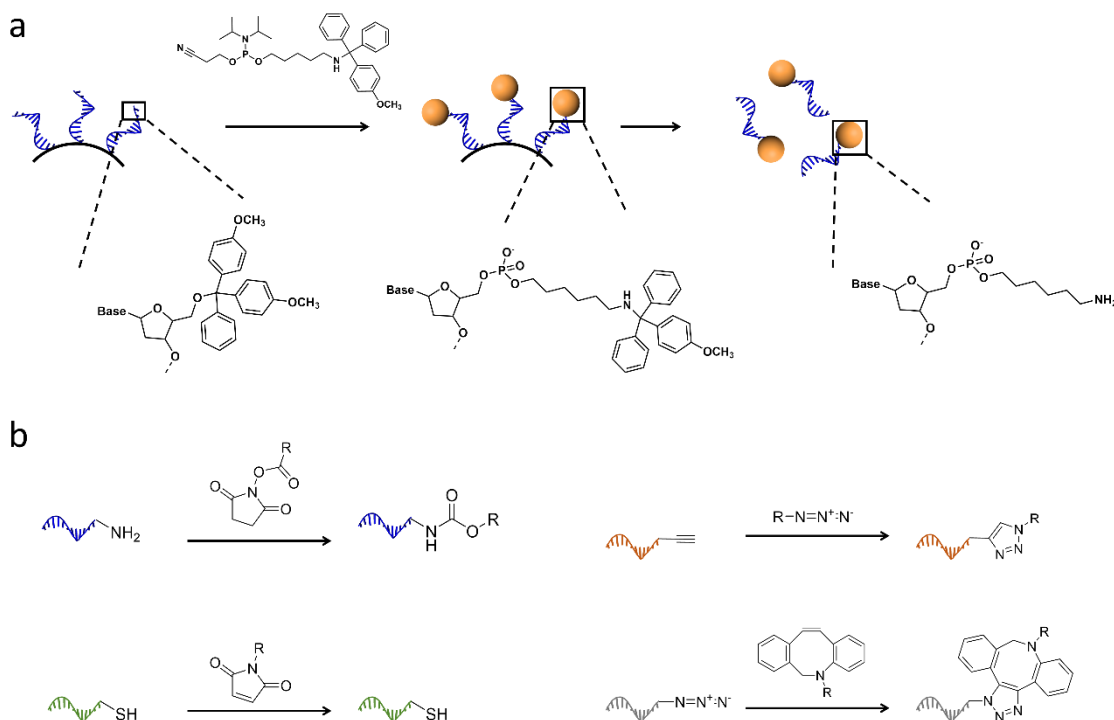


Figure 10. Modification of DNA. (a) The example of direct incorporation of an amine group to 5' of DNA. Amine containing phosphoramidite is protected with monomethoxytrityl (MMT) group. MMT group is used to separate the final product (amine DNA) from byproducts which don't have MMT groups by RP-HPLC. MMT group is able to be deprotected by acid treatment. (b) Examples of post modification of modified DNA. Amine / NHS ester, thiol / maleimide, alkyne / azide (copper-catalyzed click chemistry), and azide / dibenzocyclooctyl (copper-free click chemistry).

On the other hand, if the functional molecules can be directly incorporated into the DNA, it is expected that time and effort for the purification steps and relevant loss of materials can be minimized. Therefore, the successful synthesis of modified phosphoramidites made it possible to directly incorporate functional molecules to DNA. K. Matyjaszewski has demonstrated the straightforward method to synthesize atom transfer radical polymerization (ATRP) initiator modified phosphoramidite that is compatible with automated DNA synthesis (Figure 11)⁵⁶. ATRP-initiator phosphoramidite was synthesized by a two-step synthesis and used for automated DNA synthesis. It should be noted that there was a modification in synthesis condition to use A, T, C, and G phosphoramidites with ultra-mild protecting groups, a milder capping reagent, and shortened ammonium hydroxide treatment time (4h) to prevent the decomposition of initiator moiety during the synthesis. The obtained ATRP Initiator modified DNA was able to achieve polymer / DNA hybrid with controlled molecular weights and narrow dispersity through activators

generated by electron transfer (AGET) ATRP⁵⁶ or photochemically mediated ATRP (photo ATRP)⁵⁷.

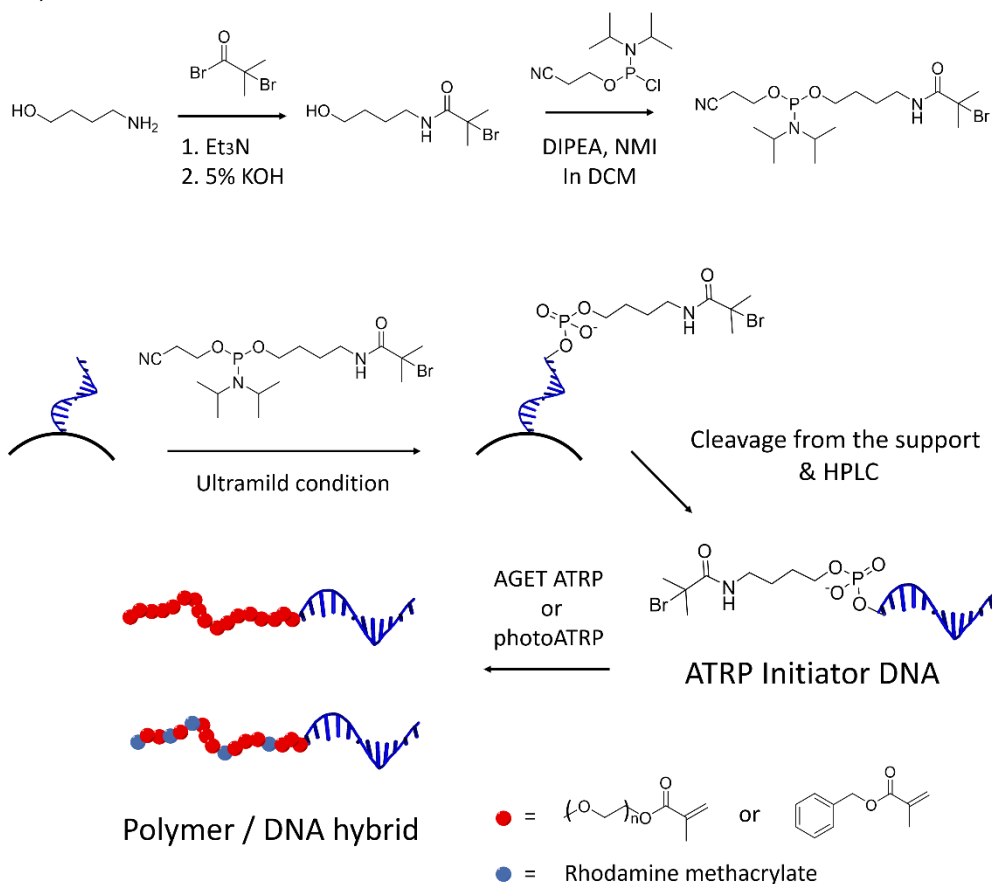


Figure 11. The synthesis and the direct incorporation of ATRP initiator to a DNA strand via automated DNA synthesis. The obtained ATRP-initiator was able to be used for AGET ATRP and photoATRP to create polymer / DNA hybrids.

1-10. Programming DNA assembly

The high programmability of DNA has been used by researchers in nanotechnology fields as a building block to construct atomically defined nanostructures with designed shapes and sizes⁵⁸. Nature also employs a distinct DNA architecture to control biological functions, i. e. Holliday junction (Figure 12 left). The basic concept of DNA nanotechnology is also to employ multiple DNA strands which recognize the correct partner and bind together with multiple DNA strands to control its self-assembly in a controlled fashion. The early idea was proposed in the early 1980s by Nadrian C. Seeman, the pioneer of DNA nanotechnology to design a DNA nanocube⁵⁹ and other DNA nanostructure aiming for these periodic structure to serve as a “molecular pegboard” to organize functional units as nanoarrays, e.g. aligning proteins onto DNA-nanogrid for structural biology.



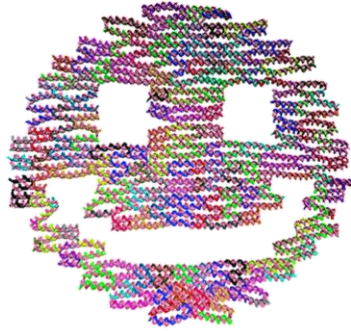
	Holliday junction	DNA Cube	DNA origami
			
Number of DNA strands	4	8	>200
Size	< 5 nm	5 - 10 nm	10 - 100 nm

Figure 12. The basic concept of DNA nanotechnology. The larger the number of DNA strands for designing their self-assembly the larger the size of the object with high precision. Holliday junction image was created from PDB: 3CRX60 by PyMOL (The PyMOL Molecular Graphics System, Version 2.0 Schrödinger, LLC). The DNA cube was adapted with permission from “Seeman, N. C. DNA in a material world. *Nature* 421, 427-431, doi:10.1038/nature01406 (2003).” Copyright (2003) Nature Publishing Group. DNA origami was adapted with permission from "Jonathan, P. K. D. et al. *Phys. Chem. Phys.* 15, 20395-20414, doi:10.1039/c3cp53545b (2013).” Copyright (2017) Royal Society of Chemistry.

A critical advance in DNA nanotechnology was demonstrated in 2006 by Paul Rothemund⁶⁰, which was denoted as the scaffold “DNA origami” method. Despite the idea of early DNA nanotechnology to use multiple short DNA strands for design principle, he introduced a long-single stranded DNA (scaffold DNA) of more than 7000 nt derived from a bacterial phage, which was folded into designed distinct shapes by aiding more than a few hundred synthesized short single-stranded DNA (staple DNA) (Figure 13). This design principle offers mainly a chance to design relatively bigger objects (~100 nm) with nanoscale precision without misfolding compared to previous trials using only multiple short DNA strands, which results in about 10 nm at maximum. Also, the recent progress of the computer-aided DNA origami design allows scientists to design one-, two, and three-dimensional DNA origami structure in literally any shape (Figure 13b and 13c), in addition, combining several 2D / 3D DNA origami objects together give a chance to create larger objects of more than 100 nm in size (Figure 13d and 13e)⁶¹⁻⁶⁶.

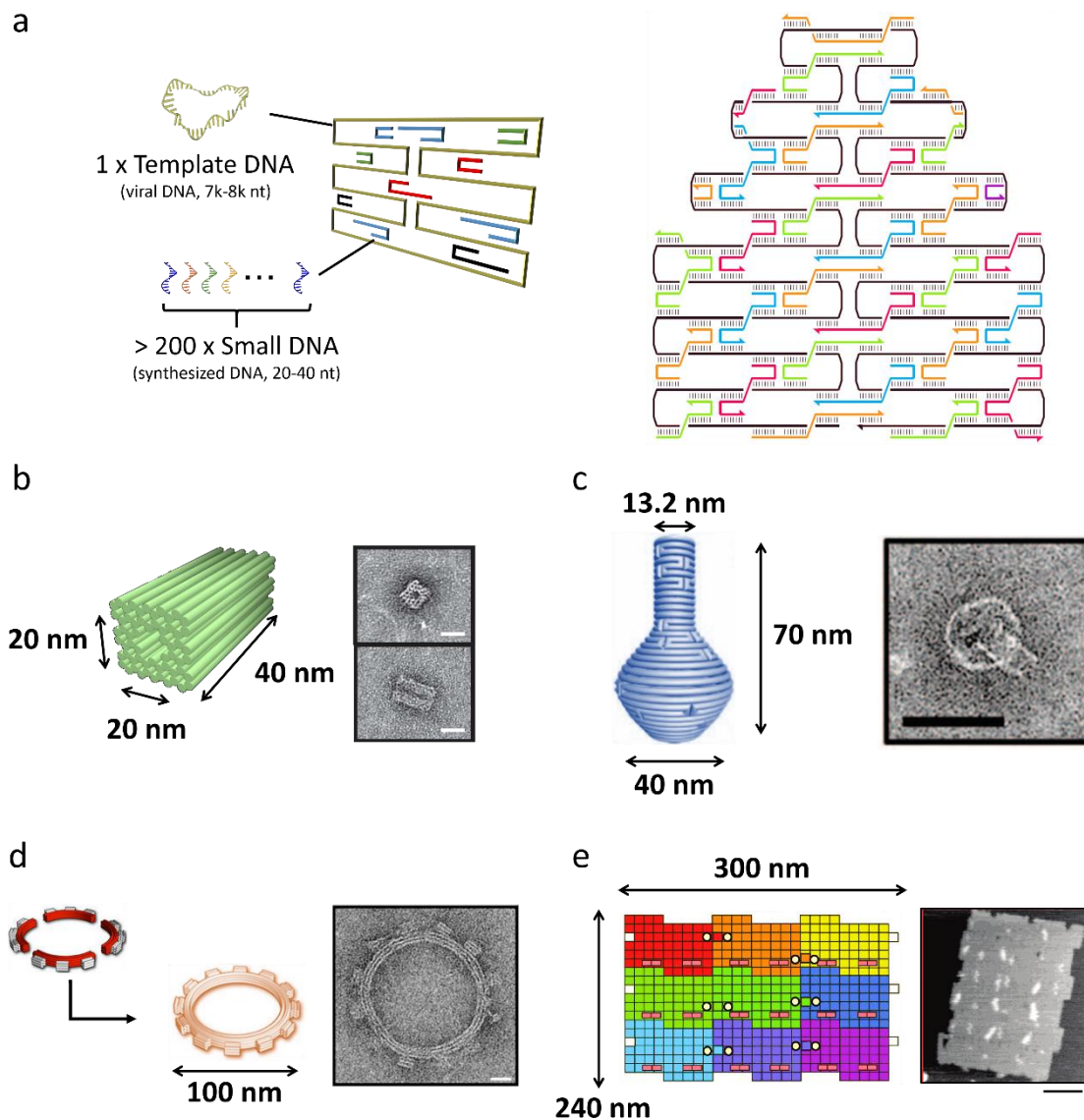


Figure 13. Design of DNA origami. (a) Schematic illustration of DNA origami design (left) and the example (right)⁶⁰. (b) 3D DNA origami cylinder with square knit⁶². (c) 3D DNA origami with curvature (vase)⁶³. (d) DNA origami gear from 4 components⁶¹. (e) DNA origami 2D assembly⁶⁴. Scale bar: 20 nm (a, d), 50 nm (c), and 100 nm (e). DNA origami in (a) was adapted with permission from “Rothemund, P. W. Folding DNA to create nanoscale shapes and patterns. *Nature* 440, 297-302, doi:10.1038/nature04586 (2006)” Copyright (2006) Nature Publishing Group. DNA cylinder was adapted with permission from “Shih, W. M. et al. Self-assembly of DNA into Nanoscale Three-Dimensional Shapes. *J. Biomol Struct. Dyn.* 26, 799-799 (2009)” Copyright (2009) Nature Publishing Group. DNA base was adapted with permission from “Han, D. R. et al. DNA Origami with Complex Curvatures in Three-Dimensional Space. *Science* 332, 342-346, doi:10.1126/science.1202998 (2011)” Copyright (2011) The American Association for the Advancement of Science. DNA gear was adapted with permission from “Dietz, H. et al. Folding DNA into Twisted and Curved Nanoscale Shapes. *Science* 325, 725-730, 24

doi:10.1126/science.1174251 (2009).” Copyright (2009) The American Association for the Advancement of Science. 2D-assembled DNA origami was adapted with permission from “Rajendran, A. et al. Programmed Two-Dimensional Self-Assembly of Multiple DNA Origami Jigsaw Pieces. ACS Nano 5, 665-671, doi:10.1021/nn1031627 (2011)” Copyright (2011) American Chemical Society.

1-11. Incorporation of functionalities into DNA origami

The unique advantage of scaffold DNA origami is that each of 200 staple DNA strands has its own position on DNA origami. This “known address” of staple DNA gives a chance to locate individual functionalities at desired positions at the nanoscale. As shown in Figure 14a, Rothemund’s 2D rectangular DNA origami of 70 nm x 100 nm x 2 nm dimension uses 216 staple DNA strands⁶⁰. According to the fundamental rule of DNA double helix, 1 turn of double helical structure is formed with 10.67 nt, which gives the basic idea that every 8th nucleotide is at 270 degree position (3/4 turn) and every 16th nt will show up on the other side of double helix (1.5 turn) (Figure 14b)⁶⁷. Since most of the staple DNA strands have 8 nt – 16 nt – 8 nt = 32 nt sequence to hybridize with three different parts of scaffold DNA to fix three DNA double helices neighboring with each other, both 5’ and 3’ are positioned on one surface of DNA origami structure (Figure 14c). Therefore, by modifying the 3’ and 5’ of staple DNA strands, the modified moieties will show up on the DNA origami surface (in other words, if the modification is not at appropriate site like somewhere between the staple DNA strands, the modified groups are buried between double helix and not accessible from the surface, or it will inhibit the formation of DNA origami in the worst case). In addition, it is also possible to separate one staple DNA strand to two at the middle, which is exposed on the other surface of DNA origami, and introduce the functional groups onto the other side of DNA origami.

Figure 15 summarizes in whole the available modification sites on the rectangular DNA origami. There are 216 positions that are available for modification on one side of the DNA origami surface and the same numbers existing on the other surface. Each modification site is located with a distance of 5.8 - 6 nm from the next. In the next paragraph, the various modification techniques will be described in detail.

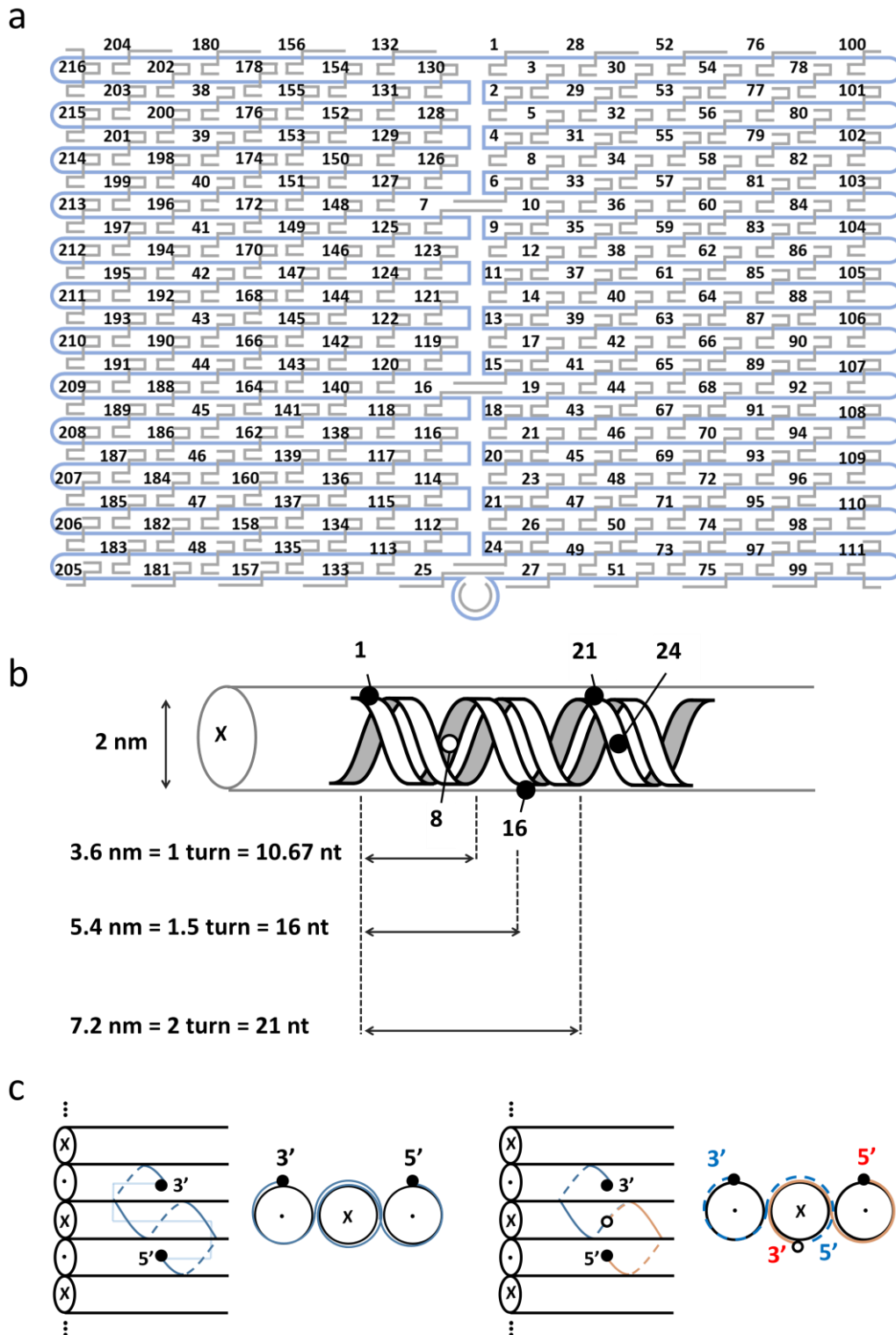


Figure 14. Principle of DNA origami. (a) Schematic illustration of Rothemund's rectangular DNA origami (70 nm x 100 nm, thickness: 2 nm) (b) Schematic view of DNA double helix and the fundamental rule of helicity. (c) Basic design concept of staple DNA strands.

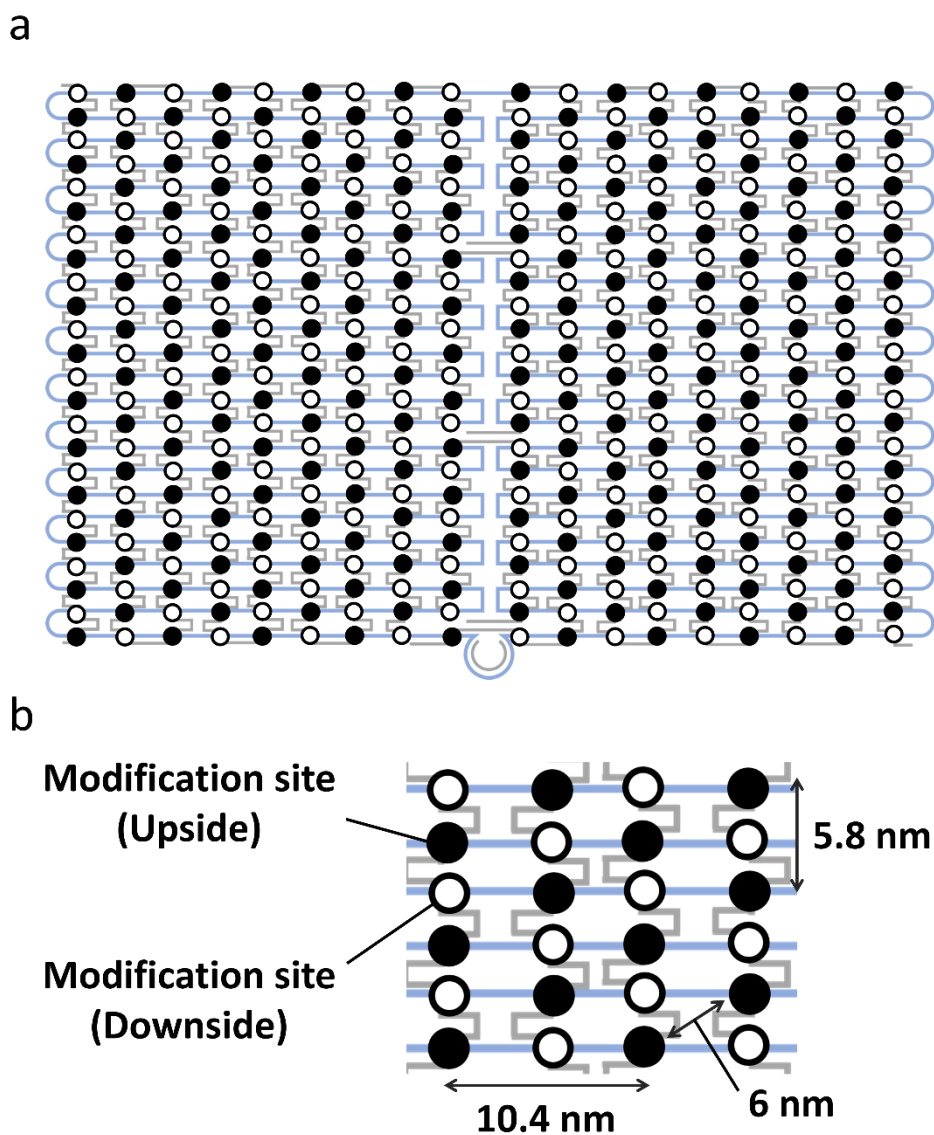


Figure 15. The modification sites of rectangular DNA origami. (a) The possible modification sites on both surface of the DNA origami are shown. The black circles and white circles represents the positions on one surface respectively. (b) The close view of neighboring modification sites and the distances between.

1-12. The modification of staple DNA strand

For the modification of staple DNA strands, a wide variety of DNA chemistry techniques are available (Figure 16); 1) small functional groups including amine, thiol, alkyne, azide, maleimide and fluorophores so on are able to be modified to DNA by automated solid-support DNA synthesis and further modifications are also options like amine / NHS ester, thiol / maleimide, and click chemistry to load additional functional groups (biotin, fluorophore, lipids and so on). 2) Extension by ssDNA which serves as a DNA handle so that other nanomaterials with the complementary DNA sequences can be captured by DNA hybridization. 3) Extension by DNA aptamer that is a specific DNA sequence and can capture its target molecule like thrombin⁶⁸ and trypsin⁶⁹. 4) Extension by Deoxyribozyme (DNAzyme), which are oligonucleotides capable of performing specific catalytic reactions. For example, G-rich DNA sequence forms a secondary structure, called G-quadruplex (G4, Figure 17)⁷⁰. G4 is the stacked layers of a guanine tetrad which are composed of four guanine bases associated together by Hoogsteen hydrogen bonding and stabilized by cations like K^+ and Na^+ sitting in the middle of the layer. It was found that G4 could associate with hemin (chloro(protoporphyrinato)iron(III)) to form G4/hemin DNAzyme, which manifests the catalytic activity of hydrogen peroxide-mediated oxidation reaction mimicking hydrogen peroxidase⁷¹.

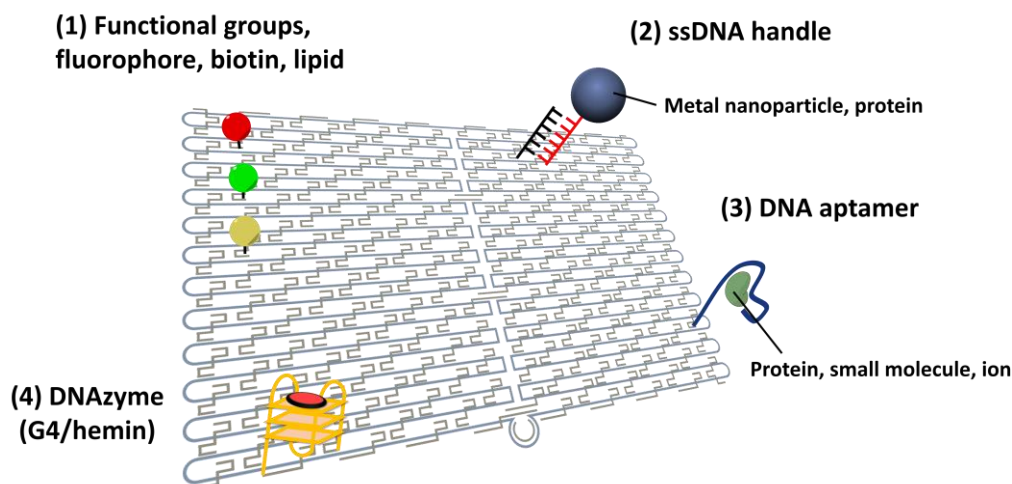


Figure 16. Functionalization of DNA origami by introducing modified staple DNA.

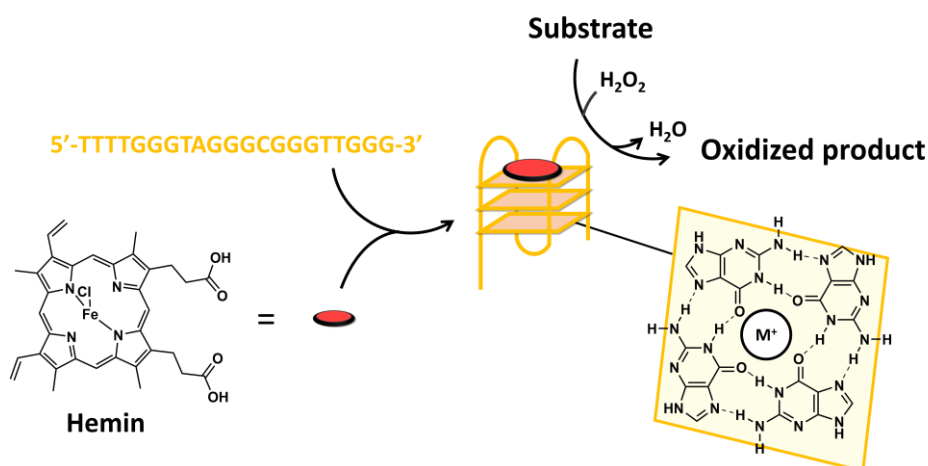


Figure 17. G4/hemin based DNA enzyme. G-rich DNA sequence (orange) forms G-quadruplex structure in the presence of metal ions like Na^+ or K^+ as stabilizer. Hemin binding onto the G-quadruplex activates its catalytic property of hydrogen peroxide-mediated oxidization reaction.

1-13. DNA origami as template for assembling nanomaterials

Due to the atomic addressability of each staple DNA strand in a designed DNA origami structure and its mesoscale size which cannot be usually accessed by other materials like protein, metal particles, DNA origami has been employed as powerful scaffolds to align, organize, assemble other nanomaterials. Figure 18 shows the immobilization of proteins, metal nanoparticles, and fluorophores onto specific positions on DNA origami. As a linker between DNA origami and the nanomaterial of interest, different options has been demonstrated; DNA hybridization^{72,73}, direct replacement of staple DNA strands⁷⁴, affinity tag (biotin⁷⁵⁻⁷⁷, aptamer^{78,79}) and supramolecular interactions⁸⁰. The well-organized nanomaterials on DNA origami is beneficial to investigate the crosstalk between neighboring particles and distance-dependent activities of cascade reactions or yield of energy transfers, which span the applications of DNA origami over a number of different fields from fundamental study for nanoelectronics, nanoplasmonics, nanooptics, and biophysics to applied sciences like nanomedicines, nanorobotics, nanochips and so on.

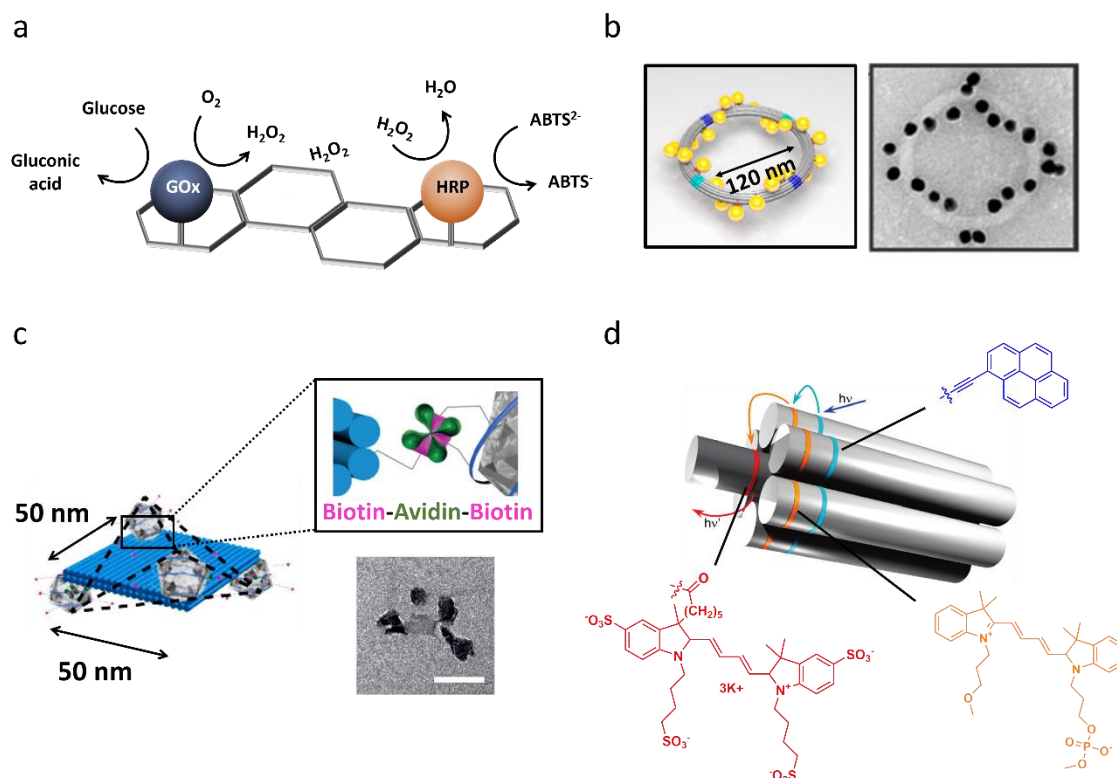


Figure 18. DNA origami templated nanomaterial assembly. (a) Enzyme cascade system with a controlled distance on DNA origami⁷². (b) plasmonic chiral platforms on gold nanoparticles immobilized on DNA origami⁷³. (c) Fluorescent nanodiamond assembly on DNA origami via biotin / avidin interaction⁷⁷. Scale bar: 100 nm (d) DNA origami directed artificial light harvesting antenna⁷⁴. (a) was adapted with permission from “Wilner, O. I. et al. Enzyme cascades activated on topologically programmed DNA scaffolds. *Nat. Nanotechnol.* 4, 249-254, doi:10.1038/Nnano.2009.50 (2009)” Copyright (2009) Nature Publishing Group. (b) was adapted with permission from “Urban, M. J. et al. Plasmonic Toroidal Metamolecules Assembled by DNA Origami. *J. Am. Chem. Soc.* 138, 5495-5498, doi:10.1021/jacs.6b00958 (2016).” Copyright (2016) American Chemical Society. (c) was adapted with permission from “Zhang, T. et al. DNA-Based Self-Assembly of Fluorescent Nanodiamonds. *J. Am. Chem. Soc.* 137, 9776-9779, doi:10.1021/jacs.5b04857 (2015)” Copyright (2015) N American Chemical Society. (d) was adapted with permission from “Dutta, P. K. et al. DNA-Directed Artificial Light-Harvesting Antenna. *J. Am. Chem. Soc.* 133, 11985-11993, doi:10.1021/Ja1115138 (2011).” Copyright (2011) American Chemical Society.

1-14. DNA origami-templated synthesis of nanomaterials

As described in the last paragraph, DNA origami was employed as powerful scaffolds to organize other nanomaterials. As a next step, it is quite interesting if one can use DNA origami as a template for not aligning but also synthesizing nanomaterials in a defined fashion. In nanomaterials, their size, shape, composition of elements, number and positions of introduced functionalities play an essential role to decide their properties. For example, it was demonstrated that different sizes of gold nanoparticles showed different cell entry behaviors, or shape parameters such as aspect ratio and curvature also influence how the material interacts with the cellular surface⁸¹. On the other hand, the shape-controlled synthesis of inorganic nanostructures is also important for nanocomputing and nanoplasmonics since the size and shape of the metal nanoparticles give influences to the optical and catalytic properties⁸². To address these issues, the template-based bottom-up synthesis has been investigated by using programmable scaffolds which can serve as a mold or template to fabricate functional nanomaterials which possess the structural information transferred from the scaffolds. For example, the interior cavity of virus capsid particles has been utilized to synthesize polymers or metal nanoparticles in defined sizes⁸³. For this purpose, DNA origami is no exception and has been employed as a promising candidate. The control of chemical reactions in single molecular level on DNA origami was also demonstrated by Kurt Vesterager Gothelf in 2010 (Figure 19a)⁸⁴. These achievements in positioning the appropriate functions at desired positions on DNA origami raised the chance of DNA origami to synthesize functional materials in a bottom-up fashion with the same programmability as DNA origami. In 2014, Ralf Seidel and Peng Yin synthesized a variety of gold and silver nanoparticles with different shapes by metal seed-incorporated 3D DNA origami structures as a nanomold (Figure 19b)^{85,86}. In these works, the position of metal growing is located at interior space of DNA origami and the shape was determined by the shape of molds. The demonstrated method here in principle allows synthesis of gold or silver nanoparticles in any arbitrary shape and dimension, which is demanded in the fields such as nanocomputing, nanooptics, and nanoelectronics. Not only inorganic materials, but also soft materials have been approached in the last few years. DNA origami structures decorated with lipid molecules at specific positions can serve as scaffold to construct enzyme-contained lipid nanomembrane or exoskeleton to fabricate liposomes with complicated shapes to mimic spiral bacteria and golgi complexes (Figure 19c)^{87,88}.

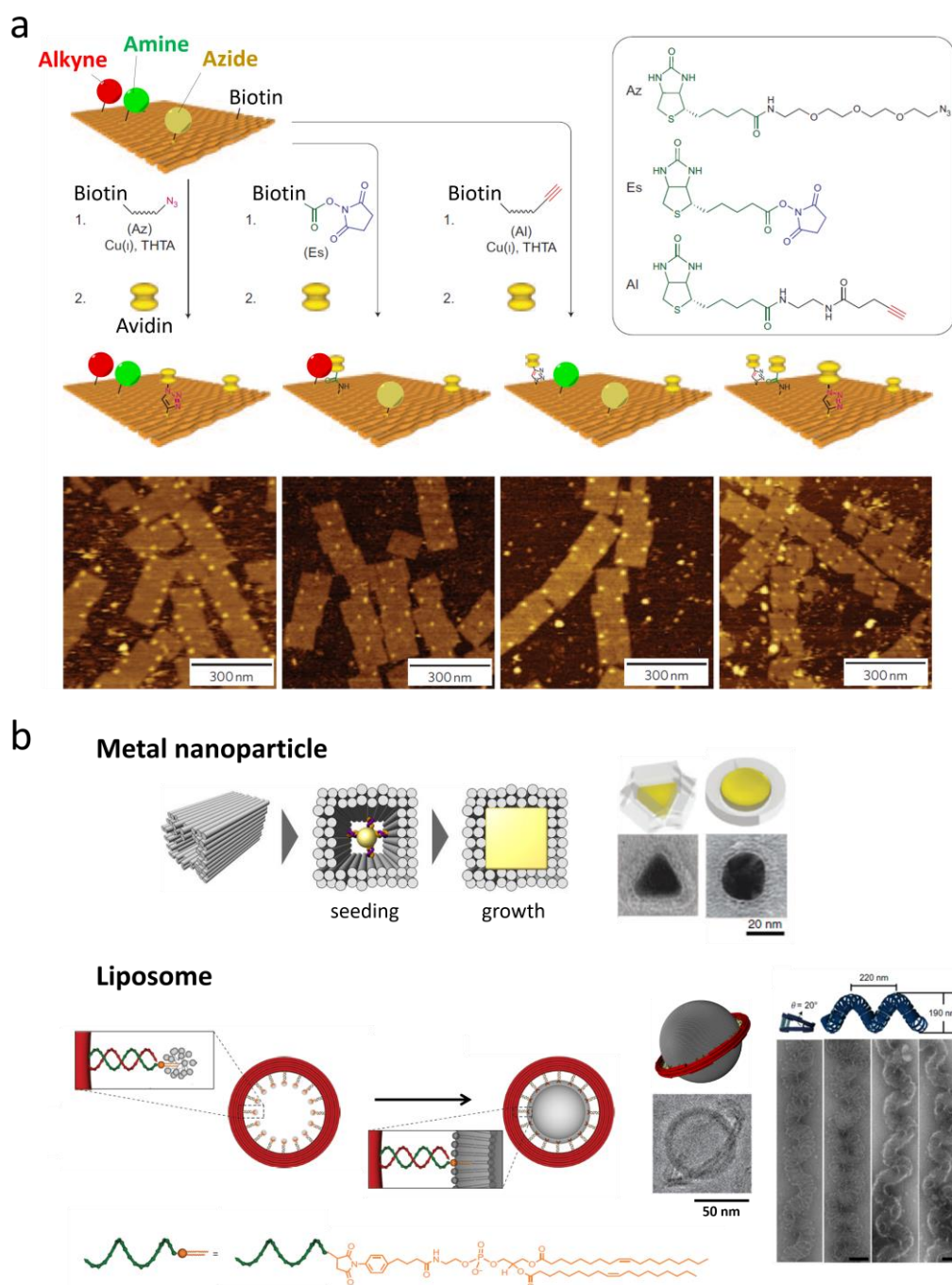


Figure 19. DNA origami-templated synthesis of nanomaterials. (a) Control over the single-molecular chemical reactions on DNA origami. Biotin was incorporated to three different functional groups (alkyne, amine, and azide) on DNA origami by the corresponding chemical reactions⁸⁴. The subsequent immobilization of avidin clearly demonstrated the correct chemical reaction occurred at the designed positions. (b) (Upper) DNA origami-templated synthesis of gold nanoparticles was conducted by a two-step procedure; firstly seeding of small gold nanoparticle in the 3D DNA origami template by DNA hybridization, and then supplying gold salt and reducing reagent for growing the gold nanostructure^{85,86}. On bottom, the inner surface of 3D DNA origami was

decorated by lipid molecules which serve as an anchor group to grow liposomes with a defined diameter when the lipid was supplied to the system. The high freedom of DNA origami design made it possible to create complex lipophilic materials^{87,88}. (a) was adapted with permission from “Voigt, N. V. et al. Single-molecule chemical reactions on DNA origami. *Nat. Nanotechnol.* 5, 200-203, doi:10.1038/Nnano.2010.5 (2010).” Copyright (2010) Nature Publishing Group. (b, upper) was adapted with permission from “Helmi, S. et al. Shape-Controlled Synthesis of Gold Nanostructures Using DNA Origami Molds. *Nano Lett.* 14, 6693-6698, doi:10.1021/nl503441v (2014)” Copyright (2014) American Chemical Society and “Sun, W. et al. Casting inorganic structures with DNA molds. *Science* 346, 717, doi:Artn 125836110.1126/Science.1258361 (2014)” Copyright (2014) The American Association for the Advancement of Science. (b, bottom) was adapted with permission from “Yang, Y. et al. Self-assembly of size-controlled liposomes on DNA nanotemplates. *Nat. Chem.* 8, 476-483, doi:10.1038/Nchem.2472 (2016)” Copyright (2016) Nature Publishing Group and “Zhang, Z. et al. Placing and shaping liposomes with reconfigurable DNA nanocages. *Nat. Chem.* 9, 653-659, doi:10.1038/Nchem.2802 (2017).” Copyright (2017) Nature Publishing Group.

In addition to transferring structural information, the nanoscale addressability of DNA origami is able to be exploited for transferring functionalities, which was demonstrated as “DNA origami-based nanoimprinting lithography” by Chunhai Fan’s group (Figure 20)⁸⁹. In their work, the surface of DNA origami was decorated by multiple ss DNA which worked both as handles to capture gold nanoparticle decorated with complementary ssDNA strands and as transferable units by the toehold-mediated strand displacement reaction. After the gold nanoparticle was released into the solution by adding detachment strands, patterning of oligonucleotides on DNA origami was transferred onto the surface of gold nanoparticles which was further used to attach differently sized gold nanoparticles to create unique gold nanoclusters which were extremely difficult to obtain by other methods.

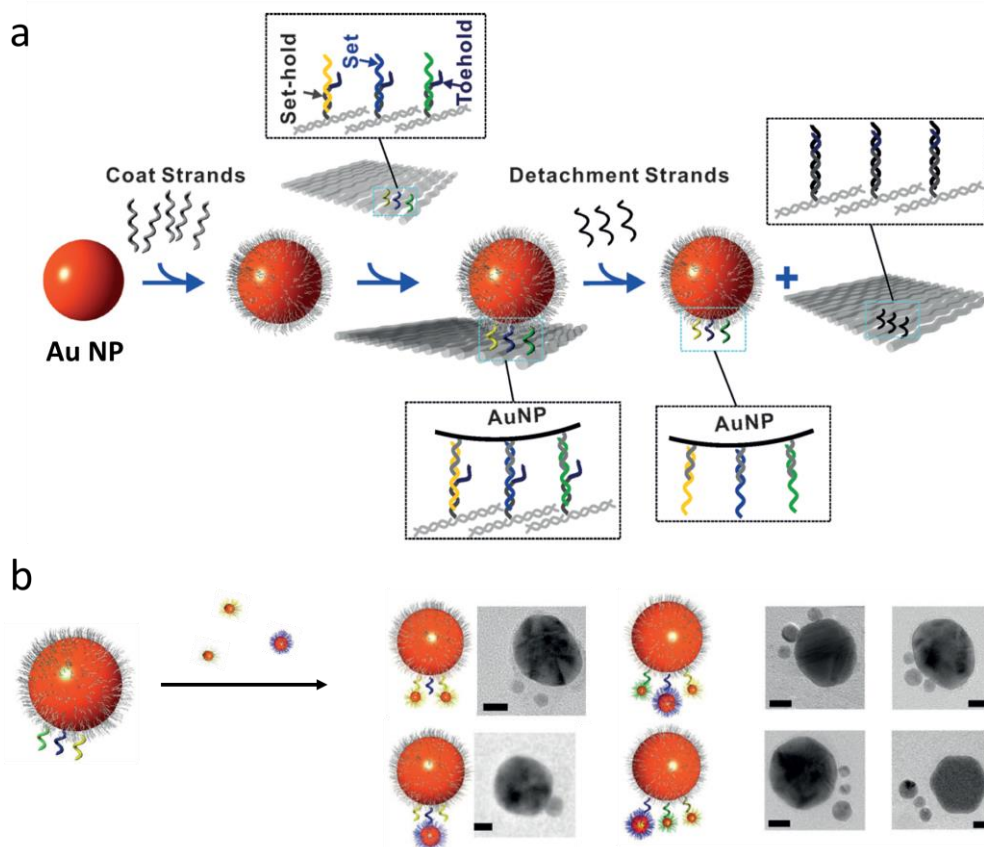


Figure 20. DNA origami-based nanoimprinting lithography⁸⁹. (a) The Au NP (30 nm diameter) modified with “Coat strands” were immobilized on DNA origami decorated with “Set-hold strands” by DNA hybridization between coat strands and set strands. Set strands were transferred to Au NP by replacement with “Detachment strands” which have completely complementary sequences to hold strands. (b) Au NP possessing multiple ssDNA sequences at specific positions can capture 10 nm Au NP and 5 nm Au NP modified with corresponding complementary sequences to set strands. Scale bar: 10 nm. Adapted with permission from “Zhang, Y. N. et al. Transfer of Two-Dimensional Oligonucleotide Patterns onto Stereocontrolled Plasmonic Nanostructures through DNA-Origami-Based Nanoimprinting Lithography. *Angew. Chem. Int. Ed.* 55, 8036-8040, doi:10.1002/anie.201512022 (2016).” Copyright (2016) John Wiley and Sons.

1-15. The stability of DNA origami

Although it has been demonstrated that DNA origami can serve as a powerful template in nanoscale, there are also some drawbacks which can hinder the development of DNA origami. For example, the stability of DNA origami is a critical issue since DNA is a soft and labile material. Usually, the melting temperature depends on the length and composition of base pairs (C-G base pairing is generally stronger than A-T base pairing) and typical DNA origami structures has shown its melting temperature between 50 and 65 degree⁹⁰. Once the DNA origami was thrown into an environment above this temperature range, scaffold DNA and a set of staple DNA strands start to dissociate and they can't hybridize completely to reform the original structure without supplying excess of staple DNA strands. Sugiyama's group found that photo-crosslinking of DNA origami by 8-methoxypsoralen could increase the heat resistance of DNA origami up to 30 degree in solution (Figure 21a)⁹¹.

For biomedical applications, high salt concentrations and nucleases are the main challenges. Most DNA origami structures requires between 5-20 mM divalent cations (Mg^{2+} and Ca^{2+}) to overcome the electrostatic repulsion forces between the negatively charged phosphodiester backbones. In biological environment, the concentration of both ions are ~2 mM in blood and less than 1 mM in cytosol (Mg^{2+} : ~0.8 mM, Ca^{2+} : < 0.0002 mM), under these conditions DNA origami cannot maintain structural integrity. Secondly, nuclease proteins, an enzyme capable of cleaving DNA phosphodiester bonds between nucleotides, can also rapidly degrade DNA origami⁹². The main function of nucleases in biological systems is DNA repair and they are contained in fetal bovine serum (FBS) which is a blood product often added to cell culture media. Usually the cell culture medium is supplemented with 10-20% of FBS that possess approximately 200-1000 u/L equivalent of nuclease activity which is enough to decompose the DNA origami in 12 h⁹². There are several approaches to address the instability of DNA origami to nuclease digestion by encapsulating DNA origami in a lipid bilayer (Figure 21b)⁹³, block copolymers (Figure 21c)⁹⁴, or oligolysine-based polymers⁹⁵. Also, it has been demonstrated that coating the DNA origami structures with virus capsid proteins⁹⁶ and cationic polymers⁹⁷ could enhance their entry into cells compared to the native DNA origami. However, using electrostatic interaction between negative DNA origami surface and positive polymers or proteins can induce aggregation behavior of encapsulated DNA origami structures and more importantly, the highly programmable property of DNA origami with functional materials can be lost because these coating methods don't have spatial addressability but simply coat the whole DNA origami surface.

1-16. DNA origami and polymer synthesis

In the previous section, polymers that electrostatically interacted with the DNA origami surface were described as a promising protection tool for overcoming the stability issues of DNA origami. Turberfield's group has incorporated a temperature responsive property to a DNA tetrahedron structure by conjugating pNIPAM to the corner of the tetrahedron⁹⁸. These previous works clearly indicate the emerging interests in DNA origami / polymer hybrid materials. Aside from utilizing the synthetic polymers to alter or control the functionalities of DNA origami, the high programmability of DNA origami should also be employed to design polymeric structures with high precision. Gothelf's group has shown the routing of single conductive polymers in desired patterns on 2D/3D DNA origami⁹⁹. They modified conductive (2,5-dialkoxy)paraphenylene vinylene (APPV) polymers with ssDNA strands to immobilize onto designed paths on DNA origami. In addition, the conformation of the directed polymer can be dynamically switched by toe-hold displacement technique¹⁰⁰. Since APPV polymers have π -conjugated systems, the system can be potentially applied to the advanced nanoelectronics and nanooptic devices.

2. Motivation

Intensive developments of polymer chemistry open access to the synthesis of defined polymer chains with desired chemical compositions, lengths and functions, which further allow the design of a large variety of polymer assemblies in micro/nanoscale, represented by micelle, polymersome, and polymer brush. In material science, these micro/nano-structured polymers are promising candidates for applications such as drug delivery systems, sensors, and surface coatings. In this respect, rational design methods to fabricate polymer architectures with high precision and the freedom of size, geometry and functions are strongly demanded. On the other hand, nature can sophisticatedly synthesize a wide variety of biopolymers like DNA, peptide, proteins and their complexes with unique geometries and corresponding functions. Therefore, there are rapidly increasing interests in mimicking/utilizing biomacromolecules or their assembled state as defined templates for programming polymer architectures in nanoscale. These interdisciplinary backgrounds strongly inspired us to exploit the novel approach for designing polymeric nanomaterials by utilizing DNA nanotechnology. The high programmability of DNA nanostructures represented by DNA origami would possess a promising potential to work as the ideal nano-factory for creating desired polymer nanoarchitectures by providing the adequate reaction space and environments. The facile and versatile design of shape and size in polymer materials with nanoscale precision would promote the development of polymer nanotechnology towards various nanodevices like nanooptics, nanosensor, nanoelectronics, nanofluidics and so on. Additionally, the wide variety of functionalized DNA origami could allow the combination of synthesized polymer nanostructures with other functional materials such as metallic nanoparticles, proteins, fluorophores and so on to fabricate novel hybrid materials with synergetic effects and smart functions.

In the presented thesis, the first system investigated is the bottom-up synthesis of nanopatterned polymers on a two dimensional DNA origami template via surface-initiated atom transfer radical polymerization (SI-ATRP). In this system, ATRP initiator-modified single-stranded DNA was synthesized and hybridized with multiple complementary DNA handles arranged on tile-shaped DNA origami. By introducing sacrificial initiators and reducing reagent, in-situ polymerization on DNA origami was achieved in a controlled manner. The DNA origami template provided the facile method to create desired polymer nanopatterns in nanoscale resolution by allowing control over the positioning of a single initiator moiety. Besides, by crosslinking the synthesized polymer nanopatterns, the geometry of crosslinked polymers programmed on DNA origami were retained after removal of the DNA origami template.

The integration of highly defined DNA nanostructure and chemical / physical properties

of synthetic polymers is quite interesting to investigate novel smart nanomaterials. Herein, the established method in the first system was applied further to the three-dimensional DNA origami structure to create a defined core-shell DNA / polymer hybrid material, which are described in the second part. 2D DNA origami tile-shape was transformed into 3D DNA origami tube-shape structure by applying a set of additional DNA strands that can adhere the side edges of DNA origami tile together. The outer surface of DNA origami tube was fully decorated with initiator moieties that confers crosslinked polymer shells after SI-ATRP, which could potentially protect the inner DNA tube from digestion by DNA-degrading enzyme. Additionally, the inner space of the DNA tube was available for further functionalization, which taken together, yielded dual-functionalized DNA / polymer hybrid nanomaterials applicable for drug delivery systems and chemical nanoreactors.

In addition to synthetic polymers, (bio)synthetic polymers are promising materials due to their biocompatibility and unique intrinsic functions. On the other hand, the different polymerization mechanisms from synthetic polymers hinder control over the polymerization process. We utilized DNA origami that possessed nanosized catalytic domains on its surface to fabricate the defined biosynthetic polymer, polydopamine. Polydopamine is a mussel-inspired biopolymer known for its high adhesive property and a wide variety of functional groups for available for post-modification, which makes it a promising surface coating material. Locally concentrated catalysts on DNA origami could create an environment which could facilitate the polymerization of dopamine only close to the catalytic domain. Therefore, the geometry of synthesized polydopamine could be programmed by the shape of the catalytic domain and the size was controlled by changing the substrate concentration. The intrinsic adhesive property of polydopamine on DNA origami could serve as molecular glue to dynamically alter the conformation of DNA origami.

Also, understanding of how well-designed self-assembled polymeric nanomaterials can function for practical applications is quite interesting. In collaboration with Dr. David Y. W. Ng, the investigation of the supramolecular self-assembly behavior of oligothiophene analogues transported into biological systems by complexation with protein was conducted. The study revealed the strong potential of a supramolecular assembly as novel platforms for biomedical sciences by proper synthetic design and control over their self-assembling characteristics.

3. Investigated systems

[3-1] Fabrication of defined nanopatterned polymers by surface-initiated atom transfer radical polymerization on DNA origami

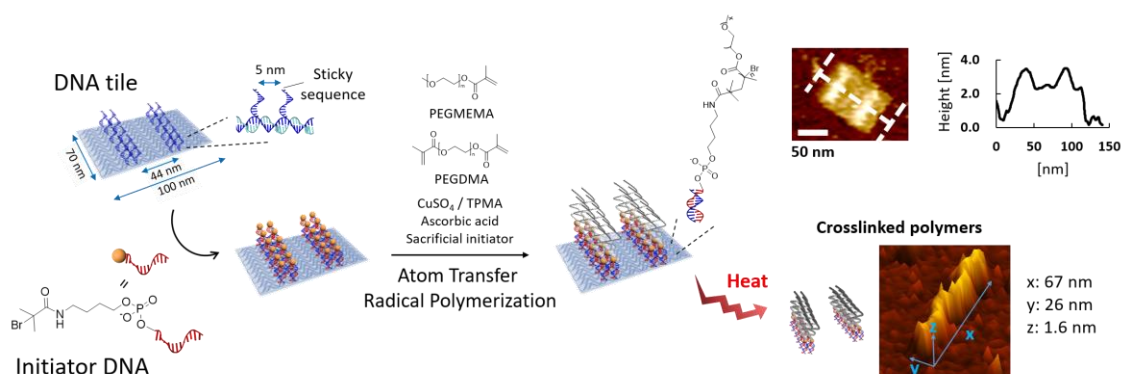


Figure 22. Surface-initiated atom transfer radical polymerization on DNA origami templates. Adapted with permission from “Yu, T. et al. Bottom-Up Fabrication of Nanopatterned Polymers on DNA Origami by In Situ Atom-Transfer Radical Polymerization. *Angew. Chem. Int. Ed.* 2016, 55, 5692-5697, doi: 10.1002/anie.201511761.” Copyright (2016) John Wiley and Sons.

As discussed in the introduction, fabricating polymer nanoarchitectures with high precision are highly attractive for numerous modern technologies. Especially, the nanopatterning of densely grafted polymers is vitally important for applications such as biochips for cell-function control, nanofluidics systems, and photonic crystal materials¹⁰¹⁻¹⁰³. Currently available techniques often rely on top-down strategies such as lithography, which has several limitations including high instrumental costs, long operation times, and low productivities. On the other hand, bottom-up strategies in principle can solve these limitations by manufacturing the precise nanopatterned polymers with low-nanometer resolution in high yields and productivity. So far, substantial efforts have been made to control polymer self-assembly by designing sophisticated monomers / polymers, although the prediction and the flexible design of e.g. geometries and sizes are still challenging.

For this purpose, exploitation of nature-derived smart and sophisticated systems for material sciences has gained tremendous interest in recent years. Biomacromolecules or their assemblies with defined geometries, sizes and a wide variety of functional groups are powerful tools for fabricating unique functional nanomaterials in a bottom-up

fashion^{40,41,50}. Compared to peptide and protein-based systems, which also provide fixed geometries and sizes, DNA is a highly tunable material and ideally suited to create distinct nanostructures, represented by DNA origami⁶⁰. Although a wide variety of materials (metallic / carbon nanoparticles^{104,105}, proteins^{106,107}, and fluorophores^{74,108}) were ordered on DNA origami scaffolds for the fundamental studies on the crosstalk between two materials positioned close proximity, chemical reactors for efficient cascade reactions, nanoantenna with high efficacy and so on, to the best of my knowledge, there has only been one study that reported the bottom-up fabrication of synthetic polymers using DNA origami. B. Ding's group elaborated the shape-controlled synthesis of polyaniline on planar DNA origami¹⁰⁹ scaffolds. Inspired by these results, a novel method for directly grafting polymer nanopatterns from the surface of a DNA origami scaffold was established, which should yield much denser polymers compared to the "grafting to" approach, in which polymers are directly conjugated to the surface, resulting sometimes in lower densities because of steric hindrance.

An appropriate selection of the most suitable polymer chemistry, which should be compatible with the DNA origami technique, is hereby crucial since although DNA origami is a powerful template, it usually cannot survive in organic solvents or at high temperatures. Among the different polymerization techniques, atom-transfer radical polymerization (ATRP) was selected as a suitable method for polymerization on DNA. ATRP is the method of choice to obtain defined polymers with controlled molecular weights, narrow polydispersity, and chain-end functionalities. In addition, the reactions proceed in aqueous solution at ambient temperature, which is essential for the stability of the DNA origami structure, and they are applicable to a variety of monomers^{110,111}.

Two dimensional rectangular DNA origami (70 nm x 100 nm)⁶⁰ was prepared from M13mp18 DNA and the corresponding staple DNA strands. To immobilize ATRP initiators onto the DNA origami, an additional DNA sequence with 15 oligonucleotides (referred as "sticky sequence") was extended from the 3' end of staple DNA strands, so that the added DNA part was exposed onto the one surface of the DNA origami. By selecting different staples, two different DNA origami patterns were designed: one with two lines and one with four spots. It should be noted here that although these two patterns were selected as representative examples, even more complicated patterns were designed by following the same approach. In addition, ATRP-initiators modified with single-stranded DNA with a complementary sequence to the sticky sequence (DNA initiator) were synthesized¹¹². Briefly, the ATRP initiator modified phosphoramidite was prepared by a two-step synthesis, and coupled to the 5' end of the DNA via automated solid-support DNA synthesis, followed by HPLC purification and characterized by MALDI-TOF MS. The successfully synthesized DNA initiators were immobilized by the sticky sequences on DNA origami via DNA hybridization to form the DNA origami macroinitiator.

To explore surface-initiated ATRP reactions on DNA origami macroinitiators, the polymerization of poly(ethylene glycol) methyl ether methacrylate (PEGMEMA) was selected owing to their biocompatibility¹¹³, water solubility, and more importantly, the expectation that the bulky side chain of PEG on the grafted polymers facilitates monitoring the polymer growth on the DNA origami surface by AFM. In the beginning, the polymerization condition was examined in the presence of free DNA initiators in solution. After careful optimization, it was found that the polymerization reaction only occurred when the initiator concentration was above 10 μM . However, such a high concentration of DNA origami macroinitiators could not be achieved in the reaction mixture due to the extremely high molecular weight of the DNA origami and the increasing solution viscosity¹¹⁴. To overcome this challenge, free sacrificial initiators were supplied to the reaction solution to increase the total initiator concentration and to ensure the generation of a persistent concentration of radicals to retain an ATRP equilibrium¹¹⁵. In general, the polymerization process was conducted in a closed double-structure small vial equipped with an inlet inside containing 50-60 μL reaction solution of the DNA origami initiator, monomer, catalyst (copper bromide, CuBr_2), and a stabilizing ligand (tris(2-pyridylmethyl) amine (TPMA)). All oxygen in the reaction mixture was removed by the freeze-pump-thaw method, and the polymerization was initiated by the continuous, slow addition of ascorbic acid for two hours to generate the reactive catalyst species¹¹⁶. After the reaction, the product was separated from the resulting free polymer chains grown from the sacrificial initiators and remaining catalyst by PEG-induced precipitation method¹¹⁴.

The obtained nanopatterned polymers on the DNA origami (DNA origami - polymer) were characterized by AFM, agarose gel electrophoresis, and time-of-flight secondary ion mass spectrometry (ToF-SIMS). In AFM, the appearance of the new objects at the designed initiator patterned areas was clearly visible. These new objects showed a height increase of about 0.5 nm from the DNA origami surface. Additionally, nanomechanical property mapping mode in AFM revealed that the formed objects provide different mechanical properties compared to the DNA origami structures (i.e., a lower Young's modulus and higher adhesion to silicon nitride cantilever), which also indicated a successful polymerization. During the AFM study of the DNA origami – polymer nanotiles with different nanopatterns (two lines and four spots), it was observed that when the DNA origami with two-line patterned polymers was deposited on mica, almost all the DNA origami revealed the polymer-grown at the surface, while in case of the one with four-spot pattern, there was no preferential surface deposition and both sides appeared equally often facing up or down. Based on this observation, I have speculated that grafted polymers could alter the surface properties of DNA origami in terms of charge, topology, and hydrophobicity, thus resulting in a favorable deposition of the more negatively charged plain DNA origami side onto the Mg^{2+} absorbed positively charged mica surface

over the polymer-grown side in two-line nanopatterns. For instance, the four-spot pattern covers a three times smaller surface area of the DNA origami, therefore the surface properties of the DNA origami were not altered significantly and no favorable deposition on mica surfaces was observed. From ToF-SIMS analysis, the secondary ion derived from the end group of the PEG chain ($C_2H_5O_2^-$) was detected in the purified DNA origami – polymer sample. Additionally, there was no nonspecific absorption of the polymers grown from sacrificial initiators to DNA origami.

The further insight into the control over the degree of the polymerization reaction on DNA origami was obtained by changing the molar ratio between the initiators and monomers. By increasing the monomer to initiator ratio, higher nanopatterned polymers were obtained. However, the heights of polymer brushes observed by AFM were still significantly shorter than the distances between adjacent initiator positions (5.8 nm), indicating that the polymers should adopt a mushroom-like collapsed structure.

Finally, we investigated if the architecture of the grafted polymeric nanostructures programmed by the DNA origami could be preserved in the absence of the template. This time, the crosslinker molecule, PEG dimethacrylate (PEGDMA) was added to the reaction mixture to obtain the crosslinked polymers on the DNA origami template. The crosslinked polymers were observed with similar shapes on the DNA origami compared to the respective polymers without crosslinker. Removal of DNA origami was performed by decreasing the Mg^{2+} concentration in the buffer and heating a 60 degree overnight. AFM imaging revealed the extracted crosslinked polymers that remained with identical dimensioned structures compared to the polymers presented on DNA origami.

In conclusion, the bottom-up fabrication of polymers with precisely designed nanopatterns on a DNA origami template scaffold by surface-initiated ATRP has been successfully conducted for the first time. This new approach could be in principle applicable to employ any DNA origami structure as a template, so that 3D polymer nanoarchitectures could be fabricated by precise 3D box- or tube-shape DNA origami. Considering the versatility of ATRP allowing to apply a wide variety of monomers and to synthesize complex polymers such as block-copolymers and branched polymers, future developments will focus on tuning the properties (charge, hydrophobicity) and to introduce new functionalities (stimuli-responsiveness, higher stability) at the desired positions of DNA origami.

These results are presented comprehensively in the manuscript [6-1].

[3-2] Step-wise design of precision polymer tube by DNA origami templated synthesis

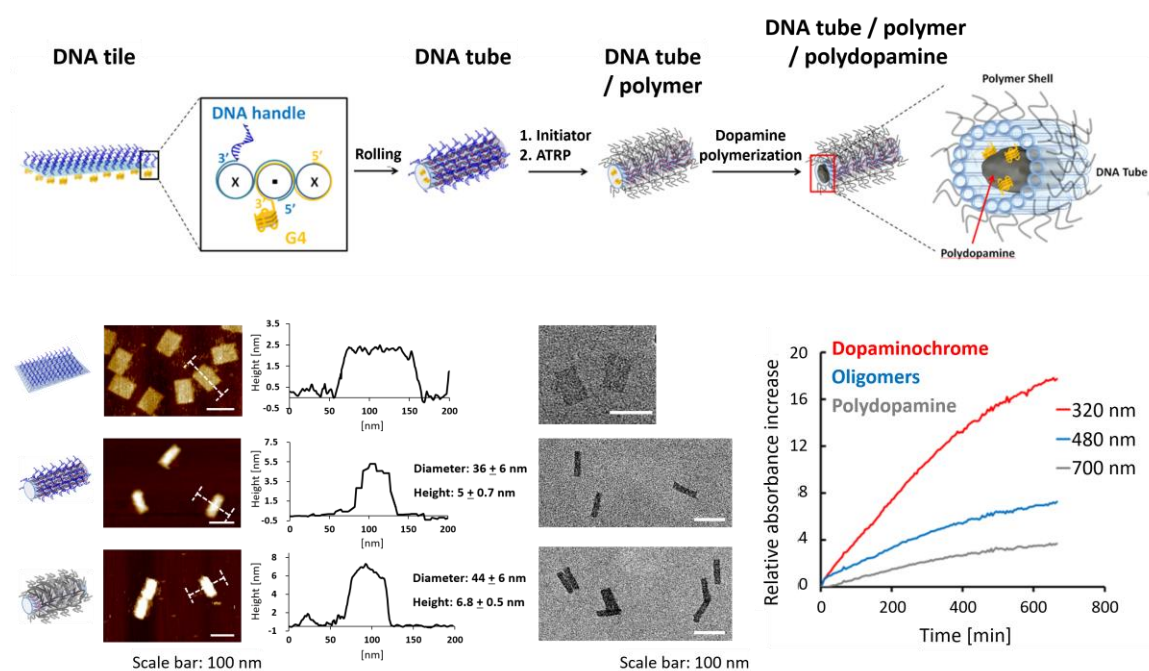


Figure 23. DNA origami-templated step-wise growth of polymers for nanoscale engineering. Adapted with permission from “Yu, T. et al. Polymer tube nanoreactors by DNA-origami templated synthesis. *Chem. Commun.* 2018, doi: 10.1039/C7CC09620H.” Copyright (2018) The Royal Society of Chemistry.

Nanomaterials engineering with defined sizes, shapes and functionalities are crucial to revolutionize a variety of nanotechnology applications such as nanomedicines, nanosensors, and chemical reactors in nanoscale. In the previous part, the surface-initiated ATRP on DNA origami was investigated as a new method to fabricate defined polymeric nanopatterns with high structural precision¹¹⁷. Not only programming functionalities with absolute positioning on DNA origami, but also the limitless freedom of DNA origami shape and size in nanoscale could be utilized as the precision template for polymeric nanostructure synthesis. Furthermore, DNA / polymer hybrid system could potentially solve the stability and the low structural rigidity of DNA origami which limit further advances of this technology. It has been observed that DNA origami designed with a single DNA double-helix layer is flexible and bending or twisting of the structure can be induced in solution and even exaggerated under dried state conditions^{96,118}. In addition, under low salt concentrations, acidic pH¹¹⁹, and high temperature⁹⁰, DNA origami rapidly degrades since DNA origami requires approximately 5 – 20 mM divalent cations (Mg^{2+} and Ca^{2+}) to overcome the repulsive forces between the highly negatively charged DNA

backbones. Also in physiological systems, nuclease enzymes can disassemble the DNA origami structure⁹². There have been several attempts to address these limitations, e.g. by protecting DNA origami with a crosslinker⁹¹, virus capsid proteins⁹⁶, lipids⁹³, cationic polymers⁹⁷, and oligo/poly-lysine based (block co)polymers^{94,95}. Some of these coatings could also enhance the cell entry by facilitating the interactions with cellular membranes, and increase the origami stability against nuclease digestion, which is particularly crucial for in vivo applications. Besides, the electrostatic interaction induced coating of the entire DNA origami surface could reduce the available space for further functionalization, i.e. the immobilization of other nanomaterials, and also the choice of the coating materials has been limited to positively charged molecules and materials. On the other hand, the surface-initiated polymerization from the DNA origami surface allows spatial control and tunable polymer properties.

Therefore, I have explored the facile and versatile design of a DNA/polymer nanomaterial with defined core-shell tube structure by folding up a two dimensional DNA origami tile into a tube followed by surface initiated polymerization from the DNA origami surface. The common two dimensional rectangular DNA origami structure⁶⁰ served as basis and in the first step, this rectangular DNA origami with modified two long edges was transformed into a tube-shape structure by applying an additional set of 16 ssDNA strands (transforming DNAs)^{120,121}. The conformational change from the tile (70 nm x 100 nm with 2 nm thickness) into a tube (22 nm in diameter and 100 nm length) was confirmed by AFM and TEM. It should be noted that in AFM, DNA tube structures were observed with a diameter of 36 ± 0.6 nm and 5 ± 0.7 nm height on average. The discrepancy between the measured dimensions in AFM and theoretical calculations could be attributed to a structural distortion by the cantilever tapping of AFM^{120,121}. For additional characterization, dynamic light scattering (DLS) measurements revealed an increase of hydrodynamic radius (R_h) from 52 nm (DNA tile) to 71 nm (DNA tube), and agarose gel electrophoresis showed a clear band shift which, taken together, indicated the efficient DNA tube formation.

Since the DNA tile surface was almost fully decorated with multiple sticky ssDNA strands, DNA initiators were introduced to the surface of the formed DNA tube for surface-initiated ATRP, which was already described in the first investigated system¹¹⁷. Similarly, the crosslinked polymers were fabricated on the surface of the DNA tube from poly(ethylene glycol) methyl ether methacrylate (PEGMEMA, average M_n 300) and PEG dimethacrylate (PEGDMA, average M_n 750). After purification, the obtained DNA tube with polymer coating (DNA tube / polymer) was again characterized by AFM, TEM, DLS, and agarose gel electrophoresis. AFM measurements showed an increase of both diameter (+ 6 nm) and height (+ 1.8 nm) compared to the DNA tube due to the formed polymer shell. On the other hand, in TEM images no obvious structural changes were observed before and after

polymer coating due to the invisibility of polymers to uranyl formate staining^{94,95,97}. However, TEM images of the DNA tube with polymer coating showed a unique phenomenon; some tube structures were aligned side to side with some gap (supporting information) which was also observed in electrostatic binding of positively charged polylysine to negatively charged DNA nanostructures⁹⁴. From DLS measurement, R_h value of 103.2 nm was obtained. Additionally, a Holtzer plot showed similar profiles before and after the polymer shell formation, which indicated that the increased R_h did not result from dimerization or oligomerization, but from the increased diameter of the DNA tube / polymer and the altered hydration behaviors attributed to the outer polymer shell.

The constructed polymer coated DNA tube possesses interior space that could be in principle further functionalized. The availability of the inner surface of the polymer coated DNA tubes was demonstrated by immobilizing DNA-based enzymes (DNAzyme) so that polymer coated DNA tube could be used as chemical nanoreactors. It has been known that G-rich DNA sequences can form a stacked G-quadruplex (G4) structure that can accommodate hemin to give horseradish peroxidase (HRP)-mimicking catalytic activity for a hydrogen peroxide (H_2O_2)-mediated oxidation reaction^{71,122}. 20 G4 moieties were immobilized inside the polymer coated DNA tubes, and hemin was loaded to activate enzymatic activity. The catalytic activity of DNAzyme-incorporated DNA / polymer tube was demonstrated by tracking an oxidation of 2,2'-azino-bis(3-ethylbenzothiazoline-6-sulphonic acid (ABTS) in the presence of H_2O_2 . Subsequently, the interior space of DNAzyme decorated DNA / polymer tube was utilized to initiate the polymerization of dopamine¹²³. Polydopamine is a bio-inspired polymer known as that oxidation of dopamine to dopaminochrome is the key-intermediating step for the polydopamine formation¹²⁴⁻¹²⁶. So, the reaction kinetics and the formation of polymerization intermediates (dopaminochrome, oligomers) and polydopamine formation were monitored and confirmed using absorbance spectroscopy, which clearly showed the successful polydopamine formation. As such the opposing placements of the G4 catalytic sites with respect to the ATRP initiators have successfully provided the basis of spatial control between inner and outer spheres of the DNA tube.

In conclusion, the systematic design and synthesis of polymer coated DNA tubes has been accomplished that revealed improved stability against nucleases most likely due to the presence of the outer polymer shell. In addition, the inner cavity of the tube was independently available for the further functionalization. This was demonstrated by incorporating DNAzyme for conducting the polymerization of dopamine inside. Furthermore, since the outer surface and the inner space can be modified independently, this design strategy is compatible with a large variety of functionalization methods for DNA origami; immobilizing different enzymes for cascade reactions¹²⁷, loading drug molecules for biomedical applications¹²⁸⁻¹³⁰, and so on. Besides, the polymer introduced

onto the outer surface would also be modifiable, for example by stimuli-responsive polymers to switch the surface properties of the DNA tube^{98,131} that could potentially transfer DNA origami into organic solvents without destroying its defined structure to broaden its application fields^{49,132,133}. Thus, the facile and versatile design proposed here could open access to creating tailor-made DNA / polymer hybrid nanomaterials for a wide variety of applications in nanotechnology.

These results are presented comprehensively in the manuscript [6-2].

[3-3] DNAzyme-assisted fabrication of polydopamine nanostructure on DNA origami template

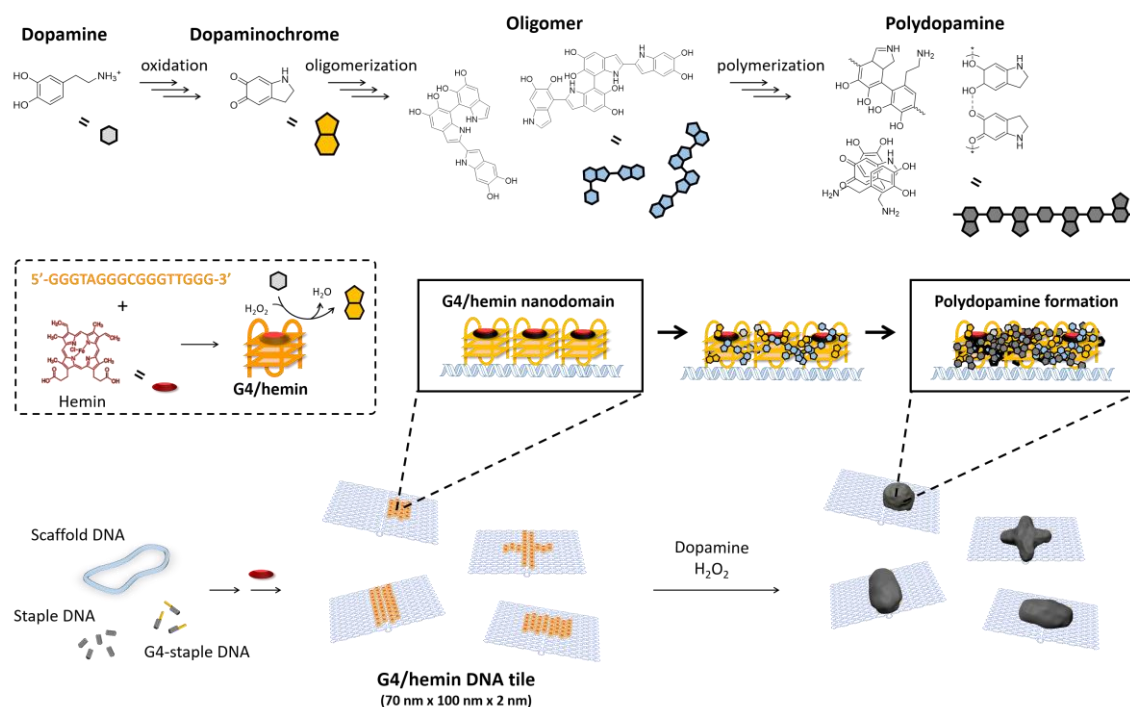


Figure 24. Polymerization mechanism of dopamine and DNAzyme-assisted bottom-up polydopamine nanostructure fabrication on DNA origami template. Adapted with permission from “Yu, T. et al. Fabrication of Defined Polydopamine Nanostructures by DNA Origami-Templated Polymerization. *Angew. Chem. Int. Ed.* 2018, 57(6), 1587-1591 doi: 10.1002/anie.201711560.” Copyright (2018) John Wiley and Sons.

In the previous projects reported above, the controlled radical polymerization reaction on the surface of DNA origami¹¹⁷ has been accomplished to construct and explore defined functional DNA / polymer nanoarchitectures. In this contribution, the highly programmable DNA origami technology that clearly provides versatile opportunities to design and construct the adequate environments for conducting polymerization reactions at the nanoscale has been applied to fabricate desired polymeric nanoarchitectures with nanoscale resolution. Bio-inspired polymer, polydopamine (PD)¹²³ has been selected as model system for the spatial controlled growth from the origami template. PD is known for its high adhesive properties and a variety of functional groups (amine, hydroxyl, and carboxylic acid) available for post-functionalization^{134,135}. In combination with its natural

biocompatibility and the robust wet adhesion properties of invertebrate mussels, it moved into spotlight as a novel coating material for very broad attention in the biotechnology field such as biomaterials and nanomedicine¹³⁶⁻¹³⁸. On the other hand, the polymerization mechanism of PD involves multi-steps (oxidation, isomerization, and oligomerization) and the chemical structures of PD are diverse¹²⁴⁻¹²⁶, which makes it difficult to control the polymerization reaction of PD.

To control PD formation, the DNA origami scaffold was utilized possessing the nanosized catalytic domain with multiple G4/hemin DNAzyme moieties. Previously, G4/hemin decorated DNA origami was employed as scaffold for the oxidative polymerization of polyaniline¹⁰⁹. Separately, it was reported that G4/hemin DNAzyme could oxidize dopamine to dopaminochrome, which is an oxidized state of dopamine and one of the intermediates for PD formation^{139,140} and that the HRP enzyme could accelerate PD formation¹⁴¹. In combining both concepts, we speculated that organizing multiple G4/hemin moieties at distinct nanodomains on DNA origami provides the local environment allowing a controlled dopamine polymerization. The DNA tile (70 nm x 100 nm dimensions) was designed with a 20 nm square domain containing 20 G4 moieties (G4 DNA tile). After incorporating hemin to the G4 domains, the catalytic properties of the DNAzyme on the DNA tile were evaluated with an ABTS assay revealing that the G4/hemin domain on the DNA tile showed an almost five fold faster reaction kinetic compared to free G4/hemin molecules at similar concentrations, which could be achieved due to a cooperative effect as a consequence of the locally concentrated G4/hemin reaction centers. Fabrication of PD nanostructures on the G4/hemin DNA tile was initially pursued in TAE / Mg buffer (20 mM Tris, 10 mM acetic acid, 1 mM EDTA, 12 mM MgCl₂, pH 5.8) since under these conditions, the activity of the DNAzyme was highest while preventing an oxidation of dopamine by dissolved oxygen. However, PD formation on the DNA tile was not observed, but many PD nanoparticles were formed in solution. Most likely, the high ionic strength and cation concentrations shielded the negative charges of the DNA backbone so that dopamine molecules did not attach there. In this way, dopamine molecules that were oxidized to dopaminochrome on the DNA nanotile would rapidly diffuse back into the bulk solution and spontaneously self-polymerize in solution as detected. This self-polymerization in solution was suppressed efficiently, when the buffer concentration was decreased by about 70 times. Under these conditions, no degradation of the DNA tile was observed and the new PD objects appeared on the DNAzyme domain. The AFM images showed the height increase of the catalytic domain by 2-3 nm after the reaction. Additionally, mechanical property mapping revealed an increase in adhesion forces by 73 pN \pm 16 pN from the DNA tile, which taken together, indicated the successful PD formation. It is hypothesized that the electrostatic interaction between positively charged dopaminochrome / dopamine and negatively charged DNA

nanotile coupled with multiple DNAzyme molecules in close proximity facilitated a high local concentration of PD intermediates including oligomers, leading to the preferential polymerization directly at the DNAzyme domain. Further characterization of PD formation was performed by UV-Vis spectroscopy to track the formation of the oxidized dopamine (dopaminochrome), oligomer, and PD by recording their optical properties at their characteristic wavelengths. Interestingly, the dopaminochrome and the oligomer were formed in both G4/hemin-DNA tile and free G4/hemin, whereas PD was only formed in the case of G4/hemin-DNA tile, which clearly indicated that multiple DNAzymes in the immediate vicinity at low ionic strength were essential for producing PD locally and directly on the DNAzyme domain. The control over the PD formation on the DNA tile was achieved by changing the amount of H_2O_2 supplied to DNAzyme. The height of the formed PD increased by supplying the larger amount of H_2O_2 , and the anchoring of PD around DNAzyme domain self-defines the final shape and the size of PD nanostructures by limiting the diffusion of H_2O_2 to the DNAzyme.

By making use of the programmability of DNA origami, different PD nanostructures (line, cross, and 3D-stripe) could be obtained by positioning the DNAzyme domains into the corresponding geometries. One of the major features of PD is related to its high adhesiveness due to a wide variety of supramolecular interactions (hydrogen bonding, π - π stacking, hydrophobic interaction, electrostatic interaction) possible on the PD nanostructure surfaces. This “supramolecular glue” effect was also observed in our system. Especially, when the line-shape PD was formed along with the long axis of the DNA tile, partially or fully folded DNA tiles were observed by AFM. The directed conformational changes of DNA origami are important to conceive smart functional DNA origami with gate-open/close systems and stimuli-responsive systems. Although there are several modulation approaches reported by using DNA-based machinery (toehold DNA displacement, DNA hinge, and aptamer), intercalating molecules¹⁴², lipid molecules¹⁴³, and proteins⁹⁶, to the best of my knowledge, the approach reported herein was the first presentation of an entirely polymer-based approach for DNA origami folding.

In comparison to common monomers used for the synthesis of polymers, dopamine is unique as it serves as monomer as well as crosslinker thereby leading to rigid and highly crosslinked materials after polymerization. Based on these highly stable and potentially shape-persistent properties of PD we have asked us whether it would be possible to extract the PD nanostructure formed on the DNA tile after removing the template. When the PD formed DNA tile was deposited on mica and treated with 1M HCl solution, DNA origami was decomposed rapidly, within 10 seconds, and only the PD nanostructures retaining the structural information (size and geometry) programmed by DNA tile were observed. The rapid degradation of DNA origami in acidic pH is due to the hydrolysis of the phosphodiester backbone, bases, and glycosidic bonds¹¹⁹. More importantly, during

AFM studies, the extracted PD nanostructures were found at the same positions as before acid treatment. Since the micro/nano-patternings of DNA origami onto the various surface were reported¹⁴⁴⁻¹⁴⁶, potentially the micro/nano-patterning of PD nanostructure in the large area could be envisaged.

In summary, the first strategy for creating defined PD nanostructures in high precision was achieved by using DNA origami template with catalytic centers. By positioning multiple catalytic moieties close to each other, dopamine molecules were locally oxidized and captured at catalytic domains for facilitating PD formation. Also, the well-known random and uncontrolled self-polymerization behavior of dopamine in solution was efficiently subverted by conducting the reaction in acidic pH. The kinetics of PD growth and the control over the height of the architecture was achieved by adjusting the H₂O₂ concentration. Coupled with the spatial programmability of functionalities on DNA origami, one could envision creating various desired shapes of PD nanostructures in 2D and 3D with unprecedented resolution. The unique adhesive properties of PD could alter the conformation of DNA origami at PD-grown areas. The robust and tightly crosslinked PD features allowed retaining of the sizes and shapes of the PD nanostructures programmed on DNA origami even after the removal of the template by a rapid and facile acid treatment. Collectively, the DNA origami templated polymerization strategy contributes to the development of precision polymeric architectures and nanostructured PD-based material science as well as the surface functionalization of DNA origami to impart novel features.

These results are presented comprehensively in the manuscript [6-3].

[3-4] Systematic study on intercellular supramolecular assembly of oligothiophene analogues

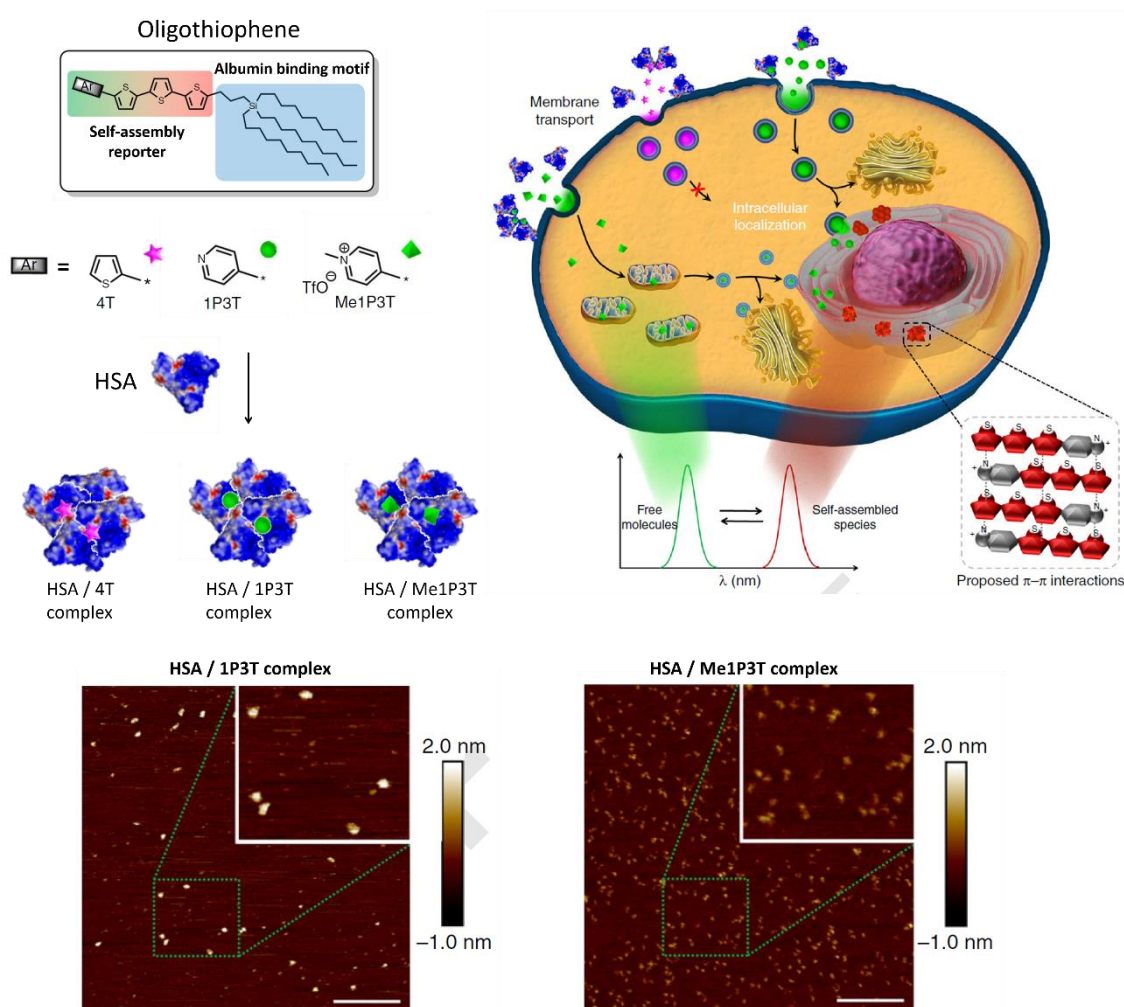


Figure 25. Complexation of a series of oligothiophenes with HSA. Each complex could traffic on different intercellular pathways driven by the tailored head group. The real-time tracking of free molecules and self-assembled species was achieved by recording their different fluorescent characteristics based on their states inside living cells and cellular compartments. Adapted with permission from "David, Y. W. Ng et al. Directing intracellular supramolecular assembly with N-heteroaromatic quaterthiophene analogues. Nat. Commun. 2017, 8, 1850 doi: 10.1038/s41467-017-02020-2." Copyright (2018) Nature Publishing Group and Creative Commons Attribution 4.0 International License (<http://creativecommons.org/licenses/by/4.0/>.)

This work described herein focuses on directed intercellular self-assembly of oligothiophene analogues and it has been achieved in a close collaboration with Dr. David

Y. W. Ng and Roman Vill, who were the main investigators. The supramolecular assembly of synthetic molecules is governed by both synthetic design to control the interactions between the components and the stimulus provided by the environment. In particular, it is important to study the supramolecular chemistry in biological systems to understand how nature elegantly organizes the various biological components (RNA, DNA, peptide, protein) in an elaborated fashion to conduct important biological functions, which could provide a strategy to develop a novel therapeutics¹⁴⁷. In this context, substituted oligothiophenes (more specifically, carbosilane substituted terthiophenes), a class of the π -conjugated heteroaromatic compounds, and its analogues were used in the study as their fluorescence changes depending on the molecular states¹⁴⁸. In the study, three differently functionalized oligothiophene molecules were designed by replacing the terminal thiophene unit with quaterthiophene, pyridine, and subsequent N-methylation. Additionally, all the oligothiophene series possess the branched alkyl chain to bind with human serum albumin (HSA) protein for forming non-toxic complexes with improved water-solubility and uptake into living cells¹⁴⁹. A series of HSA / oligothiophene complexes was well-characterized by both spectroscopic studies (UV-Vis, fluorescence correlation spectroscopy) and atomic force microscopy method (AFM) to understand their supramolecular assembly behaviors.

The systematic studies on the different intercellular behavior of synthesized complexes by the combination of confocal microscopy and selective inhibition of intercellular transport pathways revealed that the pathways within the cell were clearly determined by head functional groups. In addition, the self-assemblies of oligothiophenes inside cells were traceable by their specific red color emission. Especially, self-assembly of oligothiophene was observed in the perinuclear region, where it was also demonstrated in the study that the combination of a pathway inhibitor (bafilomycin A1¹⁵⁰) and the lowering of temperature could specifically induce the self-assembly process in a cellular organelle (mitochondria). This demonstration clearly indicated the possibility to control the location, the timing, and the degree of self-assembling materials in cells with external stimulus.

Collectively, the smart structural design of self-assembling materials could show the significant influences to their respective fates in cells. The unique findings observed in the presented study forms the foundation of a new platform for biomedical science applications such as organelle-targeted therapeutics¹⁵¹ and creation of self-assembled materials in cells to alter / tune cell functions (proliferation, migration, differentiation, apoptosis)¹⁵².

These results are presented comprehensively in the manuscript [6-4].

4. Conclusion and Outlook

In my thesis, I have investigated and established novel methods for the preparation of structurally defined polymeric nanostructures by merging DNA nanotechnology and polymer chemistry. During the last decades, the developments in polymer chemistry have enabled synthesis of defined polymers with tunable length, chemical compositions, and functionalities, which further developed to the self-assembled state of polymers represented by micelle, polymersome and polymer brush. However, compared to these well-fabricated synthetic polymers and their assemblies, Nature's portfolio provides a wide variety of precision biopolymers (peptide, protein, DNA, RNA) and their assemblies (photosynthesis system, chromatin, proteasome, and so on) with programmed geometries and smart functionalities located with greatest structural precision to conduct the important biological reactions. Therefore, it would be highly attractive if synthetic polymers could be accomplished with similar degrees of perfection, which could potentially fulfill the crucial demands for developing modern nanotechnology applications such as smart drug delivery systems, micro/nano fluidics, cell chip, and high throughput sensors. To conceive of the novel strategy of fabricating defined polymer architectures with nanoscale precision, emulating nature's system by employing and mimicking biopolymers or their assemblies as templates and reactors for synthesizing precision polymers have been extensively investigated as promising approach.

My contribution was the merge of modern DNA nanotechnology denoted as scaffold DNA origami and synthetic polymer chemistry for the first time to produce polymers of high spatial definition. After its invention in 2006, the development of DNA origami research has brought it to the stage that almost any 1D / 2D/ 3D nanostructures with a resolution of a few nanometer could be designed. In addition, since the functionalities can be positioned with the same degree of precision, DNA origami could serve as versatile templates to immobilize molecules and, more importantly, a template for nanomaterial synthesis by proper choosing and positioning of the reactive moieties.

By integrating the surface-initiated atom transfer radical polymerization and DNA origami, the novel bottom-up method for fabricating the defined nanopatterning of polymers was achieved. DNA origami allowed independent positioning of single initiator molecules for polymerization at desired locations with nanoscale resolution, which made it possible to create any nanopatterned polymers on DNA origami. The bottom-up approach in principle could promise high productivity and the controlled radical polymerization gives the chance to tune the length, chemical components, and architectures of grown polymers in high uniformity, which are essential for efficient production in industrial stages. Additionally, by crosslinking the grown polymers on DNA origami, the structural information of polymers programmed by the template could be

retained after the removal of DNA origami. This potentially indicates the chances of fabricating not only 2D nanopatterned polymers but also the defined 3D polymer nanoarchitectures.

The advantages of polymeric materials include a wide variety of chemical and physical properties that are tunable by the choice of the monomers and the polymerization methods. Therefore, polymeric materials are quite useful for modulating and enriching the properties of other materials, e.g. by directly conjugating the polymers to or by growing the polymers from the surface of the materials of interest. Along with this context, the established strategy above mentioned was further developed and utilized to create defined and a functional DNA / polymer tube. The stability of DNA origami, which is one of the major issues hindering DNA origami's application in versatile fields, was improved by the polymer coating on the outer surface of the tube-shape DNA origami. Furthermore, the spatial control of the polymer coating allowed the interior space of DNA tube to remain available for the further functionalization, which was demonstrated by immobilizing DNA-based enzyme moieties to conduct the polymerization of dopamine inside the tube.

In collaboration with Sean Harvey, the fabrication of distinct polydopamine nanostructures, a bioinspired polymer from mussel's adhesive proteins, using DNA origami technology was established. By introducing the catalytic DNAzyme nanodomains at precise positions on the DNA origami, control of the dopamine polymerization in nanoscale was achieved for the first time. Not only the different polydopamine nanoarchitectures were fabricated on the DNA origami template, but also the adhesive properties of polydopamine were transferred onto DNA origami to induce distinct conformational changes. In addition, facile acid treatment rapidly degraded the DNA origami and liberated the rigid polydopamine with defined sizes and shapes.

In collaboration with Dr. David Y. W. Ng, the investigation of the supramolecular self-assembly behavior of oligothiophene analogues transported into biological systems by complexation with protein was conducted. The study revealed the strong potential of a supramolecular assembly as novel platforms for biomedical sciences by proper synthetic design and control over their self-assembling characteristics.

In summary and future outlook, the interdisciplinary fields between polymer chemistry and DNA nanotechnology were investigated and the novel approach for designing a variety of precision polymeric nanostructures was established herein, which could further stimulate innovative future perspectives of DNA nanotechnology-promoted polymer chemistry. Combining the established surface-initiated ATRP with other polymerization methods like RAFT^{153,154}, two kinds of polymers with varying polarity could be nanopatterned on single DNA origami template, which would results in the amphiphilic nanopatterned surface such as virus system using in nature to interact with the cell surface for infection^{155,156}(Figure 26a). Besides, upscaling of the produced precision

polymers could be a key concern, which could be envisaged to be addressable by recovering and recycling the templates like the polymerase chain reaction¹⁵⁷⁻¹⁵⁹ (Figure 26b). The smart design of DNA origami device which can program polymeric nanoarchitectures with great precision will provide the future outlook of novel polymer-based systems which can rival the elaborated biomacromolecular systems in nature.

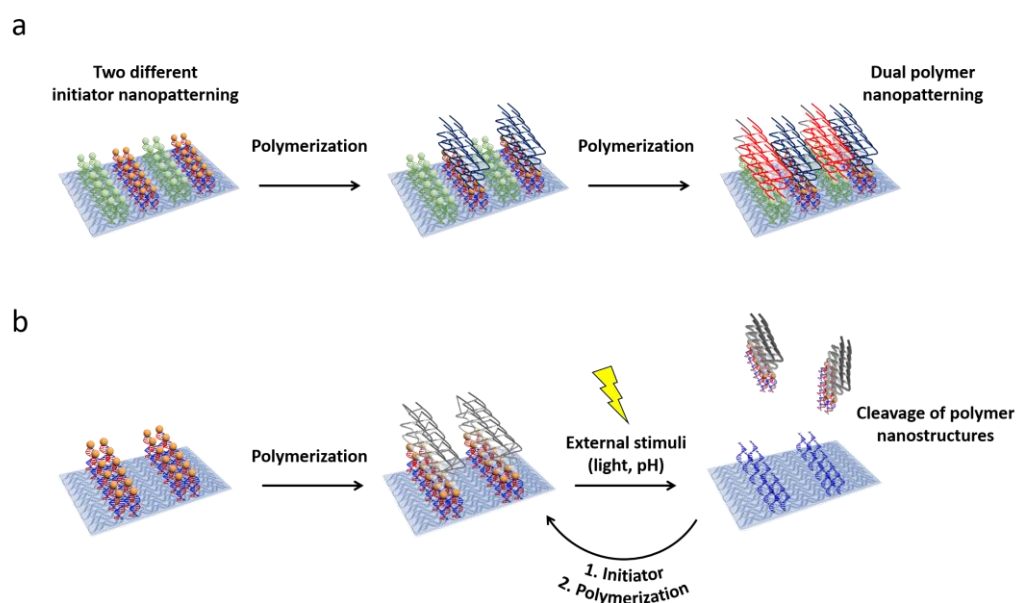


Figure 26 Outlook of DNA origami templated polymer nanoarchitectures synthesis

5. References

- 1 Wang, J. S. & Matyjaszewski, K. Controlled Living Radical Polymerization - Atom-Transfer Radical Polymerization in the Presence of Transition-Metal Complexes. *J Am Chem Soc* 117, 5614-5615, doi:Doi 10.1021/Ja00125a035 (1995).
- 2 Kato, M., Kamigaito, M., Sawamoto, M. & Higashimura, T. Polymerization of Methyl-Methacrylate with the Carbon-Tetrachloride Dichlorotris(Triphenylphosphine) Ruthenium(II) Methylaluminum Bis(2,6-Di-Tert-Butylphenoxide) Initiating System - Possibility of Living Radical Polymerization. *Macromolecules* 28, 1721-1723, doi:Doi 10.1021/Ma00109a056 (1995).
- 3 Chiefari, J. et al. Living free-radical polymerization by reversible addition-fragmentation chain transfer: The RAFT process. *Macromolecules* 31, 5559-5562, doi:Doi 10.1021/Ma9804951 (1998).
- 4 Wang, Y. J., Hosta-Rigau, L., Lomas, H. & Caruso, F. Nanostructured polymer assemblies formed at interfaces: applications from immobilization and encapsulation to stimuli-responsive release. *Phys. Chem. Chem. Phys.* 13, 4782-4801, doi:10.1039/c0cp02287j (2011).
- 5 Lutz, J. F., Lehn, J. M., Meijer, E. W. & Matyjaszewski, K. From precision polymers to complex materials and systems. *Nat. Rev. Mater.* 1, doi:Artn 1602410.1038/Natrevmats.2016.24 (2016).
- 6 Kuzyk, A. et al. DNA-based self-assembly of chiral plasmonic nanostructures with tailored optical response. *Nature* 483, 311-314, doi:10.1038/nature10889 (2012).
- 7 Borys, N. J., Walter, M. J., Huang, J., Talapin, D. V. & Lupton, J. M. The Role of Particle Morphology in Interfacial Energy Transfer in CdSe/CdS Heterostructure Nanocrystals. *Science* 330, 1371-1374, doi:10.1126/science.1198070 (2010).
- 8 Discher, D. E. Shape Effects of Filaments Versus Spherical Particles in Flow and Drug Delivery. *Proceedings of the Asme Summer Bioengineering Conference 2008*, Pts a and B, 739-739 (2009).
- 9 Geng, Y. et al. Shape effects of filaments versus spherical particles in flow and drug delivery. *Nat. Nanotechnol.* 2, 249-255, doi:10.1038/nnano.2007.70 (2007).
- 10 Zhu, J. H. et al. Disk-cylinder and disk-sphere nanoparticles via a block copolymer blend solution construction. *Nat. Commun.* 4, doi:Artn 229710.1038/Ncomms3297 (2013).
- 11 Lobling, T. I. et al. Rational design of ABC triblock terpolymer solution nanostructures with controlled patch morphology. *Nat. Commun.* 7, doi:Artn 1209710.1038/Ncomms12097 (2016).
- 12 Zhao, B. & Brittain, W. J. Polymer brushes: surface-immobilized macromolecules. *Prog. Polym. Sci.* 25, 677-710, doi:Doi 10.1016/S0079-6700(00)00012-5 (2000).

- 13 Barbey, R. et al. Polymer Brushes via Surface-Initiated Controlled Radical Polymerization: Synthesis, Characterization, Properties, and Applications. *Chem. Rev.* 109, 5437-5527, doi:10.1021/cr900045a (2009).
- 14 Stuart, M. A. C. et al. Emerging applications of stimuli-responsive polymer materials. *Nat. Mater.* 9, 101-113, doi:10.1038/NMAT2614 (2010).
- 15 Draper, J., Luzinov, I., Minko, S., Tokarev, I. & Stamm, M. Mixed polymer brushes by sequential polymer addition: Anchoring layer effect. *Langmuir* 20, 4064-4075, doi:10.1021/la0361316 (2004).
- 16 Xu, C. et al. Effect of block length on solvent response of block copolymer brushes: Combinatorial study with block copolymer brush gradients. *Macromolecules* 39, 3359-3364, doi:10.1021/ma051405c (2006).
- 17 Zoppe, J. O. et al. Surface-Initiated Controlled Radical Polymerization: State-of-the-Art, Opportunities, and Challenges in Surface and Interface Engineering with Polymer Brushes (vol 117, pg 1105, 2017). *Chem. Rev.* 117, 4667-4667, doi:10.1021/acs.chemrev.7b00093 (2017).
- 18 Ejaz, M., Yamamoto, S., Ohno, K., Tsujii, Y. & Fukuda, T. Controlled graft polymerization of methyl methacrylate on silicon substrate by the combined use of the Langmuir-Blodgett and atom transfer radical polymerization techniques. *Macromolecules* 31, 5934-5936, doi:Doi 10.1021/Ma980240n (1998).
- 19 Li, Y. F. et al. Polymer brush nanopatterns with controllable features for protein pattern applications. *J. Mater. Chem.* 22, 25116-25122, doi:10.1039/c2jm35197h (2012).
- 20 Yu, Q., Ista, L. K., Gu, R. P., Zauscher, S. & Lopez, G. P. Nanopatterned polymer brushes: conformation, fabrication and applications. *Nanoscale* 8, 680-700, doi:10.1039/c5nr07107k (2016).
- 21 Takahashi, H., Nakayama, M., Itoga, K., Yamato, M. & Okano, T. Micropatterned Thermoresponsive Polymer Brush Surfaces for Fabricating Cell Sheets with Well-Controlled Orientational Structures. *Biomacromolecules* 12, 1414-1418, doi:10.1021/bm2000956 (2011).
- 22 Yu, Q., Cho, J., Shivapooja, P., Ista, L. K. & Lopez, G. P. Nanopatterned Smart Polymer Surfaces for Controlled Attachment, Killing, and Release of Bacteria. *ACS Appl. Mater. Inter.* 5, 9295-9304, doi:10.1021/am4022279 (2013).
- 23 Paik, M. Y. et al. Patterning of Polymer Brushes. A Direct Approach to Complex, Sub-Surface Structures. *Nano Lett.* 10, 3873-3879, doi:10.1021/nl102910f (2010).
- 24 Hammiche, A. et al. Photothermal FT-IR spectroscopy: A step towards FT-IR microscopy at a resolution better than the diffraction limit. *Appl. Spectrosc.* 53, 810-815, doi:Doi 10.1366/0003702991947379 (1999).
- 25 Anderson, M. S. Infrared spectroscopy with an atomic force microscope. *Appl.*

- Spectrosc. 54, 349-352, doi:Doi 10.1366/0003702001949618 (2000).
- 26 Dazzi, A., Prazeres, R., Glotin, E. & Ortega, J. M. Local infrared microspectroscopy with subwavelength spatial resolution with an atomic force microscope tip used as a photothermal sensor. *Opt. Lett.* 30, 2388-2390, doi:Doi 10.1364/Ol.30.002388 (2005).
 - 27 Pollock, H. Towards chemical mapping at sub-micron resolution: near-field spectroscopic delineation of interphase boundaries. *Mater. Sci. Forum.* 662, 1-11, doi:10.4028/www.scientific.net/MSF.662.1 (2011).
 - 28 Dazzi, A. et al. AFM-IR: Combining Atomic Force Microscopy and Infrared Spectroscopy for Nanoscale Chemical Characterization. *Appl. Spectrosc.* 66, 1365-1384 (2012).
 - 29 Felts, J. R., Kjoller, K., Lo, M., Prater, C. B. & King, W. P. Nanometer-Scale Infrared Spectroscopy of Heterogeneous Polymer Nanostructures Fabricated by Tip-Based Nanofabrication. *ACS Nano* 6, 8015-8021, doi:10.1021/nn302620f (2012).
 - 30 Morsch, S., Liu, Y. W., Lyon, S. B. & Gibbon, S. R. Insights into Epoxy Network Nanostructural Heterogeneity Using AFM-IR. *ACS Appl. Mater. Inter.* 8, 959-966, doi:10.1021/acsami.5b10767 (2016).
 - 31 Wien, K. TOF-SIMS analysis of polymers. *Nucl. Instrum. Meth. B* 131, 38-54, doi:Doi 10.1016/S0168-583x(97)00147-X (1997).
 - 32 Chan, C. M., Weng, L. T. & Lau, Y. T. R. Polymer surface structures determined using ToF-SIMS. *Rev. Anal. Chem.* 33, 11-30, doi:10.1515/revac-2013-0015 (2014).
 - 33 Li, L. et al. Surface studies of the rearrangement of end groups of a polymer by ToF-SIMS and AFM. *Macromolecules* 33, 5588-5592, doi:Doi 10.1021/Ma991142k (2000).
 - 34 Miyasaka, T., Ikemoto, T. & Kohno, T. ToF-SIMS imaging of PE/PP polymer using multivariate analysis. *Appl. Surf. Sci.* 255, 1576-1579, doi:10.1016/j.apsusc.2008.05.137 (2008).
 - 35 Bailey, J. et al. 3D ToF-SIMS Imaging of Polymer Multi layer Films Using Argon Cluster Sputter Depth Profiling. *ACS Appl. Mater. Inter.* 7, 2654-2659, doi:10.1021/am507663v (2015).
 - 36 Li, X. Y. & Liu, D. R. DNA-Templated organic synthesis: Nature's strategy for controlling chemical reactivity applied to synthetic molecules. *Angew. Chem. Int. Edit.* 43, 4848-4870, doi:10.1002/anie.200400656 (2004).
 - 37 Yoshimura, H. Protein-assisted nanoparticle synthesis. *Colloid Surface A* 282, 464-470, doi:10.1016/j.colsurfa.2006.01.037 (2006).
 - 38 Gottlieb, D., Morin, S. A., Jin, S. & Raines, R. T. Self-assembled collagen-like peptide fibers as templates for metallic nanowires. *J. Mater. Chem.* 18, 3865-3870, doi:10.1039/b807150k (2008).

- 39 Qi, Y. Z. & Chilkoti, A. Growing polymers from peptides and proteins: a biomedical perspective. *Polym Chem-Uk* 5, 266-276, doi:Doi 10.1039/C3py01089a (2014).
- 40 Abe, S. et al. Polymerization of Phenylacetylene by Rhodium Complexes within a Discrete Space of apo-Ferritin. *J. Am. Chem. Soc.* 131, 6958-+, doi:10.1021/ja901234j (2009).
- 41 Renggli, K., Nussbaumer, M. G., Urbani, R., Pfohl, T. & Bruns, N. A Chaperonin as Protein Nanoreactor for Atom-Transfer Radical Polymerization. *Angew. Chem. Int. Edit.* 53, 1443-1447, doi:10.1002/anie.201306798 (2014).
- 42 Surin, M. From nucleobase to DNA templates for precision supramolecular assemblies and synthetic polymers. *Polym Chem-Uk* 7, 4137-4150, doi:10.1039/c6py00480f (2016).
- 43 He, Y. & Liu, D. R. A Sequential Strand-Displacement Strategy Enables Efficient Six-Step DNA-Templated Synthesis. *J. Am. Chem. Soc.* 133, 9972-9975, doi:10.1021/ja201361t (2011).
- 44 Meng, W. J. et al. An autonomous molecular assembler for programmable chemical synthesis. *Nat. Chem.* 8, 542-548, doi:10.1038/Nchem.2495 (2016).
- 45 Nielsen, P. E., Egholm, M., Berg, R. H. & Buchardt, O. Sequence-Selective Recognition of DNA by Strand Displacement with a Thymine-Substituted Polyamide. *Science* 254, 1497-1500, doi:DOI 10.1126/science.1962210 (1991).
- 46 Niu, J., Hili, R. & Liu, D. R. Enzyme-free translation of DNA into sequence-defined synthetic polymers structurally unrelated to nucleic acids. *Nat. Chem.* 5, 282-292, doi:10.1038/Nchem.1577 (2013).
- 47 Carlini, A. S., Adamiak, L. & Gianneschi, N. C. Biosynthetic Polymers as Functional Materials. *Macromolecules* 49, 4379-4394, doi:10.1021/acs.macromol.6b00439 (2016).
- 48 Vllasaliu, D., Fowler, R. & Stolnik, S. PEGylated nanomedicines: recent progress and remaining concerns. *Expert Opin Drug Del* 11, 139-154, doi:10.1517/17425247.2014.866651 (2014).
- 49 Abe, H. et al. Structure Formation and Catalytic Activity of DNA Dissolved in Organic Solvents. *Angew. Chem. Int. Edit.* 51, 6475-6479, doi:10.1002/anie.201201111 (2012).
- 50 Lucon, J. et al. Use of the interior cavity of the P22 capsid for site-specific initiation of atom-transfer radical polymerization with high-density cargo loading. *Nat. Chem.* 4, 781-788, doi:10.1038/nchem.1442 (2012).
- 51 Cobo, I., Li, M., Sumerlin, B. S. & Perrier, S. Smart hybrid materials by conjugation of responsive polymers to biomacromolecules. *Nat Mater* 14, 143-159, doi:10.1038/NMAT4106 (2015).
- 52 Pan, X. C., Lamson, M., Yan, J. J. & Matyjaszewski, K. Photoinduced Metal-Free

- Atom Transfer Radical Polymerization of Acrylonitrile. *ACS Macro Lett* 4, 192-196, doi:10.1021/mz500834g (2015).
- 53 Treat, N. J. et al. Metal-Free Atom Transfer Radical Polymerization. *J. Am. Chem. Soc.* 136, 16096-16101, doi:10.1021/ja510389m (2014).
 - 54 Watson, J. D. & Crick, F. H. C. Molecular Structure of Nucleic Acids - a Structure for Deoxyribose Nucleic Acid. *Nature* 171, 737-738, doi:10.1038/171737a0 (1953).
 - 55 Ghosh, A. et al. Indolicidin Targets Duplex DNA: Structural and Mechanistic Insight through a Combination of Spectroscopy and Microscopy. *ChemMedChem* 9, 2052-2058, doi:10.1002/cmdc.201402215 (2014).
 - 56 Averick, S. E., Dey, S. K., Grahacharya, D., Matyjaszewski, K. & Das, S. R. Solid-Phase Incorporation of an ATRP Initiator for Polymer-DNA Biohybrids. *Angew. Chem. Int. Edit.* 53, 2739-2744, doi:10.1002/anie.201308686 (2014).
 - 57 Pan, X. C. et al. Automated Synthesis of Well-Defined Polymers and Biohybrids by Atom Transfer Radical Polymerization Using a DNA Synthesizer. *Angew. Chem. Int. Edit.* 56, 2740-2743, doi:10.1002/anie.201611567 (2017).
 - 58 Seeman, N. C. DNA in a material world. *Nature* 421, 427-431, doi:10.1038/nature01406 (2003).
 - 59 Chen, J. & Seeman, N. C. The Synthesis from DNA of a Molecule with the Connectivity of a Cube. *Abstr. Pap. Am. Chem. S.* 202, 162-BIOL (1991).
 - 60 Gopaul, D. N., Guo, F. & Van Duyne, G. D. Structure of the Holliday junction intermediate in Cre-loxP site-specific recombination. *Embo. J* 17, 4175-4187, doi:10.1093/emboj/17.14.4175 (1998).
 - 61 Rothemund, P. W. Folding DNA to create nanoscale shapes and patterns. *Nature* 440, 297-302, doi:10.1038/nature04586 (2006).
 - 62 Dietz, H., Douglas, S. M. & Shih, W. M. Folding DNA into Twisted and Curved Nanoscale Shapes. *Science* 325, 725-730, doi:10.1126/science.1174251 (2009).
 - 63 Shih, W. M. et al. Self-assembly of DNA into Nanoscale Three-Dimensional Shapes. *J Biomol Struct. Dyn.* 26, 799-799 (2009).
 - 64 Han, D. R. et al. DNA Origami with Complex Curvatures in Three-Dimensional Space. *Science* 332, 342-346, doi:10.1126/science.1202998 (2011).
 - 65 Rajendran, A., Endo, M., Katsuda, Y., Hidaka, K. & Sugiyama, H. Programmed Two-Dimensional Self-Assembly of Multiple DNA Origami Jigsaw Pieces. *ACS Nano* 5, 665-671, doi:10.1021/nn1031627 (2011).
 - 66 Linko, V. & Dietz, H. The enabled state of DNA nanotechnology. *Curr. Opin. Biotech.* 24, 555-561, doi:10.1016/j.copbio.2013.02.001 (2013).
 - 67 Veneziano, R. et al. DNA NANOTECHNOLOGY Designer nanoscale DNA assemblies programmed from the top down. *Science* 352, doi:10.1126/science.1244388 (2016).

- 68 Castro, C. E. et al. A primer to scaffolded DNA origami. *Nat. Methods* 8, 221-229, doi:10.1038/Nmeth.1570 (2011).
- 69 Bock, L. C., Griffin, L. C., Latham, J. A., Vermaas, E. H. & Toole, J. J. Selection of Single-Stranded-DNA Molecules That Bind and Inhibit Human Thrombin. *Nature* 355, 564-566, doi:10.1038/355564a0 (1992).
- 70 Xiao, P. et al. An aptamer-based trypsin reactor for on-line protein digestion with electrospray ionization tandem mass spectrometry. *Anal. Biochem.* 441, 123-132, doi:10.1016/j.ab.2013.06.012 (2013).
- 71 Sen, D. & Gilbert, W. Formation of parallel four-stranded complexes by guanine-rich motifs in DNA and its implications for meiosis. *Nature* 334, 364-366, doi:10.1038/334364a0 (1988).
- 72 Travascio, P., Bennet, A. J., Wang, D. Y. & Sen, D. A ribozyme and a catalytic DNA with peroxidase activity: active sites versus cofactor-binding sites. *Chem. Biol.* 6, 779-787, doi:10.1016/S1074-5521(99)80125-2 (1999).
- 73 Wilner, O. I. et al. Enzyme cascades activated on topologically programmed DNA scaffolds. *Nat. Nanotechnol.* 4, 249-254, doi:10.1038/Nnano.2009.50 (2009).
- 74 Urban, M. J. et al. Plasmonic Toroidal Metamolecules Assembled by DNA Origami. *J. Am. Chem. Soc.* 138, 5495-5498, doi:10.1021/jacs.6b00958 (2016).
- 75 Dutta, P. K. et al. DNA-Directed Artificial Light-Harvesting Antenna. *J. Am. Chem. Soc.* 133, 11985-11993, doi:10.1021/Ja1115138 (2011).
- 76 Wong, N. Y., Xing, H., Tan, L. H. & Lu, Y. Nano-Encrypted Morse Code: A Versatile Approach to Programmable and Reversible Nanoscale Assembly and Disassembly. *J. Am. Chem. Soc.* 135, 2931-2934, doi:10.1021/ja3122284 (2013).
- 77 Linko, V., Eerikainen, M. & Kostainen, M. A. A modular DNA origami-based enzyme cascade nanoreactor. *Chem. Commun.* 51, 5351-5354, doi:10.1039/C4cc08472a (2015).
- 78 Zhang, T. et al. DNA-Based Self-Assembly of Fluorescent Nanodiamonds. *J. Am. Chem. Soc.* 137, 9776-9779, doi:10.1021/jacs.5b04857 (2015).
- 79 Rinker, S., Ke, Y. G., Liu, Y., Chhabra, R. & Yan, H. Self-assembled DNA nanostructures for distance-dependent multivalent ligand-protein binding. *Nat. Nanotechnol.* 3, 418-422, doi:10.1038/nnano.2008.164 (2008).
- 80 Godonoga, M. et al. A DNA aptamer recognising a malaria protein biomarker can function as part of a DNA origami assembly. *Sci Rep-Uk* 6, doi:10.1038/Srep21266 (2016).
- 81 Sprengel, A. et al. Tailored protein encapsulation into a DNA host using geometrically organized supramolecular interactions. *Nat. Commun.* 8, doi:10.1038/Ncomms14472 (2017).
- 82 Chithrani, B. D., Ghazani, A. A. & Chan, W. C. W. Determining the size and shape

- dependence of gold nanoparticle uptake into mammalian cells. *Nano Lett.* 6, 662-668, doi:10.1021/nl052396o (2006).
- 83 Zaleska-Medynska, A., Marchelek, M., Diak, M. & Grabowska, E. Noble metal-based bimetallic nanoparticles: the effect of the structure on the optical, catalytic and photocatalytic properties. *Adv Colloid Interfac.* 229, 80-107, doi:10.1016/j.cis.2015.12.008 (2016).
 - 84 Rother, M., Nussbaumer, M. G., Renggli, K. & Bruns, N. Protein cages and synthetic polymers: a fruitful symbiosis for drug delivery applications, bionanotechnology and materials science. *Chem. Soc. Rev.* 45, 6213-6249, doi:10.1039/c6cs00177g (2016).
 - 85 Voigt, N. V. et al. Single-molecule chemical reactions on DNA origami. *Nat. Nanotechnol.* 5, 200-203, doi:10.1038/Nnano.2010.5 (2010).
 - 86 Helmi, S., Ziegler, C., Kauert, D. J. & Seidel, R. Shape-Controlled Synthesis of Gold Nanostructures Using DNA Origami Molds. *Nano Lett.* 14, 6693-6698, doi:10.1021/nl503441v (2014).
 - 87 Sun, W. et al. Casting inorganic structures with DNA molds. *Science* 346, 717-+, doi:Artn 125836110.1126/Science.1258361 (2014).
 - 88 Yang, Y. et al. Self-assembly of size-controlled liposomes on DNA nanotemplates. *Nat.Chem.* 8, 476-483, doi:10.1038/Nchem.2472 (2016).
 - 89 Zhang, Z., Yang, Y., Pincet, F., Llaguno, M. C. & Lin, C. X. Placing and shaping liposomes with reconfigurable DNA nanocages. *Nat. Chem.* 9, 653-659, doi:10.1038/Nchem.2802 (2017).
 - 90 Zhang, Y. N. et al. Transfer of Two-Dimensional Oligonucleotide Patterns onto Stereocontrolled Plasmonic Nanostructures through DNA-Origami-Based Nanoimprinting Lithography. *Angew. Chem. Int. Edit.* 55, 8036-8040, doi:10.1002/anie.201512022 (2016).
 - 91 Song, J. et al. Direct Visualization of Transient Thermal Response of a DNA Origami. *J. Am. Chem. Soc.* 134, 9844-9847, doi:10.1021/ja3017939 (2012).
 - 92 Rajendran, A., Endo, M., Katsuda, Y., Hidaka, K. & Sugiyama, H. Photo-Cross-Linking-Assisted Thermal Stability of DNA Origami Structures and Its Application for Higher-Temperature Self-Assembly. *J. Am. Chem. Soc.* 133, 14488-14491, doi:10.1021/ja204546h (2011).
 - 93 Hahn, J., Wickham, S. F. J., Shih, W. M. & Perrault, S. D. Addressing the Instability of DNA Nanostructures in Tissue Culture. *ACS Nano* 8, 8765-8775, doi:10.1021/nn503513p (2014).
 - 94 Perrault, S. D. & Shih, W. M. Virus-Inspired Membrane Encapsulation of DNA Nanostructures To Achieve In Vivo Stability. *ACS Nano* 8, 5132-5140, doi:10.1021/nn5011914 (2014).
 - 95 Agarwal, N. P., Matthies, M., Gur, F. N., Osada, K. & Schmidt, T. L. Block Copolymer

- Micellization as a Protection Strategy for DNA Origami. *Angew. Chem. Int. Edit.* 56, 5460-5464, doi:10.1002/anie.201608873 (2017).
- 96 Ponnuswamy, N. et al. Oligolysine-based coating protects DNA nanostructures from low-salt denaturation and nuclease degradation. *Nat. Commun.* 8, doi:Artn 1565410.1038/Ncomms15654 (2017).
 - 97 Mikkila, J. et al. Virus-Encapsulated DNA Origami Nanostructures for Cellular Delivery. *Nano Lett.* 14, 2196-2200, doi:10.1021/nl500677j (2014).
 - 98 Kiviahio, J. K. et al. Cationic polymers for DNA origami coating - examining their binding efficiency and tuning the enzymatic reaction rates. *Nanoscale* 8, 11674-11680, doi:10.1039/c5nr08355a (2016).
 - 99 Wilks, T. R. et al. "Giant Surfactants" Created by the Fast and Efficient Functionalization of a DNA Tetrahedron with a Temperature-Responsive Polymer. *ACS Nano* 7, 8561-8572, doi:10.1021/nn402642a (2013).
 - 100 Knudsen, J. B. et al. Routing of individual polymers in designed patterns. *Nat. Nanotechnol.* 10, 892-898, doi:10.1038/Nnano.2015.190 (2015).
 - 101 Krissanaprasit, A. et al. Programmed Switching of Single Polymer Conformation on DNA Origami. *ACS Nano* 10, 2243-2250, doi:10.1021/acsnano.5b06894 (2016).
 - 102 Geissler, M. & Xia, Y. N. Patterning: Principles and some new developments. *Adv. Mater.* 16, 1249-1269, doi:DOI 10.1002/adma.200400835 (2004).
 - 103 Hammond, P. T. Form and Function in Multilayer Assembly: New Applications at the Nanoscale. *Adv. Mater.* 16, 1271-1293, doi:10.1002/adma.200400760 (2004).
 - 104 Kim, P. et al. Soft lithographic patterning of supported lipid bilayers onto a surface and inside microfluidic channels. *Lab Chip* 6, 54-59, doi:10.1039/b512593f (2006).
 - 105 Zhang, T. et al. DNA-Based Self-Assembly of Fluorescent Nanodiamonds. *J. Am. Chem. Soc.*, doi:10.1021/jacs.5b04857 (2015).
 - 106 Schreiber, R. et al. Hierarchical assembly of metal nanoparticles, quantum dots and organic dyes using DNA origami scaffolds. *Nat. Nanotechnol.* 9, 74-78, doi:Doi 10.1038/Nnano.2013.253 (2014).
 - 107 Fu, J. L. et al. Multi-enzyme complexes on DNA scaffolds capable of substrate channelling with an artificial swinging arm. *Nat. Nanotechnol.* 9, 531-536, doi:Doi 10.1038/Nnano.2014.100 (2014).
 - 108 Sacca, B. et al. Orthogonal Protein Decoration of DNA Origami. *Angew. Chem. Int. Edit.* 49, 9378-9383, doi:DOI 10.1002/anie.201005931 (2010).
 - 109 Lin, C. X. et al. Submicrometre geometrically encoded fluorescent barcodes self-assembled from DNA. *Nat. Chem.* 4, 832-839, doi:Doi 10.1038/Nchem.1451 (2012).
 - 110 Wang, Z. G., Liu, Q. & Ding, B. Q. Shape-Controlled Nanofabrication of Conducting Polymer on Planar DNA Templates. *Chem. Mater.* 26, 3364-3367,

- doi:10.1021/cm501445u (2014).
- 111 Siegwart, D. J., Oh, J. K. & Matyjaszewski, K. ATRP in the design of functional materials for biomedical applications. *Prog. Polym. Sci.* 37, 18-37, doi:DOI 10.1016/j.progpolymsci.2011.08.001 (2012).
 - 112 Matyjaszewski, K. & Tsarevsky, N. V. Nanostructured functional materials prepared by atom transfer radical polymerization. *Nat. Chem.* 1, 276-288, doi:Doi 10.1038/Nchem.257 (2009).
 - 113 Averick, S. E., Dey, S. K., Grahacharya, D., Matyjaszewski, K. & Das, S. R. Solid-phase incorporation of an ATRP initiator for polymer-DNA biohybrids. *Angew. Chem. Int. Ed. Engl* 53, 2739-2744, doi:10.1002/anie.201308686 (2014).
 - 114 Ryan, S. M., Mantovani, G., Wang, X. X., Haddleton, D. M. & Brayden, D. J. Advances in PEGylation of important biotech molecules: delivery aspects. *Expert Opin. Drug Del.* 5, 371-383, doi:Doi 10.1517/17425247.5.4.371 (2008).
 - 115 Stahl, E., Martin, T. G., Praetorius, F. & Dietz, H. Facile and Scalable Preparation of Pure and Dense DNA Origami Solutions. *Angew. Chem. Int. Ed.* 53, 12735-12740, doi:10.1002/anie.201405991 (2014).
 - 116 Bontempo, D. & Maynard, H. D. Streptavidin as a macroinitiator for polymerization: In situ protein-polymer conjugate formation. *J. Am. Chem. Soc.* 127, 6508-6509, doi:Doi 10.1021/Ja042230+ (2005).
 - 117 Min, K., Gao, H. F. & Matyjaszewski, K. Use of ascorbic acid as reducing agent for synthesis of well-defined polymers by ARGET ATRP. *Macromolecules* 40, 1789-1791, doi:10.1021/ma0702041 (2007).
 - 118 Tokura, Y. et al. Bottom-Up Fabrication of Nanopatterned Polymers on DNA Origami by In Situ Atom-Transfer Radical Polymerization. *Angew. Chem. Int. Edit.* 55, 5692-+, doi:10.1002/anie.201511761 (2016).
 - 119 List, J., Weber, M. & Simmel, F. C. Hydrophobic Actuation of a DNA Origami Bilayer Structure. *Angew. Chem. Int. Ed.* 53, 4236-4239, doi:10.1002/anie.201310259 (2014).
 - 120 Kim, H., Surwade, S. P., Powell, A., O'Donnell, C. & Liu, H. T. Stability of DNA Origami Nanostructure under Diverse Chemical Environments. *Chem. Mater.* 26, 5265-5273, doi:10.1021/cm5019663 (2014).
 - 121 Shen, X. B. et al. Rolling Up Gold Nanoparticle-Dressed DNA Origami into Three-Dimensional Plasmonic Chiral Nanostructures. *J. Am. Chem. Soc.* 134, 146-149, doi:10.1021/ja209861x (2012).
 - 122 Fu, Y. M. et al. Single-Step Rapid Assembly of DNA Origami Nanostructures for Addressable Nanoscale Bioreactors. *J. Am. Chem. Soc.* 135, 696-702, doi:10.1021/ja3076692 (2013).
 - 123 Travascio, P., Li, Y. F. & Sen, D. DNA-enhanced peroxidase activity of a DNA

- aptamer-hemin complex. *Chem. Biol.* 5, 505-517, doi:10.1016/S1074-5521(98)90006-0 (1998).
- 124 Lee, H., Dellatore, S. M., Miller, W. M. & Messersmith, P. B. Mussel-inspired surface chemistry for multifunctional coatings. *Science* 318, 426-430, doi:10.1126/science.1147241 (2007).
 - 125 Della Vecchia, N. F. et al. Building-Block Diversity in Polydopamine Underpins a Multifunctional Eumelanin-Type Platform Tunable Through a Quinone Control Point. *Adv. Funct. Mater.* 23, 1331-1340, doi:10.1002/adfm.201202127 (2013).
 - 126 Liebscher, J. et al. Structure of Polydopamine: A Never-Ending Story? *Langmuir* 29, 10539-10548, doi:10.1021/la4020288 (2013).
 - 127 Liu, Y. L., Ai, K. L. & Lu, L. H. Polydopamine and Its Derivative Materials: Synthesis and Promising Applications in Energy, Environmental, and Biomedical Fields. *Chem Rev* 114, 5057-5115, doi:10.1021/cr400407a (2014).
 - 128 Linko, V. et al. DNA-Based Enzyme Reactors and Systems. *Nanomaterials-Basel* 6, doi:10.3390/nano6080139 (2016).
 - 129 Jiang, Q. et al. DNA Origami as a Carrier for Circumvention of Drug Resistance. *J. Am. Chem. Soc.* 134, 13396-13403, doi:10.1021/ja304263n (2012).
 - 130 Zhang, Q. et al. DNA Origami as an In Vivo Drug Delivery Vehicle for Cancer Therapy. *ACS Nano* 8, 6633-6643, doi:10.1021/nn502058j (2014).
 - 131 Halley, P. D. et al. Daunorubicin-Loaded DNA Origami Nanostructures Circumvent Drug-Resistance Mechanisms in a Leukemia Model. *Small* 12, 308-320, doi:10.1002/sml.201502118 (2016).
 - 132 Sugawara, Y., Tamaki, T., Ohashi, H. & Yamaguchi, T. Control of the poly(N-isopropylacrylamide) phase transition via a single strand-double strand transformation of conjugated DNA. *Soft Matter* 9, 3331-3340, doi:10.1039/c3sm27230c (2013).
 - 133 Mok, H. & Park, T. G. PEG-assisted DNA solubilization in organic solvents for preparing cytosol specifically degradable PEG/DNA nanogels. *Bioconjugate. Chem.* 17, 1369-1372, doi:10.1021/bc060119i (2006).
 - 134 Chen, W., Gerasimov, J. Y., Zhao, P., Liu, K. & Herrmann, A. High-Density Noncovalent Functionalization of DNA by Electrostatic Interactions. *J. Am. Chem. Soc.* 137, 12884-12889, doi:10.1021/jacs.5b05432 (2015).
 - 135 Lee, H., Dellatore, S. M., Miller, W. M. & Messersmith, P. B. Mussel-inspired surface chemistry for multifunctional coatings. *Science* 318, 426-430, doi:10.1126/science.1147241 (2007).
 - 136 Liu, R., Guo, Y. L., Odusote, G., Qu, F. L. & Priestley, R. D. Core-Shell Fe₃O₄ Polydopamine Nanoparticles Serve Multipurpose as Drug Carrier, Catalyst Support and Carbon Adsorbent. *ACS Appl. Mater. Inter.* 5, 9167-9171,

- doi:10.1021/am402585y (2013).
- 137 Lynge, M. E., van der Westen, R., Postma, A. & Städler, B. Polydopamine—a nature-inspired polymer coating for biomedical science. *Nanoscale* 3, 4916, doi:10.1039/c1nr10969c (2011).
 - 138 Chien, H. W., Kuo, W. H., Wang, M. J., Tsai, S. W. & Tsai, W. B. Tunable Micropatterned Substrates Based on Poly(dopamine) Deposition via Microcontact Printing. *Langmuir* 28, 5775-5782, doi:10.1021/la300147p (2012).
 - 139 Ding, Y. H., Floren, M. & Tan, W. Mussel-inspired polydopamine for bio-surface functionalization. *Biosurface and Biotribology* 2, 121-136, doi:10.1016/j.bsbt.2016.11.001 (2016).
 - 140 Golub, E., Albada, H. B., Liao, W. C., Biniuri, Y. & Willner, I. Nucleoapzymes: Hemin/G-Quadruplex DNAzyme-Aptamer Binding Site Conjugates with Superior Enzyme-like Catalytic Functions. *J. Am. Chem. Soc.* 138, 164-172, doi:10.1021/jacs.5b09457 (2016).
 - 141 Albada, H. B., Golub, E. & Willner, I. Rational design of supramolecular hemin/G-quadruplex-dopamine aptamer nucleoapzyme systems with superior catalytic performance. *Chem. Sci.* 7, 3092-3101, doi:10.1039/c5sc04832j (2016).
 - 142 Li, J. et al. Dramatic enhancement of the detection limits of bioassays via ultrafast deposition of polydopamine. *Nat. Biomed. Eng.* 1, 0082, doi:10.1038/s41551-017-0082 (2017).
 - 143 Chen, H. R. et al. Dynamic and Progressive Control of DNA Origami Conformation by Modulating DNA Helicity with Chemical Adducts. *ACS Nano* 10, 4989-4996, doi:10.1021/acsnano.6b01339 (2016).
 - 144 List, J., Weber, M. & Simmel, F. C. Hydrophobic Actuation of a DNA Origami Bilayer Structure. *Angew. Chem. Int. Edit.* 53, 4236-4239, doi:10.1002/anie.201310259 (2014).
 - 145 Rafat, A. A., Pirzer, T., Scheible, M. B., Kostina, A. & Simmel, F. C. Surface-Assisted Large-Scale Ordering of DNA Origami Tiles. *Angew. Chem. Int. Edit.* 53, 7665-7668, doi:10.1002/anie.201403965 (2014).
 - 146 Gopinath, A. & Rothmund, P. W. K. Optimized Assembly and Covalent Coupling of Single-Molecule DNA Origami Nano arrays. *ACS Nano* 8, 12030-12040, doi:10.1021/nn506014s (2014).
 - 147 Hung, A. M. et al. Large-area spatially ordered arrays of gold nanoparticles directed by lithographically confined DNA origami. *Nat. Nanotechnol.* 5, 121-126, doi:10.1038/Nnano.2009.450 (2010).
 - 148 Ng, D. Y. W., Wu, Y. Z., Kuan, S. L. & Weil, T. Programming Supramolecular Biohybrids as Precision Therapeutics. *Accounts Chem. Res.* 47, 3471-3480, doi:10.1021/ar5002445 (2014).

- 149 Mishra, A., Ma, C. Q. & Bauerle, P. Functional Oligothiophenes: Molecular Design for Multidimensional Nanoarchitectures and Their Applications. *Chem. Rev.* 109, 1141-1276, doi:10.1021/cr8004229 (2009).
- 150 Krenzel, E. S., Chen, Z. J. & Hamilton, J. A. Correspondence of Fatty Acid and Drug Binding Sites on Human Serum Albumin: A Two-Dimensional Nuclear Magnetic Resonance Study (vol 52, pg 1559, 2013). *Biochemistry-Us* 52, 2382-2382, doi:10.1021/bi400314u (2013).
- 151 Yoshimori, T., Yamamoto, A., Moriyama, Y., Futai, M. & Tashiro, Y. Bafilomycin-A1, a Specific Inhibitor of Vacuolar-Type H⁺-ATPase, Inhibits Acidification and Protein-Degradation in Lysosomes of Cultured-Cells. *J Biol. Chem.* 266, 17707-17712 (1991).
- 152 Fulda, S., Galluzzi, L. & Kroemer, G. Targeting mitochondria for cancer therapy. *Nat. Rev. Drug Discov.* 9, 447-464, doi:10.1038/nrd3137 (2010).
- 153 Tanaka, A. et al. Cancer Cell Death Induced by the Intracellular Self-Assembly of an Enzyme-Responsive Supramolecular Gelator. *J. Am. Chem. Soc.* 137, 770-775, doi:10.1021/ja510156v (2015).
- 154 Rowe, M. A., Hammer, B. A. G. & Boyes, S. G. Synthesis of surface-initiated stimuli-responsive diblock copolymer brushes utilizing a combination of ATRP and RAFT polymerization techniques. *Macromolecules* 41, 4147-4157, doi:10.1021/ma800154c (2008).
- 155 Foster, E. L., Tria, M. C. R., Pernites, R. B., Addison, S. J. & Advincula, R. C. Patterned polymer brushes via electrodeposited ATRP, ROMP, and RAFT initiators on colloidal template arrays. *Soft Matter.* 8, 353-359, doi:10.1039/c1sm06406a (2012).
- 156 Hammer, B. A. G. et al. Controlling Cellular Uptake and Toxicity of Polyphenylene Dendrimers by Chemical Functionalization. *Chembiochem* 18, 960-964, doi:10.1002/cbic.201700079 (2017).
- 157 Chen, C. Y. & Liu, Q. Virus-like particles with tunable morphology derived from amphiphilic polyplexes. *Soft Mater.* 15, 191-195, doi:10.1080/1539445X.2017.1307223 (2017).
- 158 Yang, Y. Y., Endo, M., Hidaka, K. & Sugiyama, H. Photo-Controllable DNA Origami Nanostructures Assembling into Predesigned Multiorientational Patterns. *J. Am. Chem. Soc.* 134, 20645-20653, doi:10.1021/ja307785r (2012).
- 159 Takenaka, T. et al. Photoresponsive DNA Nanocapsule Having an Open/Close System for Capture and Release of Nanomaterials. *Chem-Eur. J* 20, 14951-14954, doi:10.1002/chem.201404757 (2014).
- 160 Kuzyk, A. et al. A light-driven three-dimensional plasmonic nanosystem that translates molecular motion into reversible chiroptical function. *Nat. Commun.* 7,

doi:Artn 1059110.1038/Ncomms10591 (2016).

6. Publications

In the following are the reprints of manuscripts. The reprints were made with permission of the relative journal. Furthermore, the copyrights are given on the respective cover and information of the contribution of the respective authors is listed.

[6-1] Bottom-Up Fabrication of Nanopatterned Polymers on DNA Origami by In Situ Atom-Transfer Radical Polymerization

Yu Tokura⁺, Yanyan Jiang⁺, Alexander Welle, Martina H. Stenzel, Katarzyna M. Krzemien, Jens Michaelis, Rüdiger Berger, Christopher Barner-Kowollik, Yuzhou Wu,^{*} and Tanja Weil^{*}

⁺ shared first authorship, ^{*} corresponding author

Published in Angew. Chem. Int. Ed. 2016, 55, 5692–5697

Copyright: Reproduced by permission of the publisher John Wiley and Sons.

Abstract:

Bottom-up strategies to fabricate patterned polymers at the nanoscale represent an emerging field in the development of advanced nanodevices, such as biosensors, nanofluidics, and nanophotonics. DNA origami techniques provide access to distinct architectures of various sizes and shapes and present manifold opportunities for functionalization at the nanoscale with the highest precision. Herein, we conduct in situ atom transfer radical polymerization (ATRP) on DNA origami, yielding differently nanopatterned polymers of various heights. After cross-linking, the grafted polymeric nanostructures can even stably exist in solution without the DNA origami template. This straightforward approach allows for the fabrication of patterned polymers with low nanometer resolution, which provides access to unique DNA-based functional hybrid materials.

Contribution of the respective authors:

Yu Tokura: Design and synthesis of DNA origami and ATRP-initiator modified DNA, conducting surface-initiated ATRP on DNA origami, Agarose gel electrophoresis study, extracting crosslinked polymers from DNA origami, AFM study and analysis, writing the manuscript

Yanyan Jiang: Synthesis of ATRP-initiator modified DNA, optimizing the polymerization condition on DNA origami, writing the manuscript

Alexander Welle: ToF-SIMS study, analysis, and discussion on the results

Martina H. Stenzel: Results discussion, correcting the manuscript

Katarzyna M. Krzemien: Optimization and assist of AFM study

Jens Michaelis: Assist of AFM study and discussing on the results, correcting the manuscript

Christopher Barner-Kowollik: Interpretation of the ToF-SIMS experiments, correcting the manuscript

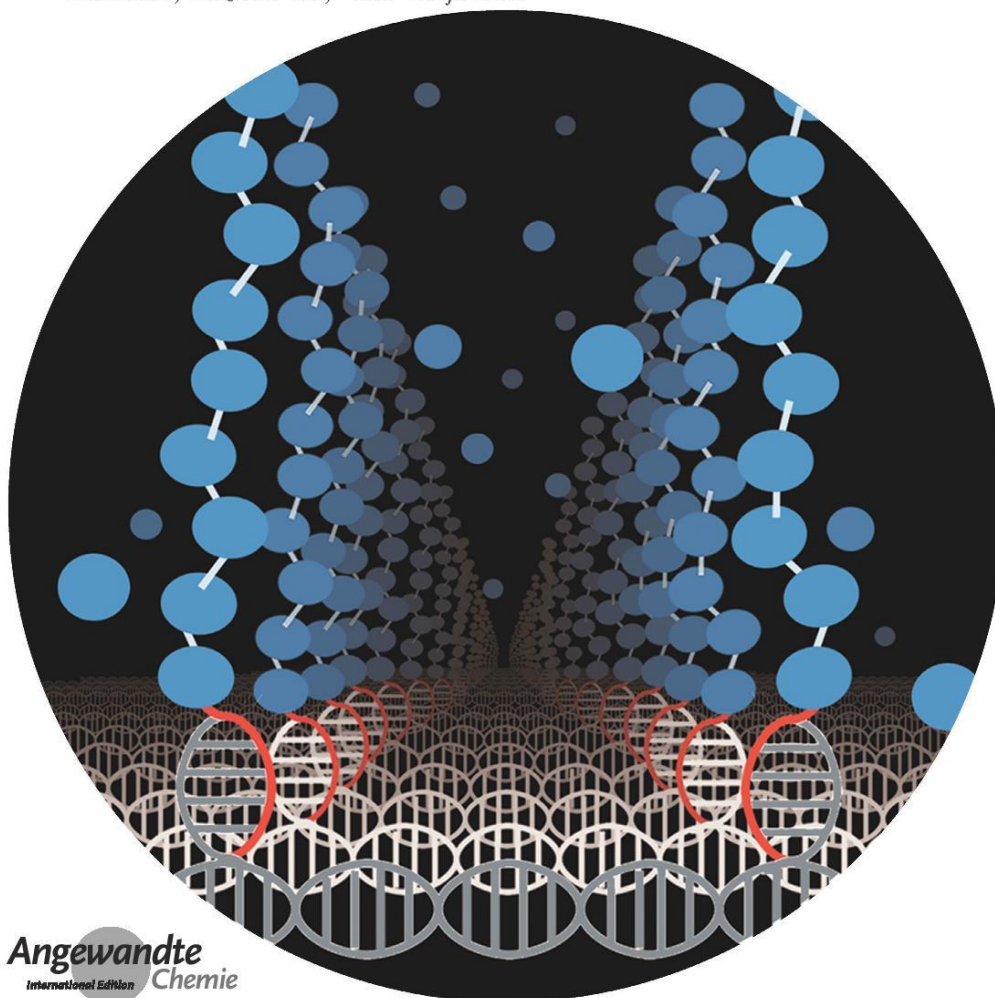
Rüdiger Berger: Assist of nanomechanical property mapping study with AFM, discussion on the results

Yuzhou Wu: Discussion on the concept and results, writing and correcting the manuscript

Tanja Weil: Acquiring funding for the project, design and discussion of the concept and results, writing and correcting the manuscript.

Bottom-Up Fabrication of Nanopatterned Polymers on DNA Origami by In Situ Atom-Transfer Radical Polymerization

Yu Tokura⁺, Yanyan Jiang⁺, Alexander Welle, Martina H. Stenzel, Katarzyna M. Krzemien, Jens Michaelis, Rüdiger Berger, Christopher Barner-Kowollik, Yuzhou Wu,^{*} and Tanja Weil^{*}



Abstract: Bottom-up strategies to fabricate patterned polymers at the nanoscale represent an emerging field in the development of advanced nanodevices, such as biosensors, nanofluidics, and nanophotonics. DNA origami techniques provide access to distinct architectures of various sizes and shapes and present manifold opportunities for functionalization at the nanoscale with the highest precision. Herein, we conduct *in situ* atom-transfer radical polymerization (ATRP) on DNA origami, yielding differently nanopatterned polymers of various heights. After cross-linking, the grafted polymeric nanostructures can even stably exist in solution without the DNA origami template. This straightforward approach allows for the fabrication of patterned polymers with low nanometer resolution, which provides access to unique DNA-based functional hybrid materials.

Nanofabrication refers to a process that generates patterned structures with a typical resolution of less than 100 nm. The nanopatterning of densely grafted polymers is vitally important to numerous modern technologies, for example, biochips for cell-growth control, micro/nanofluidic systems, and photonic crystal materials.^[1] Currently available techniques are mainly based on top-down strategies, such as lithography, which has several limitations, including high instrumental costs and long operation times. Bottom-up strategies in principle enable the fast fabrication of dense polymers. To date, it is still highly challenging to fabricate patterned polymers by bottom-up approaches with low-nanometer resolution. Substantial efforts have been made to induce polymer self-assembly by side-chain supramolecular recognition,^[2] although it is impractical to flexibly design the patterns with nanoscale precision. Alternatively, biomacromolecules with regular periodic structures, such as virus capsids, have been derived as reactors allowing for controlled polymerization in their confined nanosized interior cavities.^[3] However, the sizes and shapes of polymer structures are seldom tunable by such processes owing to the fixed 3D structures of proteins. On the other hand, DNA is a highly tunable material to create nanostructures. The precise design of artificial DNA sequences and computer-assisted predictions of DNA double-helix folding provide access to a large

variety of arbitrary 2D and 3D nanostructures, denoted as DNA origami.^[4] This technique has been investigated extensively for the bottom-up nanopatterning of proteins,^[5] nanoparticles,^[6] and chromophores.^[7] Very recently, conductive polymers containing oligonucleotide side chains were successfully assembled on DNA origami by a predefined route.^[8] Furthermore, various functional moieties can be incorporated into DNA origami to perform surface-initiated chemical reactions and be characterized by atomic force microscopy (AFM).^[9] In this context, capitalizing on DNA origami as a template for the bottom-up fabrication of precise polymer nanopatterns is highly valuable compared to existing systems.

In the current study, we report an *in situ* polymerization reaction on a DNA origami scaffold for the first time. *In situ*, or so-called “grafting from” polymerization, offers great opportunities as a method that is often more efficient and leads to denser polymers than the “grafting to” approach, in which polymers are directly conjugated to the surface, resulting sometimes in lower densities because of steric hindrance.^[10]

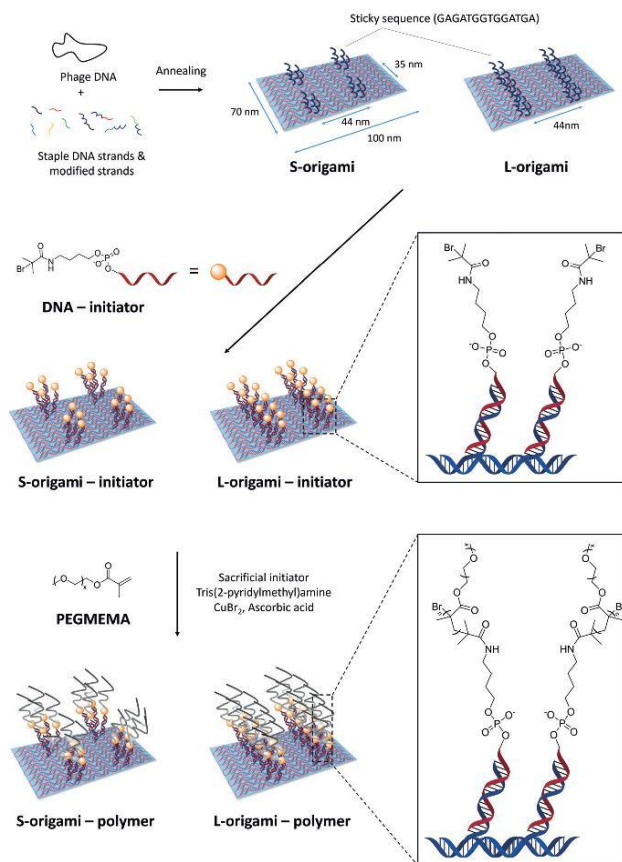
Atom-transfer radical polymerization (ATRP) was selected as a suitable method for polymerization on DNA origami. ATRP is a method of choice to obtain defined polymers with controlled molecular weights, narrow polydispersities, and chain-end functionalities. The reactions proceed in aqueous solution at ambient temperature, which is essential for the stability of the DNA origami structure, and they are applicable to a variety of monomers.^[11] To design the nanopatterned ATRP initiators, rectangular DNA origami with dimensions of 70 nm × 100 nm was prepared from the single-stranded M13mp18 DNA and modified staples (see the Supporting Information, Scheme 1 and Figure S1).^[12] Modified staples have additional sequences of 15 nt at the 3' ends, which are referred to as “sticky sequences” and extend from the surface of the DNA origami. By selecting different modified staples, two different DNA origami patterns were designed: one with two lines (L-origami) and one with four spots (S-origami). To the sticky sequences on these DNA origami patterns, complementary DNA strands with end ATRP-initiator groups (DNA initiator) were hybridized to form the DNA origami macroinitiator (L-origami initiator

[*] Y. Tokura,^[1] Y. Jiang,^[1] Dr. Y. Wu, Prof. T. Weil
Organic Chemistry III
Macromolecular Chemistry and Biomaterials, Ulm University
Albert-Einstein-Allee 11, 89081 Ulm (Germany)
E-mail: yuzhou.wu@uni-ulm.de
tanja.weil@uni-ulm.de
Y. Jiang,^[1] Prof. M. H. Stenzel
Centre for Advanced Macromolecular Design (CAMD)
School of Chemistry, University of New South Wales
Sydney, NSW 2052 (Australia)
Dr. A. Welle, Prof. C. Barner-Kowollik
Preparative Macromolecular Chemistry
Institute for Technical Chemistry and Polymer Chemistry
Karlsruhe Institute of Technology (KIT)
Engesserstrasse 18, 76131 Karlsruhe (Germany)
and
Institute for Biological Interfaces
Karlsruhe Institute of Technology (KIT)

Hermann-von-Helmholtz-Platz 1
76344 Eggenstein-Leopoldshafen (Germany)
Dr. A. Welle
Karlsruhe Nano Micro Facility
Karlsruhe Institute of Technology (KIT)
Hermann-von-Helmholtz-Platz 1
76344 Eggenstein-Leopoldshafen (Germany)
K. M. Krzemien, Prof. J. Michaelis
Institute of Biophysics, Ulm University
Albert-Einstein-Allee 11, 89081 Ulm (Germany)
Dr. R. Berger
Max Planck Institute for Polymer Research
Ackermannweg 10, 55128 Mainz (Germany)

[*] These authors contributed equally to this work.

Supporting information for this article can be found under:
<http://dx.doi.org/10.1002/anie.201511761>.



Scheme 1. In situ ATRP on DNA origami.

and S-origami initiator). Although these two patterns were selected as representative examples, even more complicated patterns could be designed following the same approach.

To explore ATRP reactions on DNA origami, the polymerization of poly(ethylene glycol) methyl ether methacrylate (PEGMEMA) was selected owing to its biocompatibility and wide applications in bionanotechnology.^[12] Furthermore, the bulky side chain of PEG on the grafted polymer facilitates monitoring the polymer growth on the DNA origami surface by AFM. In solution-based ATRP, the initiator concentration is known to play a pivotal role during the polymerization reaction.^[13] Through a systematic examination of the reaction conditions, we found that the reaction only occurred when the initiator concentration was above 10 μM (Figure S2). However, such a high concentration of DNA origami macroinitiators could not be achieved in the

reaction mixture owing to the extremely high molecular weight of the DNA origami and the increasing solution viscosity.^[14] To overcome this challenge, sacrificial initiators were employed to increase the initiator concentration in the reaction solution, which allowed the generation of a persistent concentration of radicals to establish an ATRP equilibrium. A similar strategy has been reported by Maynard et al.^[13] for ATRP reactions with the protein streptavidin as the macroinitiator molecule. Generally, the entire polymerization process was performed in a reaction volume of 20 μL consisting of the DNA origami macroinitiator (50 nM) and the sacrificial DNA initiator (33 μM) in a ratio of 1:665, PEGMEMA (average $M_n = 300$), CuBr_2 , and tris(2-pyridylmethyl)amine (TPMA). The reaction mixture was degassed by the freeze-pump-thaw method, which was followed by continuous slow addition of ascorbic acid to generate the reactive catalyst species (Figure S3). After the reaction, the free polymer chains grown from the sacrificial initiators, the catalysts, and unreacted monomers were removed

by the PEG-induced precipitation method,^[14] and the products (L-origami-polymer and S-origami-polymer) were characterized by agarose gel electrophoresis (AGE) and AFM. AGE analysis showed the different mobility of the DNA origami band (Figure S4). Furthermore, we observed the appearance of new objects at ATRP-initiator-immobilized positions on the DNA origami by AFM (Figure 1). According to the

height profile analysis, the average height increase of the DNA origami was $0.55 \text{ nm} \pm 0.02 \text{ nm}$ (standard error, S.E.) for L-origami-polymer and $0.56 \pm 0.02 \text{ nm}$ for S-origami-polymer. Quantitative nanomechanical property mapping (QNM) by AFM revealed that the formed objects have different mechanical properties than the original DNA origami (i.e., a lower Young's modulus and higher adhesion to silicon nitride cantilever), which correspond to the typical surface properties of a polymeric material (softer and more hydrophobic than DNA; Figure 1b). Together these results indicate the successful polymer growth from DNA origami at the desired positions. Remarkably, during the AFM measurement, almost all of the L-origami-polymer deposited on mica showed the polymer-grown surface upside, and hardly any plain surfaces were observed (Figure 1 and Figure S5a). On the other hand, 51 % of the S-origami-polymer molecules

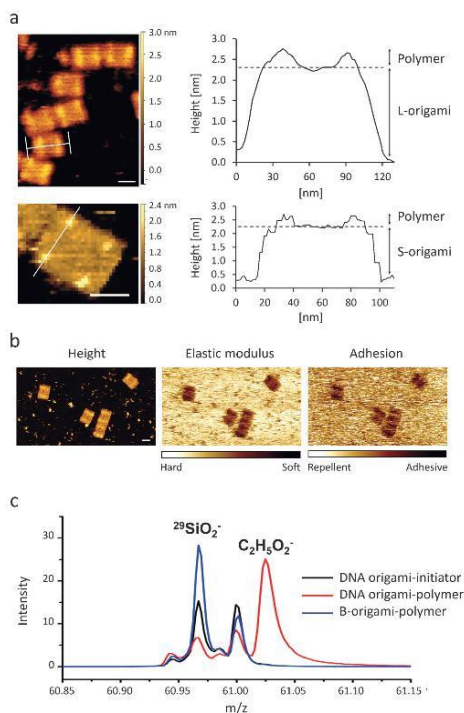


Figure 1. a) AFM images and height profiles of L-origami-polymer (top) and S-origami-polymer (bottom). Scale bars: 50 nm. b) QNM images of L-origami-polymer. c) ToF-SIMS spectrum. $^{29}\text{SiO}_2^-$ peaks are due to the mica surface.

were observed to have a polymer surface whereas the others were shown as plain surfaces (Figure S5b). Considering that DNA origami has two surfaces, namely the initiator-immobilized surface and the unmodified plain surface, this result indicates that the grafted polymers had an evident impact on the surface properties of the DNA origami (e.g., in terms of charge, surface topology, and hydrophobicity), thus resulting in a favorable deposition of the negatively charged plain origami side of the L-origami-polymer onto the positively charged mica surface over the polymer-grown side (Figure S5c). In the case of S-origami, the polymer coverage area is three times smaller than for L-origami, and therefore, the surface properties of S-origami were not altered as significantly as those of L-origami, thus no significant orientation preference was observed. This observation is consistent with previous reports by other groups that 2D DNA origami with significant surface decoration will have preferential orientations of deposition.^[5]

To further confirm the successful polymerization on DNA origami by a spectrometric method, time-of-flight secondary ion mass spectrometry (ToF-SIMS) analysis was performed.

As shown in Figure 1c, the secondary ion derived from the end group of the PEG chain ($\text{C}_2\text{H}_5\text{O}_2^-$) was detected in the purified DNA origami-polymer sample deposited on mica, but not in the sample obtained before the reaction (red and black line in Figure 1c). As the control, DNA origami without modified staples (B-origami) was prepared, mixed with the DNA initiator, and exposed to the same polymerization and purification process (B-origami-polymer, blue line, see Figure S6, Figure S7, and Table S1), from which only significant PO_3^- and PO_2^- fragments from DNA species were detected, and no PEG chain peaks were observed. This result clearly indicates that the polymers did not adhere to DNA origami by non-specific interactions.

A major advantage of the bottom-up strategy is the straightforward control of the polymer length without decreasing the conjugation efficiency.^[10d] We demonstrated that by changing the molar monomer/initiator ratios (the total amount of initiator in the reaction system), the degree of polymer growth could be tuned. As shown in Figure 2, by

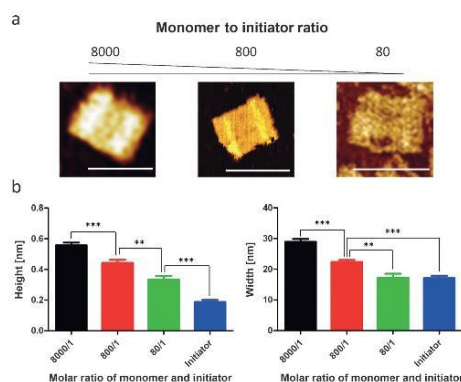


Figure 2. a) AFM images of the polymers on the origami structure made with different monomer/initiator ratios. Scale bars: 100 nm. The average height (b) and width (c) of the grafted polymers on L-origami decrease with a decreasing monomer/initiator ratio. Data represent means \pm S.E., $n = 17$. **: $p < 0.001$; ***: $p < 0.0001$.

using monomer/initiator ratios of 8000:1, 800:1, and 80:1, polymers with significantly different heights and widths were obtained. A ratio of 80:1 only gave very thin polymers with an increased height profile ($0.33 \text{ nm} \pm 0.02 \text{ nm}$). Increasing the monomer concentration to ratios of 800:1 and 8000:1 resulted in an increase in the heights of the polymer layers by $0.44 \text{ nm} \pm 0.02 \text{ nm}$ and $0.55 \text{ nm} \pm 0.02 \text{ nm}$, respectively. However, these heights are still significantly shorter than the distances between adjacent initiator positions (5.8 nm), indicating that the polymers should adopt a mushroom-like collapsed structure.^[15]

Finally, to demonstrate the unique prospects of the grafting from polymerization approach, we investigated whether the architecture of the grafted polymeric nano-

structures templated by DNA origami could be preserved in the absence of the origami scaffold. This time, PEGMEMA was polymerized on L-origami by the established method in the presence of a cross-linker molecule, PEG dimethacrylate (PEGDMA, average $M_n = 750$; Figure 3a). The cross-linked

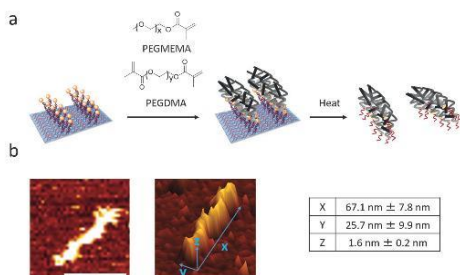


Figure 3. a) Extraction of the cross-linked polymer nanostructure. b) Corresponding AFM image of the cross-linked polymer after decomposition of the DNA origami scaffold (left), 3D view (middle), and the parameters in each direction (right). Scale bar: 50 nm.

polymers had the same shapes and properties on the DNA origami as the polymers that were obtained in the absence of the cross-linker (Figure S8). To remove the DNA origami template, the sample was diluted by a factor of 50 by the addition of water and incubated overnight at 60 °C. The stability of DNA origami is significantly affected by the temperature as well as the Mg^{2+} concentration in the buffer solution. According to AFM, only the cross-linked polymeric structure remained, and no DNA origami structures were observed (Figure 3b and Figure S9). Therefore, this treatment was sufficient to decompose the DNA origami scaffold. The average lengths and widths of the cross-linked polymers were about 67.1 nm \pm 7.8 nm and 25.7 nm \pm 9.9 nm, respectively. Considering statistical errors, these dimensions are identical to the lengths and widths of the polymers present before removal of the DNA template (length: 68.6 nm \pm 1.1 nm; width: 25.3 nm \pm 1.0 nm; Figure S8).

In conclusion, the bottom-up fabrication of polymers with precisely designed nanopatterns on a DNA origami template scaffold by in situ ATRP has been reported for the first time. The success of the polymerization was confirmed by AGE, AFM, QNM, and ToF-SIMS. With different surface coverages of the grafted polymers, the surface properties of the DNA origami were altered as demonstrated by their different affinities to mica surfaces and nanomechanical properties. Furthermore, the degree of polymerization could be tuned by varying the monomer/initiator ratio. The approach reported herein paves the way to the bottom-up fabrication of a large variety of nanoscale-patterned polymers with high density and flexibility. Polymerization from DNA origami scaffolds offers various opportunities, such as the application of cross-linkers to fix the polymeric nanostructures to remain intact even after removal of the DNA origami scaffold. In this way, a multitude of nanopatterned polymeric structures of high

precision could be grown from DNA origami and stabilized by cross-linking. As the DNA origami technique provides access to almost any arbitrary nanostructure in 2D and 3D, it could in principle be applied for the fast and flexible bottom-up manufacturing of polymers with any nanopattern, such as 2D square- and cross-shaped polymers and even 3D box- and tube-shaped polymers. Therefore, it could be attractive for a broad range of applications, including the fabrication of novel biochips and nanofluidic systems. Furthermore, modifying the different physical, chemical, and mechanical properties of polymers on DNA origami structures opens new avenues to tune the properties of DNA origami, such as increasing the stability of DNA, for example, for cellular studies or introducing additional stimulus responsiveness for developing responsive DNA materials.^[10a-c,16] Therefore, we believe that the approach reported herein will further accelerate the application of DNA origami in materials science and biomedicine.^[17]

Acknowledgements

T.W. is grateful to support by the ERC (Synergy Grant 319130-BioQ). C.B.-K. acknowledges continued funding from the Karlsruhe Institute of Technology (KIT) in the context of the Helmholtz BioInterfaces in Technology and Medicine (BIFTM) program. We thank Ulrich Ziener for critical reading of the manuscript and valuable comments.

Keywords: atom-transfer radical polymerization · DNA nanotechnology · origami nanostructures · polymerization · self-assembly

How to cite: *Angew. Chem. Int. Ed.* **2016**, *55*, 5692–5697
Angew. Chem. **2016**, *128*, 5786–5791

- [1] a) M. Geissler, Y. N. Xia, *Adv. Mater.* **2004**, *16*, 1249–1269; b) P. T. Hammond, *Adv. Mater.* **2004**, *16*, 1271–1293; c) P. Kim, S. E. Lee, H. S. Jung, H. Y. Lee, T. Kawai, K. Y. Suh, *Lab Chip* **2006**, *6*, 54–59.
- [2] M. El Garah, N. Marets, M. Mauro, A. Aliprandi, S. Bonacchi, L. De Cola, A. Ciesielski, V. Bulach, M. W. Hosseini, P. Samori, *J. Am. Chem. Soc.* **2015**, *137*, 8450–8459.
- [3] J. Lucon, S. Qazi, M. Uchida, G. J. Bedwell, B. LaFrance, P. E. Prevelige, T. Douglas, *Nat. Chem.* **2012**, *4*, 781–788.
- [4] a) P. W. Rothmund, *Nature* **2006**, *440*, 297–302; b) C. E. Castro, F. Kilchherr, D. N. Kim, E. L. Shiao, T. Wauer, P. Wortmann, M. Bathe, H. Dietz, *Nat. Methods* **2011**, *8*, 221–229; c) V. Linko, H. Dietz, *Curr. Opin. Biotechnol.* **2013**, *24*, 555–561.
- [5] a) B. Saccà, R. Meyer, M. Erkelenz, K. Kiko, A. Arndt, H. Schroeder, K. S. Rabe, C. M. Niemeyer, *Angew. Chem. Int. Ed.* **2010**, *49*, 9378–9383; *Angew. Chem.* **2010**, *122*, 9568–9573; b) J. L. Fu, Y. R. Yang, A. Johnson-Buck, M. H. Liu, Y. Liu, N. G. Walter, N. W. Woodbury, H. Yan, *Nat. Nanotechnol.* **2014**, *9*, 531–536.
- [6] a) R. Schreiber, J. Do, E. M. Roller, T. Zhang, V. J. Schüller, P. C. Nickels, J. Feldmann, T. Liedl, *Nat. Nanotechnol.* **2014**, *9*, 74–78; b) T. Zhang, A. Neumann, J. Lindlau, Y. Wu, G. Pramanik, B. Naydenov, F. Jelezko, F. Schüder, S. Huber, M. Huber, F. Stehr, A. Högele, T. Weil, T. Liedl, *J. Am. Chem. Soc.* **2015**, *137*, 9776–9779.

- [7] a) P. K. Dutta, R. Varghese, J. Nangreave, S. Lin, H. Yan, Y. Liu, *J. Am. Chem. Soc.* **2011**, *133*, 11985–11993; b) C. X. Lin, R. Jungmann, A. M. Leifer, C. Li, D. Levner, G. M. Church, W. M. Shih, P. Yin, *Nat. Chem.* **2012**, *4*, 832–839.
- [8] a) J. B. Knudsen, L. Liu, A. L. B. Kodal, M. Madsen, Q. Li, J. Song, J. B. Woehrstein, S. F. J. Wickham, M. T. Strauss, F. Schueder, J. Vinther, A. Krissanaprasit, D. Gudnason, A. A. A. Smith, R. Ogaki, A. N. Zelikin, F. Besenbacher, V. Birkedal, P. Yin, W. M. Shih, R. Jungmann, M. D. Dong, K. V. Gothelf, *Nat. Nanotechnol.* **2015**, *10*, 892–898; b) A. Krissanaprasit, M. Madsen, J. B. Knudsen, D. Gudnason, W. Surareungchai, V. Birkedal, K. V. Gothelf, *ACS Nano* **2016**, *10*, 2243–2250.
- [9] a) N. V. Voigt, T. Torring, A. Rotaru, M. F. Jacobsen, J. B. Ravnsbaek, R. Subramani, W. Mamdough, J. Kjems, A. Mokhir, F. Besenbacher, K. V. Gothelf, *Nat. Nanotechnol.* **2010**, *5*, 200–203; b) M. Endo, Y. Yang, H. Sugiyama, *Biomater. Sci.* **2013**, *1*, 347–360; c) A. H. Okholm, H. Aslan, F. Besenbacher, M. Dong, J. Kjems, *Nanoscale* **2015**, *7*, 10970–10973.
- [10] a) K. L. Heredia, D. Bontempo, T. Ly, J. T. Byers, S. Halstenberg, H. D. Maynard, *J. Am. Chem. Soc.* **2005**, *127*, 16955–16960; b) J. Liu, V. Bulmus, D. L. Herlambang, C. Barner-Kowollik, M. H. Stenzel, T. P. Davis, *Angew. Chem. Int. Ed.* **2007**, *46*, 3099–3103; *Angew. Chem.* **2007**, *119*, 3159–3163; c) P. De, M. Li, S. R. Gondi, B. S. Sumerlin, *J. Am. Chem. Soc.* **2008**, *130*, 11288; d) Y. Z. Qi, A. Chilkoti, *Polym. Chem.* **2014**, *5*, 266–276.
- [11] a) K. Matyjaszewski, N. V. Tsarevsky, *Nat. Chem.* **2009**, *1*, 276–288; b) D. J. Siegwart, J. K. Oh, K. Matyjaszewski, *Prog. Polym. Sci.* **2012**, *37*, 18–37.
- [12] S. M. Ryan, G. Mantovani, X. X. Wang, D. M. Haddleton, D. J. Brayden, *Expert Opin. Drug Delivery* **2008**, *5*, 371–383.
- [13] D. Bontempo, H. D. Maynard, *J. Am. Chem. Soc.* **2005**, *127*, 6508–6509.
- [14] E. Stahl, T. G. Martin, F. Praetorius, H. Dietz, *Angew. Chem. Int. Ed.* **2014**, *53*, 12735–12740; *Angew. Chem.* **2014**, *126*, 12949–12954.
- [15] N. Backmann, N. Kappeler, T. Braun, F. Huber, H.-P. Lang, C. Gerber, R. Y. H. Lim, *Beilstein J. Nanotechnol.* **2010**, *1*, 3–13.
- [16] L. Peng, C. Wu, M. You, D. Han, Y. Chen, T. Fu, M. Ye, W. Tan, *Chem. Sci.* **2013**, *4*, 1928–1938.
- [17] Y. Z. Wu, D. Y. W. Ng, S. L. Kuan, T. Weil, *Biomater. Sci.* **2015**, *3*, 214–230.

Received: December 19, 2015

Revised: February 5, 2016

Published online: April 5, 2016



Supporting Information

Bottom-Up Fabrication of Nanopatterned Polymers on DNA Origami by In Situ Atom-Transfer Radical Polymerization

*Yu Tokura[†], Yanyan Jiang[†], Alexander Welle, Martina H. Stenzel, Katarzyna M. Krzemien,
Jens Michaelis, Rüdiger Berger, Christopher Barner-Kowollik, Yuzhou Wu,^{*} and Tanja Weil^{*}*

anie_201511761_sm_miscellaneous_information.pdf

Table of Contents

General methods

Materials and Instruments	2
Fabrication of DNA origami	
Synthesis of DNA origami macroinitiator	
In-situ ATRP reaction	
The crosslinked polymer nanostructure extraction	
Atomic force Microscopy (<i>AFM</i>)	
Time-of-Flight Secondary Ion Mass Spectrometry (<i>ToF-SIMS</i>)	

Supplementary figures and tables

Figure S1 Design of DNA origami	5
Figure S2 Native PAGE gel of PEGMEMA polymer with DNA-initiator	
Figure S3 Home-designed device for the ATRP reaction	
Figure S4 Agarose gel electrophoresis of DNA origami before and after ATRP reaction	
Figure S5 AFM of L- and S-origami-polymer	
Figure S6 Schematic scheme of B-origami-polymer preparation	
Figure S7 Negative polarity secondary ion mass spectra	
Table S1 SIMS peak intensities, [kcts], for a constant primary ion dose of 1×10^{11} 1/cm ² , (static limit)	
Figure S8 AFM of crosslinked polymer on L-origami	
Figure S9 AFM of crosslinked polymer nanostructure after the removal of L-origami template	

References	13
-------------------	----

General methods

Materials and instruments

All solvents and chemicals were purchased from commercial sources and were used without further purification. DNA staple strands and ATRP initiator modified DNA (DNA-initiator) were synthesized by 12-Column DNA Synthesizer from POLYGEN GmbH and purified by Agilent 1260 Infinity HPLC system with Agilent Eclipse XDB-C18 column. PEGMEM (Mn = 300) and PEGDEMA (Mn = 750) monomers have been purchased from Sigma-Aldrich. Agarose gel electrophoresis was performed using Bio-Rad Mini-Sub Cell GT horizontal electrophoresis system. Bio-Rad MyCycler™ Thermal Cycler was used for annealing of MP13mp18 phage DNA and DNA staple strands to form DNA origami. For the ATRP reaction, the syringe pump (NE-300 Just Infusion™ Syringe Pump) was used. M13mp18 phage DNA was produced according to the literature.^[1]

Fabrication of DNA origami

L-origami and S-origami were assembled respectively by mixing M13MP18 phage DNA of 7k nt with desired staple strands and modified staple strands in 1 × TAE / Mg buffer (5 mM Tris, 1 mM EDTA, 5 mM NaCl, and 12 mM MgCl₂, pH 8.0) and annealing from 65 °C to 20 °C over 2 h, followed by purification with polyethylene glycol (PEG) precipitation method.^[2] Briefly, assembled L- or S- origami was treated with 15% PEG8000 (w/v), 5 mM Tris, 1 mM EDTA, and 505 mM NaCl. The solution was mixed well and centrifuged at 12000 g, at room temperature (RT) for 25 min. The supernatant was removed and the pellet was dissolved in 1 × TAE / Mg buffer.

Synthesis of DNA origami macroinitiator

L-origami or S-origami (0.75 pmol in 1 × TAE / Mg buffer) were incubated with DNA-initiator (1 nmol in 0.2 μL aqueous solution) at room temperature for 4 h, used as L- or S- origami-initiator without any purification. 1.5 μL of 20 × TAE / Mg buffer was added to the reaction mixture to keep the constant concentration of Mg²⁺. The excess amount of DNA-initiator serves as sacrificial initiator in the ATRP polymerization.

In-situ ATRP reaction

A catalyst stock solution of CuBr₂ (0.45 mg, 0.002 mmol) and Tris (2-pyridylmethyl) amine (TPMA, 4.64 mg, 0.016 mmol) were prepared in 100 μL of N,N-Dimethylformamide (DMF) and MilliQ water (1 to 1 volume) mixture. The ascorbic acid stock solution, which can generate the active catalyst species, was prepared at 5 mM in 50 mM NaCl, followed by degassing with argon bubbling for 40 mins. To

conduct the polymerization reaction, PEGMEMA ($M_n = 300$, 2.4 mg, 8 μmol), the DNA origami initiator, the catalyst stock solution (1 μL), 20 x TAE buffer (4 μL) were added. Under these conditions, the ratio of the monomer versus the total initiator concentration is 8000 to 1. The reaction solution was degassed with three freeze–pump–thaw cycles and then filled with argon. Ascorbic acid solution (36 μL) was feed into the reactor by a syringe pump at the speed of 0.3 $\mu\text{L}/\text{min}$ under stirring (Figure S3). The pump was turned off after 2 h and the reactor was incubated for another 4 h. The mixture after polymerization was purified by 15 % PEG precipitation method^[2] to obtain L-origami-polymer or S-origami-polymer. By adding 0.24 μL (800:1) or 0.024 μL (80:1) PEGMEMA monomer, the chain length of polymers on the DNA origami could be adjusted when other conditions were kept constant.

The crosslinked polymer nanostructure extraction

Crosslinked polymer nanostructure was obtained by the following procedure. Firstly, poly(ethylene glycol) methyl ether methacrylate (PEGMEMA) and poly(ethylene glycol) dimethacrylate (PEGDMA, M_n of 750) with the ratio of 7300: 700 were polymerized on L-origami by the same procedure as only PEGMEMA polymerization. After grafting crosslinked polymers on L-origami, the sample was diluted with MilliQ water and was heated at 60 degree for overnight followed by the rapid cooling on ice. Extracted polymer nanostructure was directly monitored by AFM.

Atomic force Microscopy (AFM)

Imaging and quantitative nanomechanical property mapping (QNM) were performed with a Bruker Dimension FastScan Bio AFM equipped with the ScanAsyst mode or the QNM imaging mode. The sample solution was deposited onto freshly cleaved mica surface, and left for 5 min at room temperature to allow adsorption of the DNA origami structures. After addition of 20 μL of 1 x TAE / Mg buffer, the sample was scanned with the scan rates between 1 and 3 Hz. Several AFM images were acquired at different areas of the mica surface to ensure the reproducibility of the results. All images were analyzed by using the NanoScope Analysis 1.50 and Gwyddion 2.38 software. The height profiles of 20 - 30 DNA origami structures were analyzed to calculate the average height and standard error (S.E.).

Time-of-Flight Secondary Ion Mass Spectrometry (ToF-SIMS)

Time-of-Flight Secondary Ion Mass Spectrometry was accomplished on a ToF-SIMS instrument (ION-TOF GmbH, Münster, Germany) at the Institute of Functional Interfaces, Karlsruhe Institute of Technology (KIT). This spectrometer is equipped with a Bi cluster primary ion source and a reflectron type time-of-flight analyzer. UHV base pressure was $< 5 \times 10^{-9}$ mbar. For high mass resolution, the Bi

source was operated in the “high current bunched” mode providing short Bi_3^+ primary ion pulses at 25 keV energy and a lateral resolution of approx. 4 μm . The short pulse length of 1.3 ns allowed for high mass resolution. The primary ion beam was rastered across a 500x500 μm field of view on the sample, and 128x128 data points were recorded. Primary ion doses were kept below 10^{11} ions/ cm^2 (static SIMS limit). For charge compensation on the highly insulating mica samples an electron flood gun providing electrons of 21 eV was applied and the secondary ion reflectron tuned accordingly. Spectra were calibrated on the omnipresent C^+ , CH^+ , CH_2^+ , C_2^+ , C_3^+ , or on the C^+ , CH^+ , CH_2^+ , and CH_3^+ peaks. Based on these datasets the chemical assignments for characteristic fragments were determined.

Supplementary figures and tables

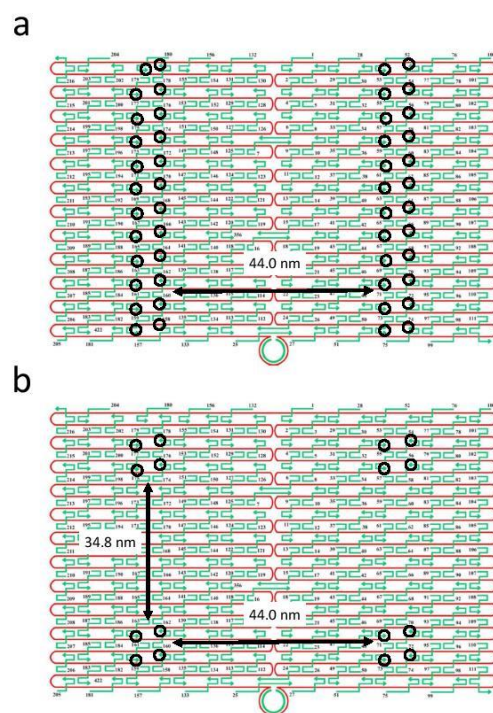


Figure S1 Design of DNA origami. Rectangular DNA origami of 70 nm × 100 nm dimension was employed.^[3] **a**, L-origami, **b**, S-origami. The modified staples for capturing DNA-initiator (5'- ATRP initiator – CTCTACCACCTAC -3'), to which additional sticky sequence (TTTTTTAGTAGGTGGTAGAG) were introduced at the 3' end, were labeled with black circles.

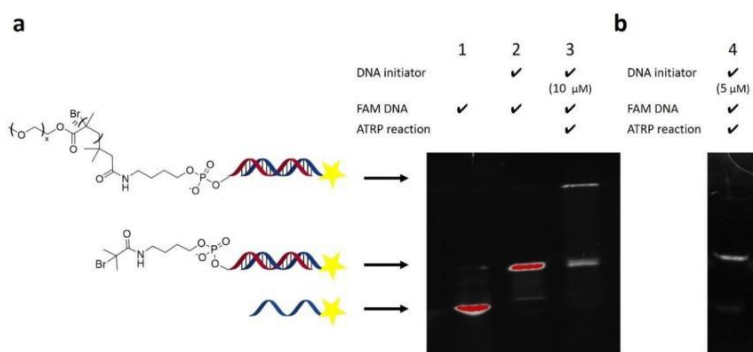


Figure S2 Native PAGE gel of PEGMEMA polymer with DNA-initiator. **a**, 6' fluorescein amidite (FAM) modified DNA (FAM DNA, lane 1), which is complementary to the DNA-initiator sequence was hybridized to DNA-initiator (10 μM, lane 2) to visualize the band because ethidium bromide staining was not efficient for the short single-stranded DNA sequence of the DNA-initiator. After the ATRP reaction with PEGMEMA monomer, the new band was appeared, indicating the successful polymerization. However, when the initiator concentration was decreased to 5 μM (**b**), there was no polymer band, which indicated that the concentration of the initiator was too low for polymerization.



Figure S3 Home-designed device for the ATRP reaction. **a**, The device was composed by a syringe pump, syringe, needle, reactor (**b**), and shaker. Inside the argon filled reactor, a small vial is standing, in which the reaction solution was contained.

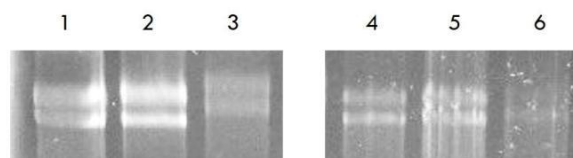


Figure S4 Agarose gel electrophoresis of DNA origami before and after ATRP reaction. 1. L-origami, 2. L-origami-initiator, 3. L-origami-polymer, 4. S-origami, 5. S-origami-initiator, 6. S-origami-polymer. Each sample was loaded to 0.8 % agarose gel in 0.5 x TBE / Mg buffer and run at 90 V for 2 hours, followed by ethidium bromide staining. The immobilization of small DNA-initiator molecules didn't give a significant effect to the mobility of the DNA origami bands. After the ATRP reaction, the shift of the DNA origami band was observed due to the polymer grafting.

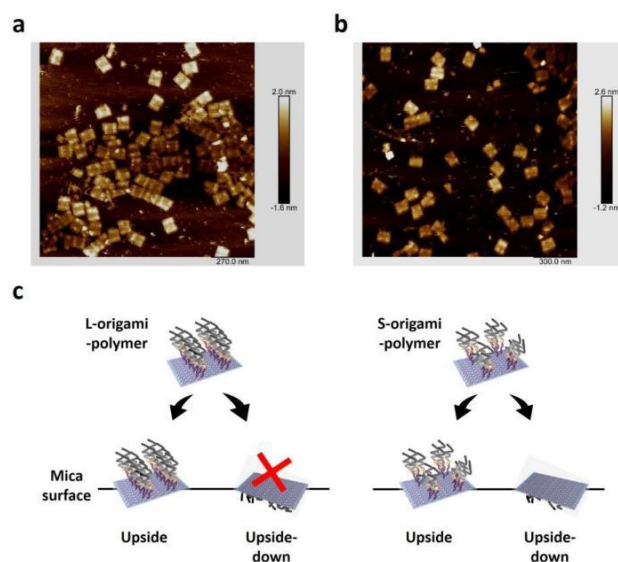


Figure S5 AFM of L- and S-origami-polymer. **a**, Purified L-origami-polymer deposited on mica surface. **b**, Purified S-origami-polymer deposited on mica surface. **c**, Schematic representation of favorable deposition of L- or S- origami-polymer onto mica surface.

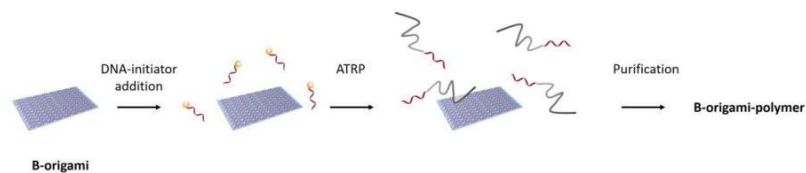


Figure S6 Scheme of B-origami-polymer preparation. Blank DNA origami without modified staple sequences (B-origami) was mixed with DNA-initiator and ATRP reaction was conducted. After the reaction, the reaction mixture was purified by PEG purification method,^[2] deposited on mica and ToF-SIMS measurement was conducted.

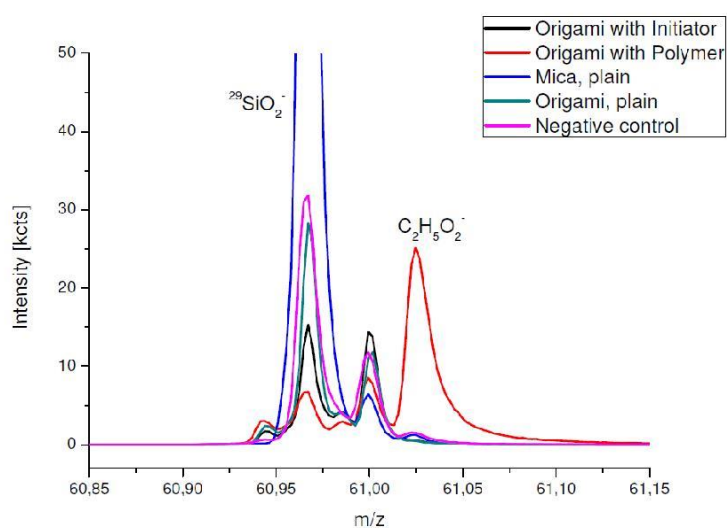


Figure S7 Negative polarity secondary ion mass spectra. DNA origami-initiator (black); DNA origami-polymer (red); clean mica (blue); DNA origami (dark green); and a negative control, Blank DNA origami after the ATRP reaction procedure (Figure S6) (purple).

Table S1: SIMS peak intensities, [kcts], for a constant primary ion dose of 1×10^{11} $1/\text{cm}^2$, (static limit).

Assignment	m/z	Origami w. Initiator	Origami w. Polymer	Mica, plain	Origami, plain	Negative control
$\text{C}_2\text{H}_3\text{O}^-$	43,017	214	1303	188	170	195
$\text{C}_2\text{H}_3\text{O}^-$	45,032	14	18	2	10	8
PO^-	46,966	8	2	9	5	13
C_2HO_2^-	56,992	14	42	5	10	13
$\text{C}_2\text{H}_2\text{O}_2^-$	58,001	310	884	67	247	263
SiO_2^-	59,963	90	57	2284	154	150
$\text{C}_2\text{H}_5\text{O}_2^-$	61,025	7	210	7	6	14
PO_2^-	62,96	802	192	89	474	1695
SiO_3H^-	76,962	119	114	1710	260	288
$^{79}\text{Br}^-$	78,908	21	8	5	14	22
PO_3^-	78,953	1667	471	245	1293	4597
$^{81}\text{Br}^-$	80,905	6	5	4	3	3
$\text{C}_4\text{H}_9\text{O}_3^-$	105,044	8	37	1	5	6
Total Counts, $\times 10^3$		76,676	77,075	42,709	74,745	69,428

The assigned peaks listed in Table S1 can be grouped into three categories: The mica substrate, SiO_2^- , and SiO_3H^- (blue colored); indicators for DNA on the surface, PO^- , PO_2^- , and PO_3^- (red colored); and characteristic PEG derived peaks like $\text{C}_2\text{H}_3\text{O}^-$ and others (yellow colored). Due to the small probing depth of a static SIMS experiment, 1 – 2 nm, shielding effects in layered samples can strongly affect secondary ion intensities. This effect is well reflected in Table S1. Due to inevitable differences in sample preparation, origamis are dispersed onto freshly cleaved mica sheets, the remaining mica signals provide a measure to determine the density of origamis within the field of view of a given SIMS experiment. Note that the lateral resolution of the applied SIMS mode is not sufficient to image individual origamis. E.g. the sample of plain origamis exhibits higher substrate signals as compared to the sample of origamis with bromine initiators attached. In turn, PO_3^- signals of the sample of plain origamis are weaker as compared to the sample of origamis with bromine initiators attached. Introducing

grafted PEG chains further contributes to this scenario: The sample of pegylated origamis shows a strong shielding of the PO_4^- signals and a weaker effect on the mica signals. A direct observation of bromine from the attached initiators with static SIMS was not possible. Note that the recorded signals at 79 and 81 m/z shown in table S1 are weak, despite the high ionization yields for bromine, and often differ strongly from the natural isotope distribution of ^{79}Br versus ^{81}Br (50,7% vs. 49,3%), indicating a strong interference with other peaks at similar m/z. However, the initiation of polymerization on bromine containing origamis, yielding pegylated origamis is demonstrated by several characteristic peaks like the ethylene glycol end group signature, $\text{C}_2\text{H}_5\text{O}_2^-$, shown in fig. S8, or the repeat unit's signal, $\text{C}_2\text{H}_3\text{O}^-$, see table S1. To demonstrate that plain origamis do not trigger PEG grafting and residues of the applied monomer do not contribute to the measured PEG signals, a negative control was performed. Therefore, plain origamis were subjected to polymerization conditions. Following that, the reaction mixtures containing origamis (with or without initiator) and monomer were purified and analyzed under identical conditions. As shown in figure S7 (purple line) and table S1 (rightmost column) only traces of poly ethylene glycol were detected in this case.

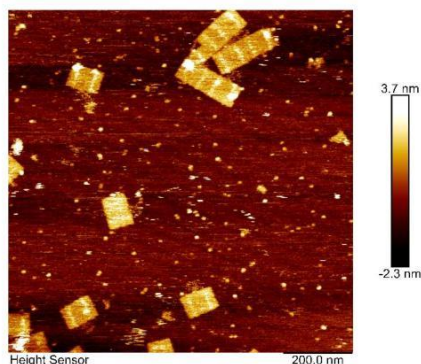


Figure S8 AFM of the crosslinked polymers on L-origami. Poly(ethylene glycol) methyl ether methacrylate (PEGMEMA, $M_n = 300$) and poly(ethylene glycol) dimethacrylate (PEGDMA, $M_n = 750$) with the ratio of 7300:700 to initiator were used for generating the crosslinked polymers on L-origami. According to the height profile analysis, the observed average height increase of DNA origami was $0.64 \text{ nm} \pm 0.04 \text{ nm}$ (standard error, S.E.), width of polymers was $25.3 \text{ nm} \pm 1.0 \text{ nm}$, and the length was $68.6 \text{ nm} \pm 1.1 \text{ nm}$, which is similar to the obtained results when only PEGMEMA and no crosslinker were used (8000:1 to initiator, Figure 2 b). Therefore, the presence of the crosslinker obviously did not affect the formed shape of the polymers on DNA origami compared to the case without crosslinker.

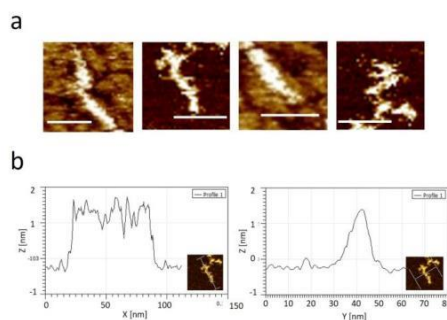


Figure S9 AFM of crosslinked polymer nanostructures after the removal of the L-origami template. **a**, AFM images of crosslinked polymeric nanostructures, the scale bar is 50 nm. **b**, The height profile of the crosslinked polymeric nanostructure in different axis.

References

- [1] G. Bellot, M. A. McClintock, J. J. Chou, W. M. Shih, *Nat. Protoc.* **2013**, *8*, 755-770.
- [2] E. Stahl, T. G. Martin, F. Praetorius, H. Dietz, *Angew. Chem. Int. Ed.* **2014**, *53*, 12735-12740; *Angew. Chem.* **2014**, *126*, 12949-12954.
- [3] a) P. W. Rothemund, *Nature* **2006**, *440*, 297-302; b) N. Y. Wong, H. Xing, L. H. Tan, Y. Lu, *J. Am. Chem. Soc.* **2013**, *135*, 2931-2934.

[6-2] Polymer tube nanoreactors by DNA-origami templated synthesis

Yu Tokura, Sean Harvey, Xuemei Xu, Chaojian Chen, Svenja Morsbach, Katrin Wunderlich, George Fytas, Yuzhou Wu*, David Y. W. Ng, and Tanja Weil*

* corresponding author

Accepted in Chem. Commun. 2018 (doi: 10.1039/C7CC09620H)

Copyright: Reproduced by permission of The Royal Society of Chemistry and Creative Commons Attribution 3.0 International License (<https://creativecommons.org/licenses/by/3.0/legalcode>).

.

Abstract:

We describe the stepwise 3D synthesis of precise polymeric objects assisted by the DNA origami nanotechnology. A common two dimensional DNA tile was transformed into a 3D DNA tube and decorated with multiple single stranded DNA handles at the outer surface to impart initiator moieties for atom transfer radical polymerization (ATRP). In the interior, the DNA nanotube was decorated with guanine quadruplexes (G4), which were transformed into peroxidase active DNAzymes. ATRP was initiated and formed a crosslinked polymer shell while its interior catalyzed the formation of polydopamine (PD). The eventual construct is a precise nanostructure with exclusive polymeric features programmed in a three dimensional space.

Contribution of the respective authors:

Yu Tokura: Design and synthesis of DNA origami, conducting surface-initiated ATRP on DNA origami, AFM study and analysis, performing agarose gel electrophoresis study, the stability assay of DNA origami, evaluating DNAzyme activity by ABTS assay, writing of the manuscript

Sean Harvey: Conducting polymerization of dopamine in DNA tube and kinetics study of polydopamine formation by absorbance spectroscopy, writing of the manuscript.

Xuemei Xu: Synthesis of DNA origami, conducting surface-initiated ATRP on DNA origami

Chaojian Chen: TEM measurement

Svenja Morsbach: DLS study and analysis, interpretation and discussion on the results

Katrin Wunderlich: Interpretation and discussion on the DLS results

George Fytas: Interpretation and discussion on the DLS results

Yuzhou Wu: Discussion on the concept and results, writing and correcting the manuscript

David Y. W. Ng: Discussion on the concept and results, writing and correcting the manuscript

Tanja Weil: Acquiring funding for the project, design and discussion of the concept and results, writing and correcting the manuscript.



Journal Name

COMMUNICATION

Received 00th January
20xx,

Polymer tube nanoreactors by DNA-origami templated synthesis

Yu Tokura,^{ab} Sean Harvey,^a Xuemei Xu,^c Chaojian Chen,^{ab} Svenja Morsbach,^a Katrin Wunderlich,^a George Fytas,^a Yuzhou Wu,^{ac*} David Y.W. Ng,^{a*} and Tanja Weil^{ab*}

Accepted 00th January 20xx

DOI: 10.1039/x0xx00000x

www.rsc.org/

We describe the stepwise synthesis of precise polymeric objects programmed by 3D DNA tube transformed from a common 2D DNA tile as precise biotemplate for atom transfer radical polymerization. The catalytic interior space of the DNA tube was utilized for synthesizing a bio-inspired polymer, polydopamine.

Three dimensional engineering of nanomaterials with precise control over sizes, shapes and functionalities represents the epitome of nanotechnology with far-reaching applications from material science to personalized medicine. From a molecular perspective, the formation of DNA origami and associated strategies^[1] to program functionalities with absolute positioning remains an unrivalled technology even in the years to come. Nonetheless, as a standalone material, polyanionic DNA is lacklustre as it generally requires a cocktail of $\text{Ca}^{2+}/\text{Mg}^{2+}$ fortified buffers to remain hydrolytically stable.^[2] Transferring the structural information of DNA origami to polymeric materials would provide access to unprecedented 3D architectures of customized material properties and presumably improved stability compared to the DNA origami scaffold.^[3]

Methodically, the emergence of DNA nanotechnology and, in particular, the "DNA origami" technique is supported by computer-aided design. As a result, precise DNA nano-objects between 20–100 nm can be created with near-limitless flexibility.^[4] This significant advantage is compounded by the capability to designate any specified positions on the 3D architecture for further modifications, which thus represents the core of nanoscale programmability. Using these principles,

a wide range of biotechnological applications including multi enzyme cascade systems^[5], drug delivery carriers^[6], and artificial ion channels^[7] have been developed. Besides these biotechnological advances, the impact of DNA origami in shaping organic^[8] and inorganic^[9] nanoarchitectures has also been increasingly investigated. In this communication, we designate a DNA tube as a shape-persistent 3D framework to direct and pattern the in-situ growth of different polymers in an orthogonal fashion. By decorating the outer surface of the DNA tube with initiators for atom transfer radical polymerization (ATRP), a templated architecture was achieved via polymerization with cross linking (Fig. 1). As a proof of concept to demonstrate 3D engineering, we functionalize the

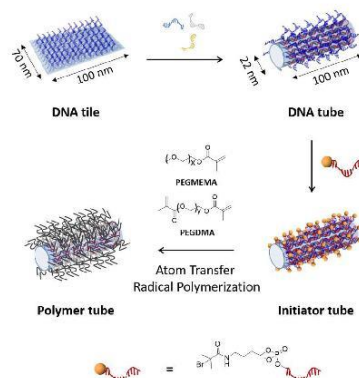


Fig. 1 DNA tiles decorated with multiple single-stranded DNA handles are transformed to DNA tubes by applying folding DNA strands. After equipping the outer surface of DNA tubes with ATRP-initiator moieties, polymers are grown on the surfaces to form polymer tube. Below, the molecular structure of initiator modified DNA is represented. The 5' end of DNA (red) is modified with bromoisobutyrate (yellow sphere).

^a Max Planck Institute for Polymer Research, Ackermannweg 10, 55128 Mainz (Germany) Email: Weil@mpip-mainz.mpg.de, David.Ng@mpip-mainz.mpg.de

^b Inorganic Chemistry I, Ulm University, Albert-Einstein-Allee 11, 89081 Ulm (Germany), E-mail: tanja.weil@uni-ulm.de

^c Hubei Key Laboratory of Bioinorganic Chemistry and Materia Medica, School of Chemistry and Chemical Engineering, Huazhong University of Science and Technology, Luoyu Road 1037, 430074 Hongshan, Wuhan, P. R. China.

*Electronic Supplementary Information (ESI) available: Details of DNA origami preparation, purification. Detail of stepwise creation methods of polymer coated DNA tube. Detail of AFM, TEM, DLS, and agarose gel electrophoresis. See DOI: 10.1039/x0xx00000x

COMMUNICATION

Construct		Theoretical (nm)	AFM (nm)	DLS, R_h (nm)
DNA Tile	L	100	99.0 ± 2.2	55 ± 3
	W	70	78.0 ± 4.0	
	H	2	3.1 ± 0.1	
DNA Tube	L	100	97.0 ± 4.9	73 ± 6
	W	22	36.0 ± 6.0	
	H	22	5.0 ± 0.7	
Polymer Tube			91.0 ± 6.4	122 ± 13
			44.0 ± 6.0	
			7.0 ± 0.5	

Table 1. Summary of dimensions of the DNA tile, DNA tube and polymer tube from theoretical, AFM, and DLS.

interior space with multiple DNA-based catalytic moieties (DNAzyme) as reaction sites for the oxidative polymerization of dopamine. By accomplishing these strategies in sequence, we show the versatility of DNA origami as a platform to exert orthogonal control over both the shape and cross-sectional components of a nanostructure.

First, the DNA tube was constructed in a stepwise fashion, starting from the DNA tile (70 nm x 100 nm with 2 nm thickness)^[1a] by annealing scaffold DNA strand (M13mp18) and 210 staple DNA strands. To functionalize its surface with ATRP initiator molecules in the subsequent step, 169 staple DNA strands were modified with an additional single-stranded DNA (ssDNA) sequence as a DNA handle (Fig. S1 and Table S2).^[10] All DNA handles are designed to appear and fully cover only one surface of the DNA tile. Thereafter, transformation of the DNA tile to the DNA origami tube (22 nm in diameter and 100 nm in length) was accomplished by applying additional 16 DNA sequences (folding DNA strands), which connect the two long edges of the DNA tile to form the DNA tube (Fig. 1 upper part).^[10] Excessive amounts of folding DNA strands were removed by PEG-induced precipitation.^[11]

Atomic force microscopy (AFM) and transmission electron microscopy (TEM) revealed the successful conversion from

DNA tile into DNA tubes (Fig. 2 and Table 1). From AFM, the dimensions of the DNA tube in 1X (TRIS)-acetate-ethylenediamine tetraacetic acid (EDTA) buffer with 12 mM $MgCl_2$ (1X TAE/Mg buffer) was determined to be 36 ± 6 nm in diameter and 5 ± 0.7 nm in height. The discrepancy (± 14 nm in diameter, ~ 17 nm in height) between these measured dimensions in AFM and the theoretical calculations could be attributed to a structural distortion of DNA tube by both the strong attractive interaction between DNA tube surface and mica surface via Mg^{2+} bridging. In addition, agarose gel electrophoresis (AGE) and dynamic light scattering (DLS) studies were conducted. In AGE, the band shift was observed after the transformation (Fig. 2 D) and DLS revealed an increase of the hydrodynamic radius (R_h) from 55 ± 3 nm (DNA tile) to 73 ± 6 nm (DNA tube) (Fig. S2). The DNA tile and the DNA tube were investigated by static light scattering (SLS) to determine the radius of gyration $R_g = 54 \pm 2$ nm, for the DNA tile, and $R_g = 83 \pm 2$ nm for the DNA tube (lower inset of Fig. S2). From R_g and R_h , the shape factor, R_g/R_h , varies for different particle architectures and geometries and is a valuable parameter for the determination of the shape.^[12] $R_g/R_h = 0.98$ for the DNA tile, and 1.14 for the DNA tube were obtained, noting that the shape changed. Next, the obtained DNA tube was equipped with 169 initiator molecules for homogeneously covering the outer surface of DNA tube with the polymer shell. Bromoisobutyrate was modified to 5' of ssDNA strand^[13] and subsequently hybridized onto the multiple ssDNA handles on the surface of the DNA tube. The surface initiated ATRP on the DNA tube was conducted using poly(ethylene glycol) methyl ether methacrylate (PEGMEMA, average M_n 300) as the monomer due to its amphiphilic character, which is widely known to stabilize sensitive biomolecules.^[14] In order to achieve a tight polymer network, PEG dimethacrylate (PEGDMA, average M_n 750) was added as a crosslinker. The surface initiated ATRP was conducted as reported

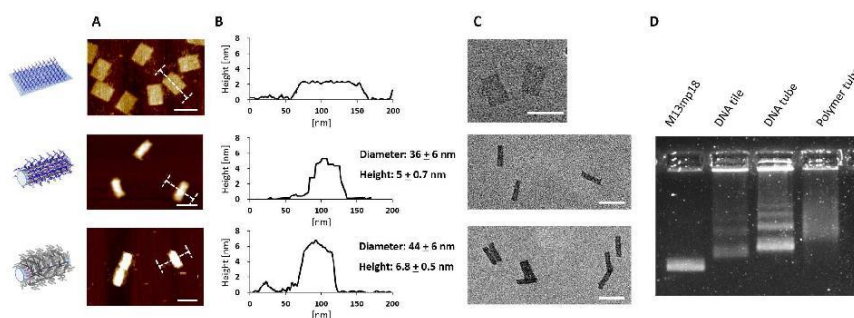


Fig. 2 (A) AFM images of DNA tile (upper), DNA tube (middle) and Polymer tube (bottom) respectively measured in liquid (1x TAE / Mg buffer). (B) Height profile of each construct depicted with I-bar in (A) and dimensions of DNA tubes and polymer tubes. (C) TEM images of each construct. Since uranyl formate staining for DNA origami doesn't visualize the coated polymer shells, there were no obvious structural changes observed between DNA tubes and polymer tubes. However, polymer tubes showed side-to-side stacking behaviour, which was not seen for the DNA tubes. (D) Agarose gel electrophoresis of each DNA construct stained with SYBR Gold. The band was shifted after transformation from tile to tube and after polymer formation. All the images were measured with purified samples. Scale bars in (A) and (C) are 100 nm.



previously.^[3b] Briefly, 20 μL reaction volume consisting of 1:665 ratio of DNA origami macroinitiator (50 nM) and sacrificial initiator (33 μM), PEGMEMA, PEGDMA, CuBr_2 and tris(2-pyridylmethyl)amine (TPMA) were combined. The reaction mixture was degassed by the freeze-pump-thaw method, followed by continuous slow addition of ascorbic acid to generate the reactive catalyst. After 2 h, the product was purified by the PEG-induced precipitation and characterized by AFM, TEM, AGE (Fig. 2) and DLS (Fig. S3).

AFM measurements of polymer coated DNA tubes (polymer tubes) revealed an increase of both the diameter (+ 8 nm) and the height (+ 2.0 nm) compared to the DNA tube due to the surrounding polymer shell. TEM images revealed no obvious structural differences, which is conceivable since the polymer shell could not be stained by uranyl formate.^[15] Nonetheless, TEM images of the polymer tube revealed a unique phenomenon as some tube structures aggregated with side on interactions (Fig. S4). This was also reported for the electrostatic binding of positively charged polylysine to a negatively charged DNA nanostructure^[15a] serving as an indication for successful polymer coating. AGE of the polymer tube revealed a further band shift to the slower mobility region possibly due to a reduction in negative surface charges and increased molecular weight by the polymer shell (Fig. 2D). Based on DLS and SLS experiments on dilute solutions of polymer tubes, the increased R_h and R_g , 122 ± 13 nm and 108 ± 3 nm (Fig. S3, Table 1) are most likely due to the grown

polymer layer and the altered hydration shell around the polymer tube. The shape factor $R_g/R_h=0.88$ is even smaller than for both DNA tile and tube that clearly implies a form change upon polymer tethering and a compact polymer structure. Furthermore, other higher-ordered interactions such as the increased hydration sphere or large aggregation of the entire construct were not observed. Stability of the polymer tubes against nuclease digestion was evaluated using dsDNA-intercalating dye, SYBR safe, as reporter molecule (Fig. S5). In the presence of 50 mU nucleases, the emission of SYBR safe in the DNA tiles and tubes decreased to 20 % and 26 % of the original signals, respectively. Under the same conditions, the polymer tube still retained about 60 % to 70 % fluorescence intensity indicating that the polymer shell protected the DNA tube from nuclease digestion. It should be noted that the ends of the DNA tube are open and in principle still accessible for nuclease digestion, which could explain the observed decrease in fluorescence intensity by about 30%.

A major advantage of the grafting-from strategy is the spatial control over the coating area and the high density of the polymer chains. For 3D nanoscale engineering, the polymer tube provides a unique opportunity to introduce further functionalities within the interior cavity. DNAzymes were introduced into the DNA tube to serve as reaction centers. Guanine-rich sequences adopt a unique secondary structure called G-quadruplex (G4) composed of stacked square planar guanine tetrads^[16]. The thus formed G4

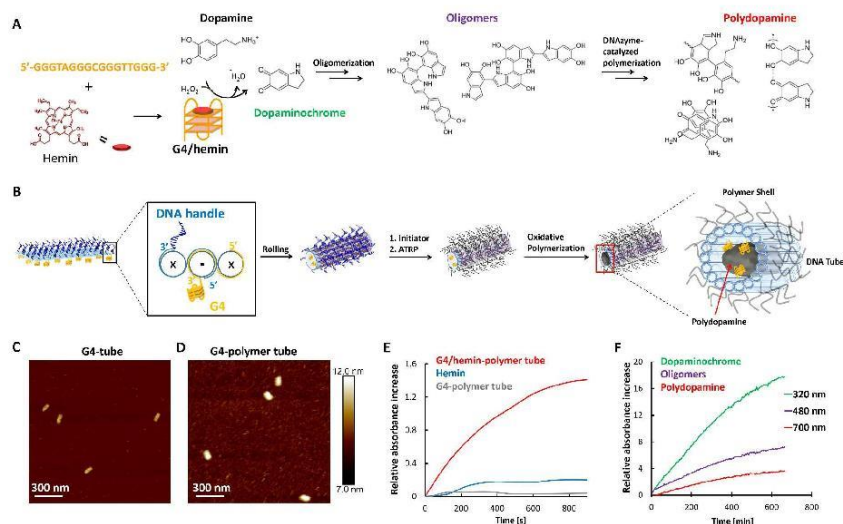


Fig. 3 (A) Scheme of G4/hemin-based DNAzyme formation and proposed mechanism of polydopamine formation. (B) Schematic illustration for the programmed and orthogonal initiation of ATRP and polydopamine formation. The G4 moieties were incorporated with the corresponding staple DNA strands being split into two strands; G4-modified strands (yellow) and DNA handle strands (blue). Both modifications were introduced at 3' of the DNA strand (Fig. S6). (C, D) AFM images of G4 incorporated DNA tube before and after polymer coating. (E) ABTS assay of G4/hemin-polymer tube. (F) Kinetics of the polymerization of dopamine initiated by the G4/hemin-polymer tubes.

COMMUNICATION

structure can accommodate hemin to activate its catalytic activity mimicking the horseradish peroxidase (HRP)^[17], i.e. acting as a redox catalyst. We functionalized the inner surface of the DNA tube with twenty G4 moieties and a polymer shell was introduced as described above (Fig. 3b and S6). The initial G4-DNA tube revealed similar dimensions (diameter: 37 ± 4 nm, height: 7.2 ± 1.0 nm, Fig. 3c) to the DNA tube itself. Polymerization via ATRP was subsequently conducted and the G4 incorporated polymer tube (G4-polymer tube) was obtained with a larger diameter of 55 ± 10 nm and a height of 11 ± 1.9 nm (Fig. 3d and Table S1).

The activity of the G4/hemin DNAzyme loaded into the polymer tube was assessed following the oxidation of 2,2'-azino-bis(3-ethylbenzothiazoline-6-sulphonic acid (ABTS)) in the presence of hydrogen peroxide. Its positive catalytic activity was compared against free hemin as well as the unloaded G4-DNA polymer tube without hemin as controls (Fig. 3e) and catalytic activity of the G4/hemin DNAzymes inside the polymer tubes was clearly demonstrated. Moreover, upon nuclease addition (50 mU, > 3500 sec observation time), 80 % of the DNAzyme activity was retained suggesting that the respective catalytic domains were protected from nuclease degradation (Fig. S7). Subsequently, peroxidase activity of the G4/hemin DNAzyme was exploited to initiate polymerization of dopamine within the polymer tube. Polydopamine is a highly crosslinked natural polymer of high structural rigidity that can be obtained by G4/hemin DNAzyme-catalyzed oxidative polymerization on DNA origami as reported by us.^[3a] G4/hemin DNAzyme oxidizes dopamine to dopaminochrome, one of the key intermediates for polydopamine formation.^[18] The reaction kinetics and the formation of polymerization intermediates (dopaminochrome, oligomers) and polydopamine formation were monitored with absorbance spectroscopy (Fig. 3f, S6). In addition, we have shown previously that the G4/hemin DNAzyme functions as a specific anchor and that polymerization of dopamine in free solution does not occur.^[3b] As such, the opposing placements of the G4 catalytic sites with respect to the ATRP initiators have successfully provided the basis of spatial control between the inner and outer space of the DNA tube.

In conclusion, we have demonstrated the construction of precisely templated DNA-polymer tubes with interfacial orthogonality towards nanoscale engineering. The well-known 2D DNA tile structure from Rothemund was transformed into a 3D DNA tube decorated with multiple ssDNA handles outside while the interior space was functionalized with G4/hemin-based DNAzymes. The DNA handles immobilized initiator molecules where surface initiated polymerization enables the growth of a densely crosslinked polymeric shell. The internal G4 was loaded with hemin and transformed into DNAzymes that initiate dopamine polymerization. By integrating two mechanistically different polymerizations while providing precision control, the proposed strategy serves as an elegant approach towards 3D polymer engineering on the nanoscale. We acknowledge support by the European Research Council (ERC, Synergy Grant 319130-BioQ) and the BMBF (Biotechnologie 2020+ initiative, "Selekomm" project). C.C

acknowledges support from the Promotionskolleg Pharmaceutical Biotechnology. We thank Dr. Rüdiger Berger for critical reading the manuscript and valuable comments.

Conflicts of interest

There are no conflicts to declare.

Notes and references

- [1] a) P. W. Rothemund, *Nature* 2006, 440, 297-302; b) Z. G. Wang, B. Q. Ding, *Acc. Chem. Res.* 2014, 47, 1654-1662; c) F. C. Simmel, *Curr. Opin. Biotech.* 2012, 23, 516-521; d) Q. Zhang, Q. Jiang, N. Li, L. R. Dai, Q. Liu, L. L. Song, J. Y. Wang, Y. Q. Li, J. Tian, B. Q. Ding, Y. Du, *ACS Nano* 2014, 8, 6633-6643; e) A. H. Okholm, J. Kjems, *Adv. Drug Deliv. Rev.* 2016, 106, 183-191.
- [2] J. Duguid, V. A. Bloomfield, J. Benevides, G. J. Thomas, *Biophys. J.* 1993, 65, 1916-1928.
- [3] a) Y. Tokura, Y. Jiang, A. Welle, M. H. Stenzel, K. M. Krzemien, J. Michaelis, R. Berger, C. Barner-Kowollik, Y. Wu, T. Weil, *Angew. Chem. Int. Ed.* 2016, 55, 5692-5697; b) Y. Tokura, S. Harvey, C. Chen, Y. Wu, Y. W. D. Ng, T. Weil, *Angew. Chem. Int. Ed.* 2017.
- [4] a) C. E. Castro, F. Kilchherr, D. N. Kim, E. L. Shiao, T. Wauer, P. Wortmann, M. Bathe, H. Dietz, *Nat. Methods* 2011, 8, 221-229; b) S. M. Douglas, A. H. Marblestone, S. Teerapittayanon, A. Vazquez, G. M. Church, W. M. Shih, *Nucleic Acids Res.* 2009, 37, 5001-5006.
- [5] G. L. Ke, M. H. Liu, S. X. Jiang, X. D. Qi, Y. R. Yang, S. Wootten, F. Zhang, Z. Zhu, Y. Liu, C. J. Yang, H. Yan, *Angew. Chem. Int. Ed.* 2016, 55, 7483-7486.
- [6] A. Ora, E. Jarvihaavisto, H. B. Zhang, H. Auvinen, H. A. Santos, M. A. Kostianen, V. Linko, *Chem. Commun.* 2016, 52, 14161-14164.
- [7] M. Langecker, V. Arnaut, T. G. Martin, J. List, S. Renner, M. Mayer, H. Dietz, F. C. Simmel, *Science* 2012, 338, 932-936.
- [8] C. Tian, H. Kim, W. Sun, Y. Kim, P. Yin, H. T. Liu, *ACS Nano* 2017, 11, 227-238.
- [9] a) B. Uprety, T. Westover, M. Stoddard, K. Brinkerhoff, J. Jensen, R. C. Davis, A. T. Woolley, J. N. Harb, *Langmuir* 2017, 33, 726-735; b) Y. L. Geng, A. C. Pearson, E. P. Gates, B. Uprety, R. C. Davis, J. N. Harb, A. T. Woolley, *Langmuir* 2013, 29, 3482-3490.
- [10] a) X. B. Shen, C. Song, J. Y. Wang, D. W. Shi, Z. A. Wang, N. Liu, B. Q. Ding, *J. Am. Chem. Soc.* 2012, 134, 146-149; b) Y. M. Fu, D. D. Zeng, J. Chao, Y. Q. Jin, Z. Zhang, H. J. Liu, D. Li, H. W. Ma, Q. Huang, K. V. Gothelf, C. H. Fan, *J. Am. Chem. Soc.* 2013, 135, 696-702.
- [11] E. Stahl, T. G. Martin, F. Praetorius, H. Dietz, *Angew. Chem. Int. Ed.* 2014, 53, 12735-12740.
- [12] W. Scharlt, *Springer Lab Man. Pol.* 2007, 1-191.
- [13] S. E. Averick, S. K. Dey, D. Grahacharya, K. Matyjaszewski, S. R. Das, *Angew. Chem. Int. Ed.* 2014, 53, 2739-2744.
- [14] S. M. Ryan, G. Mantovani, X. X. Wang, D. M. Haddleton, D. J. Brayden, *Expert Opin. Drug Del.* 2008, 5, 371-383.
- [15] a) N. P. Agarwal, M. Matthies, F. N. Gur, K. Osada, T. L. Schmidt, *Angew. Chem. Int. Ed.* 2017, 56, 5460-5464; b) J. K. Kiviahio, V. Linko, A. Ora, T. Tiainen, E. Jarvihaavisto, J. Mikkila, H. Tenhu, Nonappa, M. A. Kostianen, *Nanoscale* 2016, 8, 11674-11680.
- [16] M. Gellert, M. N. Lipsett, D. R. Davies, *PNAS* 1962, 48, 2013-8.
- [17] a) P. Travascio, Y. F. Li, D. Sen, *Chem. Biol.* 1998, 5, 505-517.
- [18] a) E. Golub, H. B. Albada, W. C. Liao, Y. Biniuri, I. Willner, *J. Am. Chem. Soc.* 2016, 138, 164-172; b) H. B. Albada, E. Golub, I. Willner, *Chem. Sci.* 2016, 7, 3092-3101.



Supporting information**Polymer tube nanoreactors by DNA-origami templated synthesis**

Yu Tokura,^{a,b} Sean Harvey,^b Xuemei Xu,^c Chaojian Chen,^{a,b} Svenja Morsbach,^b Katrin Wunderlich,^b George Fytas,^b Yuzhou Wu,^{b,c*} David Y.W. Ng,^{b*} and Tanja Weil^{a,b*}

Table of Contents

General methods	3
Materials and Instruments	
Fabrication of DNA tile with multiple DNA handles	
Transformation to DNA tube	
Synthesis of DNA tube / initiator	
Surface initiated atom transfer radical polymerization	
Atomic force Microscopy (AFM)	
Agarose gel electrophoresis	
Transmission electron microscopy (TEM)	
Dynamic and static light scattering (DLS and SLS)	
Nuclease digestion assay	
Kinetics of polydopamine formation on G4/hemin DNA nanotile	
Supplementary figures and tables	7
Figure S1 DNA tile	
Figure S2 Relaxation functions $C_{vv}(q,t)$ for the translational diffusion dynamics in aqueous solution of DNA tile (black filled squares) and DNA tube (red filled circles) at 20°C at a scattering wave vector ($q=0.009\text{ nm}^{-1}$) represented by a stretched exponential function (solid lines)	
Figure S3 Normalized field correlation functions $C_{vv}(q,t)$ at a scattering wave vector $q=0.009\text{ nm}^{-1}$ (black filled squares) and $q=0.024\text{ nm}^{-1}$ (red filled circles) for the translational diffusion dynamics in aqueous solution of polymer coated DNA tube at 20°C	
Figure S4 TEM image of stacking polymer tube	
Figure S5 Stability of different DNA origami structure against nuclease.	
Figure S6 DNAzyme-incorporated DNA tile	
Table S1 Summary of dimensions of the DNA tile, DNA tube and polymer tube from theoretical, AFM, and DLS	
Figure S7 ABTS activity of DNAzymes in polymer tubes before / after nuclease addition (50 mU)	
Table S2 Detail of staple DNA sequences	
References	22

General methods

Materials and instruments

All solvents and chemicals were purchased from commercial sources and were used without further purification. DNA staple strands and ATRP initiator modified DNA (DNA-initiator) were either synthesized by 12-Column DNA Synthesizer from POLYGEN GmbH and purified by Agilent 1260 Infinity HPLC system with Agilent Eclipse XDB-C18 column or purchased from Sigma-Aldrich. Agarose gel electrophoresis was performed using Bio-Rad Mini-Sub Cell GT horizontal electrophoresis system. Bio-Rad MyCycler™ Thermal Cycler was used for annealing of MP13mp18 phage DNA and DNA staple strands to form DNA origami. Concentration of DNA origami was determined by Spark @ 20M with Nanoquant plate™.

Fabrication of DNA tile with multiple DNA handles

DNA tile with multiple DNA handles was assembled respectively by mixing M13mp18 phage DNA of 7k nt with desired staple strands and modified staple strands in $1 \times$ TAE / Mg buffer (5 mM Tris, 1 mM EDTA, 5 mM NaCl, and 12 mM MgCl₂, pH 8.0) and annealing from 65 °C to 20 °C over 2 h, followed by purification with polyethylene glycol (PEG) precipitation method.^[1] Briefly, the DNA tile was treated with 15% PEG(8000) (w/v), 5 mM Tris, 1 mM EDTA, and 505 mM NaCl. The solution was mixed well and centrifuged at 12000 g, at room temperature (RT) for 25 min. The supernatant was removed and the pellet was dissolved in $1 \times$ TAE / Mg buffer. The same procedure was conducted twice to remove all the remaining staple DNA sequences.

Transformation to DNA tube

To DNA tile (0.5 pmol) solution was added a set of folding DNA strands (250 pmol each) and the mixture was incubated at 32 degree for overnight. The obtained DNA tube was purified again with PEG precipitation method.

Synthesis of DNA tube / initiator

DNA tubes (0.75 pmol in $1 \times$ TAE / Mg buffer) were incubated with DNA-initiator^[2] (1 nmol in 0.2 μ L aqueous solution) at room temperature for 4 h and they were used as DNA tube / initiator without any purification. 1.5 μ L of $20 \times$ TAE / Mg buffer was added to the reaction mixture to keep the constant concentration of Mg²⁺. The excess amount of DNA initiators serves as sacrificial initiator in the ATRP reaction.

Surface initiated atom transfer radical polymerization

A catalyst stock solution of CuBr_2 (0.45 mg, 0.002 mmol) and Tris (2-pyridylmethyl) amine (TPMA, 4.64 mg, 0.016 mmol) were prepared in 100 μL of N,N -Dimethylformamide (DMF) and MilliQ water (1 to 1 volume) mixture. The ascorbic acid stock solution, which can generate the active catalyst species, was prepared at 5 mM in 50 mM NaCl, followed by degassing with argon bubbling for 40 mins. To conduct the polymerization reaction, PEGMEMA ($M_n = 3001$), PEGDMA ($M_n = 750$), DNA tube / initiator, the catalyst stock solution (1 μL), 20 x TAE buffer (4 μL) were added with the ratio of PEGMEMA: PEGDMA: Initiator = 7200: 800: 1. The reaction solution was degassed with three freeze–pump–thaw cycles and then filled with argon. Ascorbic acid solution (36 μL) was feed into the reactor by a syringe pump at the speed of 0.3 $\mu\text{L}/\text{min}$ under stirring. The pump was turned off after 2 h and the reactor was incubated for another 4 h. The reaction mixture after polymerization was purified by 15 % PEG precipitation to obtain the polymer tube.

Atomic force Microscopy (AFM)

Imaging was performed with a Bruker Dimension FastScan Bio AFM equipped with the ScanAsyst mode. The sample solution was deposited onto freshly cleaved mica surface, and left for 5 min at room temperature to allow adsorption of the DNA origami structures. After addition of 70 μL of 1 x TAE / Mg buffer, the sample was scanned with the scan rates between 1 and 3 Hz. Several AFM images were acquired at different areas of the mica surface to ensure the reproducibility of the results. All images were analyzed by using the NanoScope Analysis 1.50 and Gwyddion 2.38 software.

Agarose gel electrophoresis

5 μL of sample (1.5 nM) was mixed with 1 μL of 6 x loading buffer and run with 0.8 % agarose gel in 0.5 x TBE / Mg for 120 minutes in ice bath. After running, the gel was stained by SYBR Gold for 30 minutes and the image was taken by G: Box Chemi (Syngene).

Transmission electron microscopy (TEM)

5 μL of sample (1 nM) was applied on carbon coated copper grid with hydrophilic treatment. After 10 minutes incubation, the remaining solution was removed and the sample grid was stained with 2 % uranyl formate solution for 20 seconds. The stained grid was washed with filtered water for three times and dried in air. Imaging was done with JEOL 1400 instrument and obtained images were analyzed by ImageJ software.

Dynamic and static light scattering (DLS and SLS)

Light scattering measurements were performed with an ALV/CGS3 compact goniometer system with a He/Ne laser (632.8 nm), ALV/LSE-5004 multiple-tau full-digital correlator and ALV5000 software. For temperature controlled measurements, the light scattering instrument was equipped with a thermostat from Julabo. Measurements were performed at 20 °C at 13 angles ranging from 30° to 150°. All DNA origami solution samples were adjusted to a concentration of 3.5 nM in TAE / Mg / K (0.3 mM Tris, 0.2 mM acetic acid, 0.06 mM EDTA, 0.6 mM MgCl₂, 10 mM KCl, pH 5.3). The solutions were then filtered through Hydrophilic Durapore® filters with a pore size of 0.22 µm (Merck Millipore, Billerica, USA) and transferred into dust-free quartz light scattering cuvettes (Hellma, Müllheim, Germany), which were cleaned before in sagewith acetone in a Thurmont-apparatus. The scattering wave vector q is defined as

$$q = \frac{4\pi n}{\lambda} \sin \frac{\theta}{2} \text{ with } n=1.333 \text{ being the water refractive index. The relaxation function,}$$

$C(q,t) = [G(q,t)-1]^{1/2}$ computed from the experimental scattering intensity autocorrelation function $G(q,t)$ was represented either by an inverse Laplace transform (ILT) analysis using the CONTIN algorithm.

In dilute solutions, the relaxation rate $\Gamma(q)=1/\tau(q)$ is usually diffusive defining the diffusion coefficient $D=\Gamma(q)/q^2$. For species with small size R i.e., , both the scattering intensity $I(q)$ and $D=D_0$ are q -independent with $I \sim cM$ and $D_0=k_B T/(6\pi\eta_0 R_h)$ where c , M , R_h , η_0 , k_B , and T are the probed species concentration, its molecular weight and hydrodynamic ratio, the solvent viscosity, the Boltzmann constant and the absolute temperature, respectively. For $qR \sim 1$, both $I(q)$ and $D(q)$ depend on q defining the probing length $(2\pi/q)$. The former, known as the form factor, yields (at low qR_g) the radius of gyration R_g ,

$$I(q)^{-1}=I(0)^{-1}(1+q^2 R_g^2/3) \quad (1)$$

whereas the effective D is given by,

$$D = D_0(1 + Aq^2) \quad (2)$$

with A is a parameter characterizing the shape of the diffusing species.

Nuclease digestion assay

DNA tile, DNA tube, and polymer tube were labeled with 0.5 x SYBR-safe solution by during 30 min of incubation. Different amounts (0-50 mU) of nuclease were added to the labeled DNA origami structures and incubated at 37 degree for 30 min. The fluorescence intensity of SYBR-safe was checked by Spark ® 20M with Nanoquant plate™ and

compared to the sample, to which no nuclease was added.

ABTS assay

To 0.3 nM G4-DNA tile, G4-DNA tube, and G4-polymer tube in the buffer composition (97 μ L, 20 mM Tris, 1 mM EDTA, 12 mM MgCl_2 , pH 5.3 by addition of acetic acid) was added 1 μ L of 100 nM hemin. The assay was performed by mixing the hemine added DNA origami solution with 1 μ L of freshly prepared 50 mg/ml ABTS solution and 1 μ L of 0.1M H_2O_2 . Immediately after H_2O_2 addition, the absorbance spectrum was measured by using a Tecan Spark® 20M plate reader.

Kinetics of polydopamine formation on G4/hemin DNA nanotile

G4-DNA tube (3.5 nM) in TAE / Mg / K (0.3 mM Tris, 0.2 mM acetic acid, 0.06 mM EDTA, 0.6 mM MgCl_2 , 10 mM KCl, pH 5.3) was mixed with hemin (70 nM) for 30 min at rt. 98 μ L of the solution was added to a 384 well UV transparent plate. To G4/hemin DNA nanotile solution was added 1 μ L of a freshly prepared 1M dopamine solution and 1 μ L of 1M H_2O_2 . Immediately after H_2O_2 addition, the absorbance spectrum was measured every 5 minutes for a duration of 12 hours using a Tecan Spark® 20M plate reader.

Supplementary figures and tables

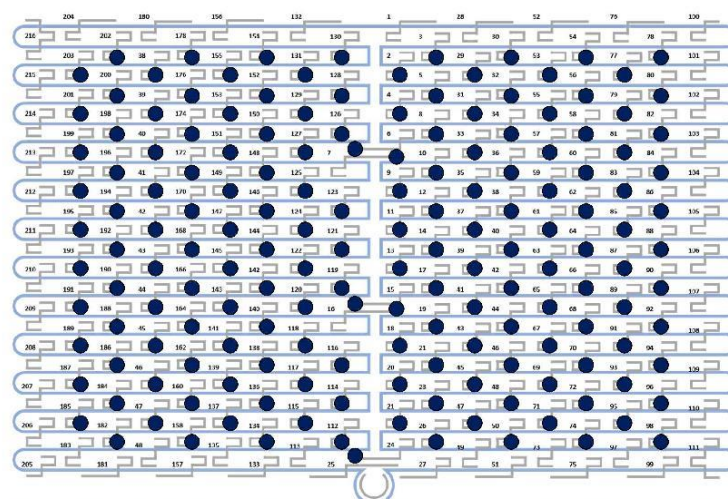


Figure S1 DNA tile. The design of DNA tile^[3] and the position of DNA handles to attach ATRP initiator moieties (dark blue circle) chosen from Cadnano software.^[4] The details of all staple strand DNA sequences are listed in Table S2.

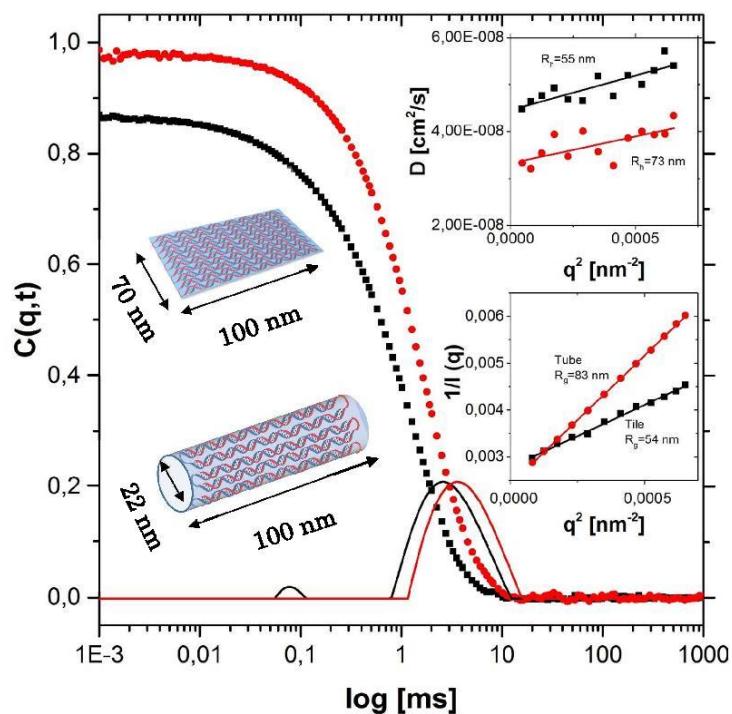


Figure S2 Relaxation functions $C_{vv}(q,t)$ for the translational diffusion dynamics in aqueous solution of the DNA tile (black filled squares) and DNA tube (red filled circles) at 20°C at a scattering wave vector ($q=0.009 \text{ nm}^{-1}$). Inverse Laplace transformation of experimental data yielded the distribution of one population for both the DNA tile and the DNA tube. Upper inset: The diffusion coefficient D vs q^2 , R_h (tile) = 55 nm and R_h (tube) = 73 nm. Lower inset: Light scattering intensity $1/I(q)$ as a function of q^2 for the DNA tile (black squares) and the DNA tube (red circles). R_g (tile)=54 nm R_g (tube) = 83 nm.

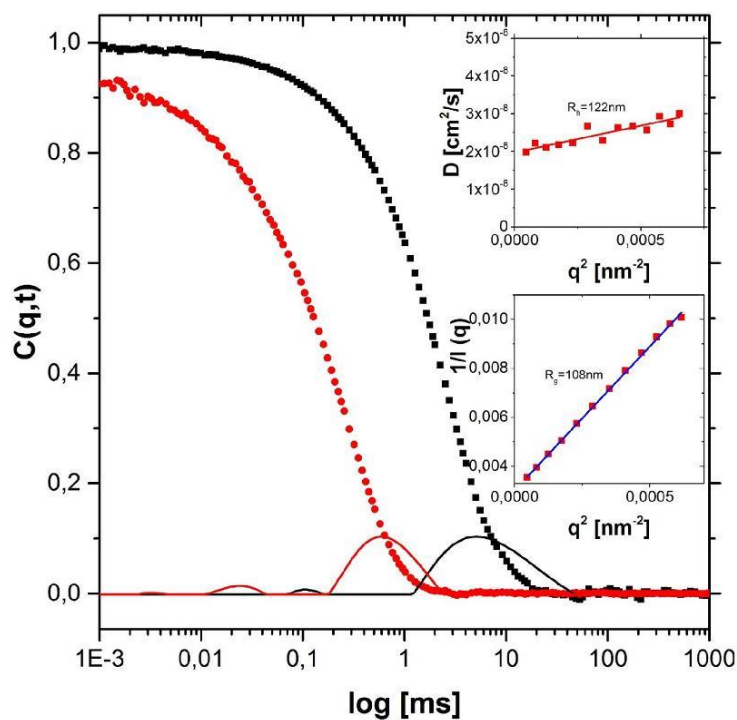


Figure S3 Normalized field correlation functions $C_{vv}(q,t)$ at a scattering wave vector $q=0.009 \text{ nm}^{-1}$ (black filled squares) and $q=0.024 \text{ nm}^{-1}$ (red filled circles) for the translational diffusion dynamics in aqueous solution of polymer coated DNA tube at 20°C . Inverse Laplace transformation of experimental data yielded to distribution of two populations for both wave vectors. Upper right inset: Double logarithmic plot of the diffusion coefficient D , $R_h=122 \text{ nm}$. Lower right inset: $1/I(q)$ versus q^2 for the polymer coated DNA tube (black squares). From equation 1, R_g was calculated. $R_g=108 \text{ nm}$.

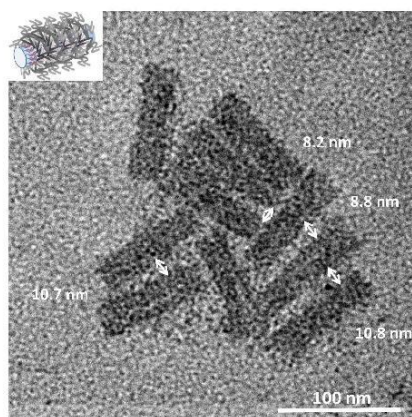


Figure S4 TEM image of stacking polymer tube.

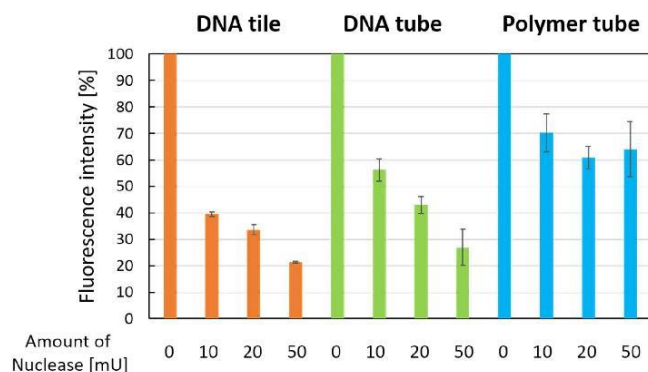


Figure S5 Stability of different DNA origami structures against nuclease digestion. DNA tile, tube, and polymer tube were labeled with SYBR-safe for 30 min. SYBR safe is a cyanine-based organic dye, which shows high fluorescence signal when it is intercalated into dsDNA. Thus, the degradation of DNA origami causes SYBR safe release from DNA origami resulting in decrease of the fluorescence intensity. Different amounts of nuclease (0-50 mU) were added to the labeled DNA origami structures and incubated at 37 degrees for 30 min. The fluorescence intensity of SYBR-safe was recorded and plotted as fluorescence intensity compared to the non-nuclease treated sample (the columns with amount of Dnase "0"). Since both ends of the DNA tubes are open, nucleases could in principle access the tube from both ends, which might explain the 30 % decrease of fluorescence intensity. However, after polymer coating, about 60 % to 70 % emission was observed for the polymer tube, compared to the DNA tube, for which only 20 % to 30 % emission intensity was recorded.

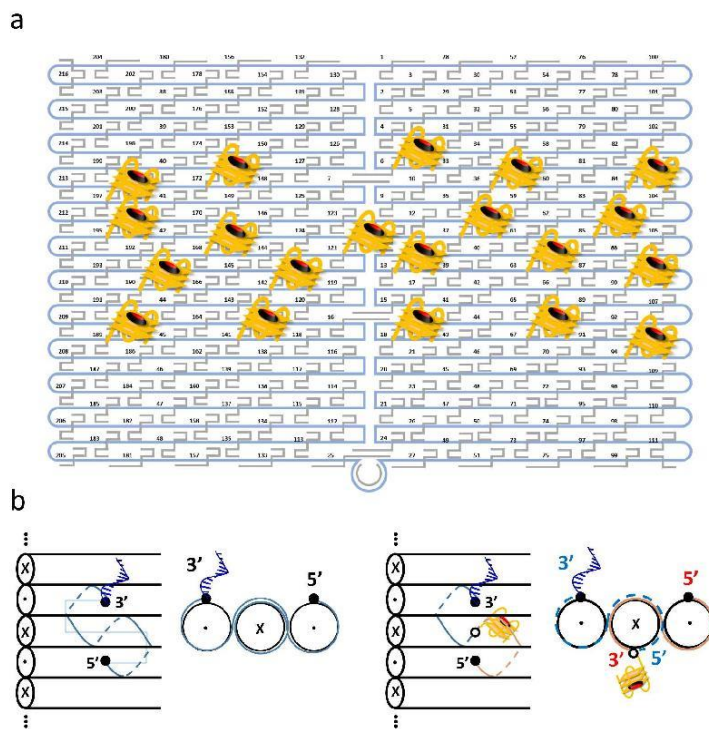


Figure S6 DNzyme-incorporated DNA tile. (a) 20 DNzyme moieties are positioned onto the surface opposite to DNA handle-introduced surface (Figure S1). (b) DNA handles are introduced to staple DNA sequence by extending its 3' that are exposed on to the surface (left). To introduce DNzyme to the opposite side to DNA handle, DNA handle extended sequences (blue, left) are divided into two sequences; DNA handle-extended part (dashed blue, right) and DNzyme incorporated part (orange, right).

Table S1 Summary of dimensions of the DNA tile, DNA tube, polymer tube, G4-incorporated DNA tube before / after ATRP (G4-tube / G4-polymer tube) from theoretical, AFM, and DLS.

Construct		Theoretical (nm)	AFM (nm)	DLS, R_h (nm)
DNA Tile	L	100	99.0 ± 2.2	55 ± 3
	W	70	78.0 ± 4.0	
	H	2	3.1 ± 0.1	
DNA Tube	L	100	97.0 ± 4.9	83 ± 2
	W	22	36.0 ± 6.0	
	H	22	5.0 ± 0.7	
Polymer Tube		-	91.0 ± 6.4 44.0 ± 6.0 7.0 ± 0.5	122 ± 13
G4-Tube	L	100	93.3 ± 3.9	
	W	22	37.0 ± 4.0	
	H	22	7.2 ± 1.0	
G4-Polymer Tube		-	95.7 ± 5.7 55.0 ± 10 11.1 ± 1.9	

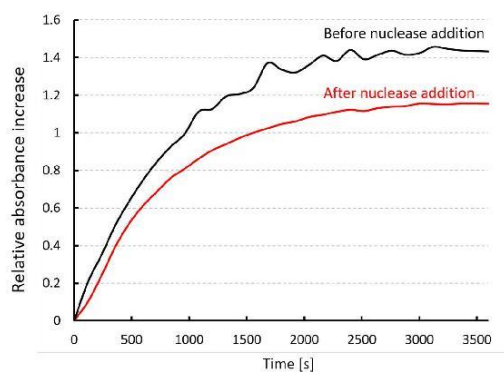


Figure S7 ABTS activity of DNazymes in polymer tubes before / after nuclease addition (50 mU). 80 % of the DNazyme activity was maintained even in nuclease presence.

Table S2 Detail of staple DNA sequences. Each number corresponds to the position shown in Figure S1. The Sequences extended with sticky DNA handle sequence at 3' are named as "3stX (X = position number)". Folding DNA sequences to transform DN tile to DNA tube are named as "FX". For preparing DNAzyme-introduce DNA tile, the sequences are separated into DNA handle-extended part (3stX half) and DNAzyme-extended part (g4-X half)

No.	Sequence
1	CAAGCCCAATAGGAACCCATGTACAAACAGTT
3st2	AATGCCCCGTAAACAGTGCCCGTATCTCCCTCATTTTTTTAGTAGGTGGTAGAG
3st3	TGCCTTGACTGCCTATTTTCGGAACAGGGATAGTTTTTTAGTAGGTGGTAGAG
3st4	GAGCCGCCCCACCACCGGAACCGCGACGGAATTTTTTTAGTAGGTGGTAGAG
3st5	AACCAGAGACCCCTCAGAACCGCCAGGGGTCAGTTTTTTAGTAGGTGGTAGAG
3st6	TTATTCATAGGGAAGGTAAATATTCATTCAGTTTTTTAGTAGGTGGTAGAG
3st7	CATAACCCGAGGCATAGTAAGAGCTTTTAAGTTTTTTAGTAGGTGGTAGAG
3st8	ATTGAGGGTAAAGGTGAATTATCAATCACCGGTTTTTTAGTAGGTGGTAGAG
3st9	AAAAGTAATATCTTACCGAAGCCCTCCAGAGTTTTTTAGTAGGTGGTAGAG
3st10	GCAATAGCGCAGATAGCCGAACAATTCAACCGTTTTTTAGTAGGTGGTAGAG
3st11	CCTAATTTACGCTAACGAGCGTCTAATCAATATTTTTTTAGTAGGTGGTAGAG
3st12	TCTTACCAGCCAGTTACAAAATAAATGAAATATTTTTTTAGTAGGTGGTAGAG
3st13	ATCGGCTGCGAGCATGTAGAAACCTATCATATTTTTTTAGTAGGTGGTAGAG
3st14	CTAATTTATCTTTCTTATCATTCATCCTGAATTTTTTTAGTAGGTGGTAGAG
3st15	GCGTTATAGAAAAAGCCTGTTTAGAAGGCCGGTTTTTTAGTAGGTGGTAGAG
3st16	GCTCATTTTCGCATTAAATTTTTGAGCTTAGATTTTTTTAGTAGGTGGTAGAG
3st17	AATTACTACAAATCTTACCAGTAATCCCATCTTTTTTTAGTAGGTGGTAGAG
3st18	TTAAGACGTTGAAAACATAGCGATAACAGTACTTTTTTTAGTAGGTGGTAGAG
3st19	TAGAATCCCTGAGAAGAGTCAATAGGAATCATTTTTTTAGTAGGTGGTAGAG
3st20	CTTTTACACAGATGAATATACAGTAAACAATTTTTTTAGTAGGTGGTAGAG
3st21	TTTAACGTTCCGGAGAAACAATAATTTCCCTTTTTTTAGTAGGTGGTAGAG
3st22	CGACAAC TAAGTATTAGACTTTACAATACCGATTTTTTTAGTAGGTGGTAGAG
3st23	GGATTTAGCGTATTAAATCCTTTGTTTTTCAGGTTTTTTAGTAGGTGGTAGAG
3st24	ACGAACCAAAACATCGCCATTAAATGGTGGTTTTTTTTAGTAGGTGGTAGAG
25	GAACGTGCGAGAAAGGAAGGGAACAAACTAT

3st26	TAGCCCTACCAGCAGAAGATAAAAACATTTGATTTTTTTAGTAGGTGGTAGAG
27	CGGCCCTTGCTGGTAATATCCAGAACGAACTGA
28	CTCAGAGCCACCACCCTCATTTTCCTATTATT
3st29	CTGAAACAGGTAATAAGTTTTAACCCCTCAGATTTTTTTAGTAGGTGGTAGAG
3st30	AGTGTAAGTAAAGTATTAAGAGGCCGCCACCTTTTTTTAGTAGGTGGTAGAG
3st31	GCCACCACTCTTTTCATAATCAAACCGTCACCTTTTTTTAGTAGGTGGTAGAG
3st32	GTTTGCCACCTCAGAGCCGCCACCGATACAGTTTTTTTAGTAGGTGGTAGAG
3st33	GACTTGAGAGACAAAAGGGCGACAAGTTACCATTTTTTTAGTAGGTGGTAGAG
3st34	AGCGCCAACCATTTGGGAATTAGATTATTAGCTTTTTTTAGTAGGTGGTAGAG
3st35	GAAGGAAAATAAGAGCAAGAAACAACAGCCATTTTTTTAGTAGGTGGTAGAG
3st36	GCCCAATACCGAGGAAACGCAATAGGTTTACCTTTTTTTAGTAGGTGGTAGAG
3st37	ATTATTTAACCCAGCTACAATTTTCAAGAACGTTTTTTAGTAGGTGGTAGAG
3st38	TATTTTGCTCCCAATCCAAATAAGTGAGTTAATTTTTTTAGTAGGTGGTAGAG
3st39	GGTATTAAGAACAAGAAAATAATTAAGCCATTTTTTTAGTAGGTGGTAGAG
3st40	TAAGTCCTACCAAGTACCGCACTCTTAGTTGCTTTTTTTAGTAGGTGGTAGAG
3st41	ACGCTCAAAATAAGAATAAACACCGTGAATTTTTTTTAGTAGGTGGTAGAG
3st42	AGGCGTTACAGTAGGGCTTAATTGACAATAGATTTTTTTAGTAGGTGGTAGAG
3st43	ATCAAAATCGTCGCTATTAATTAACGGATTCGTTTTTTAGTAGGTGGTAGAG
3st44	CTGTAAATCATAGGTCTGAGAGACGATAAATTTTTTTAGTAGGTGGTAGAG
3st45	CCTGATTGAAGAAATTGCGTAGACCCGAACGTTTTTTTAGTAGGTGGTAGAG
3st46	ACAGAAATCTTTGAATACCAAGTTCCTTGCTTTTTTTTAGTAGGTGGTAGAG
3st47	TTATTAATGCCGTCAATAGATAATCAGAGGTGTTTTTTAGTAGGTGGTAGAG
3st48	AGATTAGATTTAAAAGTTTGAGTACACGTAAATTTTTTTAGTAGGTGGTAGAG
3st49	AGGCGGTCATTAGTCTTTAATGCGCAATATTATTTTTTTAGTAGGTGGTAGAG
3st50	GAATGGCTAGTATTAACACCGCCTCAACTAATTTTTTTAGTAGGTGGTAGAG
51	CCGCCAGCCATTGCAACAGGAAAAATATTTTT
52	CCCTCAGAACCGCCACCTCAGAACTGAGACT
3st53	CCTCAAGAATACATGGCTTTTGATAGAACCACTTTTTTTAGTAGGTGGTAGAG
3st54	TAAGCGTCGAAGGATTAGGATTAGTACCGCCATTTTTTTAGTAGGTGGTAGAG
3st 55	CACCAGAGTTCGGTCATAGCCCCGCCAGCAATTTTTTTAGTAGGTGGTAGAG
3st 56	TCGGCATTCCGCCGCCAGCATTGACGTTCCAGTTTTTTTAGTAGGTGGTAGAG
3st 57	AATCACCAAATAGAAAATTCATATATAACGGATTTTTTTAGTAGGTGGTAGAG
3st 58	TCACAATCGTAGCACCATTACCATCGTTTTTCATTTTTTTAGTAGGTGGTAGAG
3st 59	ATACCCAAGATAACCCACAAGAATAAACGATTTTTTTTAGTAGGTGGTAGAG

3st60	ATCAGAGAAAGAACTGGCATGATTTTATTTTGTGTTTTTTAGTAGGTGGTAGAG
3st61	TTTTGTTTAAGCCTTAAATCAAGAATCGAGAATTTTTTTAGTAGGTGGTAGAG
3st62	AGGTTTTGAACGTCAAAAATGAAAGCGCTAATTTTTTTAGTAGGTGGTAGAG
3st63	CAAGCAAGACGCGCCTGTTTATCAAGAATCGCTTTTTTTAGTAGGTGGTAGAG
3st64	AATGCAGACCGTTTTTATTTTCATCTTGCGGGTTTTTTAGTAGGTGGTAGAG
3st65	CATATTTAGAAATACCGACCGTTACCTTTTTTTTTAGTAGGTGGTAGAG
3st66	AATGGTTTACAACGCCAACATGTAGTTCAGCTTTTTTTAGTAGGTGGTAGAG
3st67	TAACCTCCATATGTGAGTGAATAACAAAATCTTTTTTTAGTAGGTGGTAGAG
3st68	AAATCAATGGCTTAGGTTGGGTTACTAAATTTTTTTTTAGTAGGTGGTAGAG
3st 69	GCGCAGAGATATCAAAATTATTTGACATTATCTTTTTTTAGTAGGTGGTAGAG
3st 70	AACCTACCGCGAATTATTCATTTCCAGTACATTTTTTTAGTAGGTGGTAGAG
3st 71	ATTTTGCGTCTTTAGGAGCACTAAGCAACAGTTTTTTTTAGTAGGTGGTAGAG
3st 72	CTAAATAGAACAAAGAAACCACCAGGTTAGTTTTTTAGTAGGTGGTAGAG
3st73	GCCACGCTATACGTGGCACAGACAACGCTCATTTTTTTAGTAGGTGGTAGAG
3st74	GCGTAAGAGAGAGCCAGCAGCAAAAAGGTTATTTTTTTAGTAGGTGGTAGAG
75	GGAAATACCTACATTTGACGCTCACCTGAAA
76	TATCACCGTACTCAGGAGGTTTAGCGGGGTTT
3st77	TGCTCAGTCAGTCTCTGAATTTACCAGGAGGTTTTTTTAGTAGGTGGTAGAG
3st78	GGAAAGCGACCAGGCGGATAAGTGAATAGGTGTTTTTTAGTAGGTGGTAGAG
3st79	TGAGGCAGGCGTCAGACTGTAGCGTAGCAAGGTTTTTTAGTAGGTGGTAGAG
3st80	TGCCTTTAGTCAGACGATTGGCCTGCCAGAATTTTTTTAGTAGGTGGTAGAG
3st81	CCGGAACACACCACGGAATAAGTAAGACTCCTTTTTTTAGTAGGTGGTAGAG
3st82	ACGCAAAGGTCACCAATGAAACCAATCAAGTTTTTTTTAGTAGGTGGTAGAG
3st83	TTATTACGGTCAGAGGGTAATTGAATAGCAGCTTTTTTTAGTAGGTGGTAGAG
3st84	TGAACAAACAGTATGTTAGCAAACTAAAAGAATTTTTTTAGTAGGTGGTAGAG
3st85	CTTTACAGTTAGCGAACCTCCCGACGTAGGAATTTTTTTAGTAGGTGGTAGAG
3st86	GAGGCGTTAGAGAATAACATAAAAGAACACCCTTTTTTTAGTAGGTGGTAGAG
3st87	TCATTACCCGACAATAAACAACATATTTAGGCTTTTTTTAGTAGGTGGTAGAG
3st88	CCAGACGAGCGCCCAATAGCAAGCAAGAACGCTTTTTTTAGTAGGTGGTAGAG
3st89	AGAGGCATAATTTTCATCTTCTGACTATAACTATTTTTTTAGTAGGTGGTAGAG
3st90	TTTTAGTTTTTCGAGCCAGTAATAAATTCTGTTTTTTTTAGTAGGTGGTAGAG
3st91	TATGTAACCTTTTTTAAATGGAAAAATTACCTTTTTTTAGTAGGTGGTAGAG
3st92	TTGAATTATGCTGATGCAAAATCCACAATATATTTTTTTAGTAGGTGGTAGAG
3st93	GAGCAAAAACCTTCTGAATAATGAAGAAGGAGTTTTTTTAGTAGGTGGTAGAG

3st94	TGGATTATGAAGATGATGAAACAAAATTTTCATTTTTTTTAGTAGGTGGTAGAG
3st95	CGGAATTATTGAAAGGAATTGAGGTGAAAAATTTTTTTAGTAGGTGGTAGAG
3st96	ATCAACAGTCATCATATTCCTGATTGATTGTTTTTTTTAGTAGGTGGTAGAG
3st97	CTAAAGCAAGATAGAACCCTTCTGAATCGTCTTTTTTTAGTAGGTGGTAGAG
3st98	GCCAACAGTCACCTTGCTGAACCTGTTGGCAATTTTTTTAGTAGGTGGTAGAG
99	GAAATGGATTATTTACATTGGCAGACATTCTG
100	TTTTTATAAGTATAGCCCGGCCGTCGAG
101	AGGGTTGATTTTATAAATCCTCATTAAATGATATTC
102	ACAAACAATTTTAAATCAGTAGCGACAGATCGATAGC
103	AGCACCGTTTTTTAAAGGTGGCAACATAGTAGAAAA
104	TACATACATTTTGACGGGAGAATTAACACAGGGAA
105	GCGCATTATTTTGCTTATCCGGTATTCTAAATCAGA
106	TATAGAAGTTTTTCGACAAAAGGTAAAGTAGAGAATA
107	TAAAGTACTTTTCGCGAGAAAACTTTTATCGCAAG
108	ACAAAGAATTTTATTAAATTACATTTAACACATCAAG
109	AAAACAAATTTTTTCATCAATATAATCCTATCAGAT
110	GATGGCAATTTTAAATCAATATCTGGTCACAAATATC
111	AAACCCTCTTTTACCAGTAATAAAAGGGATTACCAGTCACACGTTTT
3st112	CCGAAATCCGAAAATCCTGTTTGAAGCCGGAATTTTTTTAGTAGGTGGTAGAG
3st113	CCAGCAGGGGCAAAATCCCTTATAAAGCCGGCTTTTTTTAGTAGGTGGTAGAG
3st114	GCATAAAGTTCCACACAACATACGAAGCGCCATTTTTTTAGTAGGTGGTAGAG
3st115	GCTCACAATGTAAAGCCTGGGGTGGGTTTGCCTTTTTTTAGTAGGTGGTAGAG
3st116	TTGCCCATTGCCGGAACACAGGCATTAAATCATTTTTTTAGTAGGTGGTAGAG
3st117	GCTTCTGGTCAGGCTGCGCAACTGTGTTATCCTTTTTTTAGTAGGTGGTAGAG
3st118	GTTAAATTTTAAACCAATAGGAACCCGGCACCTTTTTTTAGTAGGTGGTAGAG
3st119	AGACAGTCATTCAAAGGGTGAGAAGCTATATTTTTTTAGTAGGTGGTAGAG
3st120	AGGTAAAGAAATCACCATCAATATAATATTTTTTTTTAGTAGGTGGTAGAG
3st121	TTTCATTTGGTCAATAACCTGTTTATATCGCGTTTTTTAGTAGGTGGTAGAG
3st122	TCGCAAATGGGGCGCGAGCTGAAATAATGTGTTTTTTAGTAGGTGGTAGAG
3st123	TTTTAATTGCCCGAAAGACTTCAAACACTATTTTTTTAGTAGGTGGTAGAG
3st124	AAGAGGAACGAGCTTCAAAGCGAAGATACATTTTTTTAGTAGGTGGTAGAG
3st125	GGAATTACTCGTTTACCAGACGACAAAAGATTTTTTTAGTAGGTGGTAGAG
3st126	GAATAAGGACGTAACAAAGCTGCTCTAAAACATTTTTTTAGTAGGTGGTAGAG
3st127	CCAAATCACTTGCCCTGACGAGAACGCCAAAATTTTTTTAGTAGGTGGTAGAG

3st128	CTCATCTTGAGGCCAAAAGAATACAGTGAATTTTTTTTTTAGTAGGTGGTAGAG
3st129	AAACGAAATGACCCCGAGCGATTATTCATTCTTTTTTTAGTAGGTGGTAGAG
3st130	CTTAAACATCAGCTTGCTTTCGAGCGTAACACTTTTTTTAGTAGGTGGTAGAG
3st131	TCGGTTTAGCTTGATACCGATAGTCCAACCTATTTTTTTAGTAGGTGGTAGAG
132	TGAGTTTCGTCACCAAGTACAACTTAATTGTA
133	CCCCGATTAGAGCTTGACGGGGAAATCAAAA
3st134	GAATAGCCGCAAGCGGTCCACGCTCCTAATGATTTTTTTAGTAGGTGGTAGAG
3st135	GAGTTGCACGAGATAGGGTTGAGTAAGGGAGCTTTTTTTAGTAGGTGGTAGAG
3st136	GTGAGCTAGTTTCTGTGTGAAATTTGGGAAGTTTTTTAGTAGGTGGTAGAG
3st137	TCATAGCTACTCACATTAATTGCGCCCTGAGATTTTTTTAGTAGGTGGTAGAG
3st138	GGCGATCGCACTCCAGCCAGCTTTGCCATCAATTTTTTTAGTAGGTGGTAGAG
3st139	GAAGATCGGTGCGGGCCTCTTCGCAATCATGGTTTTTTAGTAGGTGGTAGAG
3st140	AAATAATTTTAAATTGTAAACGTTGATATTCTTTTTTTAGTAGGTGGTAGAG
3st141	GCAAATATCGCGTCTGGCCTTCCTGGCCTCAGTTTTTTAGTAGGTGGTAGAG
3st142	ACCGTTCTAAATGCAATGCCTGAGAGGTGGCATTTTTTTAGTAGGTGGTAGAG
3st143	TATATTTAGCTGATAAATTAATGTTGTATAATTTTTTTAGTAGGTGGTAGAG
3st144	TCAATCTTTTAGTTTGACCATACCAGACCGTTTTTTAGTAGGTGGTAGAG
3st145	CGAGTAGAACTAATAGTAGTAGCAAACCTCATTTTTTTAGTAGGTGGTAGAG
3st146	GAAGCAAAAAGCGGATTGCATCAGATAAAAATTTTTTTAGTAGGTGGTAGAG
3st147	TCAGAAGCCTCCAACAGGTCAGGATCTGCGAATTTTTTTAGTAGGTGGTAGAG
3st148	CCAAAATATAATGCAGATACATAAACACCAGATTTTTTTAGTAGGTGGTAGAG
3st149	CATTCAACGCGAGAGGCTTTTGCATATTATAGTTTTTTAGTAGGTGGTAGAG
3st150	ACGAGTAGTGACAAGAACCGGATATACCAAGCTTTTTTTAGTAGGTGGTAGAG
3st151	AGTAATCTTAAATTGGGCTTGAGAGAATACCATTTTTTTAGTAGGTGGTAGAG
3st152	GCGAAACATGCCACTACGAAGGCATGCGCCGATTTTTTTAGTAGGTGGTAGAG
3st153	ATACGTAAAAGTACAACGGAGATTTTCATCAAGTTTTTTAGTAGGTGGTAGAG
3st154	CAATGACACTCCAAAAGGAGCCTTACAACGCCTTTTTTTAGTAGGTGGTAGAG
3st155	AAAAAAGGACAACCATCGCCACGCGGGTAAATTTTTTTAGTAGGTGGTAGAG
156	TGTAGCATTCACAGACAGCCCTCATCTCAA
157	GTAAAGCACTAAATCGGAACCCTAGTTGTTCC
3st158	AGTTTGAGCCCTTCACCGCCTGGTTGCGCTCTTTTTTTAGTAGGTGGTAGAG
3st159	AGCTGATTACAAGAGTCCACTATTGAGGTGCCTTTTTTTAGTAGGTGGTAGAG
3st160	ACTGCCCGCCGAGCTCGAATTCGTTATTACGCTTTTTTTAGTAGGTGGTAGAG
3st161	CCCGGGTACTTTCAGTCGGGAAACGGGCAACTTTTTTTAGTAGGTGGTAGAG

3st162	CAGCTGGCGGACGACGACAGTATCGTAGCCAGTTTTTTTAGTAGGTGGTAGAG
3st163	GTTTGAGGGAAAGGGGGATGTGCTAGAGGATCTTTTTTAGTAGGTGGTAGAG
3st164	CTTTCATCCCCAAAACAGGAAGACCGAGAGTTTTTTTAGTAGGTGGTAGAG
3st165	AGAAAAGCAACATTAATGTGAGCATCTGCCATTTTTTTAGTAGGTGGTAGAG
3st166	GGTAGCTAGGATAAAAATTTTTAGTTAACATCTTTTTTAGTAGGTGGTAGAG
3st167	CAACGCAATTTTTGAGAGATCTACTGATAATCTTTTTTTAGTAGGTGGTAGAG
3st168	CAATAAATACAGTTGATTCCCAATTTAGAGAGTTTTTTTAGTAGGTGGTAGAG
3st169	TCCATATACATACAGGCAAGGCAACTTTATTTTTTTTAGTAGGTGGTAGAG
3st170	TACCTTTAAGGTCTTTACCGTGACAAAGAAGTTTTTTTAGTAGGTGGTAGAG
3st171	CAAAAATCATTGCTCCTTTTGATAAGTTTCATTTTTTTAGTAGGTGGTAGAG
3st172	TTTGCCAGATCAGTTGAGATTTAGTGGTTTAATTTTTTTAGTAGGTGGTAGAG
3st173	AAAGATTCAAGGGGTAATAGTAAACCATAAATTTTTTTAGTAGGTGGTAGAG
3st174	TTTCAACTATAGGCTGGCTGACCTTGATCATTTTTTTAGTAGGTGGTAGAG
3st175	CCAGGCGCTTAATCATTGTGAATTACAGGTAGTTTTTTAGTAGGTGGTAGAG
3st176	CGCCTGATGGAAGTTTCCATTAAACATAACCGTTTTTTAGTAGGTGGTAGAG
3st177	TTTCATGAAAATTGTGTCGAAATCTGTACAGATTTTTTTAGTAGGTGGTAGAG
3st178	ATATATTCTTTTTCACGTTGAAAATAGTTAGTTTTTTAGTAGGTGGTAGAG
3st179	AATAATAAGGTCGCTGAGGCTTGCAAAGACTTTTTTTAGTAGGTGGTAGAG
180	CGTAACGATCTAAAGTTTGTGCGTGAATTGCG
181	ACCCAAATCAAGTTTTTTGGGGTCAAAGAACG
3st182	TGGACTCCCTTTTCACCAGTGAGACCTGTCGTTTTTTTAGTAGGTGGTAGAG
3st183	TGGTTTTTAACGTCAAAGGGCGAAGAACCATCTTTTTTTAGTAGGTGGTAGAG
3st184	GCCAGCTGCCTGCAGGTCGACTCTGCAAGGCGTTTTTTAGTAGGTGGTAGAG
3st185	CTTGCAATGCATTAAATGAATCGGCCCGCCAGGGTTTTTTAGTAGGTGGTAGAG
3st186	ATTAAGTTCGCATCGTAACCGTGCGAGTAACATTTTTTTAGTAGGTGGTAGAG
3st187	TAGATGGGGGTAACGCCAGGGTTGTGCCAAGTTTTTTAGTAGGTGGTAGAG
3st188	ACCCGTCGTCATATGTACCCCGGTAAAGGCTATTTTTTTAGTAGGTGGTAGAG
3st189	CATGTCAAGATTCTCCGTGGGAACCGTTGGTGTTTTTTTAGTAGGTGGTAGAG
3st190	TCAGGTCACTTTTGCGGGAGAAGCAGAATTAGTTTTTTAGTAGGTGGTAGAG
3st191	CTGTAATATTGCTGAGAGTCTGAAAACCTAGTTTTTTAGTAGGTGGTAGAG
3st192	CAAAATTAAAGTACGGTGTCTGGAAGAGGTCATTTTTTTAGTAGGTGGTAGAG
3st193	TGCAACTAAGCAATAAAGCCTCAGTTATGACCTTTTTTTAGTAGGTGGTAGAG
3st194	TTTTTGCGCAGAAAACGAGAATGAATGTTTAGTTTTTTAGTAGGTGGTAGAG
3st195	AAACAGTTGATGGCTTAGAGCTTATTTAAATATTTTTTTAGTAGGTGGTAGAG

3st196	ACTGGATAACGGAAACAACATTATTACCTTATGTTTTTTTAGTAGGTGGTAGAG
3st197	ACGAACTAGCGTCCAATACTGCGGAATGCTTTTTTTTAGTAGGTGGTAGAG
3st198	CGATTTTAGAGGACAGATGAACGGCGCGACCTTTTTTTTAGTAGGTGGTAGAG
3st199	CTTTGAAAAGAACTGGCTCATTATTTAATAAATTTTTTAGTAGGTGGTAGAG
3st200	GCTCCATGAGAGGCTTTGAGGACTAGGAGTTTTTTTTTAGTAGGTGGTAGAG
3st201	ACGGCTACTTACTTAGCCGGAACGCTGACCAATTTTTTTTAGTAGGTGGTAGAG
3st202	AAAGGCCGAAAGGAACAACATAAGCTTTCCAGTTTTTTTAGTAGGTGGTAGAG
3st203	GAGAATAGCTTTTGCGGGATCGTCGGGTAGCATTTTTTTAGTAGGTGGTAGAG
204	ACGTTAGTAAATGAATTTTCTGTAAGCGGAGT
205	TTTTCGATGGCCCACTACGTAACCGTC
206	TATCAGGGTTTTCGGTTTGCCTATTGGGAACGCGCG
207	GGGAGAGGTTTTGTAAACGACGGCCATTCCCAGT
208	CACGACGTTTTGTAAATGGGATAGGTCAAACGCGCG
209	GATTGACCTTTTGATGAACGGTAATCGTAGCAAACA
210	AGAGAATCTTTTGGTTGTACCAAAAACAAGCATAAA
211	GCTAAATCTTTCTGTAGCTCAACATGTATTGCTGA
212	ATATAATGTTTTTATTGAATCCCCCTCAAATCGTCA
213	TAAATATTTTTTGAAGAAAAATCTACGACCAGTCA
214	GGACGTTGTTTTTATAGGGAACCGAAAGGCGCAG
215	ACGGTCAATTTTGACAGCATCGGAACGAACCCCTCAG
216	CAGCGAAAATTTTACTTTCAACAGTTTCTGGGATTTTGCTAAACTTTT
217	AACATCACTTGCCTGAGTAGAAGAACT
218	TGTAGCAATACTTTTATTGATTAGTAAT
219	AGTCTGTCCATCACGCAAATTAACCGT
220	ATAATCAGTGAGGCCACCGAGTAAAAG
221	ACGCCAGAATCCTGAGAAGTGTTTTT
222	TTAAAGGGATTTTAGACAGGAACGGT
223	AGAGCGGGAGCTAAACAGGAGGCCGA
224	TATAACGTGCTTTCTCGTTAGAATC
225	GTAATATGTTGCTTTGACGAGCACG
226	GCGCTTAATGCGCCGCTACAGGGCGC
F1	AATAATAATAATAATCAAGCCCAATAGGAACCCATGTACAAACAGTT
F25	AATAATAATAATAATGAACGTGGCGAGAAAGGAAGGGAACAACTAT
F27	CAAGCCCACTGGTAATATCCAGAACGAACCTGA

F28	CCGCCAGCCACCACCCTCATTTTCCTATTATT
F51	CTCAGAGCCATTGCAACAGGAAAAATATTTTT
F52	GGAAATACACCGCCACCCTCAGAACTGAGACT
F75	CCCTCAGACTACATTTTGACGCTCACCTGAAA
F76	GAAATGGATACTCAGGAGGTTTAGCGGGGTTT
F99	TATCACCGTTATTTACATTGGCAGACATTCTG
F132	GAACGTGGGTCACCAGTACAACTTAATTGTA
F133	TGTAGCATTAGAGCTTGACGGGGAAATCAAAA
F156	CCCCGATTTCCACAGACAGCCCTCATCTCAA
F157	CGTAACGACTAAATCGGAACCCTAGTTGTTCC
F180	GTAAAGCATCTAAAGTTTTGTGCGTAATTGCG
F181	ACGTTAGTCAAGTTTTTTGGGGTCAAAGAACG
F204	ACCCAAATAAATGAATTTTCTGTAAGCGGAGT
g4-6half	TTATTCATAGGGAAGG TTTTGGGTAGGGCGGGTTGGG
3st6half	TAAATATT CATTCACT TTTTTTGTAGGTGGTAGAG
g4-13half	ATCGGCTGCGAGCATG TTTTGGGTAGGGCGGGTTGGG
3st13half	TAGAAACCTATCATAT TTTTTTGTAGGTGGTAGAG
g4-18half	TTAAGACGTTGAAAC TTTTGGGTAGGGCGGGTTGGG
3st18half	ATAGCGATAACAGTAC TTTTTTGTAGGTGGTAGAG
g4-36half	GCCCAATACCGAGGAA TTTTGGGTAGGGCGGGTTGGG
3st36half	ACGCAATAGGTTTACCTTTTTTGTAGGTGGTAGAG
g4-37half	ATTATTTAACCAGCT TTTTGGGTAGGGCGGGTTGGG
3st37half	ACAATTTTCAAGAACG TTTTTTGTAGGTGGTAGAG
g4-63half	CAAGCAAGACGCGCCT TTTTGGGTAGGGCGGGTTGGG
3st63half	GTTTATCAAGAATCGC TTTTTTGTAGGTGGTAGAG
g4-67half	TAACCTCCATATGTGA TTTTGGGTAGGGCGGGTTGGG
3st67half	GTGAATAAACAAAATCTTTTTTGTAGGTGGTAGAG
g4-84half	TGAACAAACAGTATGT TTTTGGGTAGGGCGGGTTGGG
3st84half	TAGCAAATAAAAGAA TTTTTTGTAGGTGGTAGAG
g4-85half	CTTTACAGTTAGCGAA TTTTGGGTAGGGCGGGTTGGG
3st85half	CCTCCCGACGTAGGAA TTTTTTGTAGGTGGTAGAG
g4-90half	TTTTAGTTTTTCGAGC TTTTGGGTAGGGCGGGTTGGG
3st90half	CAGTAATAAATTCTGT TTTTTTGTAGGTGGTAGAG
g4-94half	TGGATTATGAAGATGA TTTTGGGTAGGGCGGGTTGGG
3st94half	TGAAACAAAATTTTCA TTTTTTGTAGGTGGTAGAG

g4-121half	TTTCATTTGGTCAATA TTTTGGGTAGGGCGGGTTGGG
3st121half	ACCTGTTTATATCGCGTTTTTTTAGTAGGTGGTAGAG
g4-141half	GCAAATATCGCGTCTG TTTTGGGTAGGGCGGGTTGGG
3st141half	GCCTTCCTGGCCTCAGTTTTTTTAGTAGGTGGTAGAG
g4-142half	ACCGTTCTAAATGCAA TTTTGGGTAGGGCGGGTTGGG
3st142half	TGCCTGAGAGGTGGCA TTTTTTAGTAGGTGGTAGAG
g4-168half	CAATAAATACAGTTGA TTTTGGGTAGGGCGGGTTGGG
3st168half	TTCCCAATTTAGAGAG TTTTTTAGTAGGTGGTAGAG
g4-172half	TTTGCCAGATCAGTTG TTTTGGGTAGGGCGGGTTGGG
3st172half	AGATTTAGTGGTTTAA TTTTTTAGTAGGTGGTAGAG
g4-189half	CATGTCAAGATTCTCC TTTTGGGTAGGGCGGGTTGGG
3st189half	GTGGGAACCGTTGGTG TTTTTTAGTAGGTGGTAGAG
g4-190half	TCAGGTCACTTTTGCG TTTTGGGTAGGGCGGGTTGGG
3st190half	GGAGAAGCAGAATTAG TTTTTTAGTAGGTGGTAGAG
g4-195half	AAACAGTTGATGGCTT TTTTGGGTAGGGCGGGTTGGG
3st195half	AGAGCTTATTTAAATA TTTTTTAGTAGGTGGTAGAG
g4-199half	CTTTGAAAAGAACTGG TTTTGGGTAGGGCGGGTTGGG
3st199half	CTCATTATTTAATAAA TTTTTTAGTAGGTGGTAGAG

References

- [1] E. Stahl, T. G. Martin, F. Praetorius, H. Dietz, *Angew. Chem.Int. Ed.* 2014, 53, 12735-12740.
- [2] S. E. Averick, S. K. Dey, D. Grahacharya, K. Matyjaszewski, S. R. Das, *Angew. Chem. Int. Ed.* 2014, 53, 2739-2744.
- [3] P. W. Rothmund, *Nature* 2006, 440, 297-302
- [4] S. M. Douglas, A. H. Marblestone, S. Teerapittayanon, A. Vazquez, G. M. Church, W. M. Shih, *Nucleic Acids Res.* 2009, 37, 5001-5006

[6-3] Fabrication of defined polydopamine nanostructures by DNA origami-templated polymerization

Yu Tokura⁺, Sean Harvey⁺, Chaojian Chen, and Yuzhou Wu^{*}, David Y. W. Ng^{*}, and Tanja Weil^{*}

⁺ shared first authorship, ^{*} corresponding author

Status: *Angew. Chem. Int. Ed.* 2018, 130, 1603–1607

Copyright: Reproduced by permission of the publisher John Wiley and Sons.

Abstract:

We report a versatile, bottom-up approach for the controlled fabrication of polydopamine (PD) nanostructures on DNA origami. PD is a biosynthetic polymer that has been investigated as an adhesive and promising surface coating material. However, the control of dopamine polymerization is challenged by the multi stage-mediated reaction mechanism and diverse chemical structures in PD. We utilized DNA origami decorated with multiple horseradish peroxidase-mimicking DNAzyme motifs to control the shape and size of PD formation with nanometer resolution. These fabricated PD nanostructures can serve as “supramolecular glue” for controlling DNA origami conformations. Facile liberation of the PD nanostructures from the DNA origami templates has been achieved in acidic medium. This presented DNA origami-controlled polymerization of a highly crosslinked polymer provides a unique access towards anisotropic PD architectures with distinct shapes that were retained even in the absence of the DNA origami template.

Contribution of the respective authors:

Yu Tokura: Design and synthesis of DNA origami, AFM study and analysis, performing agarose gel electrophoresis study, performing liberation of polydopamine nanostructures from DNA origami, writing the manuscript.

Sean Harvey: Optimization of the polymerization of dopamine on DNA origami, evaluating DNAzyme activity by ABTS assay, performing kinetics study of polydopamine formation, writing the manuscript.

Chaojian Chen: TEM measurement

Yuzhou Wu: Design of the project, taking the responsibility for the development of DNA templated synthesis, support with troubleshooting, writing and correcting the manuscript.

David Y. W. Ng: Troubleshooting the initiation and control of dopamine polymerization/growth under origami conditions, writing and correcting the manuscript

Tanja Weil: Acquiring funding for the project, design and discussion of the concept and results, writing and correcting the manuscript.

Fabrication of Defined Polydopamine Nanostructures by DNA Origami-Templated Polymerization

Yu Tokura[†], Sean Harvey[†], Chaojian Chen, Yuzhou Wu,^{*} David Y. W. Ng,^{*} and Tanja Weil^{*}

Abstract: A versatile, bottom-up approach allows the controlled fabrication of polydopamine (PD) nanostructures on DNA origami. PD is a biosynthetic polymer that has been investigated as an adhesive and promising surface coating material. However, the control of dopamine polymerization is challenged by the multistage-mediated reaction mechanism and diverse chemical structures in PD. DNA origami decorated with multiple horseradish peroxidase-mimicking DNAzyme motifs was used to control the shape and size of PD formation with nanometer resolution. These fabricated PD nanostructures can serve as “supramolecular glue” for controlling DNA origami conformations. Facile liberation of the PD nanostructures from the DNA origami templates has been achieved in acidic medium. This presented DNA origami-controlled polymerization of a highly crosslinked polymer provides a unique access towards anisotropic PD architectures with distinct shapes that were retained even in the absence of the DNA origami template.

Nanofabrication of polymer materials with high precision and resolution is in high demand for numerous modern technologies in the information era. From biochips for controlling cell adhesion and behavior, micro/nanofluidic systems with highly integrated functions, to photonic materials with quantum optical properties, these state-of-the-art devices contain immense information given their small footprint.^[1] Polymers, which are quintessential in many of these

devices, would naturally be required to break its limits on their fabrication. However, with current available techniques mainly based on top-down strategies, such as lithography, high instrumental costs and long operation times as well as its resolution of control limit wider use. On the other hand, although restricted by the scale of operation, bottom-up approaches have recently seen development with the assistance of DNA origami nanotechnology.^[2] DNA origami is a powerful DNA nanotechnology that offers systematic design of a large variety of defined DNA nanostructures by self-assembling scaffold DNA and staple DNA sequences.^[3] Computer-assisted design provides almost limitless access to any defined nanostructure in 2D and 3D^[4] with each DNA staple sequence encoding a specific position that can be precisely modified. This concept has been utilized to arrange metal nanoparticles,^[5] proteins,^[6] and fluorescent molecules^[7] with nanometer resolution. For higher complexity, DNA origami has been employed as a versatile framework to cast metal nanoparticles^[8] and liposomes^[9] in their confined 3D space. By integrating DNA origami with polymer chemistry, we have previously established this platform for spatially controlling “grafting from” polymer growth using atom transfer radical polymerization.^[10] In this manuscript, the DNA templated strategy was applied for the first time to control the polymerization of PD and the formation of anisotropic PD nanostructures with distinct shapes. PD is a bioinspired polymer from invertebrate mussels known for its highly uncontrolled self-polymerization and its adhesive properties.^[11] A variety of functional groups available on PD provide this adhesive property as well as an avenue for post-functionalization with polymers, biomolecules, and metal nanoparticles.^[11,12] Due to its natural biocompatibility, it immediately attracted very broad attention in the field of biomaterials and nanomedicine.^[13] Micropatterned PD surfaces efficiently captured cells, proteins, chemicals, and metals^[14] for advanced biochips and sensors. Hence, there is great interest to fabricate PD with defined nanoscale structures/patterns, which has so far remained elusive due to 1) the molecular mechanisms of PD formation, that are still not fully understood since many intermediate and short-lived chemical species are involved,^[15] 2) the rapid polymerization kinetics of dopamine, and 3) its adhesiveness that often causes aggregation or uncontrolled adsorption to any surface.

Herein, a G-quadruplex (G4)/hemin-based DNA enzyme (DNAzyme) possessing a horseradish peroxidase (HRP)-mimicking H₂O₂-mediated oxidation ability was employed as redox catalyst (Scheme 1). This strategy has been reported for catalyzing the oxidative polymerization of polyaniline,^[16] but has never been explored for controlling dopamine polymerization. In detail, the control of dopamine polymerization

[*] Y. Tokura,[†] S. Harvey,[†] C. Chen, Prof. Dr. Y. Wu, Dr. D. Y. W. Ng, Prof. Dr. T. Weil
Max Planck Institute for Polymer Research
Ackermannweg 10, 55128 Mainz (Germany)
E-mail: david.ng@mpip-mainz.mpg.de
tanja.weil@mpip-mainz.mpg.de

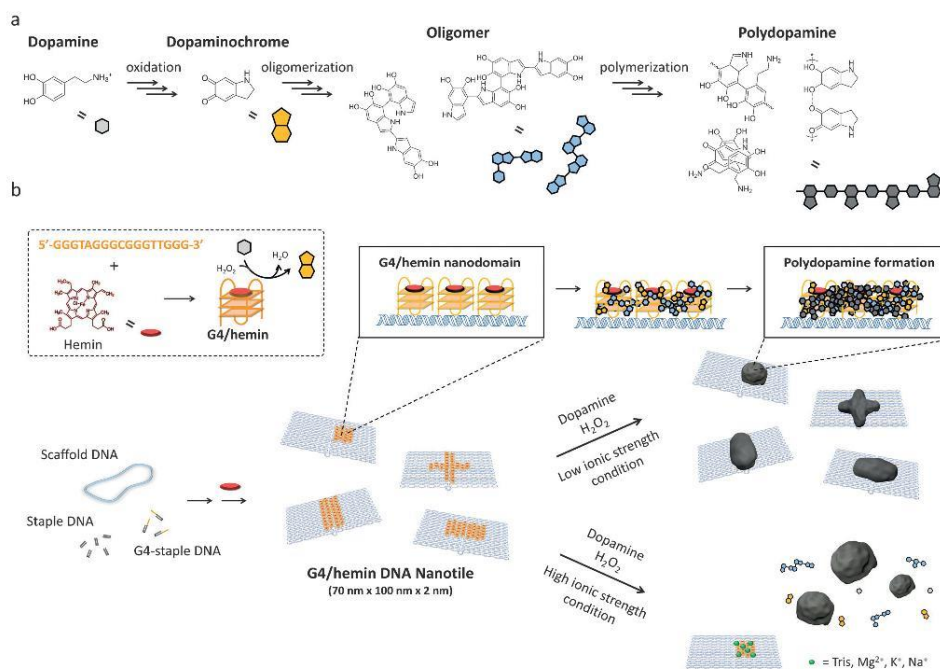
Y. Tokura,[†] C. Chen, Prof. Dr. T. Weil
Ulm University
Albert-Einstein-Allee 11, 89081 Ulm (Germany)

Prof. Dr. Y. Wu
Hubei Key Laboratory of Bioinorganic Chemistry and Material Medica, School of Chemistry and Chemical Engineering
Huazhong University of Science and Technology
1037 Luoyu Road, 430074 Wuhan (China)
E-mail: wuyuzhou@hust.edu.cn

[†] These authors contributed equally to this work.

Supporting information and the ORCID identification number(s) for the author(s) of this article can be found under <https://doi.org/10.1002/anie.201711560>.

© 2018 The Authors. Published by Wiley-VCH Verlag GmbH & Co. KGaA. This is an open access article under the terms of the Creative Commons Attribution Non-Commercial License, which permits use, distribution and reproduction in any medium, provided the original work is properly cited, and is not used for commercial purposes.



Scheme 1. a) Proposed mechanism of PD formation (also see Figure S1) and b) Illustration of fabricating defined PD nanostructure on the DNA nanotile (light blue) carrying G4 (orange)/hemin (red) DNAzyme domain. The DNAzyme domain locally oxidizes dopamine to dopaminochrome. And further processes yield PD. On the other hand, no PD formation on DNA nanotile occurs under the high ionic strength conditions (also see Figure S8).

centers on the DNAzyme, which is known to oxidize dopamine to dopaminochrome. This oxidized state of dopamine is one of the intermediates for PD formation^[17] and Gao et al has separately found that the HRP could accelerate the polymerization of dopamine.^[18] In combining both concepts, we speculate that organizing multiple DNAzyme moieties at distinct nanodomains on DNA origami provides the local environment allowing a controlled dopamine polymerization.

To introduce the DNAzyme reaction center at distinct locations on DNA origami, 20 staple DNA sequences were modified with additional G-rich sequences (TTGGGTAGG GCGGGTTGGG) at their 3' ends (see Figure S2, S3 and Table S1 in the Supporting Information). The introduced G4 moieties were designed to appear as a 20 nm square domain at the surface of the Rothemund's DNA origami rectangle sheet (Figure S3a, 70 nm x 100 nm dimensions)^[3] denoted as DNA nanotile. AFM measurements proved the correct formation of the DNA nanotile with desired dimensions and the G4 domain with an approximate 2 nm height increase at the designated positions (Figure S3c).

In the next step, DNAzyme on DNA nanotile was activated by incorporating its cofactor, hemin, resulting in

no morphological differences by AFM (Figure S3c), but a characteristic shift of the hemin Soret band was detected in the UV/Vis spectra (Figure S4) that corresponds to existing literature.^[19] The catalytic activity of DNAzyme domain on DNA nanotile was evaluated by tracking the oxidation of 2,2'-azino-bis(3-ethylbenzothiazoline-6-sulphonic acid) (ABTS) in the presence of H_2O_2 . It was observed that the activity of G4/hemin DNA nanotile was relatively low in TAE/Mg buffer (20 mM Tris, 10 mM acetic acid, 1 mM EDTA, 12 mM MgCl_2 , pH 7.8), which is commonly used for DNA origami storage and functionalization (Figure S5). The DNAzyme activity was improved by supplementing 10 mM K^+ , which is known to stabilize G4.^[20] Additionally, lowering pH to acidic conditions (pH 5.3) significantly improved the activity profile while preventing oxidation of dopamine by dissolved oxygen. It should be also noted that G4/hemin domain on DNA nanotile showed an almost five fold faster reaction kinetic compared to free G4/hemin molecules with the same concentration, which was possibly due to a cooperative effect as a consequence of the locally concentrated G4/hemin reaction centers (Figure 1a). Fabrication of a PD nanostructure on G4/hemin DNA nanotile was initially pursued in the optimized buffer as discussed above. However, no changes were observed from

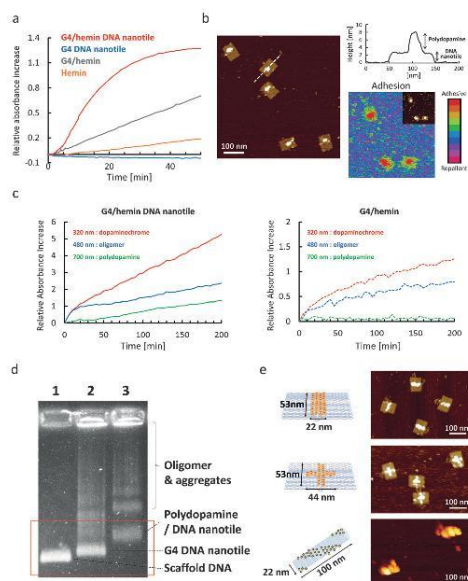


Figure 1. a) ABTS assay of G4/hemin DNA nanotile (3.5 nm containing 70 nm G4/hemin) and G4/hemin only (70 nm). b) AFM image of DNA nanotile after PD formation and adhesion mapping (inset: corresponding height image). c) Reaction kinetics of PD formation on G4/hemin DNA nanotile (3.5 nm, left) and G4/hemin only (70 nm, right). d) AGE of 1: M13MP18 DNA, 2: G4 DNA nanotile, and 3: PD/ DNA nanotile. e) Illustrations of DNA nanotile with different G4/hemin (yellow circle) positions (vertical line [top], cross patterning [middle], striped tube [bottom]) and corresponding AFM images.

the G4/hemin DNA nanotile in AFM measurements, but many small particles were found in solution (Figure S6). Most likely, the high ionic strength and cation concentrations (triethylenediamine and Mg^{2+}) could shield the negative charges of the DNA backbone.^[16] In this way, dopamine molecules that were oxidized to dopaminochrome on the DNA nanotile would rapidly diffuse back into the bulk solution and spontaneously self-polymerize in solution.

This self-polymerization in solution was suppressed efficiently, when a buffer containing low concentrations of TAE/Mg/K (0.3 mM Tris, 0.2 mM acetic acid, 0.06 mM EDTA, 0.6 mM $MgCl_2$, 10 mM KCl, pH 5.3) was applied (Figure S5). Only under these conditions, new objects appeared on the DNAzyme domain (Figure 1b). The AFM image showed the height increase of the DNAzyme domain from 2 nm to about 4–6 nm after the reaction. Additionally, mechanical property mapping revealed an increase in adhesion force by 73 ± 16 pN from the DNA nanotile (Figure 1b and S7), which taken together, indicated the successful PD formation. It is hypothesized that the electrostatic interaction between positively charged dopaminochrome/dopamine and negatively charged DNA nanotile coupled with multiple DNAzyme molecules in close proximity facilitated a high local concen-

tration of PD intermediates including oligomers, leading to the preferential polymerization directly at the DNAzyme domain (Figure S8).

To further characterize PD formation, the reaction kinetics were monitored by UV/Vis spectroscopy (Figure 1c and S9). The early oxidation (dopaminochrome, 320 nm) and polymerization products (oligomer, 480 nm) formed immediately after initiating the reaction, followed by the occurrence of PD (700 nm), after 50 min.^[21] A control reaction conducted with free DNAzyme molecules in solution could only produce dopaminochrome and oligomers, but no PD (Figure 1c and S9), clearly indicating that multiple DNAzymes in the immediate vicinity at low ionic strength were essential for producing PD locally and directly on the DNAzyme domain. Additionally, an experiment replacing dopamine with its neutral analog *L*-Dopa (at pH 5.3) revealed no polymerization (Figure S10), further strengthening the importance of the association of dopamine and its intermediates with the DNAzyme domain. As a control without hemin, PD was not formed at all due to a lack of DNAzyme activity (Figure S11). The quantity of PD and therefore the height increase was controlled and tuned with the amount of H_2O_2 added to the reaction (Figure S12). Anchoring of the PD to G4 locally limits the growth providing control over the final shape and size of the nanostructures. PD nanostructures grown on the DNA nanotile were purified by size exclusion chromatography for agarose gel electrophoresis (AGE) (Figure 1d).

Next, we applied these optimized reaction conditions to fabricate different PD nanopatterns since the framework of DNA origami allows the positioning of every single DNAzyme moiety on the DNA nanotile with molecular precision. Vertical line, horizontal line, cross and striped patterning of DNAzyme domains were designed on DNA nanotile and PD nanostructures adopting similar shapes were achieved (Figure 1e, S2, S13, and S14). And under these optimized reaction conditions, there was no polydopamine induced aggregation of DNA origami observed via AFM.

One of the major features of PD is related to its high adhesiveness, serving as glue in many applications. We have exploited the precise positioning of the adhesive PD nanostructures to induce and control DNA origami folding. By growing PD from the DNA tile with horizontal line patterning at the edge or in the middle, partially or fully folded DNA nanotile structures were observed (Figure 2, S15 and S16).

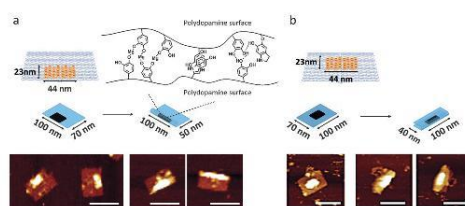


Figure 2. PD-induced folding of DNA nanotile with horizontal line-shape DNAzyme domain. Depending on the position of DNAzyme domain (a: side, and b: middle), DNA nanotile was folded either partially (a) or completely (b). Scale bar: 100 nm.

This unique feature is likely due to the secondary interaction between the functional groups on PD surfaces (Mg^{2+} bridging, hydrogen bonding, π - π stacking).

By adjusting the position of the PD “nanoglue” in the center or closer to the outer edge of the origami nanotile, different folded origami shapes could be imaged by AFM (Figure 2a and b). On the other hand, when the line DNAzyme domain was designed along the short axis (70 nm), most of the DNA nanotile structures remained as non-folded states (Figure S17). We believe that the rigid dsDNA parallel to the long axis most likely inhibited folding along its short axis where the energy required for the curvature cannot be compensated by the non-covalent interactions. This observation shows that PD could serve as “supramolecular glue” for controlling different DNA origami conformations with low nanometer resolution, which outperforms other, less precise methods, for example, by using DNA intercalators.^[22] The formation of precise polymeric architectures with nanoscale precision similar to biomolecules such as proteins, tRNA has always been a holy grail in polymer chemistry. Dopamine is unique as it serves as monomer as well as cross-linker thereby leading to rigid and highly crosslinked materials after polymerization. Therefore, PD nanostructures formed on DNA origami preserved their engineered size and geometry after removal of the template given the innate stability differences between PD and DNA. DNA origami is unstable in acidic pH and quickly degrades due to the hydrolysis of the phosphodiester backbone, bases, and glycosidic bonds.^[22] Hence, the liberation of PD nanostructures was achieved by treating the deposited PD/DNA on mica surface with 1M HCl for 10 seconds (Figure 3 and S18). Subsequent replacement of the buffer and re-engagement of AFM imaging revealed the structural preservation of the PD architecture (Figure 3).

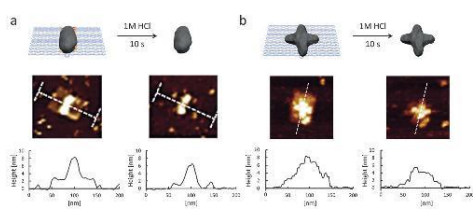


Figure 3. Extraction of PD nanostructure (a: vertical line, b: cross) from DNA nanotile via HCl treatment.

In summary, we have presented the first strategy for creating defined anisotropic PD nanostructures on DNA origami. The most valuable features of this approach are the precise localization of dopamine polymerization areas in nanoscale by using precisely patterned multiple DNAzyme as reaction centers. In the method reported herein, dopamine molecules are oxidized locally at DNAzyme domains on DNA origami resulting in the formation of PD structures with nanoscale precision. Also, the well-known random and uncontrolled self-polymerization behavior of dopamine in solution was efficiently subverted by conducting the reaction

in acidic pH. The kinetics of PD growth and the control over the height of the architecture was achieved by adjusting the H_2O_2 concentration. Coupled with the spatial programmability of functionalities on DNA origami, one could envision creating various desired shapes of PD nanostructures in 2D and 3D with unprecedented resolution.

Based on the unique secondary adhesive properties of PD, conformational changes of the DNA origami nanostructures were induced. Here, PD served as “supramolecular glue”, connecting different areas of the DNA origami in a fast and controlled fashion, which serves as a versatile tool to manipulate the post-modified conformation of DNA origami. The robust and tightly crosslinked PD features allow programmed PD nanostructures to retain their shapes after removal of the template. In this way, the organization of nanostructured PD over large surface areas^[24] as a nanoarray or the application of distinct PD shapes to probe and optimize cell interactions could be envisaged. Collectively, the strategy reported herein provides an integrated methodology for designing functional DNA nanodevices and for fabricating PD with spatial control, which will create new frontiers in DNA nanotechnology and the various fields of material science and nanomedicine.

Acknowledgements

We acknowledge the support by the European Research Council (ERC) under the program Synergy Grant 319130-BioQ and the BMBF project “Selektomm” within the Biotechnologie 2020+ initiative. C.C. thanks for support from the Promotionskolleg Pharmaceutical Biotechnology. We thank Dr. Rüdiger Berger for critical reading of the manuscript and for many valuable comments.

Conflict of interest

The authors declare no conflict of interest.

Keywords: DNA origami · DNAzyme · nanostructures · polydopamine

How to cite: *Angew. Chem. Int. Ed.* **2018**, *57*, 1587–1591
Angew. Chem. **2018**, *130*, 1603–1607

- [1] a) M. Geissler, Y. N. Xia, *Adv. Mater.* **2004**, *16*, 1249–1269; b) P. T. Hammond, *Adv. Mater.* **2004**, *16*, 1271–1293; c) P. Kim, S. E. Lee, H. S. Jung, H. Y. Lee, T. Kawai, K. Y. Suh, *Lab Chip* **2006**, *6*, 54–59.
- [2] a) M. Endo, Y. Yang, H. Sugiyama, *Biomater. Sci.* **2013**, *1*, 347–360; b) A. H. Okholm, J. Kjems, *Adv. Drug Delivery Rev.* **2016**, *106*, 183–191; c) M. Komiyama, K. Yoshimoto, M. Sisido, K. Ariga, *Bull. Chem. Soc. Jpn.* **2017**, *90*, 967–1004.
- [3] P. W. K. Rothmund, *Nature* **2006**, *440*, 297–302.
- [4] R. Veneziano, S. Ratanalert, K. M. Zhang, F. Zhang, H. Yan, W. Chiu, M. Bathe, *Science* **2016**, *352*, 1534.
- [5] a) R. Schreiber, J. Do, E. M. Roller, T. Zhang, V. J. Schuller, P. C. Nickels, J. Feldmann, T. Liedl, *Nat. Nanotechnol.* **2014**, *9*, 74–78; b) T. Zhang, A. Neumann, J. Lindlau, Y. Wu, G. Pramanik, B. Naydenov, F. Jelezko, F. Schüder, S. Huber, M. Huber, F. Stehr,

- A. Högele, T. Weil, T. Liedl, *J. Am. Chem. Soc.* **2015**, *137*, 9776–9779.
- [6] a) B. Saccà, R. Meyer, M. Erkelenz, K. Kiko, A. Arndt, H. Schroeder, K. S. Rabe, C. M. Niemeyer, *Angew. Chem. Int. Ed.* **2010**, *49*, 9378–9383; *Angew. Chem.* **2010**, *122*, 9568–9573; b) J. L. Fu, Y. R. Yang, A. Johnson-Buck, M. H. Liu, Y. Liu, N. G. Walter, N. W. Woodbury, H. Yan, *Nat. Nanotechnol.* **2014**, *9*, 531–536.
- [7] a) P. K. Dutta, R. Varghese, J. Nangreave, S. Lin, H. Yan, Y. Liu, *J. Am. Chem. Soc.* **2011**, *133*, 11985–11993; b) C. X. Lin, R. Jungmann, A. M. Leifer, C. Li, D. Levner, G. M. Church, W. M. Shih, P. Yin, *Nat. Chem.* **2012**, *4*, 832–839.
- [8] a) S. Helmi, C. Ziegler, D. J. Kauert, R. Seidel, *Nano Lett.* **2014**, *14*, 6693–6698; b) W. Sun, E. Boulais, Y. Hakobyan, W. L. Wang, A. Guan, M. Bathe, P. Yin, *Science* **2014**, *346*, 717.
- [9] a) Y. Yang, J. Wang, H. Shigematsu, W. M. Xu, W. M. Shih, J. E. Rothman, C. X. Lin, *Nat. Chem.* **2016**, *8*, 476–483; b) Z. Zhang, Y. Yang, F. Pincet, M. C. Llaguno, C. X. Lin, *Nat. Chem.* **2017**, *9*, 653–659.
- [10] Y. Tokura, Y. Y. Jiang, A. Welle, M. H. Stenzel, K. M. Krzemien, J. Michaelis, R. Berger, C. Barner-Kowollik, Y. Z. Wu, T. Weil, *Angew. Chem. Int. Ed.* **2016**, *55*, 5692–5697; *Angew. Chem.* **2016**, *128*, 5786–5791.
- [11] H. Lee, S. M. Dellatore, W. M. Miller, P. B. Messersmith, *Science* **2007**, *318*, 426–430.
- [12] a) H. Lee, J. Rho, P. B. Messersmith, *Adv. Mater.* **2009**, *21*, 431–434; b) R. Liu, Y. L. Guo, G. Odusote, F. L. Qu, R. D. Priestley, *ACS Appl. Mater. Interfaces* **2013**, *5*, 9167–9171.
- [13] a) M. E. Lyngse, R. van der Westen, A. Postma, B. Städler, *Nanoscale* **2011**, *3*, 4916–4928; b) Y. H. Ding, M. Floren, W. Tan, *Biosurface and Biotribology* **2016**, *2*, 121–136.
- [14] H. W. Chien, W. H. Kuo, M. J. Wang, S. W. Tsai, W. B. Tsai, *Langmuir* **2012**, *28*, 5775–5782.
- [15] a) N. F. Della Vecchia, R. Avolio, M. Alfe, M. E. Errico, A. Napolitano, M. d'Ischia, *Adv. Funct. Mater.* **2013**, *23*, 1331–1340; b) J. Liebscher, R. Mrowczynski, H. A. Scheidt, C. Filip, N. D. Hadade, R. Turcu, A. Bende, S. Beck, *Langmuir* **2013**, *29*, 10539–10548; c) Y. L. Liu, K. L. Ai, L. H. Lu, *Chem. Rev.* **2014**, *114*, 5057–5115.
- [16] Z. G. Wang, Q. Liu, B. Q. Ding, *Chem. Mater.* **2014**, *26*, 3364–3367.
- [17] a) H. B. Albada, E. Golub, I. Willner, *Chem. Sci.* **2016**, *7*, 3092–3101; b) E. Golub, H. B. Albada, W. C. Liao, Y. Biniuri, I. Willner, *J. Am. Chem. Soc.* **2016**, *138*, 164–172.
- [18] J. Li, M. A. Baird, M. A. Davis, W. Tai, L. S. Zweifel, K. M. A. Waldorf, M. Gale, Jr., L. Rajagopal, R. H. Pierce, X. Gao, *Nat. Biomed. Eng.* **2017**, *1*, 0082.
- [19] X. Yang, C. Fang, H. Mei, T. Chang, Z. Cao, D. Shanguan, *Chem. Eur. J.* **2011**, *17*, 14475–14484.
- [20] P. Travascio, Y. F. Li, D. Sen, *Chem. Biol.* **1998**, *5*, 505–517.
- [21] M. Bisaglia, S. Mammi, L. Bubacco, *J. Biol. Chem.* **2007**, *282*, 15597–15605.
- [22] H. Chen, H. Zhang, J. Ping, T. Cha, S. Li, J. Andreasson, J. H. Choi, *ACS Nano* **2016**, *10*, 4989–4996.
- [23] H. Kim, S. P. Surwade, A. Powell, C. O'Donnell, H. T. Liu, *Chem. Mater.* **2014**, *26*, 5265–5273.
- [24] a) A. M. Hung, C. M. Micheel, L. D. Bozano, L. W. Osterbur, G. M. Wallraff, J. N. Cha, *Nat. Nanotechnol.* **2010**, *5*, 121–126; b) A. Gopinath, P. W. K. Rothmund, *ACS Nano* **2014**, *8*, 12030–12040; c) A. Aghebat Rafat, T. Pirzer, M. B. Scheible, A. Kostina, F. C. Simmel, *Angew. Chem. Int. Ed.* **2014**, *53*, 7665–7668; *Angew. Chem.* **2014**, *126*, 7797–7801.

Manuscript received: November 10, 2017
Accepted manuscript online: December 6, 2017
Version of record online: January 15, 2018



Supporting Information

Fabrication of Defined Polydopamine Nanostructures by DNA Origami-Templated Polymerization

Yu Tokura[†], Sean Harvey[†], Chaojian Chen, Yuzhou Wu,^{} David Y. W. Ng,^{*} and Tanja Weil^{*}*

ange_201711560_sm_miscellaneous_information.pdf

Table of Contents

Experimental Procedures	3
Materials and Instruments	
Fabrication of DNA nanotile with G-quadruplex staple	
Hemin binding assay	
The ABTS assay of G4/hemin DNA nanotile	
Preparation of polydopamine on G4/hemin DNA nanotile	
Transformation of DNA nanotile to tube	
Kinetics of polydopamine formation on G4/hemin DNA nanotile	
Extraction of polydopamine nanostructure via acid treatment	
Atomic force Microscopy (AFM)	
Agarose gel electrophoresis	
Transmission electron microscopy (TEM)	
Results and Discussion	4
Figure S1. Proposed mechanism of polydopamine formation	
Figure S2. Design of G4/hemin DNA nanotile	
Figure S3. G4/hemin DNA nanotile	
Figure S4. UV-Vis spectrum of hemin incorporation to G4 DNA nanotile	
Figure S5. ABTS assay of G4/hemin DNA nanotile in different buffer compositions	
Figure S6. No polydopamine formation on DNA nanotile under the high ionic strength buffer condition	
Figure S7. Nanomechanical property mapping of polydopamine DNA nanotile and G4 DNA nanotile	
Figure S8. Proposed mechanism of polydopamine formation on DNA nanotile	
Figure S9. Tracking of polydopamine formation with free DNAzyme	
Figure S10. Polymerization of L-dopa on G4/hemin DNA nanotile	
Figure S11. Polymerization of dopamine on G4 DNA nanotile (without hemin)	
Figure S12. The effects of H ₂ O ₂ concentration and reaction time to the growth of polydopamine on G4/hemin DNA nanotile	
Figure S13. Cross patterning of polydopamine nanostructure on DNA nanotile. Scale bar: 100 nm	
Figure S14. Polydopamine DNA tube with stripy G4/hemin	
Figure S15. AFM images of polydopamine DNA nanotile with horizontal line	
Figure S16. TEM images of polydopamine DNA nanotile with horizontal line after 180 minutes reaction	
Figure S17. Polydopamine DNA nanotile with vertical line	
Figure S18. AFM image of extracted polydopamine nanostructures after HCl treatment Table S1. The list of staple DNA sequences	
Table S1. The list of staple DNA sequences	
References	17

Experimental Procedures

Materials and instruments

All solvents and chemicals were purchased from commercial sources and were used without further purification. DNA staple strands and G-quadruplex containing staple strands (G4 staple) were either synthesized by 12-Column DNA Synthesizer from POLYGEN GmbH and purified by Agilent 1260 Infinity HPLC system with Agilent Eclipse XDB-C18 column or purchased from Sigma-Aldrich. Agarose gel electrophoresis was performed using Bio-Rad Mini-Sub Cell GT horizontal electrophoresis system. Bio-Rad MyCycler™ Thermal Cycler was used for annealing of MP13mp18 phage DNA and DNA staple strands to form DNA nanotile. Concentration of DNA nanotile was determined by Spark® 20M with Nanoquant plate™.

Fabrication of DNA nanotile with G-quadruplex staple

DNA nanotile with G4 staples at different positions were prepared respectively by mixing M13MP18 phage DNA of 7k nt with desired staple strands and G4 staple strands in folding buffer (5 mM Tris, 1 mM EDTA, 5 mM NaCl, and 12 mM MgCl₂, pH 8.0) and annealing from 65 °C to 20 °C over 2 h, followed by a purification with polyethylene glycol (PEG) precipitation method^[1]. Briefly, the reaction solution containing DNA nanotile and excess of staple strands were mixed with 15% PEG8000 (w/v), 5 mM Tris, 1 mM EDTA, and 505 mM NaCl and centrifuged at 12000 rpm, at room temperature (RT) for 25 min. The supernatant was removed and the pellet was dissolved in 1 × TAE / Mg buffer (20 mM Tris, 1 mM EDTA, 12 mM MgCl₂, pH 7.8).

Hemin binding assay

G4 DNA nanotile with square domain (50 nM) was added to a 384 well UV transparent plate. Hemin (1 μM) was mixed with G4 DNA nanotile solution. Immediately after mixing, the absorbance spectrum was measured every minute for a duration of 2 hours using a Tecan Spark® 20M plate reader. The absorbance spectrum of Hemin (1 μM) alone was also measured.

The ABTS assay of G4/hemin DNAzyme on DNA nanotile

G4 DNA nanotile with square domain (3.5 nM) in different buffer composition (20 mM Tris, 1 mM EDTA, 12 mM MgCl₂, pH adjusted to 7.8 or pH 5.3 by addition of acetic acid) was mixed with hemin (70 nM) for 30 min at rt. 97.9 μL of the solution was added to a 384 well UV transparent plate. To G4/hemin DNA nanotile solution was added 1.1 μL of a freshly prepared 50 mg/ml ABTS solution and 1 μL of 0.1M H₂O₂. Immediately after H₂O₂ addition, the absorbance spectrum was measured every minute for a duration of 1 hours using a Tecan Spark® 20M plate reader. The same procedure was used each for G4 DNA nanotile only (3.5 nM), G4/hemin (70 nM), and hemin (70 nM) only. For the low ionic strength buffer, (0.3 mM Tris, 0.2 mM acetic acid, 0.06 mM EDTA, 0.6 mM MgCl₂, 10 mM KCl, pH 5.3) was used.

Preparation of polydopamine on G4/hemin DNA nanotile

G4 DNA nanotile with square domain (3.5 nM) was mixed with hemin (100 nM) in TAE / Mg / K (0.3 mM Tris, 0.2 mM acetic acid, 0.06 mM EDTA, 0.6 mM MgCl₂, 10 mM KCl, pH 5.3) for 30 min at room temperature before polymerization of polydopamine. To G4/hemin DNA nanotile solution was added 1 μL of freshly prepared dopamine (1 M) and H₂O₂ (1M), and the reaction solution was incubated at rt for 3h. The samples were purified by size exclusion chromatography (800 μL volume of Sephacryl S-400, GE Healthcare) equilibrated with a reaction buffer in Ultrafree-MC-DV (Millipore).

Transformation of DNA nanotile to tube

To DNA nanotile with stripy G4/hemin pattern solution (0.5 pmol) was added a set of folding DNA strands (250 pmol each) and the mixture was incubated at 32 degrees for overnight. The obtained DNA tube was purified again with PEG precipitation method.

Kinetics of polydopamine formation on G4/hemin DNA nanotile

G4 DNA nanotile with square domain (3.5 nM) or G4 staple (70 nM) in the decreased ionic strength buffer (pH 5.3) was mixed with hemin (70 nM) for 30 min at rt. 98 μL of the solution was added to a 384 well UV transparent plate. To G4/hemin DNA nanotile solution was added 1 μL of a freshly prepared 1M dopamine solution and 1 μL of 1M H₂O₂. Immediately after H₂O₂ addition, the absorbance spectrum was measured every 5 minutes for a duration of 12 hours using a Tecan Spark® 20M plate reader.

Extraction of polydopamine nanostructure via acid treatment

The sample solution of purified polydopamine grown DNA nanotile was added to freshly cleaved mica surface and incubated for 5 min at room temperature to deposit DNA nanotile structure on mica surface. After imaging the polydopamine / DNA nanotile by AFM, the remaining solution on mica was removed and 1 M HCl solution was added to the mica surface. After 10 seconds, HCl solution was removed and the buffer was added again. The AFM measurement was performed at the same area as before acid treatment.

Atomic force Microscopy (AFM)

Imaging was performed with a Bruker Dimension FastScan Bio AFM equipped with the ScanAsyst mode. The sample solution was deposited onto freshly cleaved mica surface, and left for 5 min at room temperature to allow adsorption of the DNA nanotile structures. After addition of 70 μL of 1 × TAE / Mg buffer, the sample was scanned with the scan rates between 1 and 3 Hz. Several AFM images were acquired at different areas of the mica surface to ensure the reproducibility of the results. All images were analyzed by using the NanoScope Analysis 1.50 and Gwyddion 2.38 software.

Agarose gel electrophoresis

5 μL of sample (3 nM) was mixed with 6 × Loading buffer and run with 0.8 % agarose gel in 0.5 × TBE / Mg for 150 min in ice bath. After running, the gel was stained by SYBR Gold for 30 min and the image was taken by G: Box Chemi (Syngene).

Transmission electron microscopy (TEM)

5 μL of sample (1 nM) was applied on carbon coated copper grid with hydrophilic treatment. After 10 minutes incubation, the remaining solution was removed and the sample grid was stained with 2 % uranyl formate solution for 20 seconds. The stained grid

was washed with filtered water for three times and dried in air. Imaging was done with JEOL 1400 instrument and obtained images were analyzed by ImageJ software.

Results and Discussion

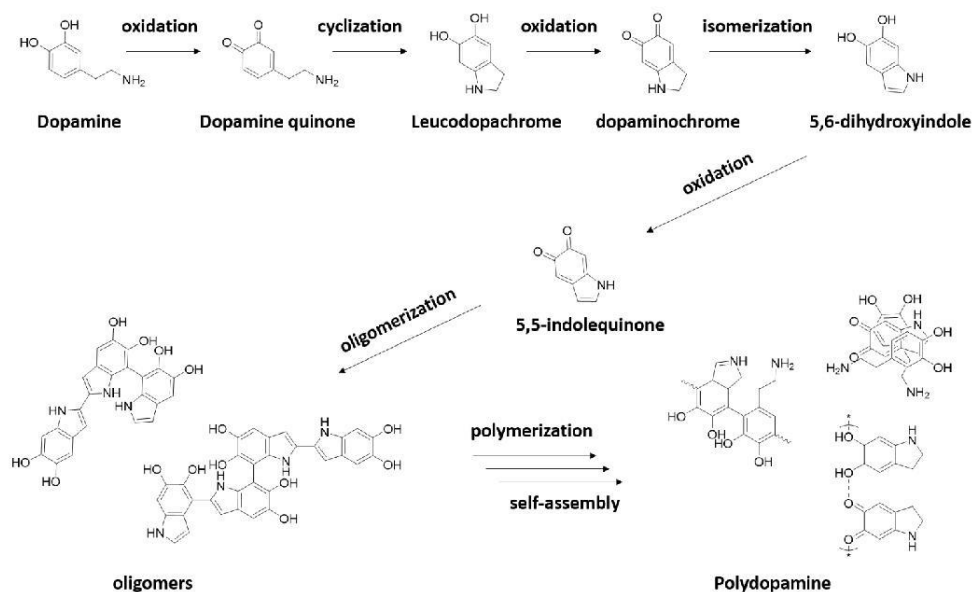


Figure S1. Proposed mechanism of polydopamine formation. Through the oxidation, isomerization, oligomerization and self-assembly polydopamine is formed via covalent bond, charge transfer, π -interactions and so on^[2].

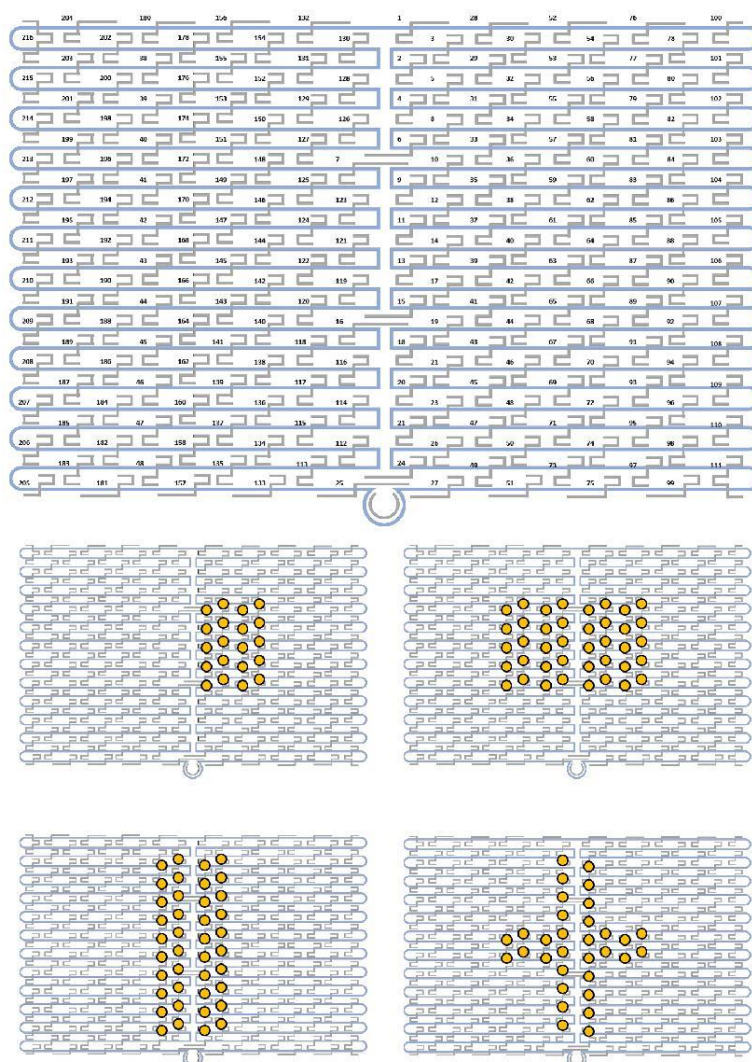


Figure S2. Design of G4/hemin DNA nanotile. Schematic of DNA nanotile^[3] and the orange circles at the bottom figures indicate the positions of G4 staple DNA sequences.

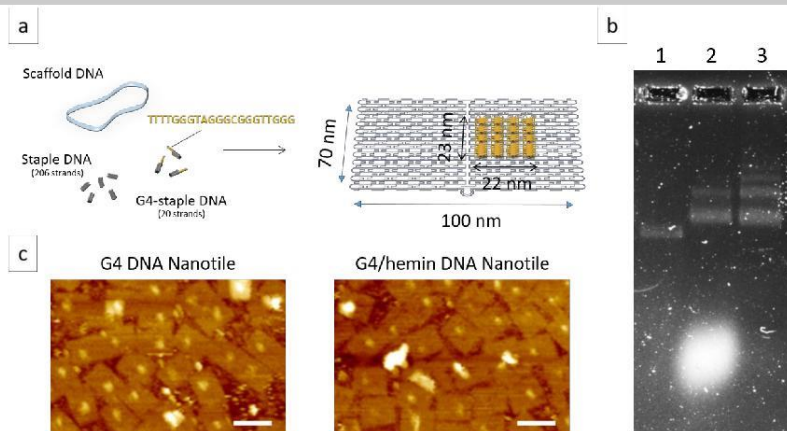


Figure S3. G4/hemin DNA nanotile. (a) Schematic illustration of DNA nanotile with 20 nm square G4/hemin domain and (b) agarose gel electrophoresis image of 1: M13MP18, 2: G4 DNA nanotile before purification, and 3: G4 DNA nanotile after purification. The staple DNA sequences were sufficiently removed after the purification. (c) AFM images before and after hemin incorporation. There was no clear difference observed before and after DNAzyme activation. Scale bar: 100 nm.

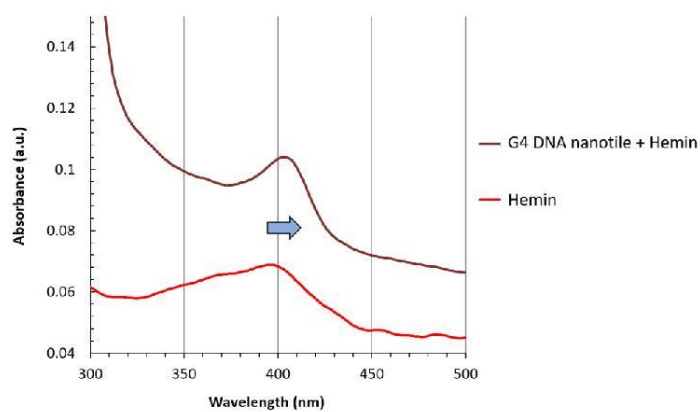


Figure S4. UV-Vis spectrum of hemin incorporation to G4 DNA nanotile. In the presence of G4 DNA nanotile, the hemin Soret band was immediately shifted from 400 nm to 405 nm due to hemin binding to G4 domain for activating DNAzyme^[4].

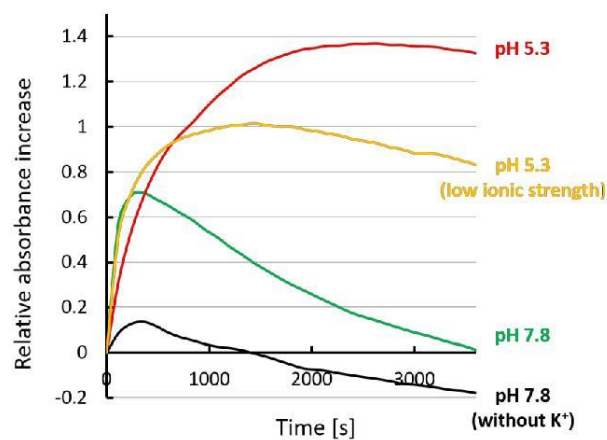


Figure S5. ABTS assay of G4/hemin DNA nanotile in different buffer compositions. It was observed that, under pH 7.8, the oxidation of ABTS will not last more than 400 seconds possibly due to the loss of DNAzyme activity, although potassium ion addition improved until certain extent (black and green). On the other hand, the improved activity was observed under acidic pH (5.3) condition (red line). By lowering the ionic strength (yellow line), the decreased DNAzyme activity was observed, but still higher than pH 7.8 condition.

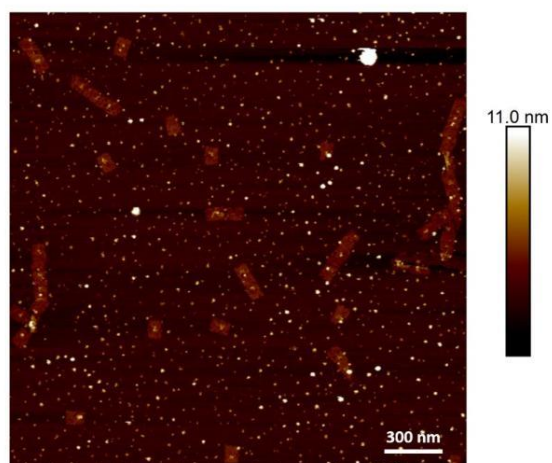


Figure S6. No polydopamine formation on DNA nanotile under the high ionic strength buffer condition.

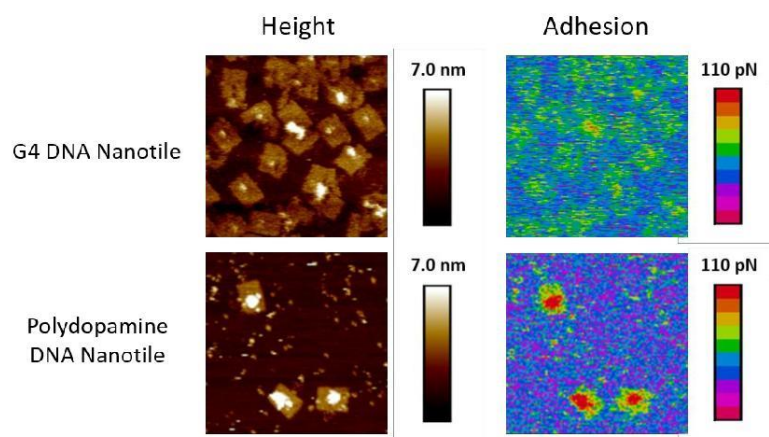


Figure S7. Nanomechanical property mapping of polydopamine DNA nanotile and G4 DNA nanotile.

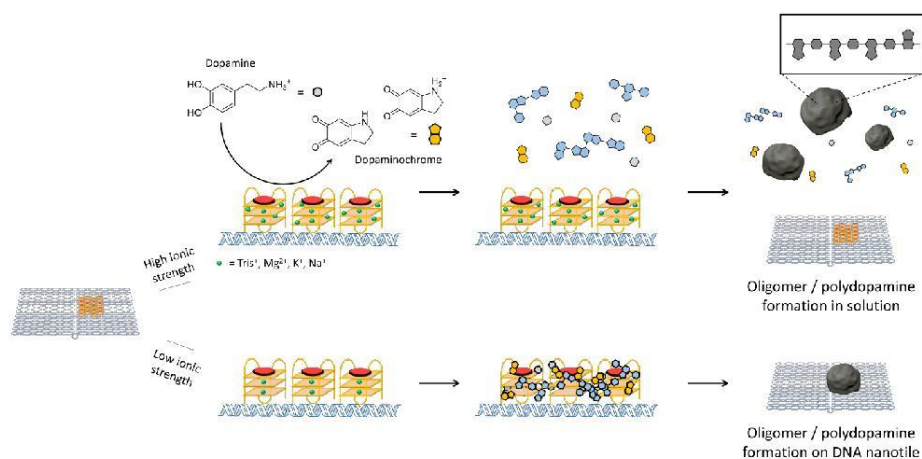


Figure S8 Proposed mechanism of polydopamine formation on DNA nanotile. Under high ionic strength condition, cations (Tris^+ , Mg^{2+} , K^+ , Na^+) shielded negative charges of the DNA backbone so that after dopamine molecules were oxidized to dopaminochrome on DNA origami, it diffused back into solution and spontaneously self-polymerized in solution. On the other hand, under low ionic strength condition, the locally concentrated dopamine, dopaminochrome, and formed oligomers facilitate the formation of polydopamine on DNA nanotile.

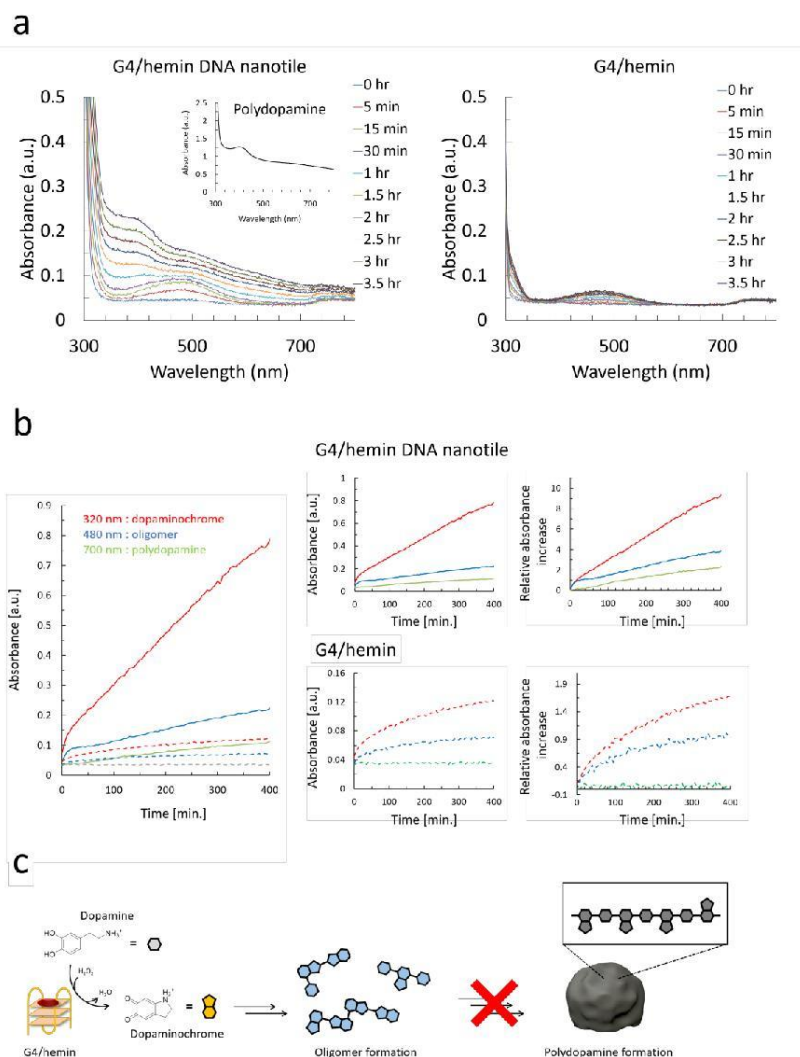


Figure S9. Tracking of polydopamine formation with free DNAzyme. (a) Absorbance spectra of dopamine polymerization on G4/ hemin DNA nanotile and G4/hemin over 3.5 hours (inset: absorbance spectra of polydopamine, dopamine [2 mg/ml] polymerized in 10 mM Tris buffer for 3.5 hr). Initial increase around 320 nm and 480 nm attributed to dopaminochrome and oligomers, respectively. Later increase in baseline (broadband absorbance) attributed to polydopamine formation. Representative wavelength at 700 nm chosen to avoid contributions from early oxidation products. (b) Dopaminochrome, oligomers, and polydopamine formation by G4/hemin DNA nanotile (3.5 nM containing 70 nM G4/hemin or free G4/hemin (70 nM)) are tracked by UV-Vis spectroscopy (the solid lines: G4/hemin DNA nanotile, dashed lines: free G4/hemin). In case of free G4/hemin molecules, the production of dopaminochrome and oligomers were lower than G4/hemin DNA nanotile. Additionally, the peak corresponding to polydopamine (700 nm, green line) didn't increase over the time (c) The schematic illustration of the reaction with free G4/hemin. Free DNAzyme can oxidize dopamine molecules to dopaminochrome. After further isomerization and oxidation, oligomers are formed, however polydopamine is not formed due to the limited production of oligomers.

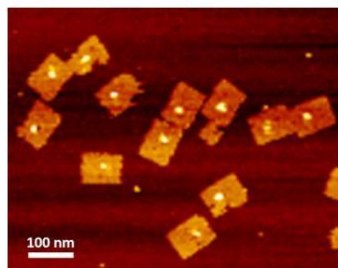
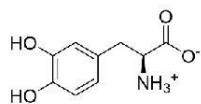


Figure S10. Polymerization of L-dopa on G4/hemin DNA nanotile. L-dopa is a derivative of dopamine having carboxylic acid group (left). Under pH 5.3 condition, it shows neutral charge which hinder its interaction with negatively charged DNAzyme domain resulting in no polymerization (right).

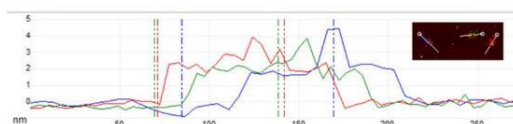
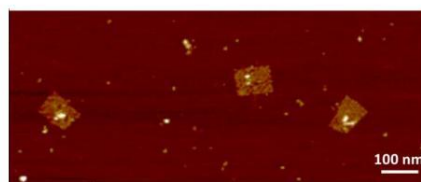


Figure S11. Polymerization of dopamine on G4 DNA nanotile (without hemin). Without hemin, no polydopamine was formed due to a lack of DNAzyme activity.

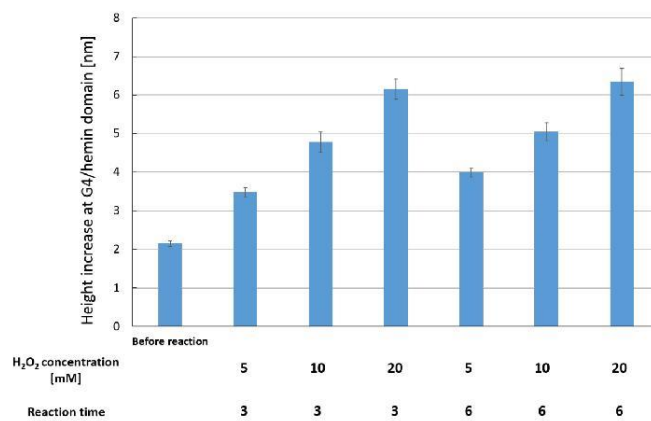


Figure S12. The effects of H_2O_2 concentration and reaction time to the growth of polydopamine on G4/hemin DNA nanotile. Means \pm S.E., $n = 28$

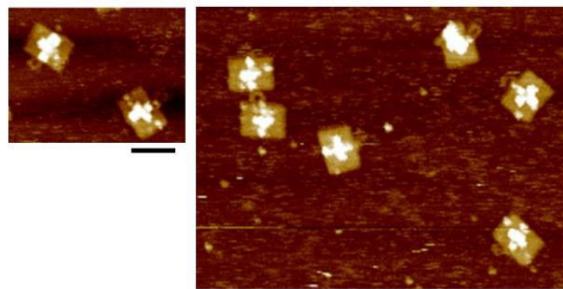


Figure S13. Cross patterning of polydopamine nanostructure on DNA nanotile. Scale bar: 100 nm.

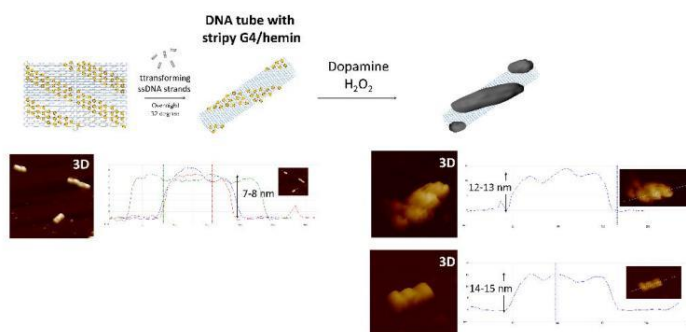


Figure S14. Polydopamine DNA tube with striped G4/hemin. (Top) Schematic illustration of tube formation and subsequent polydopamine formation. (Bottom) AFM height image and cross section of polydopamine DNA nanotube with striped G4/hemin before (left) and after polydopamine formation (right).

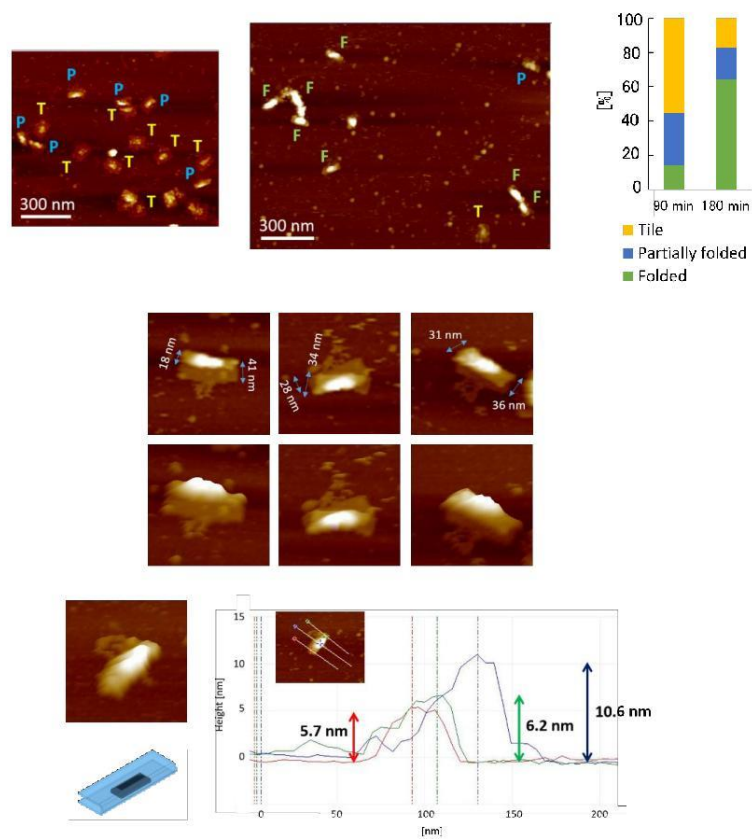


Figure S15. AFM images of polydopamine DNA nanotile with horizontal line. (Upper) AFM image after 90 min reaction time (left) and 180 minutes reaction time (right). Tile structure, partially folded structure, and folded structure were indicated by T, P, and F, respectively. The percentages of different conformation after 1.5 h and 3 h reaction time was calculated from counting 92 structures. (Bottom) Dimension and cross section of (partially) folded polydopamine DNA nanotile.

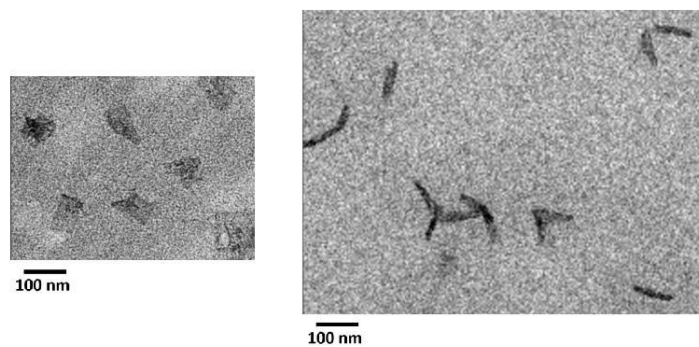


Figure S16. TEM images of polydopamine DNA nanotile with horizontal line before and after 180 minutes reaction. Scale bar: 100 nm. In TEM image, the folding was more enhanced possibly due to the drying effect.

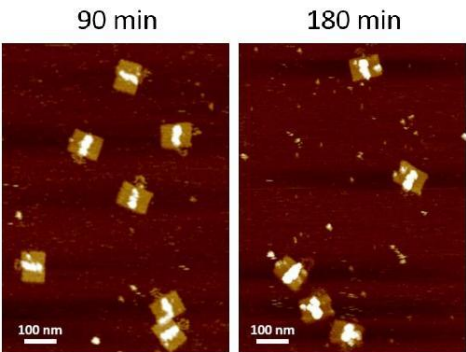


Figure S17. Polydopamine DNA nanotile with vertical line. There was no folding observed after 180 minutes reaction time.

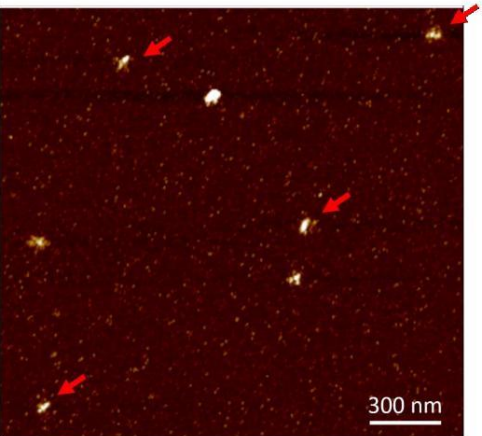


Figure S18. AFM image of extracted polydopamine nanostructures after HCl treatment. The polydopamine nanostructures were indicated by red arrows.

Table S1. The list of staple DNA sequences

No.	Sequence
1	CAAGCCCAATAGGAACCCATGTACAAACAGTT
2	AATGCCCGTAACAGTGCCCGTATCTCCCTCA
3	TGCCTTGACTGCCTATTTCGGAACAGGGATAG
4	GAGCCGCCCCACCACCGGAACCGCGACGGAAA
5	AACCAGAGACCCTCAGAACCGCCAGGGTCAG
6	TTATTCATAGGGAAGGTAAATATTCATTCAGT
7	CATAACCCGAGGCATAGTAAGAGCTTTTAAAG
8	ATTGAGGGTAAAGGTGAATTATCAATCACCGG
9	AAAAGTAATATCTTACCGAAGCCCTTCCAGAG
10	GCAATAGCGCAGATAGCCGAACAATTCAACCG
11	CCTAATTTACGCTAACGAGCGTCTAATCAATA
12	TCTTACCAGCCAGTTACAAAATAAATGAAATA
13	ATCGGCTGCGAGCATGTAGAAACCTATCATAT
14	CTAATTTATCTTTCCTTATCATTATCCTGAA
15	GCGTTATAGAAAAGCCTGTTTAGAAGGCCGG

16	GCTCATTTTCGCATTAAATTTTTGAGCTTAGA
17	AATTACTACAAATCTTACCAGTAATCCCATC
18	TTAAGACGTTGAAAACATAGCGATAACAGTAC
19	TAGAATCCCTGAGAAGAGTCAATAGGAATCAT
20	CTTTTACACAGATGAATATACAGTAAACAATT
21	TTTAACGTTTCGGGAGAAAACAATAATTTCCCT
22	CGACAACTAAGTATTAGACTTTACAATACCGA
23	GGATTTAGCGTATTAAATCCTTTGTTTTCAGG
24	ACGAACCAAAACATCGCCATTAAATGGTGGTT
25	GAACGTGGCGAGAAAGGAAGGGAACAACTAT
26	TAGCCCTACCAGCAGAAGATAAAACATTTGA
27	CGGCCTTGCTGGTAATATCCAGAACGAACTGA
28	CTCAGAGCCACCACCTCATTTTCCTATTATT
29	CTGAAACAGGTAATAAGTTTTAAACCCTCAGA
30	AGTGTACTTGAAAGTATTAAGAGGCCGCCACC
31	GCCACCCTCTTTTCATAATCAACCGTCACC
32	GTTTGCCACCTCAGAGCCGCCACCGATACAGG
33	GACTTGAGAGACAAAAGGGCGACAAGTTACCA
34	AGCGCCAACCATTTGGGAATTAGATTATTAGC
35	GAAGGAAAATAAGAGCAAGAAACAACAGCCAT
36	GCCCAATACCGAGGAAACGCAATAGGTTTACC
37	ATTATTTAACCCAGCTACAATTTTCAAGAACG
38	TATTTTGCTCCCAATCCAAATAAGTGAGTTAA
39	GGTATTAAGAACAAAGAAAATAATTAAAGCCA
40	TAAGTCTACCAAGTACCGCACTCTTAGTTGC
41	ACGCTCAAAATAAGAATAAACACCGTGAATTT
42	AGGCGTTACAGTAGGCGTTAATTGACAATAGA
43	ATCAAAATCGTCGCTATTAATTAACGGATTTCG
44	CTGTAAATCATAGGTCTGAGAGACGATAAATA
45	CCTGATTGAAAGAAATTCGCTAGACCCGAACG
46	ACAGAAATCTTTGAATACCAAGTTCTTGCTT
47	TTATTAATGCCGTCAATAGATAATCAGAGGTG
48	AGATTAGATTTAAAGTTTGAGTACACGTAATA
49	AGGCGGTCAATAGTCTTTAATGCGCAATATTA
50	GAATGGCTAGTATTAACACCGCCTCAACTAAT
51	CCGCCAGCCATTGCAACAGGAAAAATATTTTT
52	CCCTCAGAACCGCCACCCTCAGAACTGAGACT
53	CCTCAAGAATACATGGCTTTTGATAGAACCAC
54	TAAGCGTCGAAGGATTAGGATTAGTACCGCCA
55	CACCAGAGTTCGGTCATAGCCCCGCCAGCAA
56	TCGGCATTCCGCCGCCAGCATTGACGTTCCAG
57	AATCACCAAATAGAAAATTCATATATAACGGA
58	TCACAATCGTAGCACCATTACCATCGTTTTCA
59	ATACCCAAGATAACCCACAAGAATAAACGATT
60	ATCAGAGAAAGAACTGGCATGATTTTATTTTG
61	TTTTGTTTAAAGCCTTAAATCAAGAATCGAGAA
62	AGGTTTTGAACGTCAAAATGAAAGCGCTAAT
63	CAAGCAAGACGCGCCTGTTTATCAAGAAATCGC
64	AATGCAGACCGTTTTTATTTTCATCTTGCGGG
65	CATATTTAGAAATACCGACCGTTTACCTTTT
66	AATGGTTTACAACGCCAACATGTAGTTCAGCT
67	TAACTCCATATGTGAGTGAATAAACAAAATC
68	AAATCAATGGCTTAGGTTGGGTTACTAAATTT
69	GCGCAGAGATATCAAAATTTTACATTATC
70	AACCTACCGCGAATTATTCATTTCCAGTACAT
71	ATTTTGCCTCTTAGGAGCACTAAGCAACAGT
72	CTAAATAGAACAAAGAAACCACCAAGGTTAG
73	GCCACGCTATACGTGGCAGACAAACGCTCAT
74	GCCTAAGAGAGAGCCAGCAGCAAAAAGGTTAT
75	GGAATACCTACATTTTACGCTCACCTGAAA
76	TATCACCGTACTCAGGAGGTTTAGCGGGGTTT
77	TGCTCAGTCAGTCTCTGAATTTACCAGGAGGT
78	GGAAGCGACCAAGGCGGATAAGTGAATAGGTG
79	TGAGGCAGGCGTCAGACTGTAGCGTAGCAAGG
80	TGCCTTTAGTCAGACGATTGGCCTGCCAGAAT
81	CCGGAACACACCCACGGAATAAGTAAGACTCC

82	ACGCAAAGGTCACCAATGAAACCAATCAAGTT
83	TTATTACGGTCAGAGGGTAATTGAATAGCAGC
84	TGAACAAACAGTATGTTAGCAAACATAAAGAA
85	CTTTACAGTTAGCGAACCTCCCGACGTAGGAA
86	GAGGCGTTAGAGAATAACATAAAGAACACCC
87	TCATTACCCGACAATAAACACATATTTAGGC
88	CCAGACGAGCGCCCAATAGCAAGCAAGAACGC
89	AGAGGCATAATTTATCTTCTGACTATAACTA
90	TTTTAGTTTTTCGAGCCAGTAATAAATTCTGT
91	TATGTAACCTTTTTTAATGGAAAAATTACCT
92	TTGAATTATGCTGATGCAAAATCCACAAATATA
93	GAGCAAAAACCTTCTGAATAATGGAAGAAGGAG
94	TGGATTATGAAGATGATGAAACAAAATTTTCA
95	CGGAATTATTGAAAGGAATTGAGGTGAAAAAT
96	ATCAACAGTCATCATATTCCTGATTGATTGTT
97	CTAAGCAAGATAGAACCCTTCTGAATCGTCT
98	GCCAACAGTCACCTTGCTGAACCTGTTGGCAA
99	GAAATGGATTATTACATTGGCAGACATTCTG
100	TTTTATAAGTATAGCCCGCCGCTCGAG
101	AGGGTTGATTTTATAAATCCTCATTAAATGATATC
102	ACAAACAATTTTAAATCAGTAGCGACAGATCGATAGC
103	AGCACCGTTTTTAAAGGTGGCAACATAGTAGAAAA
104	TACATACATTTTGACGGGAGAAATTAACACAGGGAA
105	GCGCATTATTTGCTTATCCGGTATTCTAAATCAGA
106	TATAGAAGTTTTCGACAAAAGGTAAAGTAGAGAATA
107	TAAAGTACTTTTCGCGAGAAAACTTTTATCGCAAG
108	ACAAAGAATTTTATTAAATACATTTAACACATCAAG
109	AAAACAAATTTTTTCATCAATATAATCCTATCAGAT
110	GATGGCAATTTTAAATCAATATCTGGTCACAAATATC
111	AAACCTCTTTTACCAGTAATAAAGGGATTACACAGTCACACGTTTT
112	CCGAATCCGAAAATCCTGTTTGAAGCCGGAA
113	CCAGCAGGGGCAAAATCCCTTATAAAGCCGGC
114	GCATAAAGTTCCACACAACATACGAAGCGCCA
115	GCTCACAAATGTAAAGCCTGGGGTGGGTTTGCC
116	TTCCGCTTGGCCGAAACCAGGCATTAAATCA
117	GCTTCTGGTCAGGCTGCGCAACTGTGTTATCC
118	GTTAAAAATTTTAAACCAATAGGAACCCGGCACC
119	AGACAGTCATTCAAAGGGTGAGAACTATAT
120	AGGTAAGAAATCACCATCAATATAATATTTT
121	TTTCATTTGGTCAATAACCTGTTTATATCGCG
122	TCGCAAAATGGGGCGCGAGCTGAAATAATGTGT
123	TTTTAATTGCCCGAAAGACTTCAAAACACTAT
124	AAGAGGAACGAGCTTCAAAGCGAAGATACATT
125	GGAATTACTCGTTTACCAGACGACAAAAGATT
126	GAATAAGGACGTAACAAAGCTGCTCTAAACA
127	CCAAATCACTTGCCCTGACGAGAACGCCAAAA
128	CTCATCTTGAGGCAAAAGAAATACAGTGAATTT
129	AAACGAAATGACCCCGAGCGATTATTCTATTAC
130	CTTAAACATCAGCTTGCTTTGAGCGTAACAC
131	TCGGTTTAGCTTGATACCGATAGTCCAACCTA
132	TGAGTTTCGTCAACAGTACAAACTTAATTGTA
133	CCCCGATTTAGAGCTTGACGGGGAAATCAAAA
134	GAATAGCCGCAAGCGGTCCACGCTCCTAATGA
135	GAGTTGCACGAGATAGGGTTGAGTAAGGGAGC
136	GTGAGCTAGTTTCCTGTGTGAAATTTGGGAAG
137	TCATAGCTACTCACATTAATTGCGCCCTGAGA
138	GGCGATCGCACTCCAGCCAGCTTTGCCATCAA
139	GAAGATCGGTGCGGGCCTCTTCGCAATCATGG
140	AAATAATTTTAAATTGAAACGTTGATATTCA
141	GCAAATATCGCGTCTGGCCTTCTGCGCTCAG
142	ACCGTTCTAAATGCAATGCCTGAGAGGTGGCA
143	TATATTTTAGCTGATAAATTAATGTTGTATAA
144	TCAATTCTTTAGTTTGACCATTAACAGACCG
145	CGAGTAGAACTAATAGTAGTAGCAACCCCTCA
146	GAAGCAAAAAAGCGGATTGCATCAGATAAAAA
147	TCAGAAGCCTCCAACAGGTCAGGATCTGCGAA

148	CCAAATATAATGCAGATACATAAACACCAGA
149	CATTCAACGCGAGAGGCTTTTGCATATTATAG
150	ACGAGTAGTGACAAGAACCGGATATACCAAGC
151	AGTAATCTTAAATTGGGCTTGAGAGAATACCA
152	GCGAAACATGCCACTACGAAGGCATGCGCCGA
153	ATACGTAAAAGTACAACGGAGATTTCATCAAG
154	CAATGACACTCCAAAAGGAGCCTTACAACGCC
155	AAAAAAGGACAACCATCGCCACGCGGGTAAA
156	TGTAGCATTCCACAGACAGCCCTCATCTCCAA
157	GTAAAGCACTAAATCGGAACCCCTAGTTGTTCC
158	AGTTTGGAGCCCTTACCAGCTGGTTGCGCTC
159	AGCTGATTACAAGAGTCCACTATTGAGGTGCC
160	ACTGCCCCGCGAGCTCGAATTCGTTATTACGC
161	CCCGGTACTTTCCAGTCGGGAACGGCAAC
162	CAGCTGGCGGACGACGACAGTATCGTAGCCAG
163	GTTTGAGGGAAGGGGGATGTGCTAGAGGATC
164	CTTTCATCCCCAAAAACAGGAAGACCGGAGAG
165	AGAAAAGCAACATTAAATGTGAGCATCTGCCA
166	GGTAGCTAGGATAAAAAATTTTAGTTAACATC
167	CAACGCAATTTTGGAGAGATCTACTGATAATC
168	CAATAAATACAGTTGATTCCCAATTTAGAGAG
169	TCCATATACATACAGGCAAGGCAACTTTATTT
170	TACCTTTAAGGTCTTTACCCTGACAAAGAAAT
171	CAAAAATCATTGCTCCTTTTGATAAGTTTCAT
172	TTTGCCAGATCAGTTGAGATTTAGTGGTTTAA
173	AAAGATTACGGGGTAATAGTAAACCATAAAT
174	TTTCAACTATAGGCTGGCTGACCTTGATCAT
175	CCAGGCGCTTAATCATTGTGAATTACAGGTAG
176	CGCCTGATGGAAGTTTCCATTAAACATAACCG
177	TTTCATGAAAATTTGTGTCGAAATCTGTACAGA
178	ATATATTCTTTTTTACGTTGAAAATAGTTAG
179	AATAATAAGGTGCTGAGGCTTGCAAGACTT
180	CGTAACGATCTAAAGTTTGTCTGTAATTGCG
181	ACCCAAATCAAGTTTGTGGGTCAAAGAACG
182	TGGACTCCCTTTTACCAGTGAGACCTGTCGT
183	TGGTTTTAACGTCAAAGGGCGAAGAACATC
184	GCCAGCTGCCTGCAGGTGACTCTGCAAGGCG
185	CTTGCATGCATTAATGAATCGGCCGCCAGGG
186	ATTAAGTTCGCATCGTAACCGTGCGAGTAACA
187	TAGATGGGGGTAAACGCCAGGTTGTGCCAAG
188	ACCCGTCGTCATATGTACCCCGTAAAGGCTA
189	CATGTCAGATTCTCCGTGGGAACCGTTGGTG
190	TCAGGTCACTTTTGCGGGAGAAGCAGAATTAG
191	CTGTAATATTGCCTGAGAGTCTGGAAGACTAG
192	CAAAATTAAGTACGGTGTCTGGAAGAGGTCA
193	TGCAACTAAGCAATAAAGCCTCAGTTATGACC
194	TTTTTGCGCAGAAAACGGAATGAATGTTTAG
195	AAACAGTTGATGGCTTAGAGCTTATTTAAATA
196	ACTGGATAACGGAACAACATTATTACCTTATG
197	ACGAACTAGCGTCCAATACTGCGGAATGCTTT
198	CGATTTTAGAGGACAGATGAACGGCGCGACCT
199	CTTTGAAAAGAACTGGCTCATTATTTAATAAA
200	GCTCCATGAGAGGCTTTGAGGACTAGGGAGTT
201	ACGGCTACTTACTTAGCCGGAACGCTGACCAA
202	AAAGGCCGAAAGGAACAATAAGCTTTCCAG
203	GAGAATAGCTTTTGCGGGATCGTCGGGTAGCA
204	ACGTTAGTAAATGAATTTTCTGTAAGCGGAGT
205	TTTTCGATGGCCACTACGTAACCGTC
206	TATCAGGGTTTTCGGTTTGCCTATTTGGGAACGCGG
207	GGGAGAGGTTTTGTAAACGACGGCATTCCAGT
208	CACGACGTTTTTGAATGGGATAGGTCAAAACGGCG
209	GATTGACCTTTTGTGAACGGTAATCGTAGCAAAACA
210	AGAGAATCTTTTGGTTGTACCAAAAACAAGCATAAA
211	GCTAAATCTTTTCTGTAGCTCAACATGTATTGCTGA
212	ATATAATGTTTTTCAATTGAATCCCCCTCAATCGTCA
213	TAAATATTTTTTGAAGAAAAATCTACACCAGTCA

214	GGACGTTGTTTTTCATAAGGGAACCGAAAGGCGCAG
215	ACGGTCAATTTTGACAGCATCGGAACGAACCCCTCAG
216	CAGCGAAAATTTTACTTTCAACAGTTTCTGGGATTTTGCTAAACTTTT
217	AACATCACTTGCCTGAGTAGAAGAACT
218	TGTAGCAATACTTCTTTGATTAGTAAT
219	AGTCTGTCCATCACGCAAAATTAACCGT
220	ATAATCAGTGAGGCCACCGAGTAAAG
221	ACGCCAGAATCCTGAGAAGTGTTTTT
222	TTAAAGGGATTTTAGACAGGAACGGT
223	AGAGCGGGAGCTAAACAGGAGGCCGA
224	TATAACGTGCTTTCCTCGTTAGAATC
225	GTAATGGTTGCTTTGACGAGCACG
226	GCGCTTAATGCGCCGCTACAGGGCGC
T1	AATAATAATAATAATCAAGCCCAATAGGAACCCATGTACAAACAGTT
T25	AATAATAATAATAATGAACGTGGCGAGAAAGGAAGGGAACAACTAT
T27	CAAGCCCACTGGTAATATCCGAACGAACTGA
T28	CCGCCAGCCACCACCCTCATTTTCTATTATT
T51	CTCAGAGCCATTGCAACAGGAAAAATATTTT
T52	GGAATACACCGCCACCCTCAGAACTGAGACT
T75	CCCTCAGACTACATTTTGACGCTCACCTGAAA
T76	GAAATGGATACTCAGGAGTTTAGCGGGGTTT
T99	TATCACCGTTATTTACATTGGCAGACATTCTG
T132	GAACGTGGGTCACCAGTACAACTTAATTGTA
T133	TGTAGCATTAGAGCTTGACGGGGAAATCAAAA
T156	CCCCGATTTCCACAGACAGCCCTCATCTCCAA
T157	CGTAACGACTAAATCGGAACCTAGTTGTTCC
T180	GTAAGCATCTAAAGTTTGTCTGAATTGCG
T181	ACGTTAGTCAAGTTTTTGGGGTCAAGAACG
T204	ACCCAAATAAATGAATTTTCTGTAAGCGGAGT

References

- [1] E. Stahl, T. G. Martin, F. Praetorius, H. Dietz, *Angew. Chem. Int. Ed.* **2014**, *53*, 12735-12740.
- [2] Y. H. Ding, M. Floren, W. Tan, *Biosurface and Biotribology* **2016**, *2*, 121-136.
- [3] P. W. K. Rothmund, *Nature* **2006**, *440*, 297-302.
- [4] X. Yang, C. Fang, H. Mei, T. Chang, Z. Cao, D. Shangguan, *Chem. - Eur. J.* **2011**, *17*, 14475-14484.

[6-4] Directing intracellular supramolecular assembly with N-heteroaromatic quaterthiophene analogues

David Y.W. Ng^{*,}, Roman Vill⁺, Yuzhou Wu, Kaloian Koynov, Yu Tokura, Weina Liu, Susanne Sihler, Andreas Kreyes, Sandra Ritz, Holger Barth, Ulrich Ziener^{*}, Tanja Weil^{*}

⁺ Equal Contribution, ^{*} corresponding author

Published in *Nat. Commun.* 2017, 8, 1850

Copyright: Reproduced by permission of the publisher Nature Publishing Group and Creative Commons Attribution 4.0 International License (<http://creativecommons.org/licenses/by/4.0/>.)

Abstract:

Self-assembly in situ, where synthetic molecules are programmed to organize in a specific and complex environment i.e. within living cells, can be a unique strategy to influence cellular functions. Here, we present a small series of rationally designed oligothiophene analogues that specifically target, locate and dynamically self-report their supramolecular behavior within the confinement of a cell. Through the recognition of the terminal alkyl substituent and the amphiphilic pyridine motif, we show that the cell provides different complementary pathways for self-assembly that can be traced easily with fluorescence microscopy as their molecular organization emits in distinct fluorescent bands. Importantly, the control and induction of both forms are achieved by time, temperature and the use of the intracellular transport inhibitor, bafilomycin A1. We showcase the importance of both intrinsic (cell) and extrinsic (stimulus) factors for self-organization and the potential of such a platform towards developing synthetic functional components within living cells.

Contribution of the respective authors:

David Y.W. Ng: Initiation of the project, co-writing the manuscript, spectroscopic analysis, biological experiments, confocal microscopy study,

Roman Vill: Initiation of the project, co-writing the manuscript, chemical synthesis, spectroscopic analysis

Yuzhou Wu: Confocal microscopy study and interpretation of obtained results

Kaloian Koynov: Conducting FCS measurements and interpretation of obtained results

Yu Tokura: Structural analysis by AFM and interpretation of obtained results

Weina Liu: Supporting confocal microscopy study

Susanne Sihler: Conducting preliminary electron microscopy

Andreas Kreyes: assisting chemical synthesis

Sandra Ritz: Confocal microscopy study, discussion on the results for biological interpretation

Holger Barth: discussion on the results for biological interpretation

Ulrich Ziener: Acquiring funding for the project, design and discussion of the concept and results, correcting the manuscript, supervision of chemical synthesis

Tanja Weil: Acquiring funding for the project, design and discussion of the concept and results, writing and correcting the manuscript.

ARTICLE

DOI: 10.1038/s41467-017-02020-2

OPEN

Directing intracellular supramolecular assembly with *N*-heteroaromatic quaterthiophene analogues

David Y.W. Ng¹, Roman Vill², Yuzhou Wu¹, Kaloian Koynov¹, Yu Tokura^{1,2}, Weina Liu^{1,2}, Susanne Sihler², Andreas Kreyes², Sandra Ritz³, Holger Barth⁴, Ulrich Ziener² & Tanja Weil^{1,2}

Self-assembly in situ, where synthetic molecules are programmed to organize in a specific and complex environment i.e., within living cells, can be a unique strategy to influence cellular functions. Here we present a small series of rationally designed oligothiophene analogues that specifically target, locate and dynamically self-report their supramolecular behavior within the confinement of a cell. Through the recognition of the terminal alkyl substituent and the amphiphilic pyridine motif, we show that the cell provides different complementary pathways for self-assembly that can be traced easily with fluorescence microscopy as their molecular organization emits in distinct fluorescent bands. Importantly, the control and induction of both forms are achieved by time, temperature and the use of the intracellular transport inhibitor, bafilomycin A1. We showcase the importance of both intrinsic (cell) and extrinsic (stimulus) factors for self-organization and the potential of such a platform toward developing synthetic functional components within living cells.

¹Max Planck Institute for Polymer Research, Ackermannweg 10, 55128 Mainz, Germany. ²Institute of Organic Chemistry III, Ulm University, Albert-Einstein-Allee 11, 89081 Ulm, Germany. ³Institute of Molecular Biology, Ackermannweg 4, 55128 Mainz, Germany. ⁴Institute of Pharmacology and Toxicology, Ulm University Medical Center, Albert-Einstein-Allee 11, 89081 Ulm, Germany. David Y.W. Ng and Roman Vill contributed equally to this work. Correspondence and requests for materials should be addressed to D.Y.W.N. (email: david.ng@mpip-mainz.mpg.de) or to U.Z. (email: ulrich.ziener@uni-ulm.de) or to T.W. (email: weil@mpip-mainz.mpg.de)

The translation of biological or cellular functions into molecular design has since been regarded as the key in unlocking the development of synthetic intelligent materials as the community began to comprehend the importance of supramolecular chemistry within Nature's blueprint of life. Displayed coherently in the body, the dynamics of nanostructured biocomponents (proteins, lipids, carbohydrates, and DNA) drives cellular processes that are regulated in a highly specific way to ensure survival and proliferation. Although much efforts have been directed to understanding the influence of small molecules on cellular functions, the impact of materials at the nanometer scale assembled by seemingly individual synthetic molecules inside living cells have only very recently received increasing attention^{1, 2}.

In fact, whether it is a malignancy or a normal cellular process, it is crucial to appreciate that many of these systems exert their biological functions at the superstructure level, such as the assembly of peptide fragments into amyloid plaques that devastate neurological functions³ or the transient formation of microtubules that dictates essential intracellular transport⁴. As such, there is a need to look beyond molecular functions when it is necessary to change or modify a biological condition, especially since biological superstructures are always dynamically involved in most pathways. In this aspect, a new perspective toward developing highly specific therapeutics or to engineer artificial cells⁵ can be drawn if there is a possibility to control processes by integrating synthetic nanostructures within the cellular body^{6, 7}. Nonetheless, nanostructure assemblies of synthetic molecules within a living cell are extremely challenging to achieve due to the presence of a plethora of biological components in the environment. To circumvent this from a molecular design perspective, conjugated π -systems offer a very convenient scaffold as its orthogonality toward an environment predominated by hydrogen bonds provides a natural impetus for self-organization. Conventionally, π -conjugated heteroaromatic compounds have been extensively studied on superstructure formation in thin films

especially for charge transport applications (i.e., organic solar cells⁸, organic field-effect transistors⁹) and these devices are well understood. However, considering their self-assembly in aqueous biological medium, these molecules are rarely investigated, due to solubility, even though they possess attractive multifold functions (e.g., redox activity and fluorescence).

Among different conjugated π -systems, substituted oligothiophenes have been shown in preliminary studies to be able to bind, in a structure dependent fashion, to specific peptides and proteins often accompanied by an associated fluorescence change¹⁰. Naturally, this conformation dependent emission profile becomes an exceptional tool especially in real-time monitoring of self-assembly processes within a complex environment¹¹. This feature is even more appreciable because other well-known assembly systems in biology i.e., peptides, lipids, DNA, or proteins are incapable of providing an optical readout beyond the autofluorescence of the cell in the native state. In this aspect, Barbarella's group has shown in a seminal study the co-assembly of cell-permeable dithienothiophene-S,S-dioxide with type-I collagen to form a series of conducting microfibers within HeLa cells¹². The complementary properties of the eventual hybrid material are astounding considering that nature plays an unexpected but active role in its formation. This leads toward the notion that the integration of biological processes into the construction of intracellular assemblies can be evolved as an elegant strategy^{13, 14}. In developing such strategies into applications, Rao's group has taken advantage of the enrichment effect of intracellular nano-assemblies to amplify both the diagnostic signal and therapeutic profile within cancer cells¹⁵. On a similar note, Maruyama's group recently investigated that cancer cells can be killed purely by mechanical stress imposed by the programmed self-assembly of a peptide gelator within the cell¹⁶. Based on these studies, a strong potential toward developing an intracellular self-assembly platform as a forthcoming strategy for altering biological functions can be foreseen.

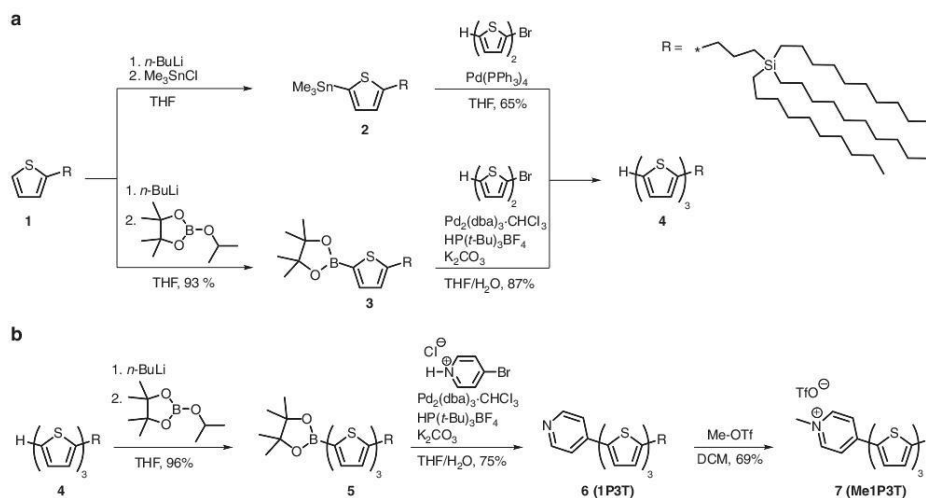


Fig. 1 Synthesis of the oligothiophene analogues. **a** Stille- VS Suzuki-Miyaura-type cross-coupling reactions to monosubstituted terthiophene **4**. **b** Synthesis of pyridine-functionalized terthiophene **6** (1P3T) via Suzuki-Miyaura-type cross-coupling and subsequent *N*-methylation reaction of latter to achieve the permanently positive charged derivative **7** (Me1P3T)

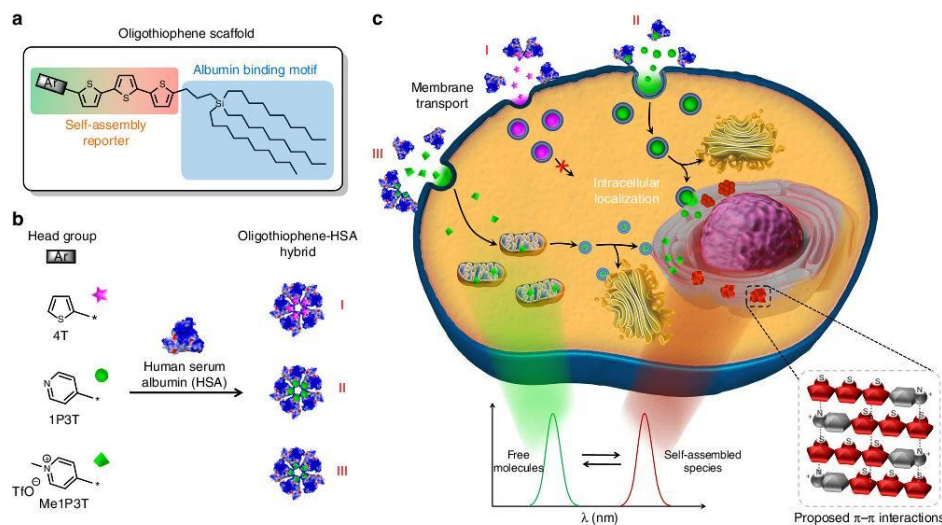


Fig. 2 Controlling intracellular assemblies. **a** Oligothiophene design containing a self-assembly reporter and an albumin binding motif. **b** Formation of stable complexes (I–III) with human serum albumin (HSA) that mediates water-solubility and cellular uptake. **c** Each oligothiophene analogue localizes and self-assembles intracellularly in a unique way based on the tailored aromatic head group (Ar), which allows real-time detection of molecular (green fluorescence) and self-assembled (red fluorescence) states. Several intracellular compartments can be specifically targeted by simply adjusting the head group (Ar) of the oligothiophene

Herein, we present carbosilane substituted terthiophenes, which are functionalized by *N*-heteroaromatic head groups of varying polarities to show that intracellular self-assembly and self-reporting systems can be rationally designed and monitored in a facile manner (Fig. 1). The oligothiophenes possess a characteristic two-color fluorescence emission that reports the arrangement of its molecular and assembled forms to elucidate intermolecular processes, associated pathways and biological responses. Pyridine with its possible quaternization was selected among existing diverse heteroaromatic scaffolds as a simplified synthetic representation to Nature's strategy of using cation- π interactions¹⁷ and *N*-methylation¹⁸ to switch and modulate DNA. Hence, by replacing the terminal thiophene unit on a quaterthiophene (4T) with pyridine (1P3T) and subsequent *N*-methylation (Me1P3T), we would sequentially assess the biological impact of (1) increasing polar interactions and electron acceptor character of the head group (Ar) as well as their impact on the terthiophene π -system, (2) how small structural changes to the oligothiophene scaffold can notably direct intracellular self-assembly. On the other hand, the carbosilane motif that incorporates long, branched alkyl chains was designed to further enhance self-organization behavior through van der Waals interactions¹⁹, as well as to support important lipid-mediated intracellular translocation²⁰. In particular, this substituent promotes binding toward human serum albumin (HSA), an ubiquitous protein in the bloodstream that has shown broad binding capabilities toward lipophilic molecules²¹, allowing their solubilization in water, as well as transport to cells. The result, therefore, is a biocompatible hybrid complex that facilitates membrane interactions and transport, with both amphiphilic quaterthiophene analogues individually displaying highly exclusive fluorescent features that provide real-time reporting of self-assembly processes inside living cells.

Results

Synthesis. In order to integrate these multifold molecular components, the synthetic route of the oligothiophene analogues was divided into three main parts (Fig. 1). The first step, depicted in Supplementary Fig. 1, involves the introduction of long alkyl chains while in the second part of the synthesis, monosubstituted terthiophene was constructed by either a Stille-type or Suzuki-Miyaura-type cross-coupling reaction (Fig. 1a). Although the synthesis of the compounds in Fig. 1a, Supplementary Fig. 1 were previously described^{19, 22}, the reaction conditions have been substantially modified and improved. Having accomplished the substituent R, the monosubstituted thiophene **1** was lithiated in the remaining α -position, followed by stannylation or borylation. Resulting **2** or **3** were coupled with 5-bromo-2,2'-bithiophene affording the corresponding terthiophene **4**. The Suzuki pathway was performed under milder reaction conditions with a more efficient palladium catalyst system compared to our previous protocol²² via Stille route leading to an improvement in yield from 65 to 87%. A further advantage of the Suzuki cross-coupling reaction is particularly the non-toxic nature of the boronic ester precursors. In order to introduce the last coupling step, the monosubstituted terthiophene **4** was again borylated (Fig. 1b). The conversion to pyridine-functionalized terthiophene **6** (1P3T) was exclusively carried out by a Suzuki-type cross-coupling reaction of monosubstituted terthienylboronic pinacol ester **5** with 4-bromopyridine hydrochloride. The Stille pathway was not pursued, because the prior mentioned coupling to **4** worked much better with the boron-containing species. Additionally, the required basic reaction conditions for Suzuki coupling reactions were utilized to neutralize, in situ, the building block from its hydrochloride salt into the free base of 4-bromopyridine. In the last step of the synthetic route, the basic functionality of 1P3T was modified via *N*-methylation reaction using methyl

trifluoromethanesulfonate to afford **7** (Me1P3T). These two analogues and the quaterthiophene **4T** form the basis of scaffold design by which the biological workflow is built upon (Fig. 2).

Self-assembly in solution. As these oligothiophenes alone are insoluble in polar solvents (i.e., DMSO, H₂O), a co-solvent system with THF in water or buffer is necessary to prevent precipitation. The maximum amount of water content tolerated by **4T** and **1P3T** (20 μ M) without precipitation is 80% v/v H₂O/THF and 95% v/v H₂O/THF for Me1P3T. Comparing the absorbance spectra, both the quaterthiophene **4T** and the pyridine-functionalized terthiophene **1P3T** exhibit a maximum at 400 nm while the quaternization of the pyridine by *N*-methylation resulted in a bathochromic shift of the absorbance ($\lambda_{\text{max}} = 439$ nm) (Supplementary Fig. 2). The broad absorption band of all three compounds can be assigned to the π - π^* transition of the conjugated backbone, whereas the redshift of the quaternized derivative Me1P3T might be attributed to the strengthening of the acceptor ability of the pyridinium moiety. In the emission spectrum ($\lambda_{\text{ex}} = 400$ nm), **4T** exhibits a maximum at 552 nm and a fine structure that is characteristic of oligothiophenes having multiple vibrational modes due to different molecular orientation and/or assembly (Fig. 3b). In comparison, **1P3T** possesses two distinct peak maxima ($\lambda_{\text{em}} = 505$ nm, 607 nm) and the large energy difference between the emission peaks suggest the formation of supramolecular structures in solution.

This phenomenon was investigated using fluorescence correlation spectroscopy (FCS) to ascertain the perceived supramolecular behavior (Supplementary Methods). In THF/H₂O, the correlation curve of **1P3T** fits a two component system indicating the presence of aggregates of sizes between 15 and 150 nm (Fig. 3f). As a control experiment, **1P3T** in THF showed a much faster diffusion coefficient with a corresponding molecular dimension of <0.5 nm. By correlating this result to the fluorescence spectrum of **1P3T**, a decrease in solvent polarity to pure THF results in disassembly of the system into a single band at 483 nm that correspond to the emission of the free molecules (Fig. 3c) while the maximum at 607 nm in THF/H₂O (Fig. 3b) can be assigned to the characteristic emission of the aggregates.

Importantly, the aggregation behavior is significantly different for the pyridinium derivative Me1P3T. In THF/H₂O where aggregates of **1P3T** were formed, Me1P3T remains, however, strictly in a molecular state (<0.5 nm) (Fig. 3g). The correlation of this molecular state of Me1P3T is also reflected on the emission spectrum (Fig. 3b, $\lambda_{\text{em}} = 500$ nm). On the contrary, in pure THF, Me1P3T showed an emission at 636 nm (Fig. 3c), which suggest a self-assembling system that is in reverse to that of **1P3T** (Fig. 3a). To demonstrate the dynamics of the supramolecular behavior, we have employed Me1P3T (which has the best solubility in polar solvents) in a concentration dependent study (Supplementary Fig. 3). With decreasing concentration of the Me1P3T, the proportion of aggregates present in solution likewise decreases. Hence, these spectral band assignments based on FCS report how amphiphilic oligothiophenes appear in polar/non-polar solvents and that these observations are not a result of a typical solvatochromism effect.

Complex formation with human serum albumin. In order to apply these oligothiophene amphiphiles in cellular studies, they need to be processible under entirely aqueous conditions. In cells, very lipophilic or amphiphilic molecules are often transported by proteins. Inspired by such natural transport opportunities, we have selected alkyl chains in our design as they are very well known to interact and bind to serum albumin (Fig. 2a, b), a protein naturally present in the human blood that is responsible

for circulating fatty acids and steroids through the body²³. HSA has a highly dynamic structure and has been known to temporarily stabilize and shuttle molecules i.e., drugs²⁴, fatty acids²⁵, and even carbon nanotubes²⁶ in water. The synthesis of the protein complex can be achieved by mixing a stock solution (20% THF/H₂O) of the oligothiophenes into a buffered solution of human serum albumin (HSA) for 16 h. THF is removed completely by freeze drying and the mixture is purified by size exclusion chromatography. The oligothiophene-HSA complexes are well soluble in water and were subsequently characterized by fluorescence spectroscopy and atomic force microscopy to understand the spectral changes upon interaction with the protein.

From the absorbance spectra, the contribution of HSA can be clearly observed at 280 nm along with the respective oligothiophene bands (Fig. 3d). Concentrations of the complexes were based on HSA due to its large molecular weight contribution (66,700 Da) compared to the oligothiophene (<1000 Da) and the 280 nm absorbance is indeed consistent throughout all three complexes. Evidently, a hypsochromic shift for all three oligothiophenes absorption can be detected, which might indicate a distortion in the planarity of the oligothiophene as a result of environmental influence. In the emission spectrum, **4T**-HSA demonstrates a characteristic molecular signal whereas both **1P3T**-HSA and Me1P3T-HSA show a mixture between molecular and aggregated forms (Fig. 3e). Due to the dynamic nature of the HSA structure and multiple binding sites, the presence of mixed signals is conceivable as the complexation of the molecules within the protein is not conformationally specific²⁷. As such, oligothiophenes can exist within the protein as a single molecule or as a small group of aggregated molecules. As the extinction of the molecules cannot be accurately determined when the oligothiophenes are complexed to the protein, a very rough estimate of ratio between protein and oligothiophene (e.g., 2 HSA proteins to 1 Me1P3T) can be seen. A higher protein to oligothiophene ratio is plausible due to the natural presence of HSA multimers in solution²⁸. Height topographic images of the oligothiophene-HSA complexes were analyzed in fluid operation AFM demonstrating a homogenous distribution of particles of ~2 nm (Fig. 3h, i), which is comparable to the native protein (Supplementary Fig. 4). In addition, these complexes are also stable in solution (FPLC, Supplementary Fig. 5) and freeze drying techniques, as oppose to standard liposomal delivery systems.

Cellular uptake, aggregation, and cellular toxicity. The primary differences between the complexed and uncomplexed form of the oligothiophenes were investigated in A549 cells. The cells were treated with the free oligothiophenes directly and imaged after 24 h. Based on the fluorescence data obtained above, we have identified two emission channels (green: 450–520 nm, red: 550–750 nm) that report the molecular and aggregated forms of the amphiphilic quaterthiophene analogues.

From the images, different internalization effects were observed for all three analogues and Me1P3T, in particular, elicited a characteristic cytotoxic response as the cells were observed to shrink and round up considerably (Fig. 4i–l). However, the spectral signature of Me1P3T is interesting as there is a high level of red emission in the remnants of the cellular membrane. This strongly suggests that Me1P3T possess a high-membrane affinity and that the environment exists within the phospholipid bilayer is favorable for the accumulation of the oligothiophene amphiphile. Hence, an experiment was conducted with phosphatidylcholine, the primary phospholipid present in the outer membrane surface to investigate the interaction in a more controlled environment. A fully water soluble system containing phosphatidylcholine (1

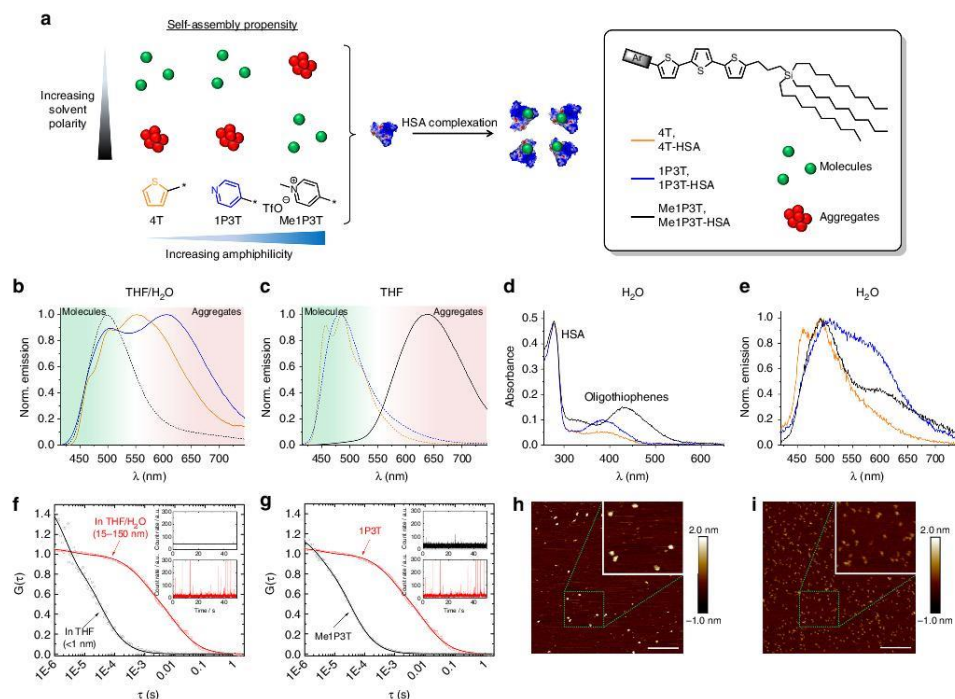


Fig. 3 Self-assembly properties of oligothiophenes and characterization of the HSA complexes. **a** Influence of the oligothiophene head group toward self-assembly. **b, c** Normalized emission spectra of 4T (orange), 1P3T (blue) and Me1P3T (black) at 20 μM in THF:H₂O = 1:4 v/v and in pure THF to investigate solvent effects. Molecular forms are distinguished by dashed lines. **d** Absorption and **e** Normalized emission spectra of oligothiophene-HSA complexes 4T-HSA (orange), 1P3T-HSA (blue) and Me1P3T-HSA (black) at 20 μM in H₂O. **f** Normalized FCS autocorrelation curves for 1P3T in THF (black circles) or THF:H₂O = 1:4, v/v. (red squares) at 1 μM . The black solid line represent a single-component ($m = 1$) fit with Supplementary Equ. 1 with $R_h \sim 0.5$ nm for 1P3T in THF solution. The red solid line represent a two component ($m = 2$) fit, indicating that various aggregates between 15 and 150 nm are present in the THF:H₂O solution. Aggregation behavior can be further observed in the respective intensity time trace plots in the inset. **g** Normalized FCS autocorrelation curves measured in 1 μM solutions (THF:H₂O = 1:4, v/v) of Me1P3T (black circles) and 1P3T (red squares). The black solid line represent a single-component ($m = 1$) fit with Supplementary Equ. 1 with $R_h \sim 0.5$ nm for Me1P3T. The red solid line represent a two component ($m = 2$) fit, indicating that various aggregates with sizes in the range 15–150 nm present in the 1P3T solution. Intensity time trace plots as insets further represent the aggregation trend. **h, i** Atomic force microscopy of 1P3T-HSA and Me1P3T-HSA, respectively, showing homogenous particles with average height profiles between 1.5 and 2 nm, indicating that the interaction between the oligothiophenes and HSA is largely defined. Scale bar = 200 nm

mM) and oligothiophene (15 μM) was formulated and observed to remain stable for days without precipitation. Fluorescence spectroscopy of the solution (Supplementary Fig. 6) showed that Me1P3T indeed demonstrates red emission maximum ($\lambda_{\text{em}} = 577$ nm). In comparison, the spectra of the oligothiophene analogues in THF resembles that in phosphatidylcholine, suggesting that the membrane-type microenvironments provide a similar environment to that by THF. Taken together, the use of THF as a co-solvent to study the respective aggregation behavior remains largely relevant. Nonetheless, the main differences comparing the two sets of spectra include the appearance of vibronic fine structures of 1P3T with phosphatidylcholine and a strong hypsochromic shift (~ 60 nm) for Me1P3T. The shift of the emission of Me1P3T toward higher energy is a consequence of the electron withdrawing capability of the pyridinium cation being partially compensated by the negative charge on phosphatidylcholine. The affinity of Me1P3T toward the host of cationic

surfactants in the literature^{29, 30}. Hence, in terms of toxicity (on both cellular and organism level), the mechanism by which the integrity of the cellular membrane is compromised by the hydrophobic cation is very well known^{31, 32}. In contrast, the treatment of 4T and 1P3T does not seem to influence the cell morphology (Fig. 4a–h) and it can be observed that the uptake of 4T is extremely limited, as its poor solubility results in precipitation from the cell medium. Co-localized signals from both green and red channels indicate that there is no difference with regards to the intracellular localization between the molecular and aggregated states.

Subsequently, we seek to quantify the toxicity effects using CellTiter-Glo luminescence assay where the functional capabilities of the mitochondria of living cells are analyzed. The IC_{50} value of Me1P3T was demonstrated to be 3.45 μM while 4T began to show toxicity $>10 \mu\text{M}$ (Fig. 5a). However, for 1P3T, no significant toxicity was detected up to 20 μM . As cellular toxicity is an especially important concern while we are exploring

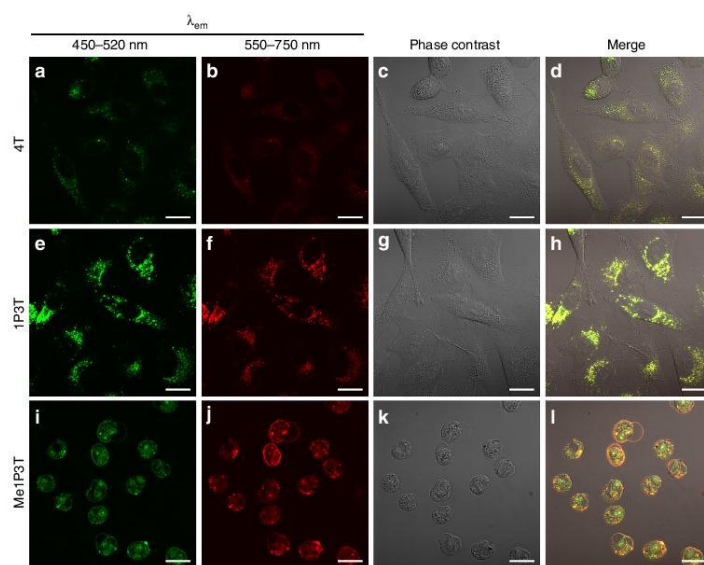


Fig. 4 Co-localized cellular uptake and morphologies of A549 cells with free oligothiophenes. Confocal laser scanning micrographs of A549 cells treated with 15 μ M oligothiophenes 4T **a–d**, 1P3T **e–h**, and Me1P3T **i–l** for 24 h at 37 °C, 5% CO₂. All samples are excited at 405 nm, where the molecular states (450–520 nm, green) and the aggregated states (550–750 nm, red) of the oligothiophenes were visualized simultaneously. Co-existence of both aggregated and non-aggregated species was represented as yellow signals. Scale bar = 20 μ m. Poor cellular internalization was observed for 4T **d**, whereas co-localization of molecular and aggregated species were detected for 1P3T **h**. Significant cell rounding indicating cellular toxicity was observed for Me1P3T **l**

intracellular processes for self-assembly, we subject the oligothiophene-HSA complexes to the same test (Fig. 5b). The toxicity effect of 4T-HSA on cell viability remained unchanged compared to its uncomplexed form whereas Me1P3T-HSA interestingly showed remarkable improvement and did not show toxicity even at 100 μ M. With these results, we proceed to conduct confocal microscopy on these oligothiophene-HSA complexes to identify plausible differences on the cellular dynamics.

Individual unique characteristics across all three analogues (4T-HSA, 1P3T-HSA, Me1P3T-HSA) were observed within A549 cells after 24 h treatment (Fig. 6). Systematically, the quaterthiophene 4T-HSA displayed improved cellular uptake behavior with co-localized signals from both molecular (green) and aggregated (red) states. However, for both 1P3T-HSA and Me1P3T-HSA, exclusive areas within the cells were observed to emit green and/or red that localized separately. Starting with the cells treated with 1P3T-HSA, green fluorescence was displayed within highly defined vesicular structures suggesting that these vesicles may play an important role in the trafficking and storage of the molecular forms of the oligothiophenes (Fig. 7a, b). The production of such large intracellular vesicles has been reported in the literature but only in selected lipid-based delivery systems and they are often found to have large size dispersities^{20, 33}. Within the perinuclear region, red fluorescent aggregates appeared to co-localize fully with green emitting molecular forms, which seem to reasonably suggest an existing equilibrium between both species. For Me1P3T-HSA, a highly scattered green fluorescence signal was observed with similar red/green co-localization in the perinuclear region (Fig. 7c, d). The similar

fluorescence signals of 1P3T and Me1P3T in the perinuclear region suggest that the process of intracellular aggregation does not depend on the protonation state of the pyridine group. In order to verify these results also on other cell lines, the localization of 1P3T and Me1P3T was tested additionally against HeLa cells and MCF-7. Although the intensity of uptake varies between cell types, the observations are comparable (Supplementary Fig. 7).

Mapping intracellular pathways and localization. Based on these results, we investigate in detail the intracellular processes to elucidate the role of HSA using pathway inhibitors and sub-cellular stains. To probe the transport function of HSA, the protein was labeled with ATTO 647 that can be excited independently from the oligothiophenes. It was clearly found that the HSA protein does not internalize into the cells at the tested concentrations (Supplementary Figs. 8, 9). This result is also supported in the literature that the primary function of HSA is the transport of nutrients and waste products between the organ-circulatory interfaces and intra-extra vasculatures³⁴. This concept was commonly known to be exploited in the albumin-paclitaxel formulation (Abraxane) for anti-cancer therapy³⁵. On the other hand, intracellular transport of HSA only happens via cell signaling or in selective cell types (i.e., Ras-transformed cells)³⁶. Therefore, the significantly reduced toxicity of Me1P3T-HSA is due to HSA preventing larger aggregates of the oligothiophenes and regulating the affinity of Me1P3T toward the cellular membrane. In this way, there is no sudden onset of oligothiophenes (indicated by lack of aggregated fluorescence membrane signal

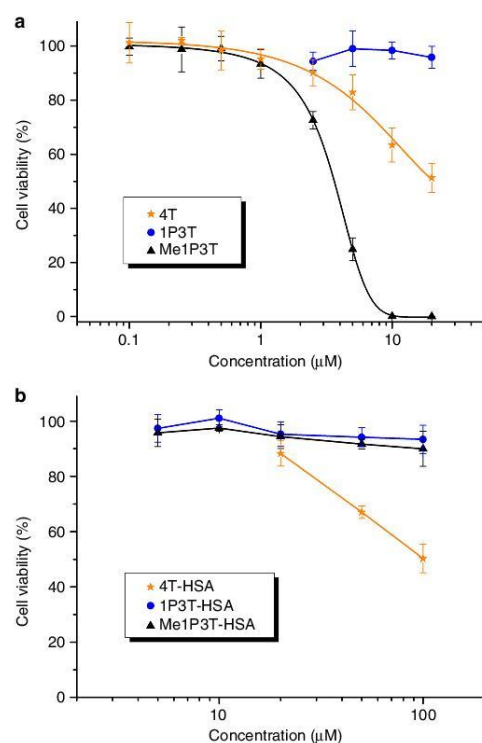


Fig. 5 Significantly reduced cellular toxicity of the oligothiophene-HSA complexes. **a, b** Precultured A549 cells were separately treated with 4T, 1P3T, Me1P3T and 4T-HSA, 1P3T-HSA, Me1P3T-HSA, respectively, at various concentrations for 24 h and analyzed in a CellTiter-Glo Luminescent Cell Viability Assay. For the free oligothiophenes, solubility of the compounds limits the test to $\leq 20 \mu\text{M}$. The intensity of luminescence directly correlates to the amount of living cells. Data presented were measured in independent triplicates. In particular, a significant toxicity difference was observed between Me1P3T (IC_{50} , $3.45 \mu\text{M}$) and Me1P3T-HSA (IC_{50} , $>100 \mu\text{M}$). The data represented as mean \pm SEM, $n = 3$

from Me1P3T-HSA) bound onto the cellular surface to cause the membrane collapse and consequently cell death.

As the molecules internalize, they are subsequently subjected to intracellular processes that dictate their movement into sub-cellular compartments and therefore influence aggregation processes. We have particularly studied the inhibition of endosomal trafficking and microtubulin-based vesicular transport, compartmental co-localization and the use of temperature to induce aggregation processes within the cell.

Bafilomycin A1, a macrolide antibiotic that inhibits H^+ -ATPase, prevents the maturation of endosomes and fusion of these vesicles with other cellular compartments thereby inhibiting intracellular transport³⁷. Therefore, bafilomycin A1 would prevent the accumulation of the oligothiophenes within the perinuclear region and impede their assembly. Moreover, it would promote better visualization and understanding of the different pathways directly associated with the respective chemical structures. Indeed, for both 1P3T and Me1P3T, red

emission of the aggregated state was absent when the cells were treated with bafilomycin and the contrast between the localization of their molecular forms becomes significantly more prominent (Fig. 8). The consistency of green fluorescence in both inhibitor treated and untreated cells implies that only the respective molecular forms of the oligothiophenes are involved in the early endocytotic pathway and that the downstream associated microenvironments i.e., organelles are necessary for self-assembly. It is therefore prospective that the fusion of vesicles into highly lipophilic and localized compartments (i.e., storage lipid droplets) interacts strongly with oligothiophenes and the alkyl chains to initiate their self-assembly. On the contrary, 4T interestingly showed no appreciable difference when treated with bafilomycin, which might suggest that the transport of this compound did not proceed further downstream and that it remained in these vesicles (Fig. 8a–d).

When the oligothiophenes are locked in place at the early stages of intracellular trafficking using bafilomycin A1, their first localization can be tracked using compartmental stains. Using MitoTracker Deep Red, the two pyridine derivatives can be distinguished because of the high tendency that lipophilic cations target the mitochondria³⁸. Indeed, the green fluorescence of Me1P3T was found to co-localize in majority with the mitochondria stain, indicating that the molecular form of Me1P3T was transported to the mitochondria (Fig. 8l). On the contrary, the vesicular structures of both 4T and 1P3T did not co-localize with the MitoTracker. As these first experiments provide an early indication that 4T showed no specific intracellular preferences for its molecular and aggregated forms, further investigations were done primarily on 1P3T and Me1P3T. Additional co-localization experiments with ER-Tracker Red and NuclearMask Deep Red (Supplementary Figs. 10, 11) demonstrate that the intracellular pathways observed do not involve the ER network nor the cell nucleus.

Therefore, we next attempt to manipulate vesicle transport dynamics by pre-treating the cells with nocodazole, an anti-neoplastic agent that prevents microtubule polymerization. With no microtubules, the cells became round and a significant reduction in the amount of intracellular vesicular structures was observed (Supplementary Fig. 12). Importantly, the fluorescence emission patterns for both 1P3T and Me1P3T remained largely similar to the normal cells, indicating that the molecular and aggregated behavior remained relatively independent on the status of the microtubule within the cell.

These biological interventions have provided deeper insights into the character and localization of these oligothiophenes. As these molecules behave and interact according to the principles of supramolecular chemistry, they respond either to the hydrophilicity/hydrophobicity of the microenvironment and/or concentration. Therefore, by performing a time lapse study of the uptake of the respective oligothiophenes, the resultant fluorescence changes can be indicative of these environmental changes within the cell. After 5 h of treatment, a dominant green fluorescence signal localized in vesicles (1P3T) or mitochondria (Me1P3T) was observed while red fluorescence of aggregates were clearly absent (Fig. 9a, b). At 24 h, the appearance of red fluorescence around the perinuclear region was clearly observed as described earlier (Fig. 9c, d). In order to prove that aggregate formation originates from the free molecules, the cells were washed (after 24 h treatment) and the medium was replaced with pure DMEM so that no new oligothiophenes could be uptaken. In these images, diminishing of green fluorescence was detected and only the perinuclear aggregation signals were observed (Fig. 9e, f). These observations clearly indicate that the amphiphiles were internalized in their molecular forms, which then traffic to different intracellular compartments to form aggregates in the

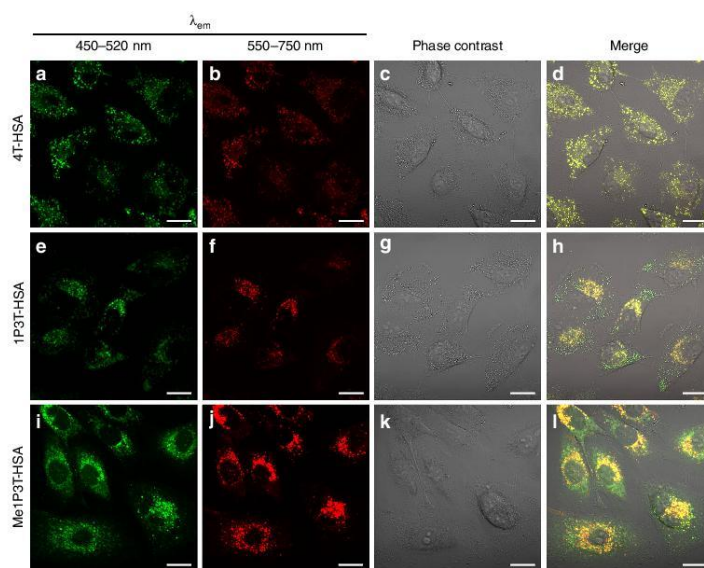


Fig. 6 Internalization, distribution and assembly of the oligothiophenes in living cells. Confocal laser scanning micrographs of A549 cells treated with oligothiophene-albumin complex 4T-HSA **a–d**, 1P3T-HSA **e–h**, and Me1P3T-HSA **i–l** at 15 μ M for 24 h (37 $^{\circ}$ C, 5% CO_2). Molecular states (450–520 nm, green) and aggregates (550–750 nm, red) are visualized simultaneously (co-localization in yellow). Scale bar = 20 μ m. All three compounds were internalized efficiently and show distinct localized fluorescence signals, which vary with the different head groups

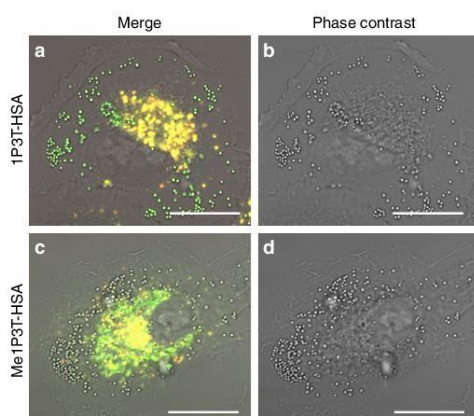


Fig. 7 Fluorescence distribution/localization of the molecular and aggregated oligothiophenes. Confocal laser scanning micrographs of A549 cells treated with 1P3T-HSA **a, b** and Me1P3T-HSA **c, d** for 24 h at 37 $^{\circ}$ C, 5% CO_2 . Scale bar = 20 μ m. The image was magnified to showcase defined features (1P3T: green vesicles; Me1P3T: non-emitting vesicles), fluorescence distribution, as well as the perinuclear localization of the aggregated states (yellow)

lipophilic regions surrounding the nucleus. Collectively, both the bafilomycin/co-localization and time dependent studies indicate evidently that the internalization process of the amphiphilic oligothiophenes specifically begin as molecular forms, which transport into specific intracellular regions and thereafter self-assemble in the lipophilic regions surrounding the nucleus (Fig. 2c).

Intracellular self-assembly induced by temperature. These previous studies give an insight into the relationship between small variations in chemical functionalities and targeted intracellular trafficking. This knowledge is fundamental for the design of smart materials within the cell where we showed that these intracellular supramolecular assemblies can be manipulated. As most supramolecular systems are largely influenced also by temperature changes, we utilize a combination of methods to specifically initiate self-assembly within targeted intracellular compartments. From the aforementioned experiments, we established that Me1P3T transports first to the mitochondria before trafficking across to the perinuclear region. By locking the translocation pathway using bafilomycin A1, the mitochondria localized Me1P3T was subjected to 4 $^{\circ}$ C treatment for 2 h (Fig. 9g–j). Comparing the fluorescence image captured at 4 $^{\circ}$ C with that of 37 $^{\circ}$ C (Fig. 8i–l), intense red emission of the aggregated forms of Me1P3T can be observed specifically in the mitochondria at 4 $^{\circ}$ C. Importantly, throughout these processes without chemical fixation, the cells look visibly healthy. As a result, by using a temperature stimulus, we showed that the aggregation behavior can be controlled through chemical design to occur in specific intracellular compartments. This ability to trigger on demand supramolecular assemblies within complex

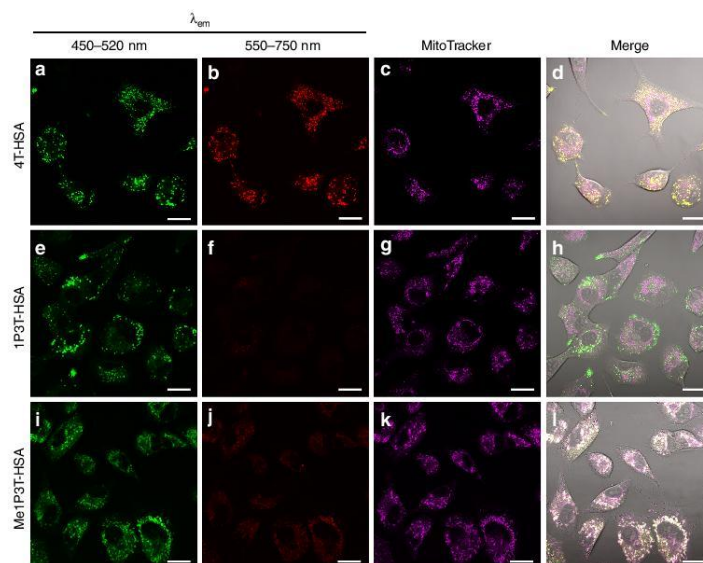


Fig. 8 Inhibition of intracellular vesicle fusion and transport by bafilomycin A1. A549 cells were treated with bafilomycin A1 (100 nM, 30 min) prior to the introduction of 4T-HSA **a–d**, 1P3T-HSA **e–h**, and Me1P3T-HSA **i–l** at 15 μ M. Images were taken after 24 h incubation at 37 °C, 5% CO₂ with the respective complex. Mitochondria of the cells were stained with MitoTracker Deep Red represented in purple color. The corresponding experiments without bafilomycin A1 are presented in Fig. 6. Scale bar = 20 μ m. Bafilomycin A1 pretreatment of cells trapped 1P3T **e** and Me1P3T **i** in their molecular states (green) within their respective compartments whereas it has no effect upon 4T **a** assembly (green and red indicating co-existence of molecular and assembled forms). **l** Co-localization studies suggest that only Me1P3T targets the mitochondria and localizes there in its molecular form (white color of the co-localization of molecular Me1P3T in green and MitoTracker in purple)

cellular environments can provide a significant impact toward creating functional nanostructures to influence cellular behavior.

Discussion

The synthesis of oligothiophene cellular reporters has been achieved by performing critical and concise chemical modifications toward the conjugated π -electron system. The resulting oligothiophene derivatives were able to respond, target and self-assemble specifically within mammalian cells. Integration of the three investigated oligothiophenes (4T, 1P3T, and Me1P3T) into HSA was essential to provide full water solubility at high concentrations (up to 100 μ M) of these otherwise insoluble molecules, resulting in the formation of non-cytotoxic complexes. Their fluorescent properties directly represent, to various degrees, nanostructural changes in solution allowing their dynamic behavior within intracellular environments to be evaluated. By interpreting these fluorescence changes, HSA is shown to be integral in mediating the cell/molecule interface where it delivers the oligothiophenes as molecules, which are subsequently recognized by the cells and sorted into different downstream pathways (Fig. 10).

We have shown that these pathways are complementarily determined by the head groups and alkyl substituent of the oligothiophene. Additionally, the intracellular processes involved are outlined by elaborated fluorescence microscopy studies. After cellular entry supported by HSA, 4T remains trapped inside vesicles while 1P3T and Me1P3T self-assembled within the perinuclear region, albeit passing through different cellular compartments. The knowledge of such compartmentalization is

crucial for promoting/inhibiting supramolecular assembly by external stimuli. Large uniform intracellular vesicles were created that demonstrate endosome-like features, which were directly controlled by bafilomycin A1. In the case of Me1P3T, the combination of bafilomycin A1 and lowering the ambient temperature efficiently locked the self-assembly process exclusively in a cellular organelle (mitochondria). This unique feature facilitates the capability to initiate self-assembly and localize aggregates, which would not be possible under standard cell culture conditions. Within these studies, we highlight the importance of structural design toward assembly in living cells where very stringent (e.g., non-toxic and cell-permeable) and dynamic intracellular processes (e.g., endocytosis, vesicle formation, and transport) are involved.

Collectively, we have presented the ability to trigger supramolecular assemblies within a complex cellular system, which provides a unique perspective toward constructing dynamic nanostructures to possibly reprogram cellular functions on a supramolecular level. Development in this area would potentially create a new platform for therapeutics where higher ordered architectures within the cells are targeted instead of a specific protein/enzyme. Furthermore, the ability to create an artificial intracellular architecture remains a powerful capability of synthetic supramolecular chemistry that may very well represent an entirely new perspective of biomedical science.

Methods

General (chemistry). ¹H NMR and ¹³C NMR spectra were recorded at room temperature on a Bruker AMX400. High temperature NMR spectroscopy was conducted on a Bruker AMX500. All NMR measurements were done in CDCl₃.

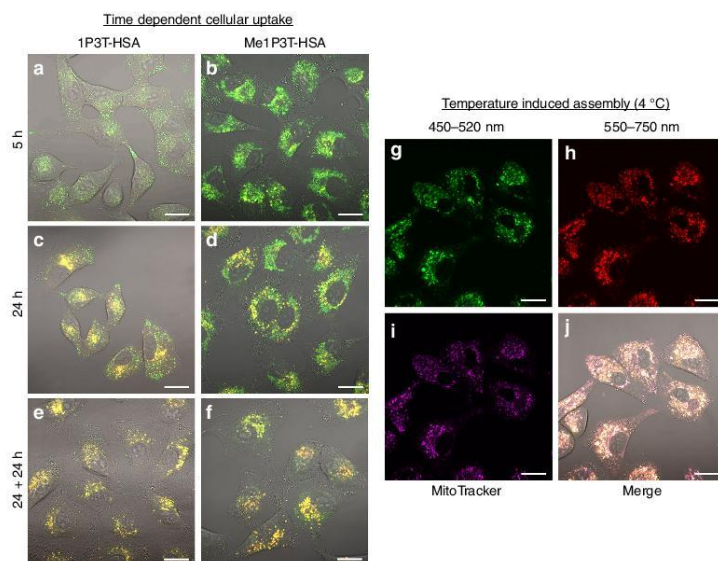


Fig. 9 Time dependent and temperature induced self-assembly. A549 cells were treated with 1P3T-HSA **a, c** and Me1P3T-HSA **b, d** at 15 μ M for 5 h and 24 h. **e, f** For an independent set of cells, the medium containing the samples was removed and added pure DMEM and incubated a further 24 h. Progression of free molecules (green) into aggregates (red, co-localized as yellow) can be clearly observed in a time dependent manner for both oligothiophene analogues. **g–j** A549 cells were pre-treated with bafilomycin and incubated with Me1P3T-HSA at 15 μ M for 24 h (37 °C, 5% CO₂). The cells were stained with MitoTracker Deep Red (purple) and they are incubated at 4 °C separately for a further 2 h and imaged via confocal laser scanning microscopy. The control experiment is shown in Fig. 8i–l. Scale bar = 20 μ m. The molecular form (green) of Me1P3T was locked in the mitochondria and forced to self-assemble into superstructures (red) by decreasing the ambient temperature. Co-localization of free molecules (green), assemblies (red) and MitoTracker (purple) represented in magenta/pink color

C₂D₂Cl₄ or CD₃OD/CDCl₃ mixture, respectively, with the solvent residual peak as an internal reference [CHCl₃: δ = 7.24 p.p.m. (¹H) and 77.0 p.p.m. (¹³C), C₂D₂Cl₄: δ = 6.00 p.p.m. (¹H), CHD₂OD: δ = 3.30 p.p.m. (¹H)]. Mass spectrometry (MALDI-TOF) was performed on Bruker Reflex III. The elemental composition was determined with an Elementar Vario EL system. The synthesis of the precursors can be found in Supplementary Information.

Synthesis of 5-(3-(Tridecylsilyl)prop-1-yl)-2,2':5',2'':5'',2'''-quaterthiophene (4T). 4T was prepared according to the literature¹⁹.

Synthesis of 4-(5-(3-(Tridecylsilyl)prop-1-yl)-2,2':5',2'':5'',2'''-terthien-5''-yl)pyridine (6, 1P3T). Terthienylboronic pinacol ester **5** (0.920 g, 1.06 mmol) was dissolved in THF (20 mL) and H₂O (6 mL) was added. The solution was degassed for 1 h. Then 4-bromopyridine hydrochloride (0.200 g, 1.03 mmol), Pd₂(dba)₃·CHCl₃ (0.088 g, 0.08 mmol), HP(*i*-Bu)₃BF₄ (0.049 g, 0.17 mmol) and K₂CO₃ (1.61 g, 11.67 mmol) were added and the reaction mixture was stirred at 81 °C for 19 h. The organic phase was separated and the aqueous phase was extracted with chloroform. The combined organic phases were dried over MgSO₄ and the solvent was evaporated. The crude product was purified by column chromatography (SiO₂/n-hexane: ethyl acetate = 2:1, ethyl acetate: n-hexane = 2:1) to give **6** as a yellow solid (0.63 g, 75%). M.p.: 72 °C. ¹H-NMR (400 MHz, CDCl₃), δ [p.p.m.]: 8.57 (dd, J(H,H) = 4.6, 1.6 Hz, 2H, 2-H₂, 6-H₂), 7.43 (dd, J(H,H) = 4.6, 1.6 Hz, 2H, 3-H₂, 5-H₂), 7.40 (d, ³J(4',3') = 3.9 Hz, 1H, 4'-H_T), 7.14 (d, ³J(3',4') = 3.8 Hz, 1H, 3'-H_T), 7.10 (d, ³J(4',3') = 3.8 Hz, 1H, 4'-H_T), 7.00 (d, ³J(3',4') = 3.9 Hz, 1H, 3'-H_T), 6.99 (d, ³J(3,4) = 3.6 Hz, 1H, 3-H_T), 6.68 (d, ³J(4,3) = 3.6 Hz, 1H, 4-H_T), 2.78 (t, ³J(α,β) = 7.3 Hz, 2H, α -CH₂), 1.68–1.61 (m, 2H, β -CH₂), 1.29–1.23 (m, 48H, CH₂), 0.85 (t, ³J(H,H) = 6.8 Hz, 9H, CH₃), 0.58–0.54 (m, 2H, γ -CH₂), 0.49–0.45 (m, 6H, SiCH₂). ¹³C-NMR (100 MHz, CDCl₃), δ [p.p.m.]: 150.3, 145.9, 141.0, 139.2, 137.9, 134.6, 134.2, 126.2, 125.1, 125.0, 124.4, 123.7, 123.6, 119.4, 34.2, 33.9, 31.9, 29.70, 29.65, 29.39, 29.34, 26.4, 23.9, 22.7, 14.1, 12.4, 12.2. MS (MALDI-TOF), m/z : 817.5 [M]⁺. Elemental analysis: Calcd. for C₅₀H₇₉NS₃Si (818.45): C 73.38, H 9.73, N 1.71; found: C 73.35, H 9.79, N 1.66.

Synthesis of N-Methyl-4-(5-(3-(tridecylsilyl)prop-1-yl)-2,2':5',2'':5'',2'''-terthien-5''-yl)pyridinium trifluoromethanesulfonate (7, Me1P3T). To a solution of **6** (48 mg, 0.06 mmol) in dry dichloromethane (10 mL) methyl trifluoromethanesulfonate (60 μ L, 0.53 mmol) was added at 0 °C. After complete addition the reaction mixture was stirred at the same temperature for 0.5 h. Then the mixture was allowed to warm to room temperature and was stirred for 3 h. The crude product was purified by column chromatography (SiO₂/dichloromethane: methanol = 5:1) to give **7** as a red solid (40 mg, 69%). M.p.: 96 °C. ¹H-NMR (400 MHz, CD₃OD:CDCl₃ = 5:1), δ [p.p.m.]: 8.65 (d, J(H,H) = 6.1 Hz, 2H, 2-H₂, 6-H₂), 8.12 (d, J(H,H) = 6.2 Hz, 2H, 3-H₂, 5-H₂), 8.02 (d, ³J(4',3') = 4.0 Hz, 1H, 4'-H_T), 7.38 (d, ³J(3',4') = 4.0 Hz, 1H, 3'-H_T), 7.35 (d, ³J(4',3') = 3.9 Hz, 1H, 4'-H_T), 7.11 (d, ³J(3',4') = 3.8 Hz, 1H, 3'-H_T), 7.09 (d, ³J(3,4) = 3.5 Hz, 1H, 3-H_T), 6.73 (d, ³J(4,3) = 3.5 Hz, 1H, 4-H_T), 4.26 (s, 3H, NCH₃), 2.82 (t, ³J(α,β) = 7.0 Hz, 2H, α -CH₂), 1.71–1.63 (m, 2H, β -CH₂), 1.32–1.24 (m, 48H, CH₂), 0.85 (t, ³J(H,H) = 6.9 Hz, 9H, CH₃), 0.61–0.57 (m, 2H, γ -CH₂), 0.52–0.48 (m, 6H, SiCH₂). ¹H-NMR (500 MHz, C₂D₂Cl₄, 357 K), δ [p.p.m.]: 8.62 (bs, 2H, 2-H₂, 6-H₂), 7.96 (bs, 2H, 3-H₂, 5-H₂), 7.84 (bs, 1H, 4'-H_T), 7.33 (bs, 2H, 4'-H_T, 3'-H_T), 7.12 (bs, 2H, 3-H_T, 3'-H_T), 6.78 (bs, 1H, 4-H_T), 4.40 (bs, 3H, NCH₃), 2.88 (t, ³J(α,β) = 7.3 Hz, 2H, α -CH₂), 1.81–1.74 (m, 2H, β -CH₂), 1.42–1.34 (m, 48H, CH₂), 0.95 (t, ³J(H,H) = 6.8 Hz, 9H, CH₃), 0.71–0.68 (m, 2H, γ -CH₂), 0.61–0.58 (m, 6H, SiCH₂). MS (MALDI-TOF), m/z : 832.5 [M]⁺. Elemental analysis: Calcd. for C₅₂H₈₂F₃NO₃S₃Si (982.55): C 63.57, H 8.41, N 1.43; found: C 63.31, H 8.52, N 1.54.

General (biology). Cell culture of A549 cells was performed in Dulbecco's Modified Eagle's Medium (DMEM, High Glucose) supplemented with 10% FBS, 1% penicillin/streptomycin and 1 \times MEM non-essential amino acid with incubation conditions set at 37 °C, 5% CO₂. CellTiter-Glo Cell Viability Assay was purchased from Promega and used according to the given protocol. Luminescence intensities are measured from Glomax Multi 96-well plate reader (Promega). Confocal laser scanning microscopy was performed using Zeiss LSM 710, Observer.Z1 and processed using Zen Blue/Black software. Separate studies were also independently performed using Zeiss TCS SPS.

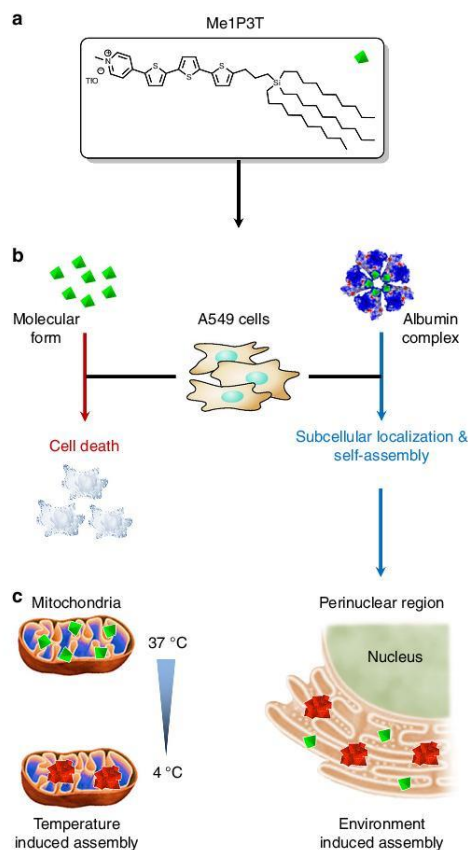


Fig. 10 Cellular response and controlled self-assembly of Me1P3T. **a, b** Cellular toxicity of the oligothiophene analogue Me1P3T (green) was first eliminated by complexation with HSA, which subsequently mediates its membrane translocation. **c** The cell sorts Me1P3T into the mitochondria followed by its transport into the perinuclear region. Self-assembly can be induced or impeded in specific compartments via external stimuli (temperature/inhibitor). In this way, Me1P3T was locked in the mitochondria using bafilomycin and initiated self-assembly by temperature reduction (red)

General preparation of water soluble oligothiophenes. Oligothiophenes (4T, 1P3T, Me1P3T) were pre-dissolved in THF at a concentration of 1 mg/mL. Human serum albumin (3.5 mg, 52.5 nmol) was dissolved in 1.2 mL of phosphate buffer (20 mM, pH 7.0) and added to the respective oligothiophenes (52.5 nmol) in 300 μ L THF. The resulting mixture was put onto an orbital shaker for 16 h at room temperature and subsequently freeze dried to remove all solvents.

The crude solid was re-dissolved in 1 mL H₂O and the solution was filtered through 0.2 μ m syringe filter. The solution was purified using Sephadex G25M (GE Healthcare) size exclusion chromatography using MilliQ water as the mobile phase. The desalted solution was subsequently freeze dried to afford the oligothiophene-albumin complex (4T-HSA, 1P3T-HSA, and Me1P3T-HSA) in \approx 80% yield.

Analysis was accomplished via Superdex 200 FPLC (ÄKTA Purifier, GE Healthcare) using phosphate buffered saline (20 mM PB, 150 mM NaCl).

Labeling of human serum albumin with ATTO 647. Human serum albumin (10 mg, 149 nmol) was dissolved in 2 mL phosphate buffer (20 mM, pH 9.0) and added

ATTO 647 *N*-hydroxysuccinimide ester (0.03 mg, 37.3 nmol) predissolved in anhydrous DMF. The reaction was stirred at room temperature for 16 h and purified using Sephadex G25M (GE Healthcare) size exclusion chromatography using MilliQ water as the mobile phase. The desalted solution was subsequently freeze dried to obtain ATTO 647-HSA in 92% yield.

Atomic force microscopy. Atomic force microscopy was measured with a Bruker Dimension FastScan Bio AFM equipped with the ScanAsyst mode. The respective 1P3T-HSA and Me1P3T-HSA solution (20 μ L, 600 nM) was deposited onto freshly cleaved mica surface and left for 5 min at room temperature to allow the protein complexes to adsorb. After an addition of additional 20 μ L of MilliQ Water into the sample, the sample was scanned at the rate between 1 and 3 Hz. Several images in different areas were taken to ensure reproducibility of the results. All images were analyzed using the NanoScope Analysis 1.50 and Gwyddion 2.38 software.

Cell culture. A549/MCF-7/HeLa cells were cultured in standard T-75 flasks using high glucose DMEM fortified with 10% fetal bovine serum, 1% penicillin/streptomycin and 1% MEM non-essential amino acids. The cells were split at near confluency and incubated at 37 °C, 5% CO₂ prior to each experiment.

Confocal microscopy imaging (standard set-up). Pre-cultured A549 cells were seeded at a density of 15,000 cells per well in an 8-well confocal microscopy chamber (Ibidi) and left to adhere overnight at 37 °C, 5% CO₂. The respective oligothiophenes (4T, 1P3T, Me1P3T) and/or oligothiophene-HSA complexes (4T-HSA, 1P3T-HSA, Me1P3T-HSA) were added into each well at concentrations (15 μ M) and incubated for 5 and 24 h separately at 37 °C, 5% CO₂. The treated cells were washed twice with DMEM to remove non-specific adsorption and imaged using Zeiss LSM 710. For fluorescence visualization, a 405 nm excitation laser was used in conjunction with emission filters at 450–520 nm and 550–750 nm to monitor the molecular and assembled species, respectively.

To exclusively monitor intracellular localization, the medium containing the oligothiophene-HSA complex was exchanged with pure DMEM after 24 h incubation. The well was aspirated and pure DMEM (300 μ L) was added. The cells were incubated for a further 24 h at 37 °C, 5% CO₂ and imaged as described above.

Confocal microscopy imaging (cellular pathway inhibitor). Pre-cultured A549 cells were seeded at a density of 15,000 cells per well in an 8-well confocal microscopy chamber (Ibidi) and left to adhere overnight at 37 °C, 5% CO₂. Bafilomycin A1 or Nocodazole (100 nM) was introduced separately into different wells and incubated for 30 min at 37 °C, 5% CO₂. The complexes (4T-HSA, 1P3T-HSA, Me1P3T-HSA) were prepared at concentrations (15 μ M) were subsequently co-incubated with the inhibitor for an additional 24 h at 37 °C, 5% CO₂. Following which, the cells were washed twice with DMEM prior to imaging using Zeiss LSM 710 and with parameters as stated above.

Confocal microscopy imaging (compartmental staining). MitoTracker Deep Red (Molecular Probes) was dissolved in DMSO (Biotect, Grade, Sigma-Aldrich) to produce a 1 mM stock solution. The staining medium was prepared by performing a 50,000 \times dilution (1 μ L stock into 50 mL DMEM) to a final concentration of 20 nM. The medium of the respective cells, incubated with the different oligothiophene-albumin complexes, were removed and added 300 μ L of the diluted staining medium. The cells were stained for 15 min at 37 °C, 5% CO₂ and were washed twice with DMEM prior to imaging. The procedures for ERTracker Red and NuclearMask Deep Red were performed using manufacturer's protocol.

Confocal microscopy imaging (low temperature measurements). Pre-cultured A549 cells were seeded at a density of 15,000 cells per well in 2 separate 8-well confocal microscopy chamber (Ibidi) and left to adhere overnight at 37 °C, 5% CO₂. Bafilomycin A1 (100 nM) was introduced separately into different wells and incubated for 30 min at 37 °C, 5% CO₂. Me1P3T-HSA was added into each well and co-incubated with the inhibitor for 24 h at 37 °C, 5% CO₂. Subsequently, one set of the microscopy chamber was transferred into a sterile 4 °C refrigerator and incubated for a further 2 h. These cells were washed with cold DMEM and left on ice prior to imaging. The other set of cells were kept at 37 °C and was treated similar to previous sections as a control experiment. Both set of cells were imaged using Zeiss LSM 710.

Cytotoxicity assay. Pre-cultured A549 cells were seeded at a density of 6500 cells per well in a white 96-well plate (half area) and allowed to adhere overnight at 37 °C, 5% CO₂. The oligothiophenes and the respective HSA-complexes were introduced at concentrations (0.1–100 μ M) and incubated for 24 h at 37 °C, 5% CO₂. CellTiter-Glo (Promega) was employed following manufacturer's protocol and the resultant luminescence read out was detected using Glomax Multi 96-well plate reader (Promega).

Data availability. The data supplementing the effect of pH and hydrocarbon solvents on 1P3T are found in Supplementary Information (Supplementary

Figs. 13, 14). The authors declare that the data supporting the findings are available within the paper and its Supplementary Information files, as well as upon reasonable requests.

Received: 20 March 2017 Accepted: 1 November 2017

Published online: 29 November 2017

References

- Shi, J., Kantoff, P. W., Wooster, R. & Farokhzad, O. C. Cancer nanomedicine: progress, challenges and opportunities. *Nat. Rev. Cancer* **17**, 20–37 (2017).
- Ng, D. Y. W., Wu, Y., Kuan, S. L. & Weil, T. Programming supramolecular biohybrids as precision therapeutics. *Acc. Chem. Res.* **47**, 3471–3480 (2014).
- Citron, M. Alzheimer's disease: strategies for disease modification. *Nat. Rev. Drug Discov.* **9**, 387–398 (2010).
- Akhmanova, A. & Steinmetz, M. O. Control of microtubule organization and dynamics: two ends in the limelight. *Nat. Rev. Mol. Cell Biol.* **16**, 711–726 (2015).
- Church, G. M., Elowitz, M. B., Smolke, C. D., Voigt, C. A. & Weiss, R. Realizing the potential of synthetic biology. *Nat. Rev. Mol. Cell Biol.* **15**, 289–294 (2014).
- Huber, M. C. et al. Designer amphiphilic proteins as building blocks for the intracellular formation of organelle-like compartments. *Nat. Mater.* **14**, 125–132 (2015).
- Palivan, C. G. et al. Bioinspired polymer vesicles and membranes for biological and medical applications. *Chem. Soc. Rev.* **45**, 377–411 (2016).
- Lloyd, M. T., Anthony, J. E. & Malliaras, G. G. Photovoltaics from soluble small molecules. *Mater. Today* **10**, 34–41 (2007).
- Mei, J., Diao, Y., Appleton, A. L., Fang, L. & Bao, Z. Integrated materials design of organic semiconductors for field-effect transistors. *J. Am. Chem. Soc.* **135**, 6724–6746 (2013).
- Åslund, A., Nilsson, K. P. R. & Konradsson, P. Fluorescent oligo and polythiophenes and their utilization for recording biological events of diverse origin —when organic chemistry meets biology. *J. Chem. Biol.* **2**, 161–175 (2009).
- Mishra, A., Ma, C.-Q. & Bäuerle, P. Functional oligothiophenes: molecular design for multidimensional nanoarchitectures and their applications. *Chem. Rev.* **109**, 1141–1276 (2009).
- Palamà, I. et al. Live-cell-permeant thiophene fluorophores and cell-mediated formation of fluorescent fibrils. *J. Am. Chem. Soc.* **133**, 17777–17785 (2014).
- Barbarella, G. & Di Maria, F. Supramolecular oligothiophene microfibers spontaneously assembled on surfaces or coassembled with proteins inside live cells. *Acc. Chem. Res.* **48**, 2230–2241 (2015).
- Rosu, C. et al. Protein-assisted assembly of π -conjugated polymers. *Chem. Mater.* **28**, 573–582 (2016).
- Ye, D. et al. Biorthogonal cyclization-mediated in situ self-assembly of small-molecule probes for imaging caspase activity in vivo. *Nat. Chem.* **6**, 519–526 (2014).
- Tanaka, A. et al. Cancer cell death induced by the intracellular self-assembly of an enzyme-responsive supramolecular gelator. *J. Am. Chem. Soc.* **137**, 770–775 (2015).
- Mahadevi, A. S. & Sastry, G. N. Cation- π interactions in nature: interaction: its role and relevance in chemistry, biology, and material science. *Chem. Rev.* **113**, 2100–2138 (2013).
- Chatterjee, J., Rechenmacher, F. & Kessler, H. N-methylation of peptides and proteins: an important element for modulating biological functions. *Angew. Chem. Int. Ed.* **52**, 254–269 (2013).
- Kreyes, A. et al. The longest β -unsubstituted oligothiophenes and their self-assembly in solution. *Chem. Mater.* **22**, 6453–6458 (2010).
- Rajendran, L., Udayar, V. & Goodger, Z. V. Lipid-anchored drugs for delivery into subcellular compartments. *Trends Pharmacol. Sci.* **33**, 215–222 (2012).
- Krenzle, E. S., Chen, Z. & Hamilton, J. A. Correspondence of fatty acid and drug binding sites on human serum albumin: a two-dimensional nuclear magnetic resonance study. *Biochemistry* **52**, 1559–1567 (2013).
- Kreyes, A. et al. Predictability of thermal and electrical properties of end-capped oligothiophenes by a simple bulkiness parameter. *Chem. Mater.* **25**, 2128–2136 (2013).
- Hammond, G. L. Plasma steroid-binding proteins: primary gatekeepers of steroid hormone action. *J. Endocrinol.* **230**, R13–R25 (2016).
- Kuan, S. L. et al. Dendronized albumin core-shell transporters with high drug loading capacity. *Biomacromolecules* **14**, 367–376 (2013).
- He, X. M. & Carter, D. C. Atomic structure and chemistry of human serum albumin. *Nature* **358**, 209–215 (1992).
- Boyer, P. D. et al. Enhanced intracellular delivery of small molecules and drugs via non-covalent ternary dispersions of single-wall carbon nanotubes. *J. Mater. Chem. B* **4**, 1324–1330 (2016).
- Curry, S., Mandelkow, H., Brick, P. & Franks, N. Crystal structure of human serum albumin complexed with fatty acid reveals an asymmetric distribution of binding sites. *Nat. Struct. Mol. Biol.* **5**, 827–835 (1998).
- Bryan, J. K. Molecular weights of protein multimers from polyacrylamide gel electrophoresis. *Anal. Biochem.* **78**, 513–519 (1977).
- Inácio, A. S. et al. In vitro surfactant structure-toxicity relationships: implications for surfactant use in sexually transmitted infection prophylaxis and contraception. *PLoS ONE* **6**, e19850 (2011).
- Schreier, S., Malheiros, S. V. P. & de Paula, E. Surface active drugs: self-association and interaction with membranes and surfactants. Physicochemical and biological aspects. *Biochim. Biophys. Acta Biomembr.* **1508**, 210–234 (2000).
- Li, H., Zhang, S., Wang, B., Cui, S. & Yan, J. Toxicity of cationic lipids and cationic polymers in gene delivery. *J. Control Release* **114**, 100–109 (2006).
- Knudsen, K. B. et al. In vivo toxicity of cationic micelles and liposomes. *Nanomedicine* **11**, 467–477 (2015).
- Hofmann, D., Messerschmidt, C., Bannwarth, M. B., Landfester, K. & Mailänder, V. Drug delivery without nanoparticle uptake: delivery by a kiss-and-run mechanism on the cell membrane. *Chem. Commun.* **50**, 1369–1371 (2014).
- Fanali, G. et al. Human serum albumin: from bench to bedside. *Mol. Aspects Med.* **33**, 209–290 (2012).
- Yardley, D. A. nab-Paclitaxel mechanisms of action and delivery. *J. Control Release* **170**, 365–372 (2013).
- Commissio, C. et al. Macropinocytosis of protein is an amino acid supply route in Ras-transformed cells. *Nature* **497**, 633–637 (2013).
- Yoshimori, T., Yamamoto, A., Moriyama, Y., Futai, M. & Tashiro, Y. Bafilomycin A1, a specific inhibitor of vacuolar-type H(+)-ATPase, inhibits acidification and protein degradation in lysosomes of cultured cells. *J. Biol. Chem.* **266**, 17707–17712 (1991).
- Fulda, S., Galluzzi, L. & Kroemer, G. Targeting mitochondria for cancer therapy. *Nat. Rev. Drug Discov.* **9**, 447–464 (2010).

Acknowledgements

T.W. is grateful to the financial support of the ERC Synergy grant 319130-BioQ and the Horizon2020 project Hyperdiamond. U.Z. gratefully acknowledges support of the present work by the Deutsche Forschungsgemeinschaft (DFG) project ZI567/4-3. H.B. thank the support from DFG Sonderforschungsbereiche (SFB) 1149-A04 and 1279-C02. R.V. acknowledges financial support from Fonds der Chemischen Industrie (FCI).

Author contributions

D.Y.W.N. and R.V. initiated the project and co-wrote the paper with the support from U. Z. and T.W. Chemical synthesis was performed by R.V. with support from A.K. and supervised by U.Z. Spectroscopic analysis was achieved by R.V. and D.Y.W.N. Preliminary electron microscopy was done by S.S. AFM was measured by Y.T. FCS measurements were done by K.K. Biological experiments were performed by D.Y.W.N. Confocal microscopy was performed by D.Y.W.N., Y.W. with support from W.L. and S. R. Biological interpretations were discussed extensively with expertise from S.R. and H.B. Supervision of work and research outcomes were done by T.W.

Additional information

Supplementary Information accompanies this paper at <https://doi.org/10.1038/s41467-017-02020-2>.

Competing interests: The authors declare no competing financial interests.

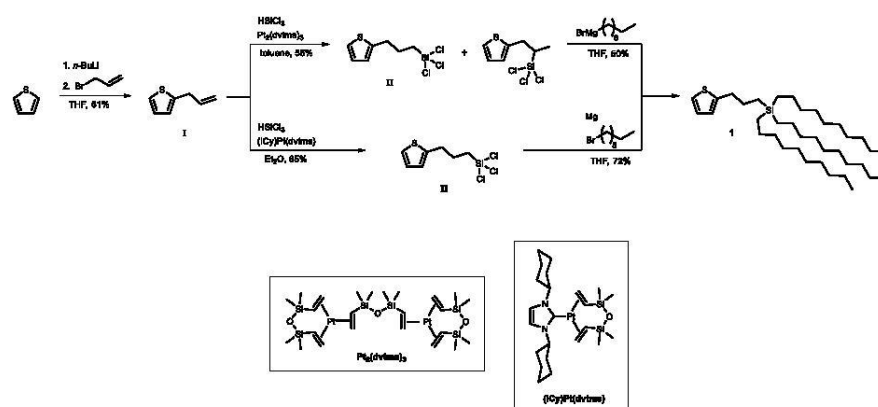
Reprints and permission information is available online at <http://npg.nature.com/reprintsandpermissions/>

Publisher's note: Springer Nature remains neutral with regard to jurisdictional claims in published maps and institutional affiliations.

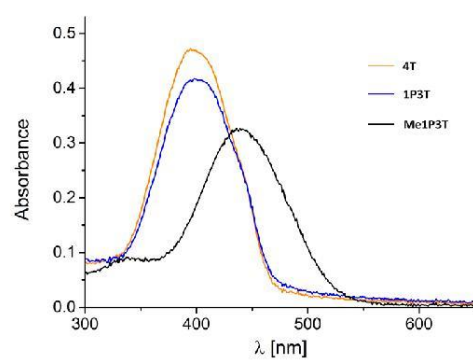


Open Access This article is licensed under a Creative Commons Attribution 4.0 International License, which permits use, sharing, adaptation, distribution and reproduction in any medium or format, as long as you give appropriate credit to the original author(s) and the source, provide a link to the Creative Commons license, and indicate if changes were made. The images or other third party material in this article are included in the article's Creative Commons license, unless indicated otherwise in a credit line to the material. If material is not included in the article's Creative Commons license and your intended use is not permitted by statutory regulation or exceeds the permitted use, you will need to obtain permission directly from the copyright holder. To view a copy of this license, visit <http://creativecommons.org/licenses/by/4.0/>.

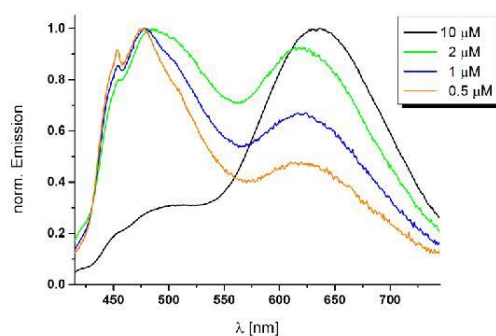
© The Author(s) 2017



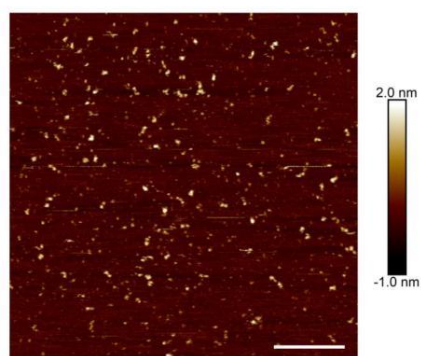
Supplementary Figure 1. Synthesis of monosubstituted thiophene **1** via construction of a branched carbosilane.^{1,2}



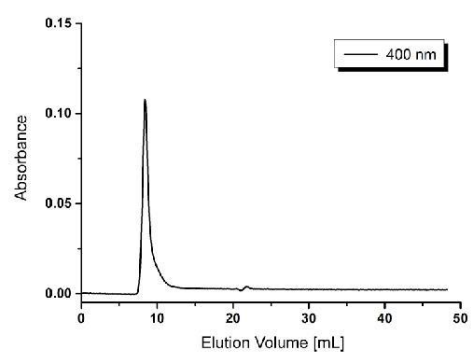
Supplementary Figure 2. Absorbance spectrum of each oligothiophene analogue (20 μ M) in THF/H₂O (1 : 4).



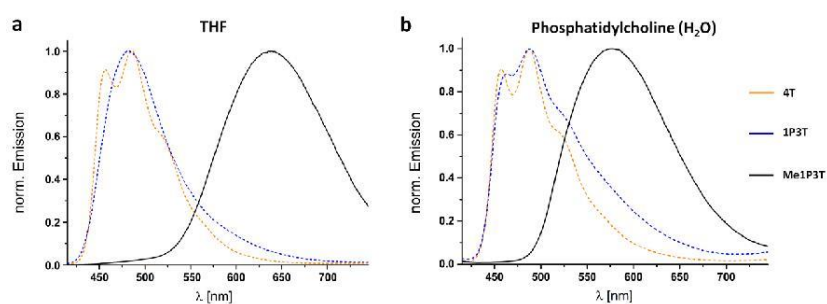
Supplementary Figure 3. Concentration dependency of the aggregation process of **Me1P3T** in THF/H₂O (1 : 4) detected using fluorescence spectroscopy ($\lambda_{exc} = 400$ nm). With increasing concentrations, the proportion of aggregates existing in solution is increased. All spectra are recorded immediately after preparation.



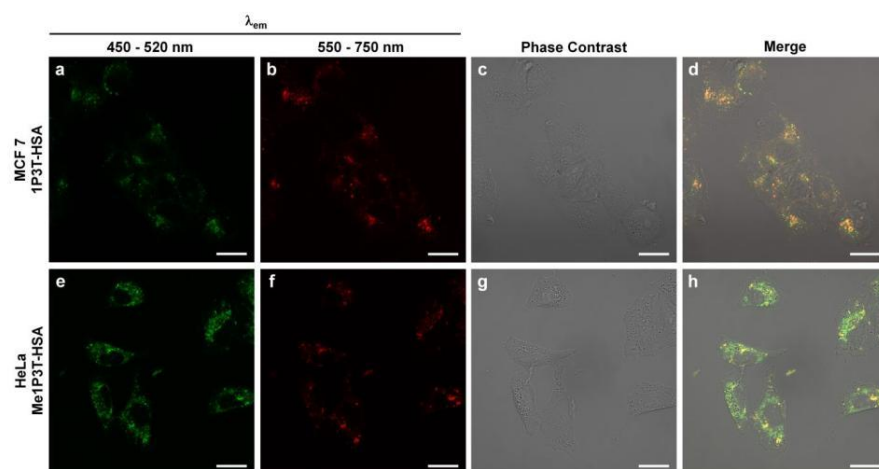
Supplementary Figure 4. Atomic force microscopy (liquid tapping mode) of native human serum albumin in H₂O. Height topological profile of particles measuring ~2 nm was detected. Scale Bar = 200 nm.



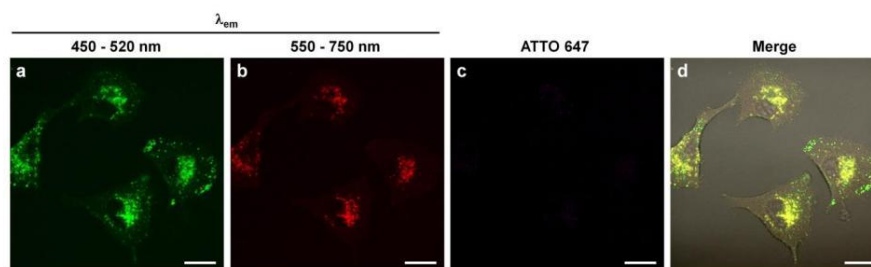
Supplementary Figure 5. Representative fast protein liquid chromatography of oligothiophene/human serum albumin complex (1P3T-HSA) on Superdex® 200 10/300 column. Mobile phase: 20 mM phosphate buffer, 150 mM NaCl.



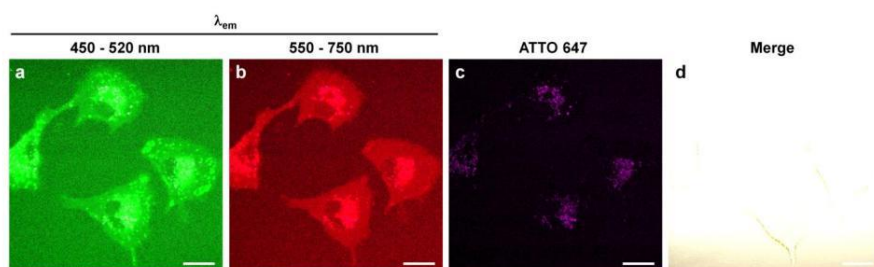
Supplementary Figure 6. Normalized emission spectra ($\lambda_{\text{ex}} = 400$ nm) of each oligothiophene analogue ($20 \mu\text{M}$) in **a** THF and **b** phosphatidylcholine (1 mM in H_2O). Dashed lines represent predominant molecular state whereas solid lines represent predominant aggregated state.



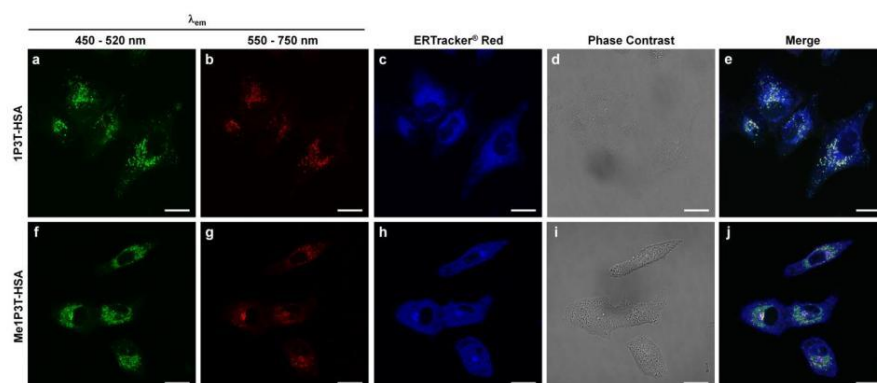
Supplementary Figure 7. Confocal laser scanning microscopy of **1P3T-HSA** in MCF-7 cells (**a-d**) and **Me1P3T-HSA** in HeLa cells (**e-h**) at 15 μ M for 24 h (37 $^{\circ}$ C, 5% CO_2). Uptake of the respective oligothiophene analogues were detected and similar aggregation behavior shown as co-localized signals of green and red within the cells. Scale bar = 20 μ m.



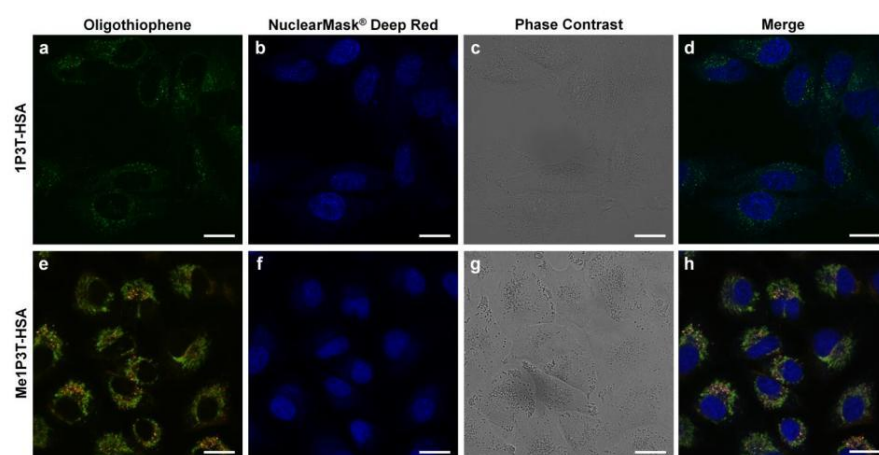
Supplementary Figure 8. Confocal laser scanning micrographs of A549 cells treated with ATTO 647 labelled **1P3T-HSA** (15 μM) for 24 h at 37 °C, 5% CO₂. **a** Molecular (450 - 520 nm, green) and **b** aggregated (550 - 750 nm, red) states of **1P3T** are visualized simultaneously. **c** Excitation of ATTO 647 at 633 nm reveals that HSA is not internalized. Scale bar = 20 μm.



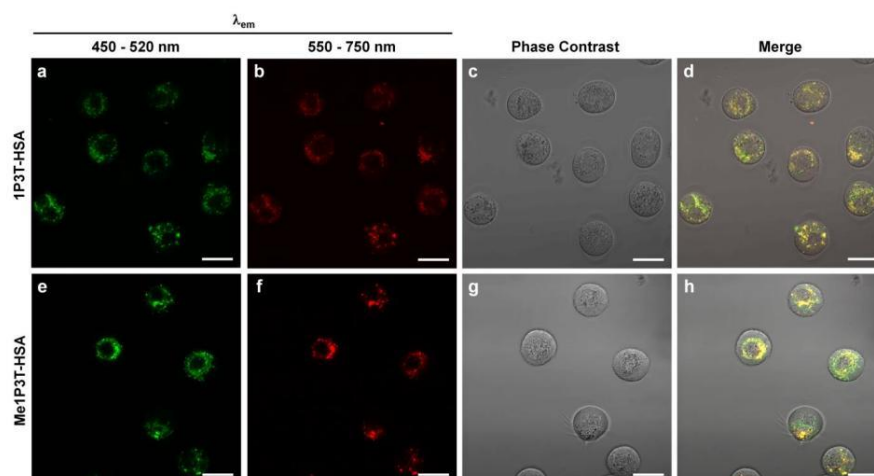
Supplementary Figure 9. Exaggeration of contrast and brightness enhancement of Supplementary Figure 8 (+80% contrast, +80% brightness, edited with Adobe Photoshop®) to show the very minor quantities of ATTO 647 labelled HSA (**c**) present in the cell. Scale bar = 20 μm .



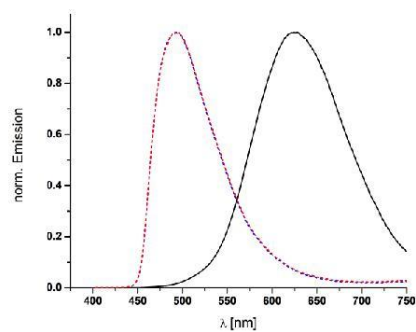
Supplementary Figure 10. Co-localization study of oligothiophene-HSA complexes **1P3T-HSA** (a-e) and **Me1P3T-HSA** (f-j) at 15 μ M for 24 h (37 °C, 5% CO₂). No co-localization signals with ERTracker® Red were detected for both molecular and aggregated forms of each oligothiophene analogue. Scale bar = 20 μ m.



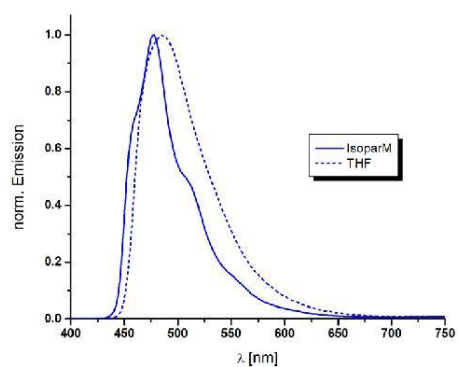
Supplementary Figure 11. Co-localization study of oligothiophene-HSA complexes **1P3T-HSA** (a-d) and **Me1P3T-HSA** (e-h) at 15 μM for 24 h (37 °C, 5% CO₂). No co-localized signals with NuclearMask® Deep Red can be detected from both molecular and aggregated forms of oligothiophenes. Scale bar = 20 μm.



Supplementary Figure 12. Analysis of microtubule dependence on the intracellular transport of oligothiophene-HSA complexes **1P3T-HSA** (a-d) and **Me1P3T-HSA** (e-h) at 15 μ M for 24 h (37 $^{\circ}$ C, 5% CO_2). A lower number of vesicles (lipid droplets) within each cell was observed as a result of both the reduction in cellular volume and the absence of microtubuli. However, the aggregation behavior of the oligothiophenes remains largely unaffected. Scale bar = 20 μ m.



Supplementary Figure 13. Normalized emission spectra of pyridine-functionalized terthiophene **1P3T** (0.3 mM in THF:H₂O = 4:1, v:v, dashed blue) including *in situ* protonation (solid black), deprotonation (dashed red). Reversibility upon addition of HCl followed by NaOH is shown.



Supplementary Figure 14. Normalized emission spectra of pyridine-functionalized terthiophene **1P3T** (400 μ M). Vibronic fine structures can be clearly seen for IsoparM in contrast to THF. Marginal shift of the maximum emission can be observed.

Supplementary Methods

Synthesis

General. 1-Bromodecane (Merck), *n*-butyllithium (*n*-BuLi, 2.5 M in *n*-hexane), trichlorosilane (all Acros), thiophene, allylbromide, 1,3-divinyl-1,1,3,3-tetramethyldisiloxaneplatinum(0) (Pt(dvtms), ~2% Pt in xylene), magnesium, 2-isopropoxy-4,4,5,5-tetramethyl-1,3,2-dioxaborolane, tris(dibenzylideneacetone)dipalladium(0)-chloroform adduct (Pd₂(dba)₃·CHCl₃), tri-*tert*-butylphosphonium tetrafluoroborate, potassium carbonate, 4-bromopyridine hydrochloride (all Aldrich), methyl trifluoromethanesulfonate and dichloromethane anhydrous (all Alfa Aesar) were purchased and used without further purification. Diethyl ether and tetrahydrofuran (THF) were dried over sodium and stored over molecular sieves 4 Å under argon atmosphere. 2-Allylthiophene³ (**I**), [Pt(*N,N'*-dicyclohexylimidazol-2-ylidene)(divinyltetramethyldisiloxane)]⁴ (ICy)Pt(dvtms), 2-trimethylstannyl-5-(3-(tridecylsilyl)prop-1-yl)thiophene¹ (**2**), 5-bromo-2,2'-bithiophene⁵ and 5-(3-(tridecylsilyl)prop-1-yl)-2,2':5',2'':5'',2'''-quaterthiophene¹ (**4T**) were prepared according to the literature. ¹H NMR and ¹³C NMR spectra were recorded at room temperature on a Bruker AMX400. High temperature NMR spectroscopy was conducted on a Bruker AMX500. All NMR measurements were done in CDCl₃, C₂D₂Cl₄ or CD₃OD/CDCl₃ mixture respectively, with the solvent residual peak as an internal reference [CHCl₃: δ = 7.24 ppm (¹H) and 77.0 ppm (¹³C), C₂HDCl₄: δ = 6.00 ppm (¹H), CHD₂OD: δ = 3.30 ppm (¹H)]. Mass spectrometry (MALDI-TOF) was performed on Bruker Reflex III. The elemental composition was determined with an Elementar Vario EL system.

2-(3-(Trichlorosilyl)prop-1-yl)thiophene (II). To (ICy)Pt(dvtms) (37.8 mg, 61.4 μmol) 2-allylthiophene (**I**) (7.63 g, 61.4 mmol) and dry diethyl ether (20 mL) were added at room temperature. Right after stirring at 36 °C for 30 min, a solution of trichlorosilane (15.5 mL, 153.6 mmol) in dry diethyl ether (25 mL) was added dropwise within 2 h. After complete addition the reaction mixture was heated at 36 °C for 17 h. After distillation in vacuo **II** was obtained as a colorless liquid (13.6 g, 85%), which was directly used for the next step. Characterization in agreement with literature.¹

2-(3-(Tridecylsilyl)prop-1-yl)thiophene (1). To a stirred suspension of magnesium turnings (11.18 g, 460 mmol) in dry THF (40 mL) a small amount of a solution of 1-bromodecane (83.0 mL, 400 mmol) in dry THF (80 mL) was added until the reaction was initiated. Subsequently, further dry THF (40 mL) and 2-(3-(trichlorosilyl)prop-1-yl)thiophene (**II**) (14.80 g, 57 mmol) were added to the rest of the 1-bromodecane solution and this mixture was added slowly. After stirring under reflux for 19 h the reaction was quenched by addition of saturated aqueous NH₄Cl solution and the organic phase was separated. The aqueous phase was extracted with diethyl ether and the combined organic phases were dried over MgSO₄. Subsequently, the solvent and *n*-decane were removed by distillation in vacuo. Then the residual crude product was purified by column chromatography (SiO₂/*n*-hexane). **1** was obtained as a colorless liquid (23.7 g, 72%). Characterization in agreement with literature.¹

2-(4,4,5,5-Tetramethyl-1,3,2-dioxaborolanyl)-5-(3-(tridecylsilyl)prop-1-yl)thiophene (3). To a solution of **1** (24.850 g, 43.06 mmol) in dry THF (160 mL) *n*-BuLi (20.7 mL, 51.67 mmol) was added dropwise at -78 °C. After complete addition the reaction mixture was stirred at the same temperature for 1 h. Then the mixture was allowed to warm to room temperature and stirred for 1 h. 2-Isopropoxy-4,4,5,5-tetramethyl-1,3,2-dioxaborolane (12.3 mL, 60.28 mmol) was slowly added at -78 °C and the solution was stirred afterwards at the same temperature for 1 h. Subsequently, the solution was allowed to warm to room temperature and was stirred for 16 h. The reaction mixture was treated with saturated aqueous NH₄Cl solution and the organic

phase was separated. The aqueous phase was extracted with diethyl ether and the combined organic phases were dried over MgSO_4 . The solvent was evaporated to afford **3** as a yellow oil (28.2 g, 93%), which was directly used for the coupling step without further purification. $^1\text{H-NMR}$ (400 MHz, CDCl_3), δ [ppm]: 7.45 (d, $^3J(3,4) = 3.4$ Hz, 1H, 3-H), 6.84 (d, $^3J(4,3) = 3.4$ Hz, 1H, 4-H), 2.83 (t, $^3J(\alpha,\beta) = 7.5$ Hz, 2H, $\alpha\text{-CH}_2$), 1.68-1.60 (m, 2H, $\beta\text{-CH}_2$), 1.31 (s, 12H, BOCCH_3), 1.30-1.24 (m, 48H, CH_2), 0.86 (t, $^3J(\text{H,H}) = 6.8$ Hz, 9H, CH_3), 0.57-0.52 (m, 2H, $\gamma\text{-CH}_2$), 0.47-0.43 (m, 6H, SiCH_3).

5-(3-(Tridecylsilyl)prop-1-yl)-2,2':5',2''-terthiophene (4). Thienylboronic pinacol ester **3** (5.150 g, 7.32 mmol) and 5-bromo-2,2'-bithiophene (1.706 g, 6.96 mmol) were dissolved in THF (50 mL) and H_2O (11 mL) was added. The solution was degassed for 1 h. Then $\text{Pd}_2(\text{dba})_3\cdot\text{CHCl}_3$ (0.227 g, 0.22 mmol), $\text{HP}(t\text{-Bu})_3\text{BF}_4$ (0.128 g, 0.44 mmol) and K_2CO_3 (3.04 g, 21.97 mmol) were added and the reaction mixture was stirred at room temperature for 19 h. The organic phase was separated and the aqueous phase was extracted with diethyl ether. The combined organic phases were dried over MgSO_4 and the solvent was evaporated. The crude product was purified by column chromatography ($\text{SiO}_2/n\text{-hexane}$) to give **4** as a yellow solid (4.5 g, 87%). Characterization in agreement with literature.² The alternative route to **4** via Stille-type cross-coupling reaction was previously published.²

5-(4,4,5,5-Tetramethyl-1,3,2-dioxaborolanyl)-5''-(3-(tridecylsilyl)prop-1-yl)-2,2':5',2''-terthiophene (5). To a solution of **4** (3.820 g, 5.15 mmol) in dry THF (40 mL) $n\text{-BuLi}$ (2.5 mL, 6.18 mmol) was added dropwise at -78°C . After complete addition the reaction mixture was stirred at the same temperature for 2 h. Then the mixture was allowed to warm to room temperature and stirred for 1 h. 2-Isopropoxy-4,4,5,5-tetramethyl-1,3,2-dioxaborolane (1.5 mL, 7.21 mmol) was slowly added at -78°C and the solution was stirred afterwards at the same temperature for 1 h. Subsequently, the solution was allowed to warm to room temperature and was stirred for 16 h. The reaction mixture was treated with saturated aqueous NH_4Cl solution and the organic phase was separated. The aqueous phase was extracted with dichloromethane and the combined organic phases were dried over MgSO_4 . The solvent was evaporated to afford **5** as a green solid (4.3 g, 96%), which was directly used for the coupling step without further purification. $^1\text{H-NMR}$ (400 MHz, CDCl_3), δ [ppm]: 7.50 (d, $^3J(3,4) = 3.6$ Hz, 1H, 3-H), 7.19 (d, $^3J(4,3) = 3.6$ Hz, 1H, 4-H), 7.09 (d, $^3J(\text{H,H}) = 3.8$ Hz, 1H, 3'-H or 4'-H), 6.98 (d, $^3J(\text{H,H}) = 3.8$ Hz, 1H, 3'-H or 4'-H), 6.97 (d, $^3J(3'',4'') = 3.5$ Hz, 1H, 3''-H), 6.66 (d, $^3J(4'',3'') = 3.6$ Hz, 1H, 4''-H), 2.77 (t, $^3J(\alpha,\beta) = 7.3$ Hz, 2H, $\alpha\text{-CH}_2$), 1.68-1.60 (m, 2H, $\beta\text{-CH}_2$), 1.33 (s, 12H, BOCCH_3), 1.32-1.23 (m, 48H, CH_2), 0.85 (t, $^3J(\text{H,H}) = 6.8$ Hz, 9H, CH_3), 0.58-0.53 (m, 2H, $\gamma\text{-CH}_2$), 0.49-0.45 (m, 6H, SiCH_3).

Optical Spectroscopy

Fluorescence spectroscopy was performed on a Horiba FluoroMax-3 and Tecan Spark® multimode microplate reader. Absorbance measurements were conducted as well on the Tecan Spark® multimode microplate reader. All spectra were recorded at room temperature.

Oligothiophenes (**4T**, **1P3T**, **Me1P3T**) were freshly dissolved in THF to afford a 1 mM stock solution. The solutions were subsequently diluted to 20 μM for absorption and fluorescence spectroscopy respectively. In co-solvent systems (i.e. $\text{THF:H}_2\text{O} = 4:1$, v:v), the stock solution was always first diluted with THF followed by the addition of water to achieve the required solvent composition.

For the oligothiophene complexes (**4T-HSA**, **1P3T-HSA**, **Me1P3T-HSA**), the solutions were first dissolved into a stock solution of 300 μM using MilliQ water. The samples were further diluted into triplicates to afford 20 μM . The absorbance and fluorescence were then measured in a 384-well UVstar® microplate (Greiner Bio-One).

To achieve steady-state aggregation/disaggregation of the respective oligothiophenes, all prepared solutions were left standing at room temperature for 24 h before measurement. Each solution was excited at 400 nm with emission scan from 420 - 750 nm.

Phosphatidylcholine Experiment

Phosphatidylcholine was first dissolved in MeOH to create a 500 mM solution. The oligothiophenes (**4T**, **1P3T**, **Me1P3T**) were separately dissolved in THF to create a 10 mM solution. Phosphatidylcholine (500 mM, 2 μ L) was mixed with the respective oligothiophenes (10 mM, 2 μ L) and added water (998 μ L). The solution was mixed vigorously on a vortex shaker for 1 h. The final solution (1 mL) containing 1 mM phosphatidylcholine, 20 μ M oligothiophene was measured on Horiba FluoroMax-3.

Fluorescence Correlation Spectroscopy (FCS)

FCS experiments were performed on a commercial confocal microscope, LSM 880 (Carl Zeiss, Jena, Germany) equipped with a C-Apochromat 40x/1.2W water immersion objective. The fluorophores were excited by a diode laser (405 nm) fiber-coupled to the microscope. Emitted fluorescence light was collected with the same objective, passed through a confocal pinhole and directed to a spectral detection unit (Quasar, Carl Zeiss). In this unit emission is spectrally separated by a grating element on a 32 channel array of GaAsP detectors operating in a single photon counting mode. In all experiments the emission in the spectral range 420 – 700 nm was considered. A stainless steel chamber Attofluor (Thermo Fisher Scientific) holding a 25 mm round coverslip was used as a sample cell for the studied solutions. For each sample, a series of measurements with a total duration of 5 min were performed. The time-dependent fluctuations of the fluorescent intensity $\delta I(t)$ were recorded and analyzed by an autocorrelation function $G(\tau) = 1 + \langle \delta I(t) \delta I(t+\tau) \rangle / \langle I(t) \rangle^2$. As it has been shown theoretically for an ensemble of m different types of freely diffusing identical fluorescence species, $G(\tau)$ has the following analytical form⁶:

$$G(\tau) = 1 + \frac{1}{N} \left[1 + \frac{f_T}{1 - f_T} e^{-\tau/\tau_T} \right] \sum_{i=1}^m \frac{F_i}{\left[1 + \frac{\tau}{\tau_{Di}} \right] \sqrt{1 + \frac{\tau}{S^2 \tau_{Di}}}} \quad (1)$$

Here, N is the average number of diffusing fluorescence species in the observation volume, f_T and τ_T are the fraction and the decay time of the triplet state, $S = z_0/r_0$ is the so-called structure parameter with z_0 and r_0 representing the axial and radial dimensions of the confocal volume. F_i is the fraction of the i -th species and τ_{Di} is their diffusion time through the observation volume that is related to their diffusion coefficient, D_i , through $D_i = r_0^2/4 \tau_{Di}$. The experimentally obtained $G(\tau)$ were fitted with Supplementary Equation 1, yielding the corresponding diffusion times and subsequently the diffusion coefficients of the fluorescent species. Finally, the hydrodynamic radii R_h were calculated (assuming spherical particles) using the Stokes-Einstein relation: $R_h = k_B T / 6\pi\eta D$, where k_B is the Boltzmann constant, T is the temperature, and η is the viscosity of the solution. As the value of r_0 depends strongly on the specific characteristics of the optical setup a calibration was done using a reference standard with known diffusion coefficient, i.e. ATTO 425.

General (Biologicals)

Dulbecco's Modified Eagle's Medium (DMEM) high glucose, fetal bovine serum, penicillin/streptomycin and Sephadex® gel G25M are purchased from GE Healthcare. Staining reagents such as ERTracker® Red, NuclearMask® Deep Red and MitoTracker® Deep Red are bought from Invitrogen (Molecular Probes). Human serum albumin (>96%), Bafilomycin A1 from *Streptomyces griseus* (>90%), Nocodazole, MEM non-essential amino acid solution (100x) and associated buffer salts were purchased from Sigma Aldrich and were used directly without further purification. ATTO 647 *N*-hydroxysuccinimidyl ester was bought from ATTO-TEC. The purity of water (H₂O) used in all experiments are of MilliQ ultrapure grade.

Supplementary References

- 1 Kreyes, A. *et al.* The longest β -unsubstituted oligothiophenes and their self-assembly in solution. *Chem. Mater.* **22**, 6453-6458 (2010).
- 2 Kreyes, A. *et al.* Predictability of thermal and electrical properties of end-capped oligothiophenes by a simple bulkiness parameter. *Chem. Mater.* **25**, 2128-2136 (2013).
- 3 Zhang, Y., Wang, C., Rothberg, L. & Ng, M.-K. Surface-initiated growth of conjugated polymers for functionalization of electronically active nanoporous networks: synthesis, structure and optical properties. *J. Mater. Chem.* **16**, 3721-3725 (2006).
- 4 Markó, I. E. *et al.* Highly active and selective platinum(0)-carbene complexes. Efficient, catalytic hydrosilylation of functionalised olefins. *Adv. Synth. Catal.* **346**, 1429-1434 (2004).
- 5 Carpita, A., Rossi, R. & Veracini, C. A. Synthesis and ¹³C nmr characterization of some π -excessive heteropolyaromatic compounds. *Tetrahedron* **41**, 1919-1929 (1985).
- 6 Rigler R. and Elson E.S., Fluorescence Correlation Spectroscopy. Springer Verlag New York (2001).

7. Curriculum vitae

Personal information

Name: Yu Tokura

Date of birth: 05/01/1990

Place of birth: Japan

Nationality: Japan

Education

2016, July – Present	PhD student
Max-Planck-Institute for Polymer Research. Mainz, Germany	
2014, July – Present	PhD student
Institute of Organic Chemistry III, Ulm University, Ulm, Germany	
2014, April – 2014, Jun	Visiting scientist
Institute of Organic Chemistry III, Ulm University, Ulm, Germany	
2012, July – 2012, September	Research Internship
Nuffield Department of Clinical Medicine, University of Oxford, Oxford, UK	
2012, April – 2014, March	M. Sc.
Graduate school of Engineering, Kyoto University, Kyoto, Japan (GPA : 3.5)	
2008, April – 2012, March	B. Sc.
Faculty of Engineering, Kyoto University, Kyoto, Japan (GPA : 3.73)	

8. List of publications

Manuscripts submitted or in revision

1. S. L. Kuan, S. Fischer, S. Hafner, T. Wang, T. Syrovets, W. Liu, Y. Tokura, D.Y. W. Ng, A. Riegger, C. Förtsch, D. Jäger, T. F. E. Barth, T. Simmet, H. Barth, and T. Weil "Boosting Anti-Tumor Drug Efficacy with Chemically Engineered Multidomain Proteins" *Submitted*.

Published manuscripts

2. Y. Tokura, S. Harvey, X. Xu, C. Chen, S. Morsbach, K. Wunderlich, G. Fytas, Y. Wu, D. Y. W. Ng, and T. Weil. "Polymer tube nanoreactors by DNA-origami templated synthesis" *Chem. Commun.*, 2018. DOI: 10.1039/C7CC09620H.
3. Y. Tokura, S. Harvey, C. Chen, Y. Wu, D. Y. W. Ng, and T. Weil. "Fabrication of Defined Polydopamine Nanostructures by DNA Origami-Templated Polymerization" *Angew. Chem. Int. Ed.* 2018, 130, 1603-1607
4. T. Duan, L. He, Y. Tokura, X. Liu, Y. Wu, and Z. Shi. "Construction of tunable peptide nucleic acid junctions" *Chem. Commun.* 2018, DOI: 10.1039/C8CC00108A
5. D. Y. W. Ng, R. Vill, Y. Wu, K. Koynov, Y. Tokura, W. Liu, S. Sihler, A. Kreyes, S. Ritz, H. Barth, U. Ziener, and T. Weil. „Directing intracellular supramolecular assembly with N-heteroaromatic quaterthiophene analogues" *Nat. Commun.* 2017, 8, 1850
6. A. Riegger, C. Chen, O. Zirafi, N. Daiss, Debashish Mukherji, K. Walter, Y. Tokura, B. Stöckle, K. Kremer, F. Kirchhoff, D.Y.W. Ng, P.C. Hermann, J. Münch, and T. Weil. "Synthesis of Peptide-Functionalized Poly(bis-sulfone) Copolymers Regulating HIV-1 Entry and Cancer Stem Cell Migration" *ACS Macro Lett.* 2017, 6, 241–246.
7. Y. Tokura, Y. Jiang, A. Welle, M.H. Stenzel, J. Michaelis, C. Barner-Kowollik, Y. Wu, and T. Weil. "Bottom-up fabrication of nano-patterned polymers on DNA origami nanotile by in-situ atom transfer radical polymerization" *Angew. Chem. Int. Ed.* 2016, 55, 19, 5692-5697.
8. S. L. Kuan, C. Förtsch, D.Y.W. Ng, S. Fischer, Y. Tokura, W. Liu, Y. Wu, H. Barth, and T. Weil. "A Supramolecular Approach towards Bioinspired PAMAM-Dendronized Fusion Toxins" *Macromol. Biosci.* 2016, 16, 6, 803–810.

Manuscript in preparation

9. W. Liu, F. Boldt, Y. Tokura, T. Wang, B. K. Agrawalla, Y. Wu, and T. Weil. "Encoding function in protein-oligonucleotide precision biopolymers"

9. List of conferences

"Programming polymer nanoarchitectures by DNA origami technology" 253rd American Chemical Society, National Meeting & Exposition, San Francisco, California, U.S.A., April 2017 (Oral presentation)

"Programming polymer nanoarchitectures by DNA origami technology" The GDCh-Division of Macromolecular Chemistry, Biennial meeting, "Polymers: from Structure to Function", Halle, Germany, September 2016 (Poster presentation)

"Programming polymer nanoarchitectures by DNA origami technology" Leibnitz Institute for Interactive Materials, Young Polymer Scientist Forum, Aachen, Germany, July 2016 (Oral & Poster presentation)

"Nanofabrication and Patterning of Polymers on DNA Nanotile" IUPAC 11th International Conference on Advanced Polymers via Macromolecular Engineering, Yokohama, Japan, October 2015 (Poster presentation)

10. Abbreviations

A: adenine

AFM: atomic force microscopy

ATRP: atom transfer radical polymerization

ARGET ATRP: activator (re)generated by electron transfer atom transfer radical polymerization

C: cytosine

calc: calculated

CPG: controlled pore glass

CRP: controlled radical polymerization

DMT: 4,4'-dimethoxytrityl

DNA: deoxyribonucleic acid

DNAzyme: Deoxyribozyme

dsDNA: double stranded DNA

EDTA: ethylenediaminetetraacetic acid

eq.: equivalent(s)

G: guanine

G4: guanine quadruplex

MALDI-TOF MS: matrix-assisted laser desorption/ionization time-of-flight mass spectrometry

NHS: N-hydroxysuccinimide

nm: nanometer

NMR: nuclear magnetic resonance

OEGA: oligo(ethylene glycol)ethyl ether acrylate

PAGE: polyacrylamide gel electrophoresis

PD: polydopamine

PNA: peptide nucleic acid

PNIPAAm : poly(N-isopropylacrylamide)

RAFT: Reversible Addition–Fragmentation chain Transfer

RP-HPLC: reverse phase high performance liquid chromatography

QNM: quantitative nanomechanical property mapping

SIP: surface-initiated polymerization

SI-ATRP: surface initiated atom transfer radical polymerization

ssDNA: single stranded DNA

T: thymine

TAE: tris acetate EDTA

TBE: tris borate EDTA

TCA: trichloroacetic acid

TEM: Transmission Electron Microscopy

TOF-SIMS: Time-of-Flight Secondary Ion Mass Spectrometry

Tris: tris(hydroxymethyl)aminomethane

tRNA: transfer- ribonucleic acid

um: micrometer

UV-Vis: Ultraviolet • Visible Absorption Spectroscopy

2D: two dimensional

3D: three dimensional

11. List of figures

Figure 1. The basic scheme of ATRP

Figure 2. Design of polymer assembly

Figure 3. General scheme of polymer brush fabrication

Figure 4. Fabrication of micro/nano patterned polymer brush surface

Figure 5. General AFM scheme

Figure 6. General schematic depiction of ToF-SIMS

Figure 7. Biomacromolecular templated polymer synthesis

Figure 8. 3D Structure of ds DNA

Figure 9. The general scheme on one cycle of DNA synthesis

Figure 10. Modification of DNA

Figure 11. The synthesis and the direct incorporation of ATRP initiator to DNA strand via automated DNA synthesis

Figure 12. The basic concept of DNA nanotechnology

Figure 13. Design of DNA origami

Figure 14. Principle of DNA origami

Figure 15. The modification sites of rectangular DNA origami

Figure 16. Functionalization of DNA origami by introducing modified staple DNA

Figure 17. G4/hemin based DNA enzyme

Figure 18. DNA origami templated nanomaterial assembly

Figure 19. DNA origami-templated synthesis of nanomaterials

Figure 20. DNA origami-based nanoimprinting lithography

Figure 21. The approaches to improve the stability of DNA origami

Figure 22. Surface-initiated atom transfer radical polymerization on DNA origami template

Figure 23. DNA origami-templated step-wise growth of polymers for nanoscale engineering

Figure 24. Polymerization mechanism of dopamine and DNAzyme-assisted bottom-up polydopamine nanostructure fabrication on DNA origami template

Figure 25. Complexation of a series of oligothiophenes with HSA.

Figure 26 Outlook of DNA origami templated polymer nanoarchitectures synthesis

12. Declaration of Originality in academic work

Ich versichere hiermit, daß ich die Arbeit selbständig angefertigt habe und keine anderen als die angegebenen Quellen und Hilfsmittel benutzt sowie die wörtlich oder inhaltlich übernommene Stellen als solche kenntlich gemacht habe.

Ulm, den

.....

(Yu Tokura)

I hereby declare that this thesis and the work reported herein was composed by and originated entirely from me. Information derived from the published and unpublished work of others has been acknowledged in the text and references are given in the list of sources.

Ulm, den

.....

(Yu Tokura)

13. Acknowledgement

It is my great pleasure to take this special opportunity to express my sincere gratitude to all the people who kindly helped me throughout my PhD days. Without them and their great help, it would have been not possible for me to conduct my PhD study and come to where I am now.

First and foremost, I would like to express my most cordial appreciation for my supervisor, Prof. Dr. Tanja Weil. She kindly welcomed me to start my PhD under her great supervision, and through my PhD study, always gave my valuable suggestions and correct research directions to go. Thanks to her kind and encouraging supports, I could fully concentrate on my study and withstand hardships appeared on my way. Also, I was fully impressed and influenced by her way of doing research – always energetic, open, and fair, to which I want to show my full respect. I am greatly honored to be supervised by her.

Prof. Dr. Yuzhou Wu was my trustful advisor, giving me creative ideas, sincerely answering to my questions all the time, and helping me when I encountered difficulties during my research. I wish to thank her for all the helps which she gave to me and express that I learned a lot of things from her not only the experimental aspects but also how to actively and friendly interact with collaborators to develop the reaction field, and a way of giving powerful and persuasive presentations.

Special thanks go to Dr. Seah Ling Kuan and Dr. David Y. W. Ng, who have helped me a lot of times in Ulm period, and especially after moving to Mainz. I deeply appreciate their plentiful knowledge and experiences in research and also great helps for me to settle in Mainz and smoothly restart my experiments in Max-Planck institute for Polymer Research.

I am indebted to my past and present colleagues in Prof. Dr. Tanja Weil's group both in Ulm and in Mainz for creating a comfortable and encouraging working environments. Among them, I would like to especially thank Marco Raabe, Sean Harvey, Maksymilian Zegota, Johanna Quambusch, Jasmina Gacanin, Weina Liu, Christiane Seidler, Andreas Riegger, Stefanie Sieste, Chaojian Chen, Michaela Pieszka, Dr. Katrin Wunderlich, and Prof. Wang Tao. We have worked together and also spent a lot of enjoyable time together. I would like to also thank Dr. Lamla, Ms. Zimmerman, Dr. Hoffmann-Richter, Ms. Sciel, Ms. Schnee and apl. Prof. Ziener for technical supports, and Ms. Munz, Ms. Michaelis, Ms. Rapp, and Ms.

Zheng for administrative supports.

Furthermore, I would like to extend my gratitude toward my collaborators: Prof. Dr. Jens Michaelis from Ulm University, Dr. Yanyan Jiang from University of New South Wales, Dr. Rüdiger Berger from Max-Planck institute for Polymer Research. They all have made immense contributions to my research.

Importantly, I would like to thank my friends and family for their encouragement, understanding, and accompanying during my PhD period.